# MOSFIRE: MULTI-OBJECT SPECTROMETER FOR INFRA-RED EXPLORATION

## Detailed Design Report

April 6, 2007
Version 2.00

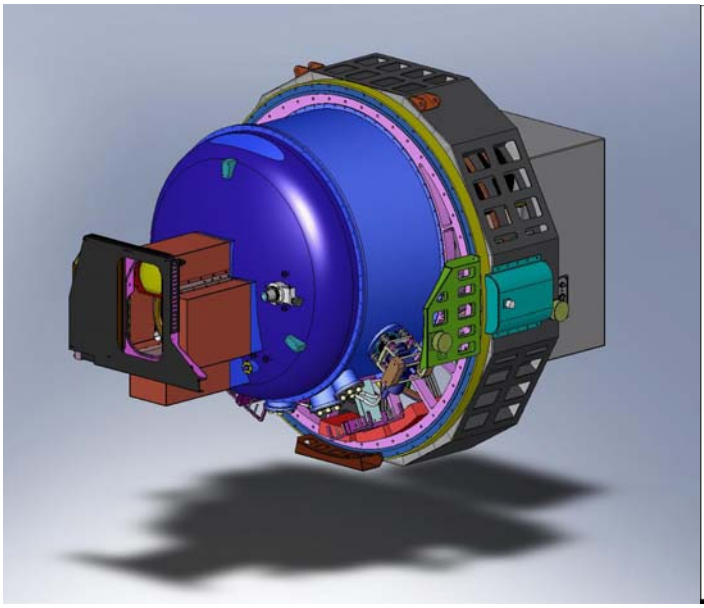

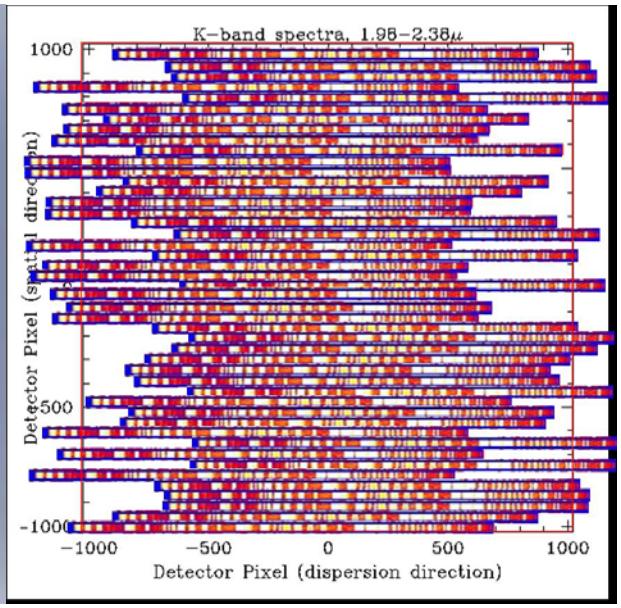

## Table of Contents

## Table of Contents

## Table of Contents

## Table of Contents

## Table of Contents

## Table of Contents

## Figures and Tables

## Figures and Tables

## Figures and Tables

## Figures and Tables

## Figures and Tables

# 1 EXECUTIVE SUMMARY

The MOSFIRE Detailed Design Report is presented. MOSFIRE is a near-IR (~0.97-2.45 μm) spectrograph for the Cassegrain focus of Keck 1. The optical design provides imaging and multi-object spectroscopy over a field of view (FOV) of 6.14' x 6.14' with a resolving power of R~3,270 for a slit width of 0.7" (2.9 pixels along dispersion). The detector is a sensitive 2K x 2K H2-RG HgCdTe array with a 2.5 μm cut-off. A special feature of MOSFIRE is that its multiplex advantage of up to 46 slits is achieved using a cryogenic Configurable Slit Unit or CSU (being developed in collaboration with the Swiss Centre for Electronics and Micro Technology, CSEM) that is reconfigurable under remote control in less than 5 minutes without any thermal cycling of the instrument. Slits are formed by moving opposable bars from both sides of the focal plane. An individual slit has a length of 7.3" but bar positions can be aligned to make longer slits. When the bars are removed to their full extent and the grating is changed to a mirror, MOSFIRE becomes a wide-field imager.

During the detailed design phase, all of the major, perceived risks have been mitigated or retired, and issues raised at the preliminary design review have been addressed. Our all-spherical refractive optical design has been advanced to the construction level and all materials needed to fabricate the lenses are in hand or soon will be. A non-cryogenic CCD-based optical guider has also been designed and many of the lenses for it have already been fabricated at the UCO/Lick shops. CSEM built and tested a 2-bar cryogenic CSU that meets our specification for variable gravity operation, carried out a detailed thermal analysis and developed the electronics and software needed to drive the prototype. CSEM recently passed their critical design review and are now ready for full scale production. Since PDR, all aspects of the MOSFIRE mechanical design have been detailed and analyzed. Finite element analysis of the large cylindrical enclosure and internal structure shows that the instrument is intrinsically stiff, and a detailed thermal analysis shows that the temperature distribution is isothermal. Using only two large CCR heads, the instrument will achieve operating temperature in about 7 to 8 days. In addition to the CSU, the other cryogenic mechanisms are a dual filter wheel, a rotating pupil mechanism and a turret carrying a single diffraction grating and a plane mirror mounted back-to-back. Two fixed positions for the grating are provided and order-sorting filters give essentially full coverage of the K, H, J and Y bands using 3$^{rd}$, 4$^{th}$, 5$^{th}$ or 6$^{th}$ order respectively. A folding flat following the field lens is equipped with piezo transducers to provide tip/tilt for flexure compensation at the 0.1 pixel level. A titanium flexure driven by a small motor installed in the detector head provides focus motion to aid in setting up the instrument; a prototype of this unit has been built. Because each lens is to be mounted in an individual cell using bonded flexures, extensive testing of the bonds was carried out for every kind of lens material. In addition, dummy lenses of aluminum and precision lens cells were developed along with sophisticated handling and alignment jigs during the detailed design phase. Software and electronics have also advanced to the detailed design level, including warm operation of the SIDECAR ASIC for detector control, servers and interfaces for all aspects of instrument control, and packaging of all electronics in a thermally controlled cabinet at the rear of the instrument.

MOSFIRE is clearly a very challenging instrument to design and build. Having developed the concept to the detailed design stage, and having evaluated the performance through analysis and prototypes, we are confident that the instrument will meet or exceed all requirements.

## 2 INTRODUCTION

One year ago, at the completion of the preliminary design study, we reported that many of the outstanding issues related to instrument performance and technical risk had been mitigated and that the design was ready to proceed to the next stage. The optical design had been advanced to the detailed design level, CSEM had been contracted to develop a cryogenic prototype of the CSU, cryogenic mechanisms had been kept to a minimum, software and electronics heritage from OSIRIS was adopted, and a single 2K x 2K HgCdTe H2-RG detector (similar to JWST) was selected. Thanks to an award from the Telescope System Instrumentation Program (TSIP) and a generous gift from Gordon and Betty Moore, MOSFIRE is fully funded at a total cost of $12M. To date, the project remains on budget and only slightly behind schedule due mainly to funding logistics rather than technical difficulties. Following completion of the detailed design review (DDR), MOSFIRE will be ready to continue into the construction phase. Due to some inevitable programmatic slippage, installation at the Keck Observatory is now planned for the end of 2009.

Our goals for this detailed design phase included a complete mechanical and thermal analysis of the design, testing of concepts through the use of prototypes, early purchase of critical components such as the optical materials, interactions with potential vendors and detailed documentation of all aspects of the design. Every facet of the design has been advanced to a detailed level including the production of shop drawings, schematics and operational code. No reduction in scope has occurred. In fact, the optical design has enabled us to request an additional slit bar from CSEM to bring the total number of slits to 46. Provision for calibration lamps has been added. Two, repeatable grating tilts are now available instead of one in order to improve coverage of the J and Y bands. A detector focus drive with a larger range of travel has been designed to aid during initial set up. The curved focal plane of the Keck telescope will be approximated with three steps in the CSU (instead of two) and the slits jaws will have a slight tilt to help over-sample the images during nodding, and to allow for the use of optimal background subtraction algorithms.

MOSFIRE is being developed for the W. M. Keck Observatory (WMKO) by the University of California, Los Angeles (UCLA), the California Institute of Technology (CIT) and the University of California, Santa Cruz, (UCSC). The MOSFIRE Co-Principal Investigators are Ian McLean of UCLA and Charles Steidel (CIT), with other leading roles in optics, instrumentation and software being played by Harland Epps (UCSC), Keith Matthews (CIT) and James Larkin (UCLA). Engineering resources at CIT, UCLA, UCSC and CARA are being combined to build MOSFIRE. The project is managed by WMKO Instrument Program Manager, Sean Adkins.

## 3 SPECIFICATIONS AND REQUIREMENTS

Top level science requirements for MOSFIRE were established in large part by an ad hoc group (Keck Observatory Next Spectrograph Advisory Group, or “KONSAG”) that considered the minimum scientific requirements of a cost-capped near-IR imaging spectrometer for the Keck Observatory. Most of the major MOSFIRE design choices flowed directly from this report (and some of the current MOSFIRE team members participated in the KONSAG study). The principle requirements were:

- Wavelength range of at least 1 to 2.4 μm, to complement optical imaging spectrometers at the WMKO operating from 0.3 to 1 μm.
- Simultaneous wavelength coverage of at least one atmospheric band at a time.
- Spectral resolution of at least R = 3000 achieved with a 0.75" entrance slit.
- Field of view of >5' for imaging, > 5' by 2' for spectroscopy
- Multiplex factor >15
- Background-limited spectroscopy over the full wavelength range in reasonable exposure times.
- Image quality should not degrade the median near-IR seeing by more than 10%, and spectral resolution should not degrade by more than 15% at the edges of the usable field.

Given that the MOSFIRE design is now quite mature, and the KONSAG requirements have been met or exceeded in every respect, in this document we focus our attention on the implementation of the design choices.

## 3.1 Changes since the PDR

There have been two significant changes in scope (both adding functionality, and both addressing recommendations made by the PDR committee) for the MOSFIRE design since PDR.

The first change provides an additional fixed grating angle designed to improve the centering of orders 5 and 6 (for J- and Y-band spectroscopy, respectively) on the detector; see MMDN24 for implementation details. To achieve the additional tilt a shim is inserted by a simple mechanism between the grating and the stop, thus changing the grating angle by slightly more than a degree, from 42.614 degrees to 41.524 degrees. In addition, the blaze angle specification of the grating (see MODN06) has been modified to better balance the location of blaze peaks with respect to the central wavelengths of each spectral order.

The second significant change is the addition of Neon and Argon calibration arc lamps to the front end of the instrument, just behind the dust cover. These lamps will provide wavelength calibrations that may be acquired in the afternoon during the process of obtaining calibrations for a night's anticipated observing. Line lamps will supplement information provided by the OH lines in the night sky. Use of the lamps is discussed further below in Section 3.2.9 (Calibration Plans).

## 3.2 Flow Down of Science Requirements to Technical Requirements

The key MOSFIRE design choices are summarized in Table 1, and the science-driven rationale for these choices is discussed briefly in the following sections. A more detailed set of requirements can be found in the MOSFIRE Requirements Document.

| | |
|---|---|
| **Wavelength coverage** | 0.975 to 2.40 μm; 110.5 line/mm grating used in orders 6,5,4,3 (Y, J, H, K), with choice of two grating tilts optimized for H, K or Y, J. |
| **Spectral Resolution** | Rθ=2290 ⇒ R=3270 w/0.7" slit, (2.9 pixels) |
| **Simultaneous Wavelength Range** | Coverage is 0.45 μm (21%) in K band; 1.97 to 2.42 μm for a slit at the center of the field; H band coverage 1.48 to 1.81 μm for the same slit |
| **Pixel Scale** | 0.18" in imaging mode |
| **Field Size** | 6.12' slit length, 6.14' field for imaging; slits can be placed anywhere within the imaging field of view. |
| **Multiplex** | Cryogenic Configurable Slit Unit (CSU): 46 remotely configurable slits each 7.3" long; configurable as a smaller number of longer slits. Each slit width can be adjusted arbitrarily. |
| **Image Quality** | Design delivers < 0.25" rms diameter images over 0.97 to 2.40 μm with no re-focus. |
| **Stability** | <0.3 pixel residual image motion at detector over 2 hr observation. Open-loop flexure compensation using tip/tilt mirror, look-up table. |
| **Guiding** | Optical CCD guider, offset by 6.6' from the center of the MOSFIRE field, field of view of 2.8' square on a 1024x1024 detector with 0.164" sampling. |
| **Throughput: spectroscopy** | >30% not including telescope, on order blaze |
| **Mask configuration time** | <5 minutes for full re-configuration; goal <2.5 minutes |
| **Filters** | Minimum complement is order sorting filters for K, H, J, Y; additional Ks photometric filter for imaging. Goal: up to 5 additional photometric broad or narrow-band filters. |
| **Lyot stop** | Two position tracking pupil mask [circumscribed or slightly under-sized, matching hexagonal shape of pupil image (for H, K bands)] |
| **Detector** | 2048 x 2048 Rockwell Scientific Hawaii-2RG and ASIC; 18 μm pixels, long-wavelength cutoff @2.5 μm; low charge persistence; highest QE |

**Table 1: Summary of the MOSFIRE Design Parameters**

### 3.2.1 Spectral Resolution

Spectral resolution serves a two-fold purpose: first, there is a minimum resolution required to allow measurement of spectral features or to resolve kinematic signatures for faint objects; second, a minimum resolution is required for maximum sensitivity because, over most of the 1-2.5 μm range, the background is dominated by discrete OH emission lines and not by sky continuum. There is no perfect resolution that optimizes sensitivity for all applications simultaneously. However, most studies have concluded that R~3,000 is required for effective OH suppression over substantial fractions of each atmospheric band, particularly in the J and H bands (e.g., Martini and DePoy 2000). R~3,000 is also required for measuring radial velocities to ~10 km $s^{-1}$, velocity dispersions down to σ~30-40 km $s^{-1}$ as required for intrinsically faint galaxies, and for providing access to unique spectral features in Galactic sources. Although seeing in the near-IR can often be in the 0.3"-0.4" range on Mauna Kea, many potential targets for multiplexed spectroscopy are resolved, and would suffer from significant slit losses with very narrow entrance slits. Thus, R > 3,000 must be achieved with a ~0.7" slit that we believe will be the most commonly used aperture size for faint object work. The current design achieves R = 3,270 using a 110.5 line/mm

grating similar to the one made for the Gemini GNIRS spectrometer; for the commonly-quoted 2-pixel projected slit (0.48" for MOSFIRE) the nominal resolution is R = 4,770. A custom (larger size) master is being manufactured for MOSFIRE, with a blaze angle of 21.93 degrees (6.35 μm effective first-order blaze with the 40 degree included (camera-collimator) angle used by MOSFIRE), chosen to optimize the blaze function for each spectral order with respect to the bandpass.

### 3.2.2 Field of View and Spectral Coverage

One of the primary design goals of MOSFIRE was wavelength coverage of at least a full atmospheric band while preserving the spectral resolution. This is difficult to achieve without a mosaic of detectors in the camera focal plane. For reasons of detector cost, increasing difficulty in the optical design, the cost of larger optics, and the optical performance impact, there was a strong impetus to map the spectral format onto a single 2K x 2K detector. Here there was some leeway to trade spatial sampling for spectral coverage (e.g. using more focal reduction), although this too is limited by the difficulty in designing extremely fast cameras with acceptable performance. A plate scale of 0.18"/pixel was the initial design goal, to provide reasonable sampling of the typical near-IR seeing of ~0.5" for both imaging programs and for spatial resolution along slits. In the MOSFIRE case, the design choice of a reflection grating in the manner we are proposing, with an anamorphic magnification factor of 1.34, provides additional effective focal reduction in the dispersion direction, thus gaining spectral coverage without sacrificing spectral resolution. As a result, one can place slits over a wide range in "X" position within the MOSFIRE field of view and still record most or all of each atmospheric window, for each slit, on a single detector. The effective spatial sampling in the dispersion direction is 0.24"/pixel, so that the projected slit will be 2.9 and 2.1 pixels respectively for slits of 0.7" and 0.5". Thus, the adopted configuration meets the desired goals for spectral resolution and spectral coverage on a single detector, eliminating the complication of spectral and/or spatial "gaps" that occur in the case of a detector mosaic and which make data reduction considerably more complex.

Figure 1 shows the locations of spectra in each of the four MOSFIRE spectral bands for a set of 46 slits randomly placed within a 6.1' x 3' field. The black square outline represents the 2K x 2K detector. In the K and H bands, a grating tilt of 42.614 degrees (the "primary" grating setting) centers the spectra on the detector, and only a small amount of wavelength coverage is lost for slits at the most extreme X-positions. For the Y and J bands, the spectra are more optimally placed on the detector using the "secondary" grating tilt of 41.525 degrees – full spectral coverage for each spectrum is obtained for these bands.

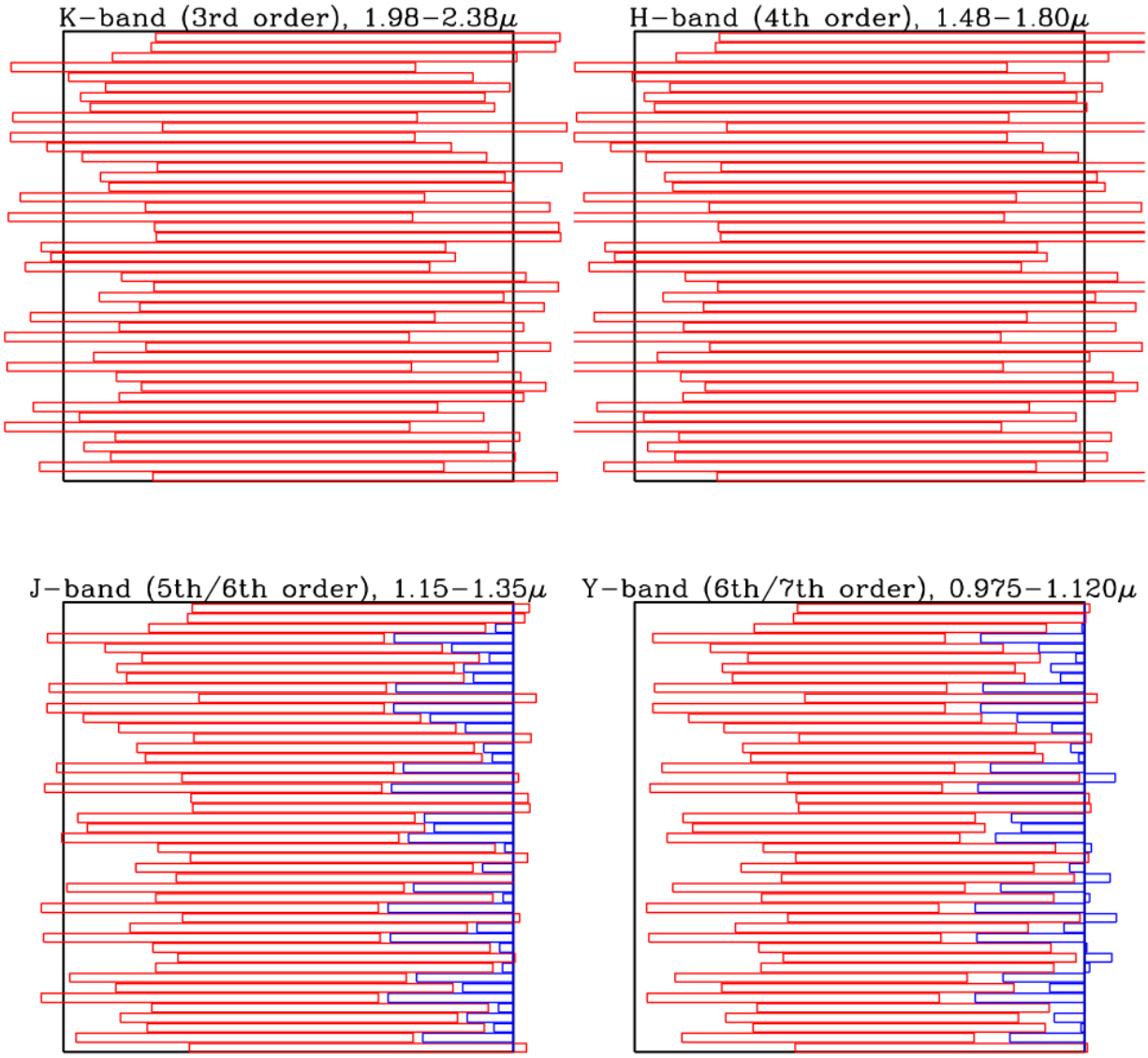


**Figure 1: Spectral Format, 46 Randomly Generated Slits Deployed over 6.12' x 3'**
In this figure, the slit positions were identical for all 4 bands but the secondary grating tilt was used for Y, J spectra.

Ray tracing of the end-to-end telescope plus MOSFIRE optical design has shown that slits placed *anywhere* within the MOSFIRE imaging field maintain very good spectroscopic image quality. This flexibility, together with two alternative grating tilts, allows one to ensure that a particular wavelength is recorded for every slit, or to obtain spectra of objects distributed over a larger field at the expense of uniform spectral coverage. Some example configurations are shown in Figure 2.

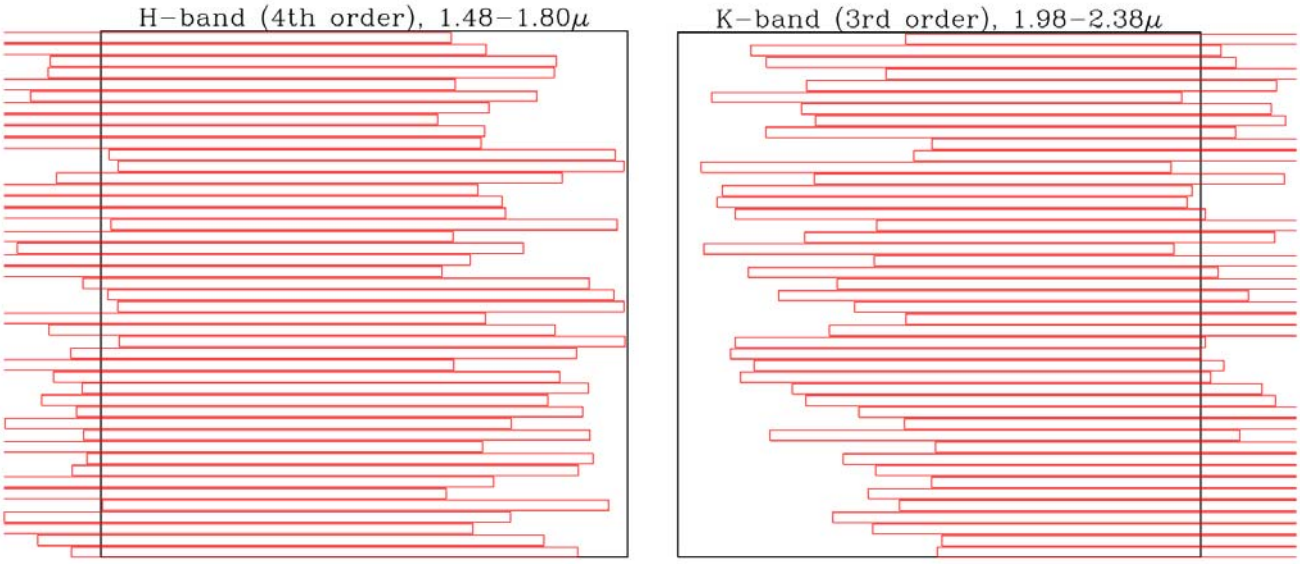


**Figure 2: Examples of Flexibility in Spectroscopic Configurations**
The left panel of the figure shows H-band spectra for a 6.12' by 3.0' portion of the field, but shifted -1.5' from being "centered" on the MOSFIRE field. The right panel shows K-band spectra using a 6.12' by 4' portion of the field, but the "secondary" grating tilt (e.g., supposing that features at 2.0 μm are important for every target).

### 3.2.3 Configurable Slit Unit

While the principal reason for adopting a configurable slit unit (CSU) instead of machined or laser-cut focal plane slit masks is to avoid design and operational issues that would be very costly in the long term, and would require frequent cryogenic cycling of a separate fore-dewar in order to install and remove focal plane masks, there are also scientific advantages to configuring the masks remotely. It will be possible for users to reconfigure masks in real-time to adjust to changing conditions (e.g. narrowing or widening of slits as seeing conditions change) or to allow for immediate reaction to discoveries or required changes in strategy in the course of executing an observing program. Flexibility is particularly important at WMKO, which is likely to remain classically scheduled into the foreseeable future. Optimal use of observing time and the pursuit of higher risk or experimental programs will benefit significantly from a CSU. The CSU allows for deployment of slits over the full imaging field of view of the instrument (6.8' diameter field projected onto a 6.14' square detector as shown in Figure 3).

The disadvantages of a CSU, compared to disposable focal plane masks, are that it will not be possible to use "tilted" slits (where the angle of each slit is different to follow the major axis of targets), or to place more than 1 slit on the same row (for higher multiplexing at the expense of spectral coverage). The former is unlikely to be used much for near-IR work because nodding along the slit is likely to be required for accurate sky subtraction. The proposed CSU will have a bar pitch of 5.8 mm and this allows an acceptable slit length of 7.3" in the Keck f/15 focal plane

and provides for up to 46 slits within the MOSFIRE field of view. In assigning slits to targets of very high surface density (> 5 arcmin$^{-2}$), it should be possible to assign every slit to an object and still allow for small telescope nods along the slits for improving background subtraction. For significantly lower target surface density, a smaller number of objects will be accommodated, and adjacent slits can be combined to form a longer slit with no dead regions in between, so that multiple (continuous) slits of arbitrary length can be constructed in ~8" intervals. Example CSU configurations are discussed below in the context of scientific use cases. It should be noted that with the same telescope position and PA, only about 10% fewer objects are observed than in the (more conventional) case where slits could have arbitrary length with a minimum of 7.3"; in other words, the fixed format of the CSU bars makes only a small compromise in terms of the efficiency of observing targets. For targets with lower surface density on the sky, the "quantized" nature of the slit lengths will have a still less important effect on efficiency.

A significant concern for the most efficient use of MOSFIRE in multi-object spectroscopy mode is the time required to re-configure it from one mask setup to another, or from imaging mode to spectroscopic mode. We now have a good understanding of the reconfiguration times, summarized in Table 2 (see MSDN63 for details). The CSU currently meets the requirement of < 5 minute reconfiguration time for any change of configuration within a 6.12' by 3' field when operated at its nominal 1Hz speed.

| **Configuration Description** | **Configuration Time (range)** |
|---|---|
| 6.12' x 3' field multi-slit ⇒ 6.12' x 3' multi-slit | 254 to 274 s (4.23 to 4.56 minutes) |
| Imaging ⇒ random full-field multi-slit | 178 to 192 s (2.97 to 3.20 minutes) |
| Re-deploy alignment boxes ⇒ slits | 34 to 146 s (0.57 to 2.43 minutes) |
| Close down alignment boxes onto same object | 8 s (0.13 minutes) |
| 6.12' x 3' field ⇒ 2' centered long slit | 118 to 128 s (1.98 to 2.07 minutes) |
| Full-field multi-slit ⇒ full-field multi-slit | 324 to 406 s (5.40 to 6.77 minutes) |

**Table 2: CSU Re-configuration Times for Nominal 1 Hz Operation**

In principle, it is possible to improve these times by moving opposing bars (i.e., those forming the same slit) in coarse mode simultaneously, or by running the CSU at 1.5Hz rather than the nominal 1Hz. The feasibility (and cost) of either of these possibilities is still under study. At present, the most typical reconfigurations of the CSU can be made in about 4.5 minutes or less. Most such re-configurations can be started while the telescope and rotator are slewing to a new position and coarse alignment using the guider is being accomplished.

An essential aspect of the MOSFIRE design has been to insure that the CSU bars remain at or below 130 K so that they do not contribute significant thermal background for longer wavelength observations. As the masking bars have significant mass in order to maintain accuracy in all possible gravity orientations, the radiation load on the bars must be kept small enough to allow them to maintain both low and uniform temperatures during the course of a night. Detailed thermal analysis of the instrument has resulted in a front baffle design that achieves these objectives (see section 5.2).

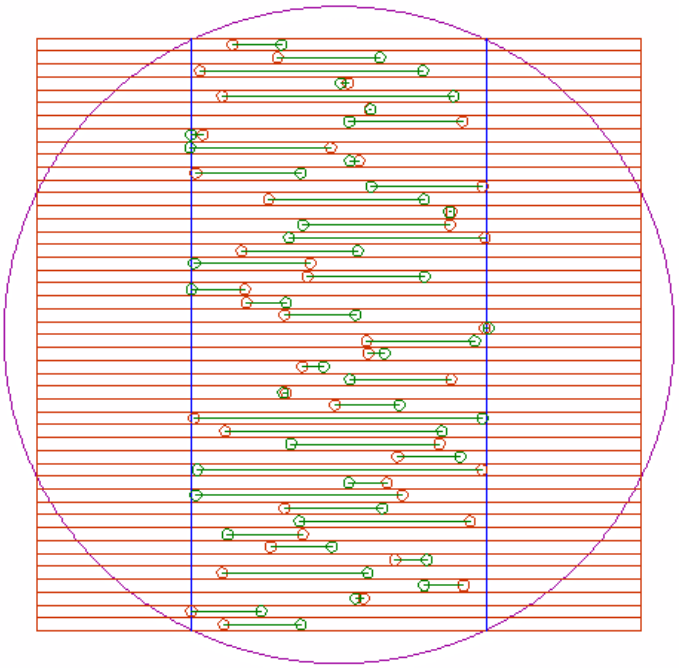

**Figure 3: Schematic Illustration of a Typical CSU Re-configuration**
The green line segments depict the movement of each bar-pair in the focal plane. The rectangular region illustrated is 6.12' by 3'on the sky, while the full available field for slit deployment is represented by the region inside the 6.8' diameter circle and within the 6.12' square for the detector.

### 3.2.4 Spectrograph Stability

MOSFIRE will be background-limited in all of its modes of operation, and thus the spectral sensitivity is ultimately limited by the intensity of the background and by the precision with which the background can be subtracted. With the exception of the long wavelength end of the K-band window, the background is dominated by atmospheric OH emission. Unless the spectrograph is very stable over time, spectral regions in the vicinity of bright OH lines will be rendered unusable by systematic errors in sky subtraction. Our goal for residual flexure *after* correction is 0.1 pixel (<3% of a spectral resolution element) with the maximum acceptable value <0.3 pixel (~10% of a typical spectral resolution element). This requirement, together with the spectral resolution requirements above, is chosen to maximize the sensitivity and useful spectral regions by getting between OH lines and then insuring that sky subtraction residuals will be minimized in regions close to OH lines. The viability of controlling instrument flexure at this level using an open-loop scheme has been demonstrated already in ESI, another Keck instrument (Kibrick et al. 2000, 2003). This desired level of stability is also necessary to allow for efficient acquisition of multi-slit or long slit spectroscopic targets, and for the use of calibrations (e.g., flat fields, arc lamps) that may be obtained during the afternoon rather than during the night.

### 3.2.5 Acquisition and Guiding

External CCD-based guiders have been used successfully on most of the Keck instruments, including the near-IR instruments NIRC and NIRSPEC. Placing a fixed guider outside of the MOSFIRE cryostat, viewing a separate portion of the f/15 focal surface, was another up-front decision made to avoid the cost and complexity of internal guiders. Based on experience with NIRSPEC, suitable optical guide stars can be found even at the Galactic poles during full moon if

the guider field is ≥7 arcminutes$^2$ (S.B. Larsen 1996). As designed, the MOSFIRE guider has a field of view of 2.8' square (for an area of 7.8 arcmin$^2$), centered 6.6' from the center of the MOSFIRE (and telescope) optical axis. The guider uses a fixed filter making it sensitive to light with an effective wavelength of 850 nm (~I band), thus minimizing the effects of moonlight and of differential refraction between the guider and science wavelengths

It is conceivable that guide stars will be scarce in the most heavily obscured regions of the Galaxy; here it is anticipated that the flexibility to rotate the position angle of the spectrograph (providing access to an annulus several times larger in sky area for potential guide stars) will allow optical (I band) guiding even in the most extreme regions. Field acquisition will be done using the guider for coarse alignment, requiring that the guider coordinate system and its relation to the near-IR focal plane be known to better than a few tenths of an arc second. The use of the guider during coarse alignment is described in detail in MGDN01 and MSDN03.

### 3.2.6 Detector & Sensitivity

The MOSFIRE optical design is predicated on the 18 μm pitch of the Teledyne (formerly Rockwell Scientific) Hawaii 2-RG detector. The demonstrated superior performance of the H2-RG in terms of charge persistence and dark current relative to the earlier generation of Hawaii devices makes it a far better choice in an instrument that depends on being background limited and as free as possible from sky subtraction artifacts. High quantum efficiency (QE >65%) will be required to achieve our instrument throughput goals. Because of the long lead time associated with the procurement of these detectors, we have submitted a purchase order to Teledyne that includes an engineering grade detector (to be delivered immediately) and the option to choose from among 3 science grade detectors.

The detection rate for sky in between OH lines in the darkest parts of the Y, J, and H bands (for even the most optimistic estimates) is 0.3 $e^-$/s/pixel for a 0.7" slit assuming ~3 pixel sampling in the dispersion direction (R = 3,270). A dark current of <0.03 $e^-$/s/pixel and an effective read noise below ~5$e^-$ would easily result in background-limited performance for most exposures; typical spectroscopic integrations are expected to be in the range 600 to 1800s, but much shorter exposures would be possible without paying a significant detector noise penalty. Test results provided by Teledyne suggest that charge persistence is not a serious problem with the H2-RG devices; the absence of persistence is crucial for an instrument used both as an imager and a spectrometer. The goals for total throughput of MOSFIRE from the slitmask to the detector have been set to match that of the best single-slit near-IR spectrometers (e.g., NIRSPEC). Table 3 and Table 4 summarize the estimated throughput of MOSFIRE, showing that the goal is achievable as long as good AR coatings (<1.5% average reflection losses per surface) can be obtained for the optics. It is clear that the AR coatings may represent the single largest risk to overall performance.

Table 4 summarizes the estimated sensitivity of MOSFIRE using conservative estimates of the night sky background between OH emission lines (for spectroscopy) and broadband for imaging.

| Component | Transmission/Reflectance | | |
|---|---|---|---|
| | 1.0μm | 1.6μm | 2.2μm |
| Dewar Window (double) | 0.95 | 0.95 | 0.95 |
| Collimator (6 x 2 surfaces) | 0.84 | 0.84 | 0.84 |
| Fold flat (protected Ag) | 0.99 | 0.99 | 0.99 |
| Camera (7 x 2 surfaces) | 0.84 | 0.84 | 0.84 |
| Internal transmission of all glasses | 0.94 | 0.92 | 0.77 |
| Filter | 0.90 | 0.90 | 0.90 |
| Detector (Hawaii2-RG) | 0.80 | 0.80 | 0.80 |
| Lyot stop (pupil vignetting) | 1.00 | 1.00 | 0.90 |
| **Net Imaging Throughput** | **0.45** | **0.44** | **0.33** |
| Grating (on blaze) | 0.65 | 0.75 | 0.83 |
| **Net Spectroscopy Throughput** | **0.29** | **0.33** | **0.27** |

Notes to table: Average reflection loss is 2.4% per surface for ZnSe and 1.2% per surface for all others. The grating efficiency is as built for replicas of the similarly-specified GNIRS grating (order 6, 4, 3 for the 3 entries).

**Table 3: MOSFIRE Throughput Estimate**

| Passband | Spec. Sky Brightness, mag arc $sec^{-2}$ Vega (AB) | Vega (AB) mag for S/N=10 in 1000 s, R=3270 with 0.7" slit | Line flux for S/N=10 (unresolved line) in 1000s, R=3270 ( erg $s^{-1}$ $cm^{-2}$) | Imaging sky brightness, mag arc $sec^{-2}$ Vega (AB) | Vega (AB) mag for S/N=10 in 1000s, broadband |
|---|---|---|---|---|---|
| Y (0.97 to 1.13μm) | 17.3 (17.9) | 20.9 (21.5) | $0.9 \times 10^{-17}$ | 16.3 (16.9) | 24.4 (25.0) |
| J (1.15 to 1.35μm) | 16.8 (17.7) | 20.4 (21.3) | $0.8 \times 10^{-17}$ | 15.7 (16.6) | 23.7 (24.6) |
| H (1.48 to 1.80μm) | 16.6 (18.0) | 20.1 (21.5) | $0.5 \times 10^{-17}$ | 13.4 (14.7) | 22.5 (23.9) |
| K (1.95 to 2.40μm) | 14.4 (16.3) | 18.6 (20.5) | $0.9 \times 10^{-17}$ | 13.2 (15.0) | 21.7 (23.6) |

Notes: spectroscopic limits assume 0.05 $e^-$/s dark current and effective read noise of 4$e^-$/pixel, with background for spectral regions between OH lines, evaluated over a 3 pixel resolution element and assuming a 0.5 $arcsec^2$ extraction aperture. Imaging limits assume 3 x 3 pixel (0.54") aperture for a point source under good seeing conditions.

**Table 4: Predicted MOSFIRE Spectroscopic and Imaging Performance**

### 3.2.7 Filter Complement

Given our design choice to use a single reflection grating in multiple orders, order sorting filters are essential to the MOSFIRE design. The minimum filter complement would be passbands designed for spectroscopy in 3rd, 4th, 5th, and 6th orders of the grating, corresponding closely to the photometric K, H, J, and Y passbands. The MOSFIRE filter wheels accommodate a total of 10 filters in two wheels (each carrying 5 filters and an "open"). A $K_s$ filter for imaging will also be installed. More specialized intermediate-band filters for the additional 5 filter slots may be provided using external funds, and are TBD. The filters being delivered as part of the MOSFIRE project are summarized in Figure 4 and Table 5.

| Filter | Cut-on/Cut-off (μm) |
|---|---|
| Yspec | 0.975/1.120 |
| Jspec | 1.150/1.350 |
| Hspec | 1.460/1.810 |
| Kspec | 1.930/2.400 |
| Ks | 1.990/2.310 |

**Table 5: MOSFIRE filters and bandpasses**

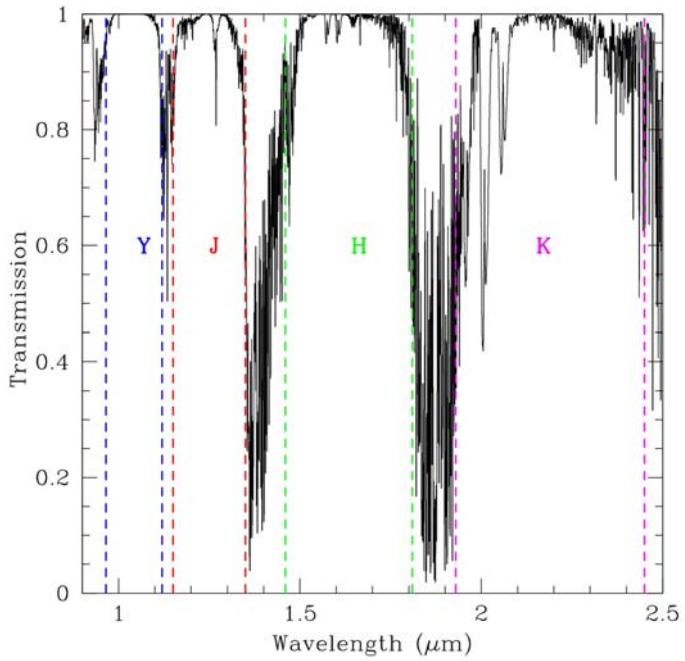


**Figure 4: MOSFIRE Spectroscopic (order sorting) Filter Passbands**
The MOSFIRE filter passbands are shown relative to the near-IR atmospheric transmission on Mauna Kea.

### 3.2.8 Lyot Stop

Because MOSFIRE has been designed to achieve background-limited performance across its entire wavelength range, and as much of the science case for MOSFIRE depends on sensitivity, the design accommodates a two-position Lyot stop. The stop will circumscribe the pupil for shorter near-IR wavelengths to minimize vignetting and maximize throughput, but it will be stopped down to the shape of the pupil image, and track the rotation of the pupil, for longer wavelengths where stray thermal radiation would significantly increase the background (primarily for K-band observations). Detailed design of this mechanism is described in MMDN23; it is based on a successful design used previously for the NIRC2 instrument at WMKO.

### 3.2.9 Calibration Plans

This section describes how MOSFIRE's various science modes will be calibrated, and the planned facilities for obtaining the necessary calibration data. Note that the DDR version of MOSFIRE includes plans for line lamps (separately controlled Ne and Ar arc lamps, located just behind the dust cover/hatch in the forward region of the "snout" at the front of the instrument). The rationale for the change is to provide wavelength calibration data without having access to the night sky, and for calibration of very short exposures (e.g. calibration stars) which otherwise would not have enough OH lines for adequate sampling of the wavelength solutions. The Ne and Ar lamps will be controlled via the MOSFIRE control GUI, and will be used primarily during the afternoon calibrations described below. Illumination of the front of MOSFIRE (with no attempt to reproduce the beam of the telescope, which is impractical for the wide field of the instrument) with the arc lamps will require having the dust cover closed. A similar system for calibration lamps is used on ESI, LRIS, and DEIMOS, the 3 optical wide-field spectrometers at WMKO.

Spectroscopic flat fields will be obtained by projector-lamp illumination of the inside of the Keck I dome. As with current spectroscopic dome flats for optical instruments at WMKO, the telescope is pointed at an elevation of 45 degrees toward the illuminated part of the dome, and the lamps are turned on (remotely) by either the user or summit personnel. WMKO personnel are still experimenting with lamps and projector combinations that will provide adequate illumination out to 2.4 μm, but we do not anticipate that there are any significant problems to be encountered.

Dark calibrations will be obtained by placing the two MOSFIRE filter wheels into a configuration that blocks all light from reaching the detector (effectively, a "cold plug" at 120K). Normally the dust cover would also be closed for dark calibrations

#### 3.2.9.1 Afternoon Calibrations

In the afternoon prior to the night's observing the user will cycle through the (science) mask configurations to be used during the upcoming night, and determine the necessary calibration data required for reduction. Most users will want to obtain direct images of the "acquisition" versions of each science mask (with alignment star boxes) that can be analyzed to measure the expected positions of the boxes on the detector for use during fine acquisition (similar to the practice with DEIMOS or LRIS currently). The "science" versions of the same masks would then be configured

on the CSU and the order-sorting filter and the grating inserted into the beam to replace the imaging mirror. The spectroscopic calibrations will include line lamps (Ne+Ar) that will provide wavelength information for each slit, and spectroscopic (dome) flat fields. The spectroscopic flat fields will be obtained off the interior of the dome, illuminated with a projector lamp. The MOSFIRE FCS will be activated during these calibrations, so that the illumination of the detector will be within a fraction of a pixel of the night-time observations. For users intending to obtain long-slit observations in addition to multi-slit, the same type of calibrations (arcs and flat fields) would be taken with the default MOSFIRE long slit mask configuration (or a custom user-designed long-slit configuration). It should be possible to cycle through all anticipated mask configurations in ~1 hour or less in the late afternoon of an upcoming night. Once the desired exposure levels are determined, it should be possible to script a set of afternoon calibration observations to run automatically. Additional calibrations may be obtained after a night's observing when the dome has been closed for morning twilight.

#### 3.2.9.2 Night-time Calibrations

The near-IR night sky naturally contains a large number of sharp, strong emission features that can provide excellent reference for obtaining accurate wavelength solutions. It is anticipated that many MOSFIRE users will take arc lamp spectra in the afternoon for initial wavelength solutions, and then use night sky features to correct for small amounts of residual flexure or differences due to non-uniform pupil illumination in the arc lamp flats. No special observations will be necessary to obtain the OH line observations, although for very short spectroscopic integrations, only a few lines may be bright enough to measure accurately in some spectral regions.

The most common night-time calibration will be observations of standard stars that will serve as references for radial velocity or velocity dispersion measurements, correction of telluric absorption features, or flux calibration. Most such observations would be efficiently carried out using a long single slit, which for the present purposes we assume will be the default MOSFIRE long-slit configuration consisting of a continuous slit of 2′ in length (15 masking bars) at the center of the MOSFIRE field. The method for acquiring a star onto the slit is described in MSDN03. The care with which observations of standard stars must be carried out will depend on the application. For telluric corrections of high S/N spectra, where a precise match of the line spread function and the pixel sampling would be desirable, the star should be observed at many positions along the slit, which would allow for a spectrally over-sampled spectrum of the star to be produced (via a technique akin to the modeling of the background using b-splines – see MSDN23). This spectrum can then be sampled in precisely the same way as the spectrum of each object on a multi-slit mask before dividing out telluric features. This approach would minimize the effects of finite spectral sampling of line profiles with typical slit widths. What is required for success of this technique is a stable line spread function over the MOSFIRE field (the spectroscopic images are pixel sampling limited over the full field and the control over the slit width on the CSU is very precise), adequate flat fielding, and very good 2-D wavelength solutions for every slit and the standard star observation. Undoubtedly some experimentation with real data will be necessary to optimize the techniques; further development will occur during commissioning. In any case, there is a great deal of inherent flexibility in how calibrations may be obtained using MOSFIRE—the main question is

how efficiently they may be obtained. Obviously, the goal is to minimize night-time calibration overhead while still obtaining adequate quality calibration.

For faint object programs (where continuum S/N will be low), it will be less important to correct for telluric features in the object continuum; however, typically a standard star will be observed after completion of a target field (or at the start or end of a night's observing) to allow for flux calibration and/or telluric correction of objects that are detected in the continuum. Of greater concern in these cases might be the ability to flux-calibrate many slits using a single observation of a star. Because the long-slit spectrum will include the entire spectral range of a given band, there will be sufficient spectral coverage to match that of a slit anywhere in the MOSFIRE field of view.

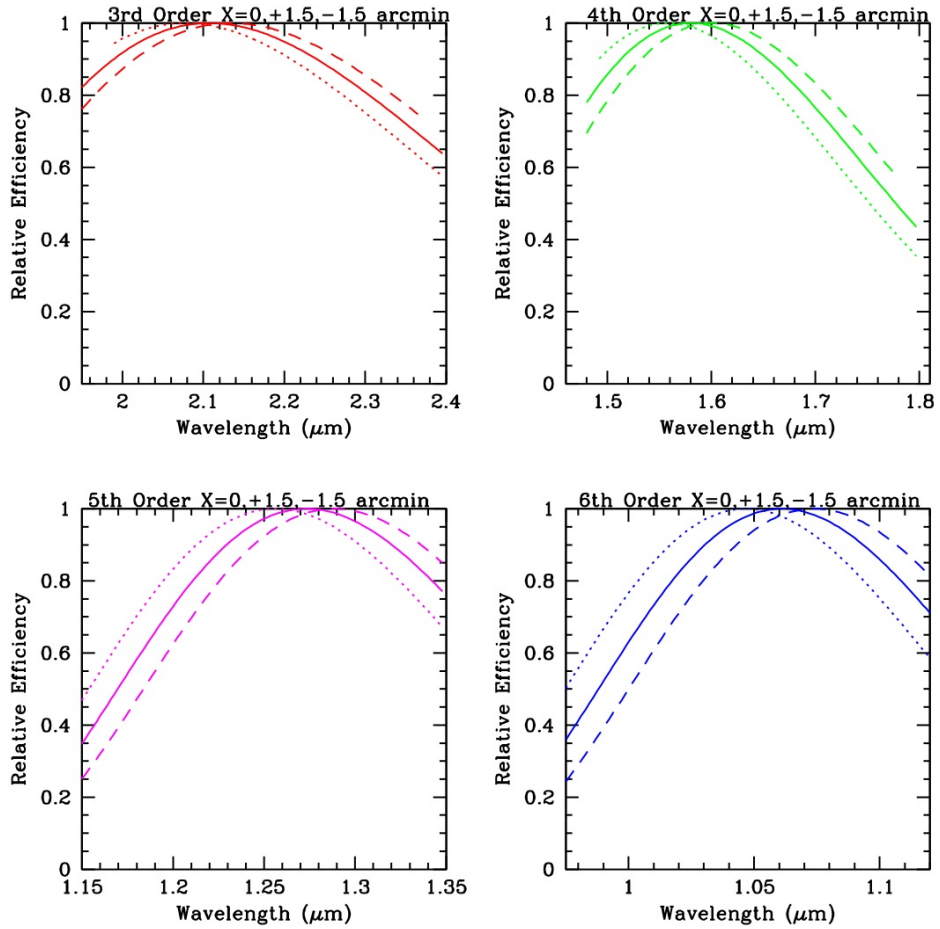


**Figure 5: Expected Blaze Functions and Blaze Shifts vs. Field Position for MOSFIRE.**
The dotted and dashed curves represent slits displaced by +1.5′ and -1.5′ from field center.

However, small effective blaze shifts as a function of field position are inevitable. Such variations can be calculated analytically (see Figure 5) or they can be empirically calibrated (using stellar spectra or simply the night sky spectra as a function of field position). Experience with this issue on other imaging spectrographs suggests that applying a single calibration curve to all slits will generally be adequate for most applications.

#### 3.2.9.3 Astrometric Calibrations of MOSFIRE

Optimal use of MOSFIRE will require tying together accurate plate solutions for the guider, the telescope focal surface (i.e., the CSU coordinates), and the detector. The mapping of RA and Dec onto the guider field and the telescope focal plane can be predicted using the Zemax models of the optics. Distortions from the telescope optics at the CSU plane are predicted to be smaller than 0.02% (1 part in 5000, or <0.08" over the 6.8' diameter MOSFIRE field), so that once the plate scale calibration is checked with on-sky observations, there will be a very simple relationship between RA/Dec and mm on the CSU (the prediction is a plate scale of 0.72515 mm/"). Knowing this will allow any external astrometry to be used to design MOSFIRE slit masks, without the need for "pre-imaging" through MOSFIRE itself.

Coarse acquisition of slit mask fields will require knowledge of the mapping between the guider field and the MOSFIRE CSU field. As designed, there is an offset of 6.60' between the center of the guider field and the center of the MOSFIRE field. The guider field is predicted to have a plate scale of 0.164"/pixel with ~1% distortion at the corners of the field. The plate solution of the guider, and the offset with respect to the MOSFIRE field, will be verified and calibrated during commissioning.

Mapping of the telescope/CSU focal surface onto the detector in imaging mode will be required for accurately predicting the location at the detector of alignment boxes used for fine acquisition. The predicted plate scale at the MOSFIRE detector for the pre-construction optical design is 99.951 microns/", or 0.1801"/pixel, with 0.2403% pincushion distortion at the extrema of the field (this includes the telescope and MOSFIRE optics). Again, the precise as-built plate solution for MOSFIRE will be calibrated during commissioning (the solution for the mapping of the CSU plane to the detector can be established in the lab during integration) and will be incorporated into the DRP and MASCGEN/MSCGUI. Once established, it will be possible to embed a world coordinate system into the header of any MOSFIRE image, making it straightforward to produce astrometrically correct images for mosaics, or for designing slit masks using MOSFIRE images.

### 3.3 Specifications

Table 1 above defined the basic, first level requirements for MOSFIRE. Several additional parameters flow down from the science requirements and these are summarized in Table 6. The optical design is achromatic but focus adjustment is desirable during initial integration and testing. Space for additional filters is an important consideration if it does not otherwise compromise the design. Two grating positions give the optimum arrangement for the four spectral regions covered by MOSFIRE and this option can be achieved without compromising repeatability. A means for compensating for flexure is important and the instrument must have a guide camera and a calibration unit.

| Parameter | Requirement (or Goal) |
|---|---|
| Optical focus | Achromatic (focus adjustment if possible) |
| Collimated beam size | 125 mm (derived from requirement on R) |
| Pupil image | Accessible for Lyot stop & mechanism |
| Filters | Diameter 170 mm, min of 5, max of 10 filters. |
| Guider | 1024 x 1024 CCD with 0.164" pixels, externally mounted, warm optics; co-mount with arc lamps |
| Window | No condensation, provide dust cover |
| CSU | Multiple requirements, see CSEM compliance Matrix |
| Vacuum enclosure (dewar) | Fits with Keck I Cassegrain volume & weight constraints |
| Flexure | ~3.0 (1.5 goal) pixel shift (uncorrected) over 2 hours |
| Flexure compensation | 10:1 reduction by look-up table & tip/tilt mechanism |
| Imaging/Spectroscopy mode change | Turret mechanism, fixed grating & mirror, reproducible to 0.1 pixel; 2 grating stop positions |
| Operating temperatures | 120 K; detector at 77 K nominal |
| Cool down time | 7 to 10 days, closed-cycle refrigeration |
| Detector dark current | < 0.03 $e^-$/s/pixel |
| Detector read noise | ~ 5 $e^-$ rms (with multiple reads) |
| Software | Support easy set up of CSU, support flexure correction look-up tables |

**Table 6: Additional or Derived MOSFIRE Parameters Used for the System Design**

## 3.4 Scientific Use of MOSFIRE: Example Cases

In order to illustrate how MOSFIRE would be used for actual observing programs at the telescope, in the following sections we outline two specific "use cases" intended to be representative. For these cases we describe the programs, including the planning of the observations, obtaining the data at the telescope, and obtaining relevant calibration data. More general procedural information on the use of MOSFIRE can be found in section 5.6 under software (and in MSDN03), while technical details on mask design and mask configuration files can be found in MSDN16, MSDN17 and MSDN18, as well as in the software section 5.4.3.2.16.1. Further information on MSALIGN, the on-sky mask alignment software, can be found in MSDN64.

### 3.4.1 Extragalactic Case

The science case chosen as an example is a spectroscopic survey of high redshift galaxies in the redshift range $2.0<z<2.6$. The objective is to measure precise redshifts, star formation rates, chemical abundances, and kinematics for galaxies in this redshift range in a particular survey field. In the targeted redshift range, star forming galaxies and AGN will have the Hα transition redshifted into the K-band atmospheric window. Hα fluxes provide a robust estimate of the galaxy star formation rate; even for relatively dust-obscured galaxies (e.g. Erb et al. 2006, ApJ 647,128), the Hα surface brightness provides an estimate of the cold gas available for star formation (Erb et al. 2006, ApJ, 646, 107), and the Hα line widths provide dynamical mass estimates. The ratio [NII]/Hα is a simple but powerful measure of chemical enrichment, which can be enhanced with

measures of the ratio [OIII]/Hβ, accessible in the H-band atmospheric window over the targeted redshift range (see Table 7).

The typical Hα flux for star forming galaxies at these redshifts is ~$10^{-17}$ ergs $s^{-1}$ $cm^{-2}$, corresponding to a star-formation rate of a few solar masses per year. Galaxies suitable for spectroscopy can be easily selected using photometric criteria in deep optical and/or near-IR images (see, e.g., Steidel et al. 2004, ApJ, 604, 534), and to an optical apparent magnitude of R=25.5, the surface density of targets in the z=2-2.6 range is ~6 $arcmin^{-2}$.

| Redshift | 3650 A | 4000Å Break | [OIII] 5007 | Hα |
|---|---|---|---|---|
| 2.0 | 1.095 μm | 1.200 μm | 1.502 μm | 1.969 μm |
| 2.3 | 1.204 μm | 1.320 μm | 1.652 μm | 2.166 μm |
| 2.6 | 1.314 μm | 1.440 μm | 1.803 μm | 2.363 μm |

**Table 7: Transition Wavelengths**

MOSFIRE itself will be the instrument of choice for obtaining the necessary very deep near-IR images necessary to detect the same galaxies in the continuum, which range from K~19-23 and have J-K~1-3 depending on star formation history. Integrations of 1-2 hours in K, and 2-3 hours in J, will provide good photometric measurements for even the faintest objects being targeted. The spectroscopic observations are planned to detect Hα with S/N > 25 so that [NII]/Hα as low as 0.1 can be measured for individual galaxies (currently such ratios can be detected only in composite spectra; see Erb et al. 2006, ApJ, 644, 813). This will require integrations of ~7200s per mask (shorter integrations will be more than adequate to measure redshifts).

High redshift galaxies with no current star formation (i.e., "red and dead" galaxies) are now known to exist at redshifts beyond z~2 but spectroscopy is extremely difficult, and little has been done with single-object near-IR spectrometers because of the very long integration times required. To reach these targets in significant numbers requires continuum spectroscopy of objects to K~20.5 (J~23.0). The strongest spectroscopic features in the rest-frame optical for "passively evolving" galaxies will be found in the Balmer/4000 Å break region, which will be redshifted into the Y/J bands, as summarized in the Table 7. While candidate red galaxies in the targeted redshift range are relatively easily identified using near-IR color criteria (e.g., J-K>2.3; see Franx et al. 2003, ApJ, 587, L79), successful spectroscopy depends on a careful approach. Many red galaxies still have significant lingering star formation, such that emission line spectroscopy (i.e., Hα) remains the most efficient means of measuring their redshifts. Thus, in most cases, it is worth attempting even very red galaxies in the K-band prior to shifting to the Balmer/4000 Å break region for continuum spectroscopy. The surface density of red galaxies to K~21 is ~1 arc $minute^{-2}$, of which ~20% will be without any current star formation based on our current understanding (e.g., Reddy et al. 2006, ApJ, 644, 792). Thus, a typical MOSFIRE footprint will contain ~40 such red galaxies,

but only ~10 of them are likely to be passive. To obtain useful spectra of these objects in the Y or J band will require continuum S/N~10 per resolution element, which can be obtained in 10-hour (36000 s) integrations with MOSFIRE at J~22.5; continuum spectroscopy at K~20 would require ~10000 s of total integration time. Taken together, the near-IR selected galaxies and the optically selected objects account for almost all of the star formation and stellar mass in galaxies during the peak epoch of their formation.

In the rest of this case, we outline details of how such a z~2.5 "spectroscopic census" might be carried out using MOSFIRE. We take as an example the field HS1700+64, a survey field for which deep photometry in the optical passbands U, G, R, the near-IR J and Ks, and Spitzer/IRAC and Spitzer/MIPS 24 μm are available. It is also a field in which a large galaxy over-density at <z> = 2.300 has been identified (Steidel et al. 2005, ApJ, 626, 44) based on optically-selected galaxies, where MOSFIRE will be capable both of obtaining significant new information on the known proto-cluster members, as well as identifying many new members across the whole range of star formation rate and star formation history. In terms of the surface density of candidate galaxies, both near-IR and optically selected, HS1700+64 is otherwise quite typical.

#### 3.4.1.1 Observation Planning

The first step for MOSFIRE slitmask design is to construct a list of targets, with accurate RA, Dec, and relative numerical priority, within the field to be studied. In this case, we confine ourselves to a region on the sky of size 8.5' by 8.5' over which existing deep near-IR data are in hand (obtained using the Palomar 5 m telescope with ~12 hour integrations in each of the J- and Ks- bands). With good external astrometry, there is no reason that the images used for target selection need have been obtained using MOSFIRE or even the Keck telescopes (in this case, they were not). However, the steps would be identical if images taken with MOSFIRE were to be used for slitmask design. Along with the targets of interest, one also needs a list of potential alignment stars with positions measured on the same astrometric system, within the same field of view. In practice, these stars can be the very same stars that have been used for optical multi-object spectroscopy in the same field, which have generally been those with V~19 to 21.

A histogram of the K-band magnitudes of alignment stars in various survey fields is shown in Figure 6. Most of these stars have K<19, and the surface density has already been shown to be adequate to provide several stars per MOSFIRE-sized field based on experience with LRIS, an instrument with a very similar sized footprint on the sky (LRIS is 7.5' by 5', whereas MOSFIRE is ~6.1' by 6.1'). The main criterion for alignment stars is that they are common enough to provide >~5 stars per MOSFIRE footprint, and that they can be significantly detected in the near-IR in short (~30 s) integrations to be used in the fine acquisition of the slitmask field at the telescope.

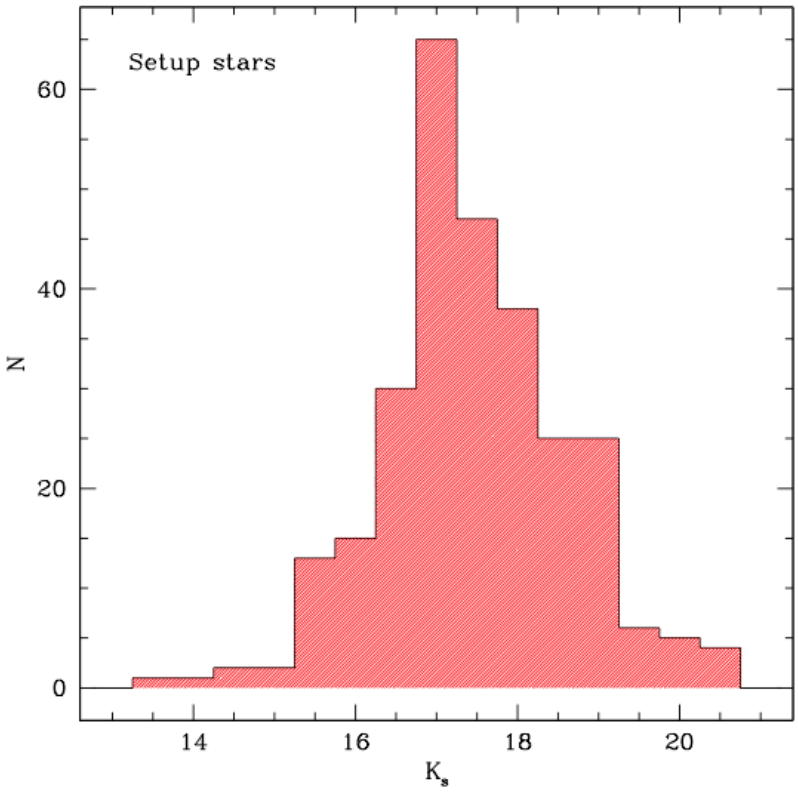


**Figure 6: Magnitude Distribution for Potential Alignment Stars**
assuming a typical high-Galactic-latitude extragalactic survey field.

In typical seeing of 0.5" (FWHM), MOSFIRE will detect stars with K<19 with S/N>25 in 30 s, thus K~19 will be the recommended magnitude limit for useful alignment stars. The bright limit for alignment stars is set by the minimum integration time and the need to be able to centroid the stars accurately. In typical seeing the bright limit is probably near K~11 to 12.

For objects with a very high surface density on the plane of the sky, it would be possible to observe as many as 46 objects with one MOSFIRE configuration. In practice, with a total surface density ~6 arc $min^{-2}$, there will be a total of ~100 to 120 targets per MOSFIRE footprint. However, the discrete nature of the slits (which of course cannot overlap in the Y-direction) and the need to place objects near the centers of the shortest slits (7.3" in length) to allow for nodding, will limit the number of targets that may be accommodated on a single mask.

For the purposes of illustration, we have generated a MOSFIRE slit mask using candidate z~2.5 galaxies in the HS1700+64 field. As input to the MOSFIRE Automatic Slit Configuration Generator (MASCGEN), we have specified in this case to allow slit placement in the inner 4' of the field in the X-direction (i.e., ±2' of the field center).

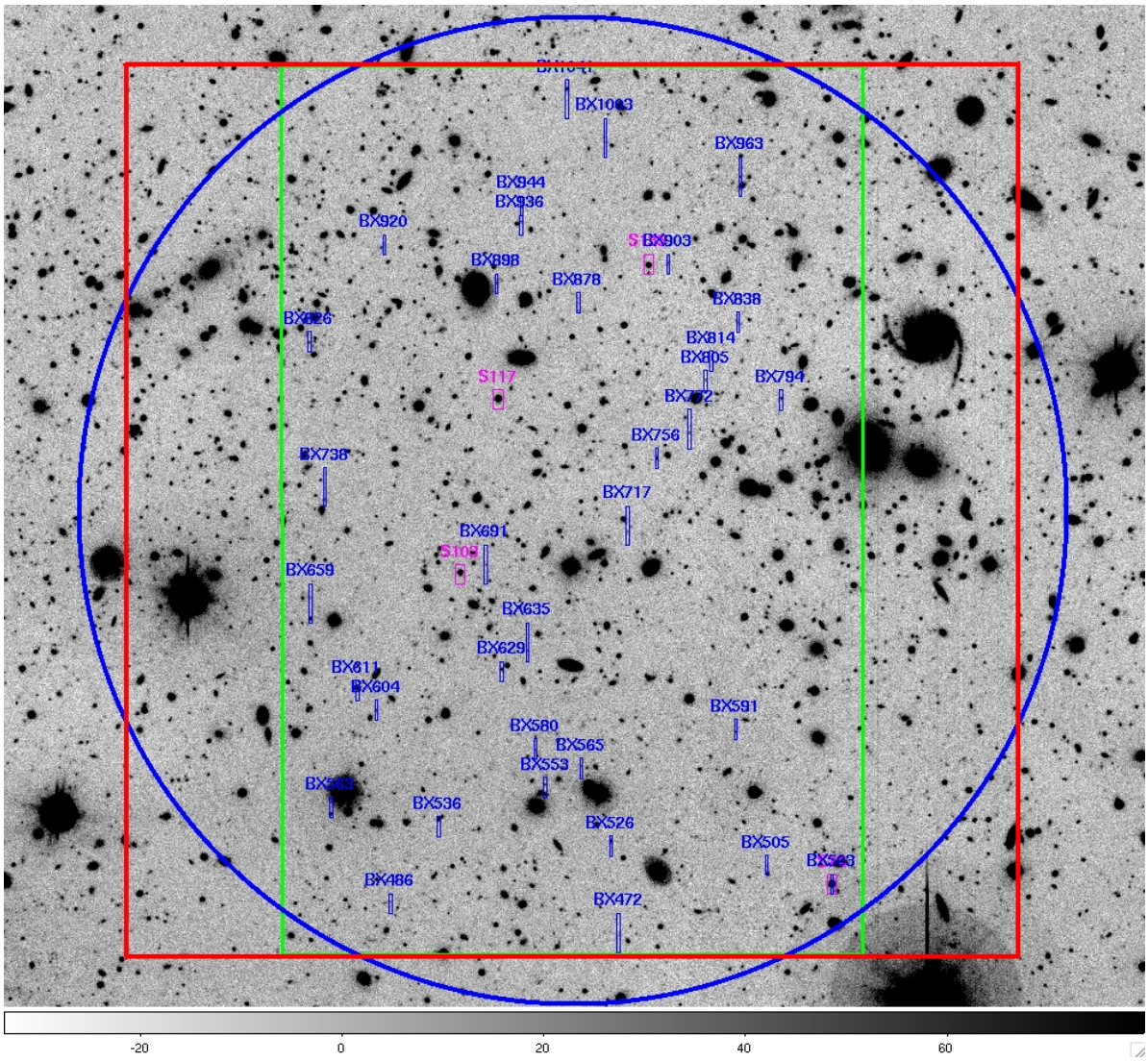


**Figure 7: Mask Layout Using a 6.1' by 4' Portion of the MOSFIRE Field (green rectangle)**
Dark blue slits are either single bar (7.3") or two bars (15.3") in length. Also indicated are four 4.0" by 7.3" alignment boxes for use in mask alignment at the telescope (magenta).

Within the 6.1' by 4' footprint, there are a total of 144 objects in the input list for slit assignment. In addition, there are a total of 20 possible alignment stars. Also as part of the input to MASCGEN/MSCGUI, we have specified that objects must fall > 2" from the edge of any slit, meaning that only the inner ~3.3" of each bar can be used. In some cases, with a fixed MOSFIRE footprint, there is no target that will fall in the swath of sky available to a particular bar. In such a case, a slit comprised of 2 aligned bars can be formed, for which the swath available for objects assignment increases to the central ~11.3" of the new 15.3" slit. Because the targets have been assigned numerical priorities (in this case, based on their distance from the line of sight to a background QSO and apparent R magnitude), high priority targets that fall close to a bar edge may be automatically assigned a longer slit if the sum of the priorities of objects that obey the slit edge distance criteria for the two bars is smaller. Thus, most masks will be comprised of slits of varying

length (in multiples of ~7.5"), resulting in configurations with fewer slits than available masking bars. In the case illustrated here, a total of 36 slits results, of which 10 are 15.3" slits made from two adjacent masking bars each.

Figure 7 shows an image of the field, on which is overlaid the MOSFIRE field with the assigned slits. Figure 8 also shows 4 selected alignment stars with 4" by 7.3" alignment "boxes" drawn on the image. These alignment stars are used for the fine acquisition of the field while at the telescope. It is generally good practice to have these stars distributed over the field of view for the most accurate measurements of small rotational corrections during fine alignment. In addition, the MASCGEN/MSCGUI software produces an image as would be seen in the MOSFIRE guider field for the chosen pointing and position angle, along with the predicted guider pixels on which each star will fall. The guider information is used at the telescope for coarse alignment in order to bypass the need for obtaining a direct image of the field without the mask in place.

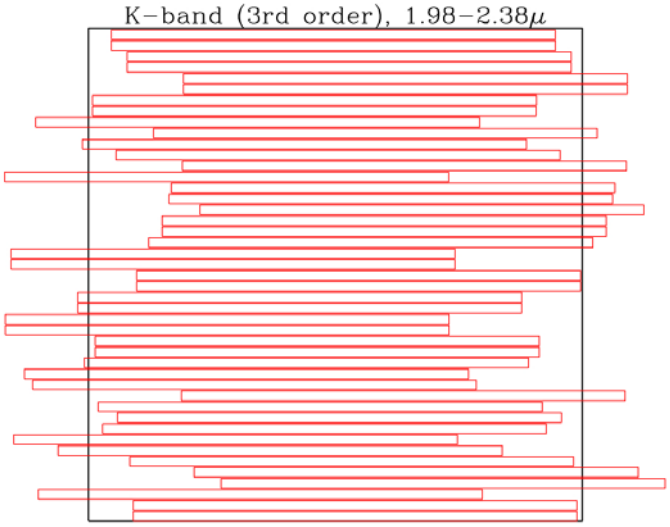


**Figure 8: Positions of K-band Spectra Relative to the Detector for the Slitmask of Figure 7**
Slits formed from two contiguous bars are evident.

As is the case with all multi-object imaging spectrometers, the wavelength coverage of each slit will depend on its placement within the field of view—the narrower the range used for slit assignment in the X field direction, the more likely that all slits will observe the full range in wavelength available in the spectral band. While designing a MOSFIRE mask, the user will be presented with information on the resulting spectral coverage similar to that shown in Figure 8, which shows (schematically) the location of each spectrum with respect to the detector for the mask design in Figure 7. Clearly, the recorded K-band spectrum will be missing some wavelengths for some of the slits, due to the user's choice to allow slits to be placed anywhere within a 6.1' by 4' region. For objects with relatively low surface density, there will always be a trade-off between the number of objects that can be assigned slits and the number of slits that would allow full wavelength coverage.

The same mask design can be used for J-band observations. The default for Y and J band is to use a secondary tilt of the MOSFIRE grating which more closely centers orders 6 and 5 on the detector. Using this tilt, the J band spectral coverage for the same mask design is shown in Figure 9. Clearly, a higher fraction of the slits will record the full J band spectrum, simply because the spectra are shorter than for the K band.

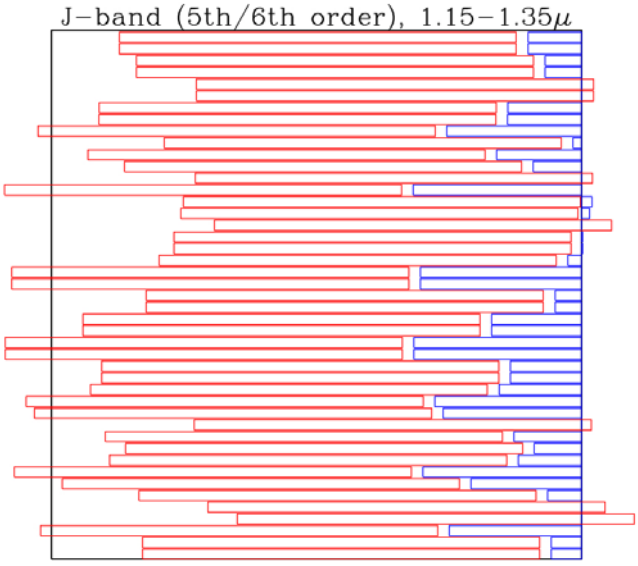


**Figure 9: The Positions of the J-band Spectra for 5th (red) and 6th (blue) Order**
Spectra shown are for the slitmask illustrated in Fig. 7. Note that nearly full J-band spectral coverage is obtained for all of the slits.

### 3.4.1.2 Field Acquisition at the Telescope

As will be the case for MOSFIRE multi-object spectroscopy in general, the first step in acquiring the field will be to begin the instrument reconfiguration (while the telescope is slewing to the field): the CSU begins deployment into the "fine alignment" configuration, which is identical to the "science configuration" except for the bars assigned to the 4 alignment stars (see Figure 7), the imaging mirror is inserted, the filter is changed (if necessary), and the rotator move necessary for the planned PA of the observation is begun. Given the pointing accuracy of Keck I, the telescope operator will normally acquire a bright star on the guider to check the local pointing, after which the telescope is pointed to the nominal center of the MOSFIRE field. The guider image can be used, by comparison with the image produced in the mask design stage, to verify that the field is correct. At this point, the observer asks the telescope operator to place one of the potential guide stars at the pre-determined pixel position on the guider, and guiding is commenced. Once the CSU reconfiguration has completed, the alignment stars should be located within the alignment boxes. The first step for fine acquisition is to obtain a pair of short exposures, both while guiding. The first exposure offsets the telescope by a relatively small amount, and an image is obtained (a typical exposure time would be ~30 seconds), after which the telescope is offset back to the original position and an identical exposure is obtained. The first exposure is used by the alignment software to precisely locate the position of the 4 alignment boxes on the detector, using the CSU

configuration information as an initial guess at the box positions. This exposure is then subtracted from the second alignment exposure (to provide background subtraction), and the precise positions of the 4 alignment stars (in detector coordinates) are measured. The relative positions of the alignment stars and the box edges are then compared to the values expected by the mask configuration information. Using this comparison, MSALIGN (see MSDN64) calculates the combination of the change in rotator angle and telescope offset necessary to place the alignment stars at the desired location within the boxes. After approval by the user, these moves are sent to the telescope (while guiding). Positioning can be re-checked, if desired, by obtaining another image through the mask, and repeating the analysis of the star/box positions. At this point, all targets should be correctly placed in their respective slits and science may begin.

The observer then selects the order-sorting filter desired (if different from that used for acquisition) and deploys the grating (at one of the two angles, depending on order). Meanwhile, the user re-deploys the bars that have been used for alignment stars onto science targets (such as in the case illustrated in Figure 7) or the slits can be closed down onto the alignment stars themselves. Once in place, a sequence of spectroscopic observations can begin.

Most observers will want to use small nods in the slit direction to improve background subtraction. For point sources or faint galaxies, nods of amplitude ~2" will generally suffice. In the present case, we would choose ±1" from the fiducial position, to avoid losing targets off the ends of slits (if larger nods are desired, the user would specify different criteria for object placement within slits at the mask design stage). The user can choose to begin a series of exposures with such a nod pattern using the exposure GUI, or the user can choose to obtain one spectroscopic exposure at a time and perform the slit nods manually. In all bands, spectroscopic observations will be background limited after 60 to 100 s (assuming detector performance of < 0.03 $e^-$/s dark current and effective read noise per pixel of ~5$e^-$), so that the user has a great deal of flexibility in choosing the length of individual exposure times. In this case, we choose 900 s integrations to limit overhead due to nodding, so that the planned K-band integrations of 2 hours would be composed of 8 x 900 s integrations, 4 in each of two nod positions. The fiducial object positions within each slit has been recorded in the header for the slit description extension, so that with the relative nod distance for each integration, the expected object position within each slit is available to the data reduction pipeline (see below).

#### 3.4.1.3 Calibrations

In the afternoon, prior to the night's observing, the user will cycle through the (science) mask configurations to be used during the upcoming night, and determine the necessary calibration data required for reduction. These will include line lamps (Ne+Ar) that will provide wavelength information for each slit, and spectroscopic (dome) flat fields. The spectroscopic flat fields will be obtained off the interior of the dome, illuminated with a projector lamp. The MOSFIRE FCS will be activated during these calibrations, so that the illumination of the detector will be within a fraction of a pixel of the night-time observations.

MOSFIRE programs targeting faint objects like the ones described in this note will generally be most concerned with the quality of the background subtraction, where systematic errors must be

minimized in order to detect targets that are as faint as < 1% of the (inter-line) sky background. Such high quality background subtraction has been demonstrated for NIRSPEC (and other) data in which a combination of standard differencing procedures coupled with two-dimensional "b-spline'' subtraction of residuals is used; this method will be implemented by MOSFIRE's DRP.

Of less concern for faint object programs (where continuum S/N will be low) will be correction of telluric features in the object continuum; however, typically a standard star will be observed after completion of a target field (or at the start or end of a night's observing) to allow for flux calibration and/or telluric correction of objects that are detected in the continuum. The standard star observation would be obtained using the default MOSFIRE long-slit acquisition, in which the central ~14 bars (~2') are deployed to the center of the MOSFIRE field, except for the central bar, which would be opened wider to form a single alignment box. The star would first be placed on the guider at a position that is calibrated relative to the center of the MOSFIRE field, and then the telescope is offset to place the star into the alignment box. A short exposure in imaging mode will allow MSALIGN to calculate the necessary telescope offset to place the target at the center of the alignment box, and to send the move command to the telescope. When the user is happy with the centering, the central bar can be closed down to the same width as the rest of the long slit, and the grating can then be inserted to replace the imaging mirror. The star observations can then be obtained, with standard nodding along the slit.

While the line lamp spectra will be useful for establishing the initial wavelength solutions for each slit, and for allowing observers to check the spectral coverage of each slit during the afternoon, the OH lines in the night sky spectrum will generally be used to obtain precision adjustments to the wavelength solution. These lines will be present in every spectrum, and allow corrections to the wavelength solutions that would be caused by differences in illumination of the slits between the arc lamp calibrations and the night-time observations, and any residual flexure in the instrument between the afternoon and the time of the science exposures. The night sky spectra also provide features that are used to model the background in 2-D by the b-spline routine that is part of the DRP (see MSDN23).

### 3.4.2 Galactic Science Case

The science case chosen as an example of a Galactic program is a spectroscopic survey of low-mass stars and brown dwarfs in nearby star-forming regions. In general, the global objectives are spectral classification and cluster membership identification, with the goal of tracking the initial mass function well into the sub-stellar regime. More specifically, the primary goal of the science program described in this note is the detection of the very lowest mass members of the region by their spectroscopic signatures.

Given the detection of over 200 extra-solar planets by Doppler reflex motion since 1995, one of the most pressing questions in astronomy today is whether or not planets are common occurrences. Studying how, with what frequency, with what masses, and in what environments do brown dwarfs (BDs) and planetary mass objects (PMOs) form may have a critical input to this question. Using both space and ground-based methods, many groups have conducted large area surveys of young star forming regions to find their lowest-mass members. Young clusters have several advantages:

1. A large sample with a similar age is obtained, as the stars are spatially grouped together and tend to be roughly coeval. The ages of field objects are not as well known.
2. Young BDs and PMOs are typically several orders of magnitude brighter when young making it possible to detect much lower-mass objects at greater distances.
3. Young clusters have small physical sizes, lessening contamination by background and foreground objects.

At the ages of typical young cluster (between 1 – 3 Myr) an object cool enough to exhibit methane absorption would be between 1 – 5 $M_{jupiter}$, depending on the model chosen. Such objects are predicted to be between $18^{th}$ – $20^{th}$ magnitude at H for a distance of 150 pc (Burrows et al. 2001, Rev. Mod. Phys., 73, 719; Baraffe et al. 2002, A&A, 382, 563). Large area surveys allow a complete census of the cluster's population down to the lowest mass objects, which in turn allows us to accurately characterize the initial mass function for stars, brown dwarfs, and PMOs. Broadband infrared surveys of such clusters are complicated by the presence of dusty cocoons that surround the young BDs and PMOs. Reddening causes confusion between spectral types in the usual JHK color-color diagram. At UCLA, we developed a new system of narrow band filters in the near infrared that can be used to classify stars and BDs (Mainzer & McLean, 2003, ApJ, 597, 555; Mainzer et al. 2004, ApJ, 604, 832). This set of four filters, spanning the H band, can be used to identify molecular features unique to BDs and PMOs, such as $H_2O$ and $CH_4$. The four filters are centered at 1.495 μm ($H_2O$), 1.595 μm (continuum), 1.66 μm ($CH_4$), and 1.75 μm ($H_2O$). Using two $H_2O$ filters allows us to solve for the reddening to individual objects. The four physical colors can be converted into three reddening-free indices, $\mu_1$, $\mu_2$, and $\mu_3$. This technique, which is equivalent to extremely low resolution spectroscopy, can be used to survey large areas to provide rough spectral classifications for all the objects in the area, ranging from spectral types O to T (as shown in Figure 10).

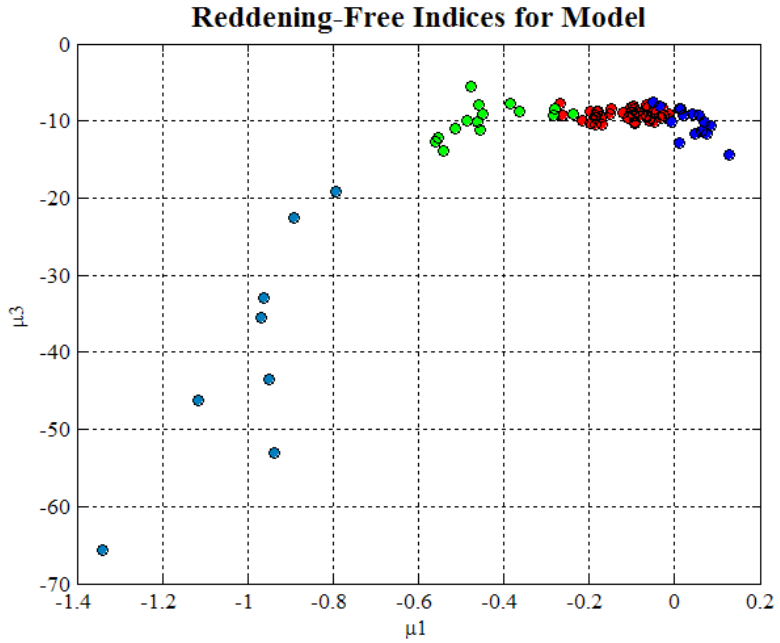


**Figure 10: Reddening-free Indices ($\mu_1$, $\mu_3$) for 85 Different Objects**
Range in spectral type is O to T. Blue = O – K; red = M1 – M9; green = L1 – L8; cyan = T1 – T8.

While smaller telescopes in the 3-5m aperture range can be used for the initial imaging and photometry, what is exceptionally difficult is to confirm the spectral classification by spectroscopy and deduce additional physical properties. With the young, hot Jupiter-mass objects lying in the range from 18 to 20 magnitude for the nearest clusters, only the Keck telescope can obtain spectroscopy, and even then, each faint target will require many hours of integration. Fortunately, many low mass targets will fall within the 6.1' x 6.1' field of MOSFIRE and therefore the opportunity exists to characterize many clusters members at the same time. If narrow band H2O and CH4 filters were available then deep imaging with MOSFIRE could detect PMOs directly.

Star-forming regions range in size and target density, from the sparsely populated Rho Ophiuchus region to the dense Orion Molecular Cloud. For the example shown below we will choose the Orion region (Figure 11). Later, we will develop examples for many other regions.

In the rest of this section we outline how a spectroscopic survey of a star-forming region might be carried out using MOSFIRE.

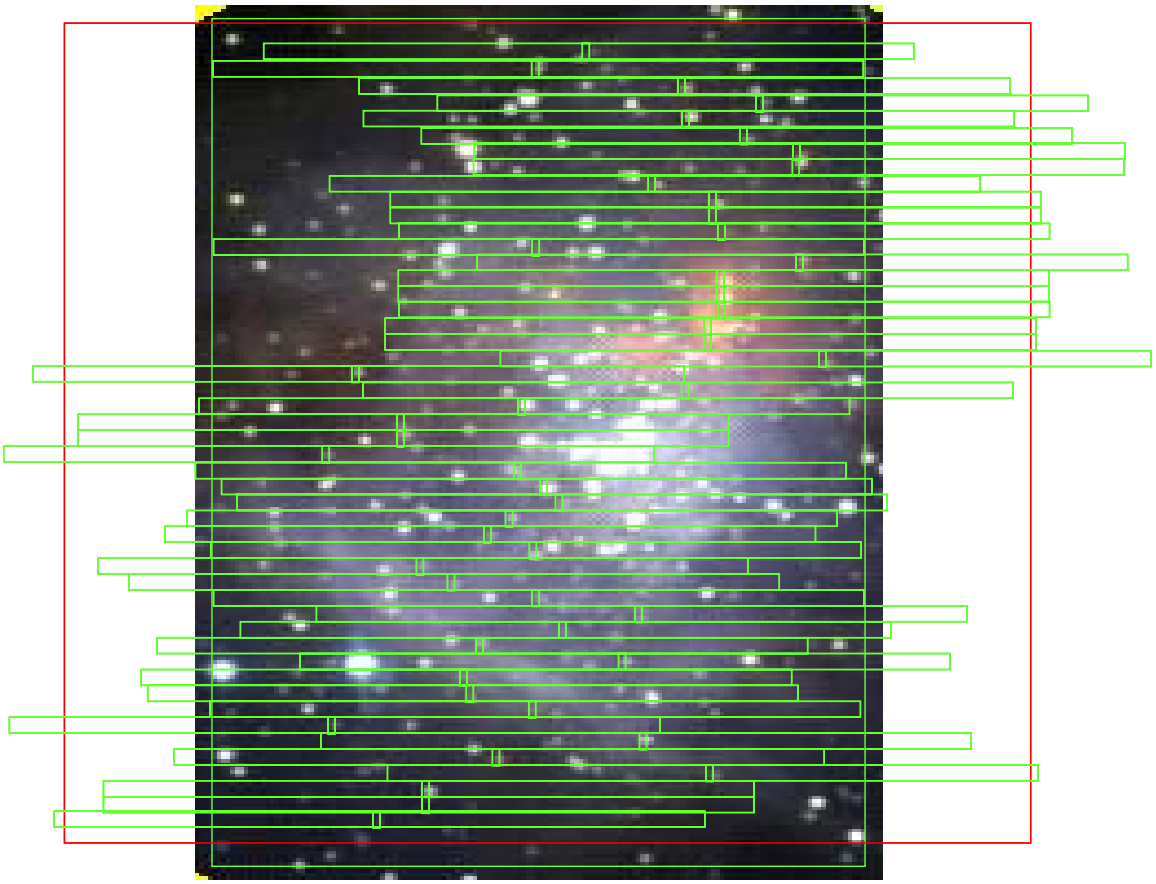

**Figure 11: 6.12′ x 3′ Region of the Orion Nebula Showing the Deployment of 46 Slits Over the Field**
Image is a JHK color composite from 2MASS. Five slits are double-length. Red box shows the approximate extent of the MOSFIRE detector and the green rectangles illustrate the H band spectrum. In all cases, the most important spectral features are on the detector. Objects other than low mass stars are included.

#### 3.4.2.1 Observation Planning

The first step for MOSFIRE slitmask design is to construct a list of targets, with accurate RA, Dec, and relative numerical priority, within the field to be studied. In this case, we confine ourselves to a region on the sky of size 6.0' x 3.0' over which existing deep near-IR data are in hand (obtained using FLITECAM on the Lick 3-m telescope). As for the previous science example, the astrometry is also derived from external data, although the steps involved would be identical if MOSFIRE were also the source for the images.

Along with the targets of interest, one also needs a list of potential alignment stars with positions measured on the same astrometric system, within the same field of view. In practice, this may be difficult in star-forming regions unless 2MASS sources are available or an image of the region has already been obtained with MOSFIRE. Most regions will have stars with $K < 19$. The main criterion for alignment stars is that they are common enough to provide ~5 stars per MOSFIRE footprint, and that they can be significantly detected in the near-IR in short (~30 s) integrations to be used in the fine acquisition of the slitmask field at the telescope. In the present case, many of the targets themselves may be bright enough to use as alignment stars, and after alignment the boxes can be closed down to slits on the targets.

For the purposes of illustration, we have generated a MOSFIRE slit mask for the candidate field. As input to the MOSFIRE Automatic Slit Configuration Generator (MASCGEN), we have specified in this case to allow slit placement in the inner 3' of the field in the X-direction (i.e., ±1.5' of the field center). Within the 6.1' by 3' footprint, there are ~100 objects in the input list for slit assignment. In addition, there are a total of 10 possible alignment stars. Also as part of the input to MASCGEN, we have specified that objects must fall >2" from the edge of any slit, meaning that only the inner ~3.3" of each bar can be used. In the case illustrated a total of 41 slits are used of which 5 are 15.3" slits made from two adjacent masking bars each.

Figure 13 shows an image of the field, on which is overlaid the MOSFIRE field with the assigned slits. Alignment stars with standard 4" by 7.3" alignment “boxes” are not drawn on the image, but several of the Orion targets could be used for alignment. The process of designing the mask configuration is very similar to that described for the extragalactic case above, with the following exception: in some star forming regions, stars bright enough in the I band to be used as guide stars on the MOSFIRE guider ($I < 19$) may be relatively scarce, so that some care will be needed that the position angle and pointing center of the mask is such that there will be at least one suitable star falling on the guider field. The MASCGEN/MSCGUI software allows for the user to obtain images and catalogs for the guider field given the MOSFIRE PA and pointing center.

#### 3.4.2.2 Field Acquisition at the Telescope

Field acquisition for this program would proceed as in the previous example, with the following exception: it may be the case in some regions of high stellar surface density that the “sky” image taken through the fine alignment version of the mask will have to be obtained prior to setting up on the field, to ensure that the alignment box images do not contain unwanted stellar sources.

Similarly, the user will have taken care that the chosen alignment stars are the brightest objects falling within the alignment boxes, in order not to confuse the mask alignment software.

In all bands, spectroscopic observations will be background limited after ~60 to 100 s (assuming detector performance of <0.03 $e^-$/s dark current and effective read noise per pixel of ~5$e^-$), so that the user has a great deal of flexibility in choosing the length of individual exposure times. In this case, we choose 900 s integrations to limit overhead due to nodding, so that the planned H-band integrations of 2 hours would be composed of 8 x 900 s integrations, 4 in each of two nod positions. The fiducial object positions within each slit are recorded in the header for the slit description extension, and information on the nod amplitudes will also be accessible in the header, to be use by the DRP.

#### 3.4.2.3 Calibrations

In the afternoon, prior to observing, spectroscopic flat fields and arc lamp exposures will have been obtained for all configurations, as in section 3.4.1 above. For programs such as the present one which depend on continuum spectroscopy (as opposed to emission lines), most users will want to be able to remove telluric features in the spectra. Correction of telluric spectral features in the observed spectrum is typically accomplished using a standard star that is observed close in time and at the same airmass as the target. Obviously, it would be tedious to place a calibration star in every slit of a given mask. However, models suggest that this should not be necessary. MOSFIRE produces pixel-sampling limited line profiles at all field positions, and a spectrally over-sampled calibration star spectrum can be obtained by placing the star at several positions along the MOSFIRE long slit. This over-sampled spectrum can then be sampled in exactly the same manner as the spectrum of the object on each slit. Provided that each slit in the mask can be flat-fielded and wavelength calibrated, the extracted spectra at each location in the mask can be divided by the re-sampled calibration star spectrum to remove the atmospheric absorption features. This procedure will be included as part of the MOSFIRE DRP, and will be fine-tuned using data obtained during commissioning. Standard star observations would be obtained using the default MOSFIRE long-slit acquisition, as in the previous science example.

## 3.5 System Overview

The system organization of MOSFIRE is by defined by a detailed product structure. The top level of this product structure is shown in Figure 12. A work breakdown structure (WBS) related to the product structure has been developed as well and serves to aid in a bottom up cost analysis.

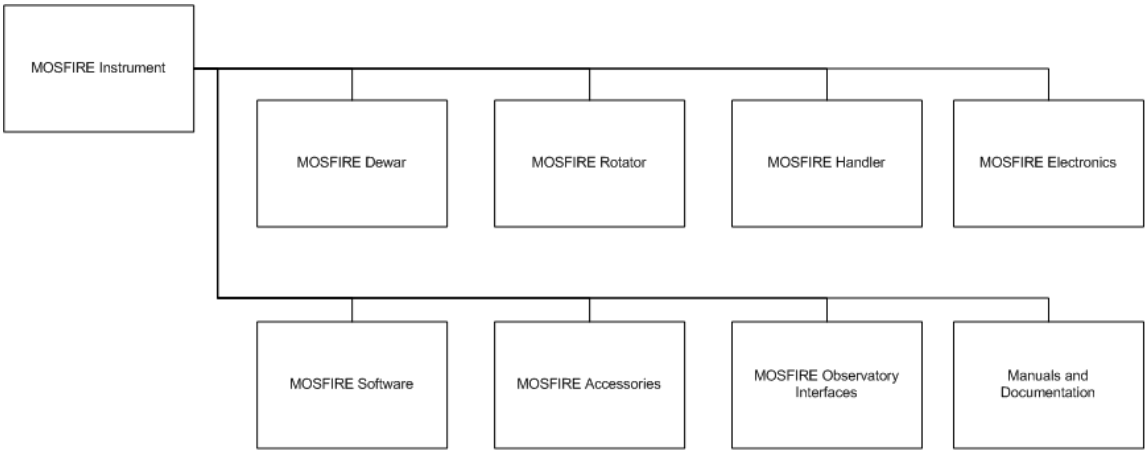


**Figure 12: Top Level MOSFIRE Product Structure**

## 3.6 Compliance Matrix for Requirements

The Compliance Matrix is available as Appendix document A.3 on the MOSFIRE web site. All other appendices, and documentation from CSEM, are posted on the web site rather than appended to this document.

# 4 DETAILED DESIGN ACTIVITIES

## 4.1 Description of major work performed

The MOSFIRE detailed design phase had two primary objectives. First, complete the design, fabrication and assembly documentation for the system and all components, hardware or software, and show that the final design complies with all specifications and applicable standards. The second objective was to present the project plan to completion, including a schedule and budget. The key objectives of the MOSFIRE detailed design phase are the following:

1. Produce detailed designs for all MOSFIRE sub-systems
2. Create fabrication drawings for MOSFIRE sub-systems
3. Place material fabrication orders for all of the MOSFIRE optical components
4. Identify other long lead time items, identify vendors and obtain quotations
5. Place orders for long lead items if the critical path requires it; e.g. grating, filters, detector
6. Perform prototype testing for cryogenic lens mount designs including testing of all required material combinations for bonded flexures
7. Build and test a prototype for the detector head and focus mechanism
8. Design and build prototype handling jigs for the optical components
9. Prepare functional requirements documents for all software including use cases, test plans and validation plans
10. Prepare configuration control plans for documentation and software
11. Prepare final error budgets for optics, flexure, weight, thermal and power
12. Prepare operations concepts including observing scenarios
13. Describe how calibrations will be accomplished and establish requirements for calibration facilities
14. Complete cryogenic testing of the CSU EUX prototype and begin the full scale development of the CSU
15. Develop performance predictions and risk mitigation strategies
16. Review and update the project plan to completion, including the schedule and budget
17. Address issues raised at the PDR

MOSFIRE's design flows down from the science requirements, and these requirements, along with the operational concepts provide context for the detailed design. The detailed design activity is documented for each sub-system and component, hardware or software, in sufficient detail to begin fabrication and procurement. All written reports are maintained on the MOSFIRE Team web page, and designs are documented in those reports and in formal Design Notes.

As the cryogenic configurable slit mask unit (CSU) is a fundamental component of the instrument, a program to develop and test a prototype of the slit mask unit was undertaken. Cryogenic tests of this prototype led to improvements in the design. In addition, CSEM carried out a detailed thermal analysis of the CSU and provided sample bars to the MOSFIRE team to enable light leakage tests to be performed. The CSU passed its critical design review on-schedule in mid-March. Consequently, the CSU is now ready for full scale development.

Again, because we identified the optical components as a high-risk area, we developed the optical design to essentially the detailed level by PDR and began to place orders for optical materials very early in the detailed design phase. Consequently, all materials are now in hand or soon will be, and the construction design is ready to release for fabrication of the lenses. We also identified the diffraction grating and large order-sorting filters as potential high-risk and long-lead items. These components are now on order.

To support the MOSFIRE lenses we developed a system of flexures mounted in a retaining ring or cell and bonded to the optical material using a pad of metal with matching thermal properties. Pull tests (both tensile and shear) were performed on each and every glass-metal combination to ensure that this methodology would work, and several prototypes of the lens cells themselves were built and tested. In addition, by making dummy lenses out of aluminum we have also been able to develop handling and alignment jigs. These experiments will continue right up until real lenses have to be installed.

Another area of risk is the HgCdTe H2-RG detector from Teledyne Imaging Sensors (formerly Rockwell Scientific) and the associated SIDECAR ASIC control chip that eliminates much of the classical electronics associated with IR and CCD arrays. An ASIC board designed for bench-top use has been operated for many months to enable local software development. In addition, Teledyne have recently been placed under contract to deliver an engineering grade device and a cryogenic ASIC carrier board to enable us to evaluate the entire system from end-to-end. A prototype detector head has been fabricated and installed in a LN2 test chamber awaiting arrival of the new board, cables and chip. In addition, as the detector focus mechanism has no previous heritage among other IR instrument at WMKO, a prototype of the titanium flexure and drive module has been built and tested.

Extensive finite element analysis modeling of the MOSFIRE vacuum chamber and internal structure (the optical benches), together with an analysis of the Cassegrain bearing, has been undertaken to demonstrate that the requirements can be met. Similarly, we sub-contracted Space Dynamics Labs to perform a detailed static and dynamic thermal analysis of the proposed design to ensure that, among other things, the desired goal of using only two large closed-cycle refrigerators could be achieved.

Other activities included extensive discussions with vendors about fabrication issues, a detailed development of science “use” cases and associated software, a study of calibration issues, and an early investigation of everything that would be needed for assembly, alignment, commissioning and maintenance, both in California and on Mauna Kea. In addition, careful attention was paid to the issues raised by the PDR committee. Most of these have already been mentioned as part of the DDR activities, but more specific statements will be made in next section.

# 5 DETAILED DESIGN

## 5.1 Optical Design

### 5.1.1 Introduction

It is assumed that the reader is familiar with the optics sections in TSIP Proposal 2005, in TSIP Proposal 2006 and in PDR Report-v4.0. Those documents can all be found on the MOSFIRE Team Web Page under the general heading, "Preliminary Design." More detailed information can be found on the Team Web Page under the general heading "Documentation/Optical" by scrolling down and clicking on the link, "MOSFIRE Optics Reports."

It should be mentioned that all of the optical designing and optimization were carried out with Epps' proprietary optical design code called, "Optical aberration reduction and system analysis" (Oarsa) and his associated support codes. Spot diagrams, image analysis, layout drawings, foot print diagrams and related calculations were done with the commercially available code, Zemax, which also provides a convenient means of documenting and sharing the various optical prescriptions with other MOSFIRE team members. Zemax prescriptions for the construction designs described and referenced below are available on the Team Web Page also.

In the information to follow, it may seem surprising that the MOSFIRE optical design has not evolved substantially, relative to that proposed in TSIP 2005. Instead, the design has matured steadily by small but important incremental steps. Some concern was expressed during the PDR review to the effect that the optical design might be more effective if done differently. Epps replied to that important question on April 17, 2006, in a letter to PI McLean. Excerpts from that letter follow:

---

Regarding the questions that reviewers raised about whether the collimator and/or camera optics could be made simpler, cheaper, with more throughput, etc., I can only say that at the present time, I don't know how to do it. I've tried pretty hard on all counts and the optics as they now exist in our preconstruction design represent the best that I've been able to do. I'd be delighted if the reviewers or their colleagues or their favorite optical designer(s) could come up with better solutions. If they do that, I'd be the first one to insist that we build the best designs, no matter who originated them.

In any design situation, a competent designer will limit himself to a set of technologies that is consistent with the design goals, including cost limitations and delivery schedule in addition to performance characteristics. I have done that in the MOSFIRE optics for example, by restricting my materials selection to *exclude* NaCl (salt), PbF2 (lead fluoride), ZnS (Cleartran), and optical glasses whose transmission characteristics are poorer than S-FTM16. I chose not to use aspheric surfaces unless the designs demanded them (which they did not).

There's no way I can prove that something can't be done. In answer to the reviewers, all I can say is, "interesting idea... why don't you give it a try and let me hear how it works out."

---

### 5.1.2 Description

The underlying guideline for the MOSFIRE optical design has always been to keep it mechanically compact and as simple as possible to fabricate. A folded, all-spherical design was adopted as the basis of our original proposal for those reasons. It matured steadily as we progressed through TSIP 2006 to our PDR last April. During the past year, the preconstruction collimator and camera designs shown in PDR Report-v4.0 have been refined further. They have been brought to a "construction design" status. By this we mean that the optical materials needed to fabricate them have almost all been received, that the melt-sheet index corrections for the optical glass elements have been included in the designs and that the lens forms have all been analyzed and approved for mechanical viability. The guider optics are nearly finished and we are ready now to proceed with production of the science optics.

#### 5.1.2.1 End-to-End Layout

Figure 13 is a depiction of the current overall MOSFIRE layout. All components in the optical path, including the CSU, are shown. The construction optical design for the guider is described in Section 5.1.2.10.

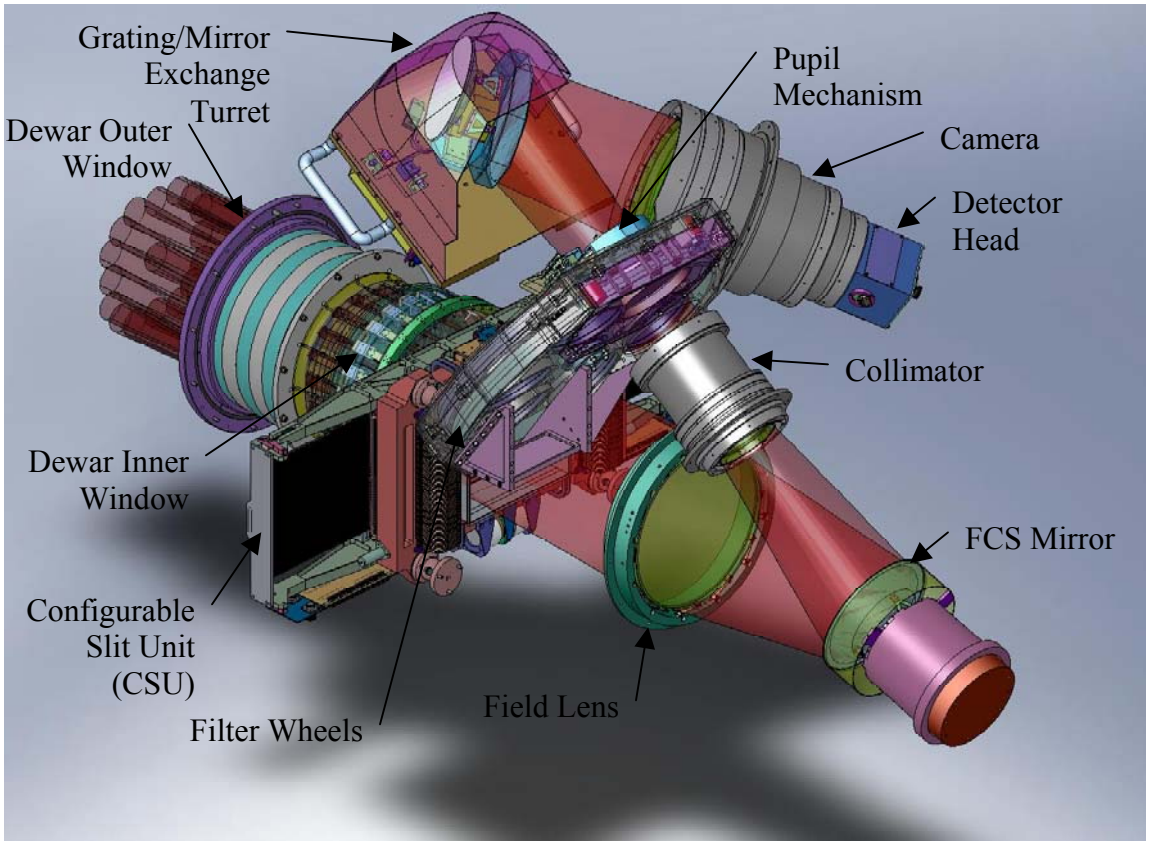


**Figure 13: MOSFIRE Optical Layout**

#### 5.1.2.2 Entrance Aperture

The Keck 1 primary mirror area is equivalent to that of a circle with a 5000.00 mm radius. However its serrated edge fits within a circumscribed circle with a much larger, 5474.46 mm radius. For convenience, we have approximated the primary mirror's entrance aperture by a circle with a 5156.61 mm radius, which covers all but the outermost parts of six "ears" whose total area is only about 2.2% of the active mirror area. The outer regions of the primary mirror are properly weighted by this approximation such that a high degree of aberration correction is achieved. The full circumscribed circle is used (where appropriate) for determining clear aperture diameters.

#### 5.1.2.3 Dewar Windows

A large (388.0 mm full diameter) entrance window is required to accommodate the 6.8′ diameter field of view. This window is located in a tube or snout at the front of the dewar. In order to withstand the pressure differential under vacuum, while keeping the maximum stress within the "glass" below ~500 psi, an Infrasil-302 window about 34.9 mm thick is required. To prevent condensation from forming as the center of this large window cools by radiation, a second, thinner (17.0 mm) Infrasil-302 window is located 228.6 mm away in the vacuum. An aluminum tube and baffles between the windows are resistively heated as described in the mechanical section to provide radiation to maintain the outer window above the average Observatory dome temperature. Detailed thermal analysis shows that this arrangement will not affect the optical performance and that it will have a negligible impact on the thermal background.

#### 5.1.2.4 Collimator and Pupil

The telescope's effective focal length is 149.572 m as it is used with MOSFIRE, such that the effective f/ratio is f/14.50. Thus the collimator's focal length must be 1813.0 mm so as to produce a (stipulated) 125.0-mm beam diameter. The collimator is a critical optical component. It must capture a physically large, 6.8' diameter field of view and it must also produce a sharply focused, accessible pupil image so that a cold Lyot stop (mask) can be inserted to eliminate stray thermal radiation. We have refined the lens-element shapes for optimal optical performance and ease of construction. We have also reoptimized the design to vacuum at the adopted operating temperature of T = 120.0 K. Final thermal corrections have been put into the construction design(s), including the front window at T = 2.0 ºC and the camera's field flattener at T = 77.0 K. The arrangement is shown in Figure 14.

The 6-element collimator contains a large CaF2 field lens separated from a second lens group. A folding flat (not shown) will be placed between these groups. Note the curved Keck 1 focal surface. This curvature (~2.124 m radius) is taken into account in the CSU design. A close-up view of the collimator's five rear elements is shown in Figure 15, together with the pupil-image location. The (monochromatic) pupil diameter is 125.0 mm as intended. The pupil image is stationary over all field angles to ~2.5% in the K-band and to ~3.6% in the H-band where a Lyot stop will be used. This lens group has been shortened slightly relative to the preconstruction design. The pupil location has been extended toward the grating to provide additional clearance between the Lyot stop mechanism and the camera barrel. A 10.0-mm thick Infrasil-302 substrate has been included

for the K-band and Ks-band filters. The other filters will use 10.0-mm N-BK7 substrates but the index differences are negligible in parallel light. The filters will be titled 6.0 degrees with respect to the optical axis to avoid ghost images.

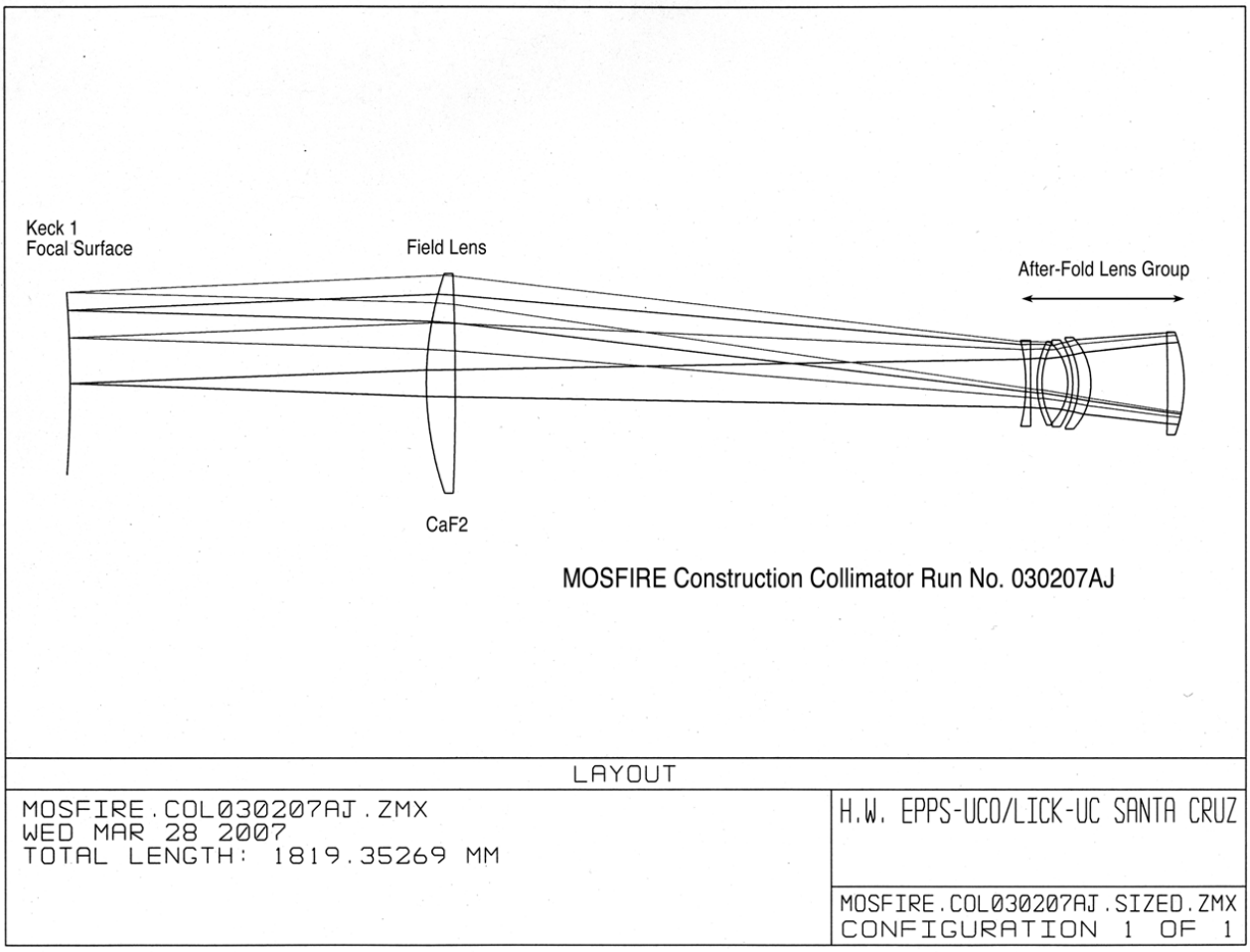


**Figure 14: The 6-element Collimator**

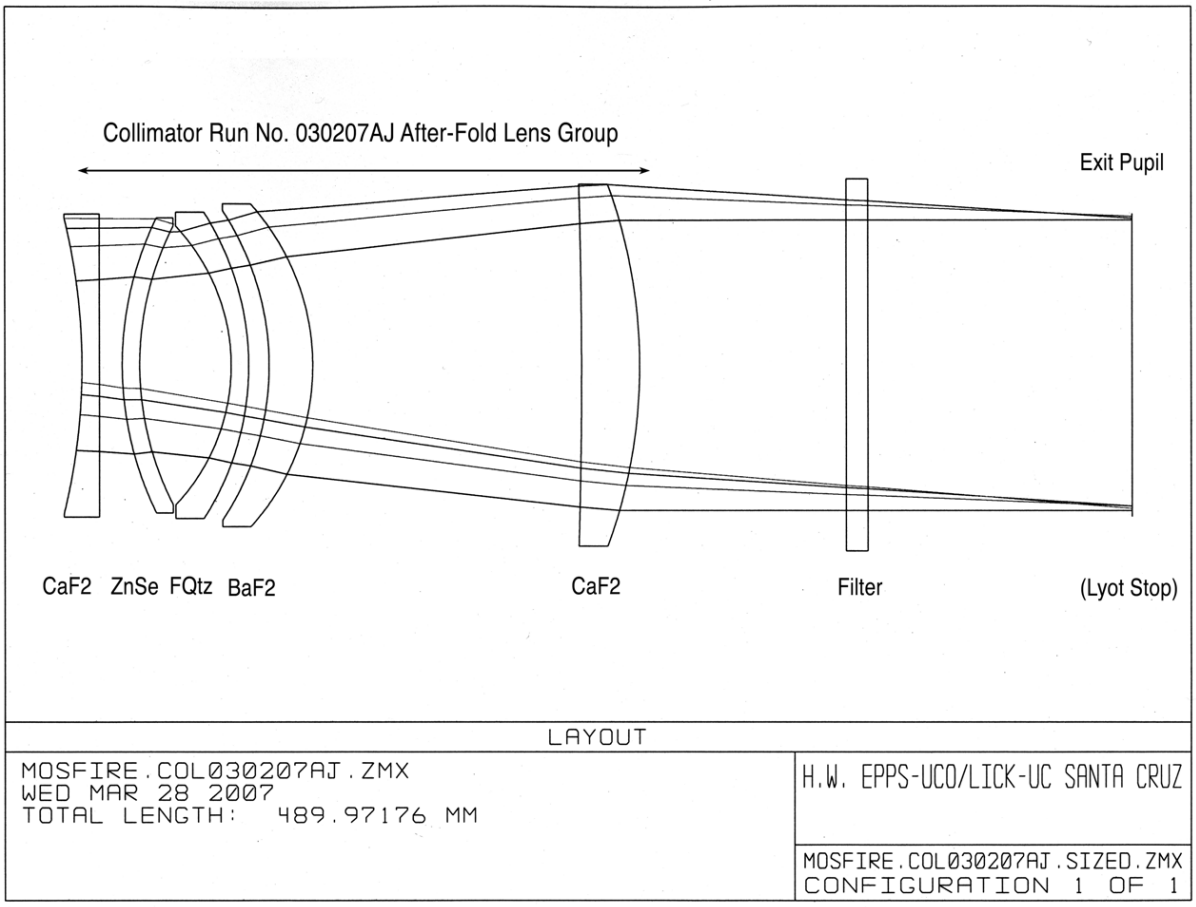


**Figure 15: Close up View of the 5 Rear Collimator Elements Showing the Pupil Image Location**
The diameter of the pupil is 125.0 mm. FQtz refers to Heraeus Infrasil-302.

When re-imaged by a "perfect" camera, the construction collimator shows rms image diameters of only 0.05" +/- 0.01", averaged over all field angles and all wavelengths in the 0.90 μm to 2.50 μm spectral range without refocus, with a maximum lateral color of 0.07" rms. These residual aberrations are entirely negligible relative to those of the real construction camera.

The collimator's pupil-imaging performance, neglecting diffraction, is illustrated in Figure 16, which shows negligible transverse aberration in the pupil. The effects of diffraction will primarily be important in K-band spectroscopy when sub-arcsecond slit widths are used. Those effects have been taken into account in the Lyot stop mask design.

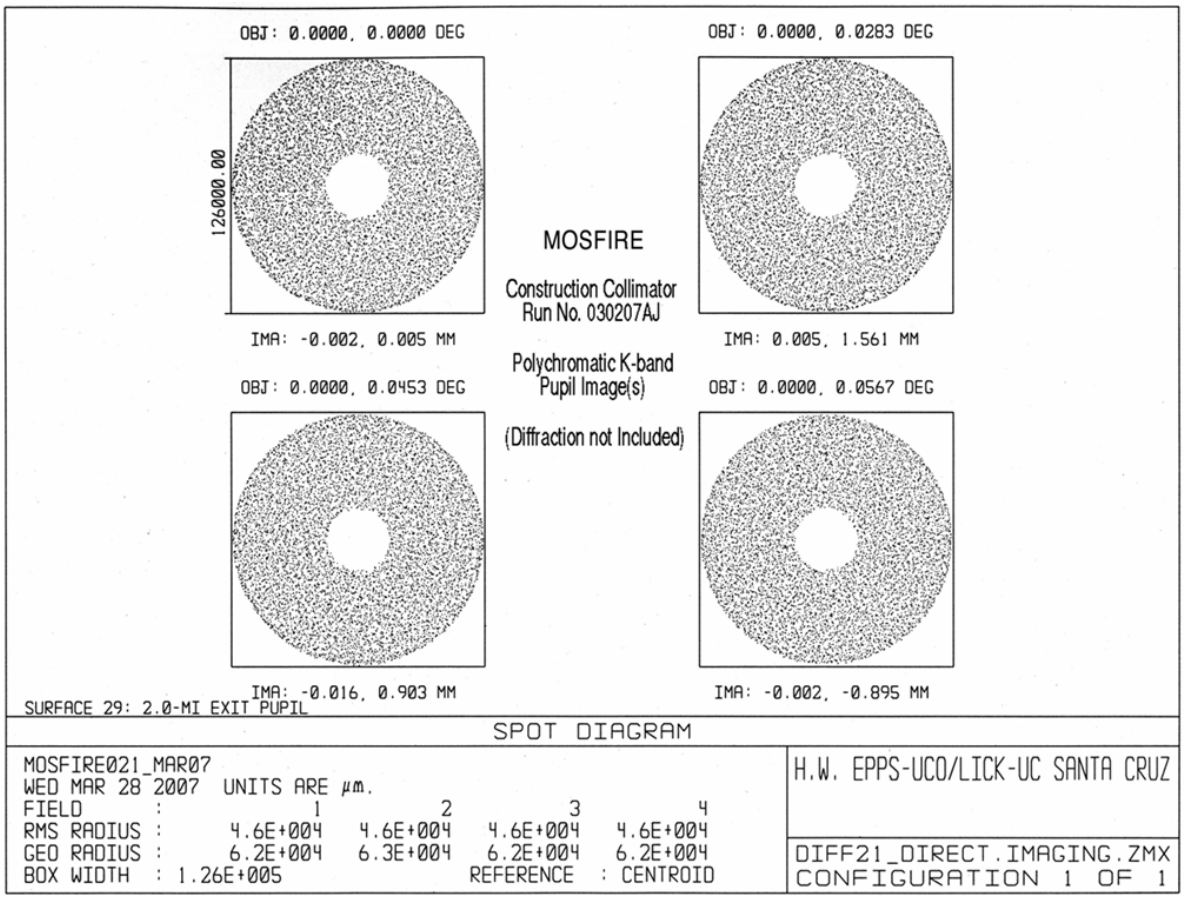


**Figure 16: Polychromatic K-band Pupil Images Without Diffraction**

The pupil images are shown for 0', 1.7', 2.72' and 3.4' field radii. The box size is 126.0 mm. Less than 1.0 mm of pupil smear is evident. Diffraction effects from the narrowest (~0.7") slits will cause larger but acceptable smear in the K-band.

The monochromatic 2.0 μm exit pupil is located 7.7 mm toward the grating, relative to its location in the preconstruction design. The full field of view has a 3.4' field radius (Frad). The amount of pupil walk (in mm) is given in Table 8 for passbands that will be used with a Lyot stop mask.

| Passband | Frad=40% | 50% | 55% | 60% | 70% | 80% | 90% | 95% | 100% |
|---|---|---|---|---|---|---|---|---|---|
| 2.0 μm | 1.26 | 1.35 | 1.34 | 1.29 | 1.03 | 0.53 | -0.24 | -0.75 | -1.36 |
| K-band | 1.43 | 1.57 | 1.58 | 1.55 | 1.34 | 0.90 | 0.17 | -0.31 | -0.89 |
| Ks-band | 1.41 | 1.54 | 1.55 | 1.52 | 1.30 | 0.85 | 0.12 | -0.37 | -0.95 |
| H-band | 0.93 | 0.93 | 0.88 | 0.78 | 0.43 | -0.16 | -1.04 | -1.60 | -2.26 |

**Table 8: Pupil Walk in mm as a Function of Field Radius (Frad)**

NOTE: 100% corresponds to 3.4'.

When the system is used in the Y-band and the J-band, the Lyot mask will retract, leaving an open hole. In that case, the exit pupil image is defined by the full extent of the serrated Keck 1 primary mirror and the amount of pupil walk is somewhat larger, due to unavoidable axial chromatic aberration in the pupil-image location.

Ray tracing shows that the required open-hole diameter is determined by the shortest wavelength in the Y-band (0.975 μm). Its full diameter is about 138.4 mm. Stray light rejection would be maximized with this calculated hole size. However an open-hole diameter of 143.0 mm has been recommended. It is prudent to maintain the extra room because the pupil image can wander significantly if the Keck 1 telescope mirrors are not aligned in a coaxial manner and/or the mechanical axis of the rotator bearing is not aligned coaxially with the telescope's optical axis.

#### 5.1.2.5 Camera

The camera system is always challenging in applications where the field of view is large and the scale reduction from the telescope image scale is significant. The large (327.5 mm) distance from the Lyot stop to the grating, combined with the (300.0 mm) distance from the grating to the camera causes convoluted, anamorphic, wavelength and field-angle dependent compound-pupil presentations, which further complicate the design. The resulting camera requires a 250.0 mm focal length and a 270.0 mm entrance aperture such that it operates at f/0.93 (under-filled), which is unprecedented for a cryogenic 0.975 μm to 2.40 μm infrared camera of these dimensions. Its field radius is 6.0 degrees to cover the corners of the H2-RG array.

Nevertheless, we have produced the 7-element all-spherical construction camera design shown in Figure 17. It satisfies all the goals for MOSFIRE, including the need to provide for direct imaging in the K, H, J, and Y passbands as well as spectral coverage in those passbands for any object located within a rectangle at the telescope focal surface whose dimensions are ±3.06′ along the slits and ±1.50′ perpendicular to the slits.

The current Zemax prescription for the construction optical design in direct-imaging mode is DIFF21_DIRECT.IMAGING.ZMX, which contains our construction collimator (Run No. 030207AJ) and our construction camera (Run No. 030607AF). This Zemax prescription and the required glass file, MOSFIRE.AGF, can be found on the Team Web Page under "Documentation/Optical." It was used to calculate the spot diagrams and image evaluation below.

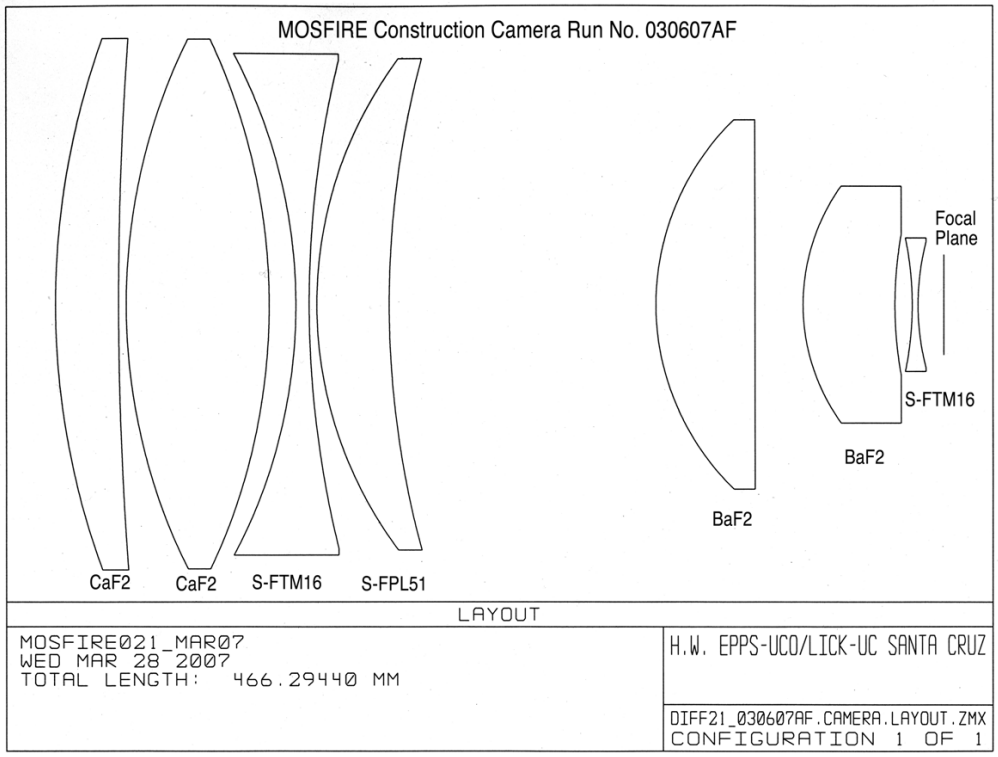


**Figure 17: The 7-element MOSFIRE Camera, Including Field Flattener and Detector Focal Plane**
For clarity, the rays have been suppressed to better show the lens forms.

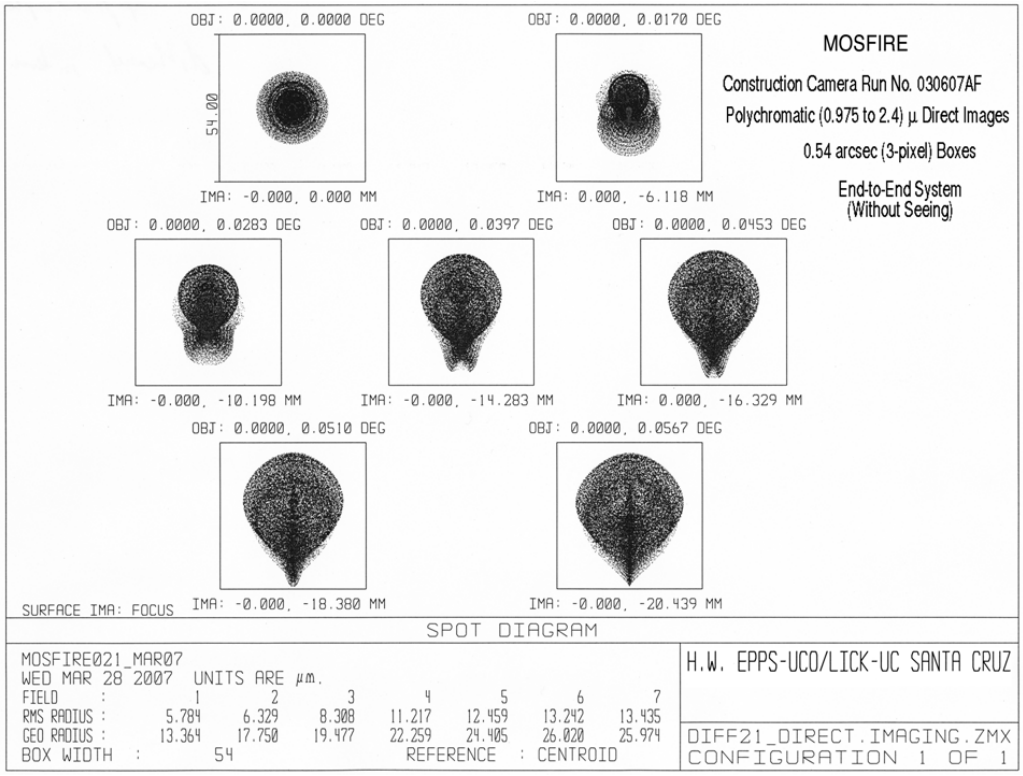


**Figure 18: End-to-end Direct-Imaging Performance Spot Diagrams**

The end-to-end direct-imaging performance of the telescope, collimator and camera combination is excellent, as seen in Figure 18. These polychromatic spot diagrams show a "wide-open" passband, which includes 20 wavelengths from 0.975 μm to 2.40 μm plotted simultaneously without refocus, for field angles that are 0.0, 30%, 50%, 70%, 80%, 90% and 100% of the full 6.8' field of view that is available for direct imaging. The area-weighted average rms image diameters are only 0.23" ± 0.06" and all of the light falls within 3-pixel (0.54") boxes. Imaging will be even better in the K, H, J, and Y passbands, which can be focused independently with the sensitive, built-in focus mechanism in the camera.

The current Zemax prescription for the construction optical design in spectroscopic mode is DIFF21_030207AJ_030607AF.ZMX, which can also be found on the Team Web Page under "Documentation/Optical." It was used to calculate the spot diagrams and image evaluation below.

Image quality in spectroscopic mode is harder to illustrate because of the many possible combinations of object locations and passbands. Furthermore, it is not well described by rms image diameters because the aforementioned anamorphism and compound-pupil presentations unavoidably result in some images whose geometries are asymmetric and irregular, including "tails" and other artifacts. Instead, we have adopted a spectroscopic image-quality goal for MOSFIRE that seeks to put 80% or more of the light in any given image into a (2 x 2)-pixel Nyquist sampling box, centered on the image centroid. This criterion is appropriate, as it is well known that optics become pixel-sampling limited under that condition.

A representative sample of *worst-case* spectroscopic images was calculated without refocus for three extreme objects placed 3.06' off-axis (at the top end of the slit), with offsets of -1.5', 0.0' and +1.5'. Our 110.5 groove/mm grating was set to a 42.614-degree angle for K and H, so as to put 2.18 μm light at the field center in 3$^{rd}$ order and 1.635 μm light at field center in 4$^{th}$ order. The grating was set to a 41.524-degree angle for J and Y, so as to put 1.248 μm light at field center in 5$^{th}$ order and 1.04 μm light at field center in 6$^{th}$ order. To determine whether or not a given image would be counted in the analysis, the criteria adopted were that it must fall on the detector and it must fall within the following wavelength ranges: 3rd-order K (1.93 μm to 2.40 μm); 4th-order H (1.46 μm to 1.81 μm); 5th-order J (1.15 μm to 1.35 μm); and 6th-order Y (0.975 μm to 1.12 μm). The resulting spectral-image ensquared energy concentrations, as percentages in a (2 x 2)-pixel Nyquist box averaged over all objects and wavelengths, are given in Table 9.

The worst images were mostly at the extreme-wavelength ends of the spectrum and/or at the very corners of the detector. At nearby wavelengths or just a couple of mm away from the corner, those worst-case images got much better. We conclude from this worst-case evaluation procedure that MOSFIRE's spectroscopic imaging performance will be strongly pixel-sampling limited in all cases.

| Order | Band | Average | Worst |
|---|---|---|---|
| 3rd | K | 92.6% ±4.6% | 87% |
| 4th | H | 91.8% ±2.3% | 89% |
| 5th | J | 90.3% ±5.3% | 81% |
| 6th | Y | 91.6% ±4.8% | 84% |

**Table 9: MOSFIRE Spectral Image Energy Concentrations**

#### 5.1.2.6 End-to-End Direct-Imaging Scale and Distortion

Ray tracing shows that, near the optical axis, the end-to-end system has a transverse image scale of 99.951 μm/" which is very close to the intended 100.0 μm/" value. The construction collimator and camera were designed such that their individual contributions to distortion tend to cancel. An end-to-end residual pincushion distortion of only 0.24% at the edge of the 6.8' field of view was achieved.

#### 5.1.2.7 Cryogenic Refractive Indices Used in the Construction Designs

The MOSFIRE science optics make use of 6 optical materials which are: CaF2, BaF2, ZnSe, Fused Quartz, S-FPL51 and S-FTM16. These optics will be used in vacuum at T = 120.0 K. The construction designs can only be as good as the correctness of the cryogenic indices used to optimize them, which ideally should be good to perhaps a few parts in the 5th decimal place. In preparation for moving the preconstruction collimator and camera designs to full-up construction designs, Epps initiated an extensive, "final" review of his cryogenic refractive index models. Details of that review are given in MOSFIRE Optics Reports #19 and #20. That study is summarized briefly here.

Epps' cryogenic index models for CaF2, BaF2 and ZnSe are based upon thermo-optic (dn/dT) coefficients reported by Feldman, et al., (1979). However the CHARMS group at Goddard Space Flight Center has published more recent high-precision measurements, made with modern BaF2 and ZnSe samples in support of the JWST program. Their models differ slightly from his. Epps chose to use the CHARMS models because they represent optical material that is more likely to be the same as our material. The CHARMS group has also measured a modern sample of CaF2. However that data is presently sequestered and unavailable, although Epps may be able to obtain it before we are forced by scheduling constraints to release our construction designs for production.

We are on less well established ground with Fused Quartz, S-FPL51 and S-FTM16. Fused Quartz is based on dn/dT values and other information for Fused Silica and scaled to the ratios of Quartz/Silica given at just two temperatures in the Heraeus catalog. S-FPL51 is based upon sparse but recently published dn/dT values from Yamamuro, et al., (2006), which look reasonable, compared with room-temperature values. However, these values could be systematically wrong as one goes colder. S-FTM16 is based on cryogenic measurements given by Brown, Epps and Fabricant in a PASP paper (2004). New measurements of S-FTM16 are underway at M3 Measurement Solutions Inc., as described in Optics Report #19. Prisms of Heraeus Infrasil-302 (Fused Quartz) and S-FPL51 have been made by Planar Optics Inc. Those will also be measured

by M3. We expect to have all of that data before the fabrication release date also. If so, we will compare it with Epps' models, try to otherwise evaluate its reliability and respond accordingly.

In summary, we prefer to think of our present construction designs as being "provisional" in the sense that we may choose to reoptimize them one final time, based upon what additional cryogenic refractive index information we are able to obtain on an acceptable time scale. However, based upon intercomparisons of all the various cryogenic index data we have as of now, as seen in Optics Report #20, we are confident that if we build the present designs, they will work satisfactorily.

#### 5.1.2.8 Ghost Image and Ghost Pupil Analysis

Extensive direct ray tracing studies to evaluate ghost images and ghost pupils in the *pre-construction* design are described in detail in Optics Report #10. Bounces off of the detector and one lens surface (detector/lens), as well as 91 different combinations of double-bounce (lens/lens) ghosts were considered. No (detector/lens) ghost images were found. Those were mitigated on-the-fly during the optimization by Oarsa. No significant ghost pupils were found although those had not been mitigated automatically.

The worst ghost image seen was that due to a double-bounce off of both sides of the field flattener in the camera. It has an rms diameter of 498 μm, which results in 3.49 magnitudes of geometric dilution, in addition to the 9.60 magnitudes of dimming expected if the coated surfaces have an average residual reflectivity of about 1.2%. It was found that this ghost image could be improved by thinning the field flattener from its preconstruction value of 4.0 mm, down to 3.0 mm. This was in fact done for the construction camera design.

The construction designs have not yet been evaluated for ghost images and ghost pupils because doing so is labor intensive and we may yet decide to re-optimize the construction designs if improved cryogenic indices are obtained prior to the release date for production of the science optics. However we certainly will perform a full ghost image and ghost pupil analysis before any design is released and we will mitigate whatever ghosts may be found on an individual basis.

#### 5.1.2.9 Grating/Mirror and Filters

The MOSFIRE grating choice was initially based on an existing 110.5 grooves/mm master that was produced as part of the GNIRS project and which has also been used to produce replicas for other near-IR spectrometers. It was always our intention to have a custom grating master fabricated for MOSFIRE, but the GNIRS grating master provides a good "backup" choice since its properties (110.5 grooves/mm and a blaze angle of 22.0 degrees) are very close to ideal for MOSFIRE, with the exception of its physical size. The MOSFIRE grating must have a ruled elliptical area of size ~10.5 inches (266.7 mm) by 7.4 inches (187.96 mm) to allow spectra to be obtained using slits placed anywhere within the MOSFIRE imaging field of view without vignetting, and it must be efficient in orders 3-6 when used at the 40 degree included angle. Final grating specifications are outlined in MODN06. Given the >12-month lead time for the production of a new master large enough to accommodate our needs, a purchase order for the grating has been submitted to Newport (formerly Richardson Grating Lab).

The nominal grating angle of 42.614 degrees nicely centers spectra for slits at the center of the MOSFIRE field of view in the H and K bands, but the Y and J bands end up slightly "short" at the same angle. This fact led us incorporate a second grating angle of 41.524 degrees that will be the default for observations in the Y and J bands. Using a simple mechanism that places a shim in front of the normal stop for the grating mechanism as described in detail in MMDN24, the second angle is achieved without compromising grating repeatability. The specified grating blaze angle of 21.93 degrees attempts to optimize the location of the blaze peak with respect to the useful bandpass for each order. We expect that it will be possible to obtain >50% grating efficiency across all of Y, J, H, K bands (with peaks higher than 80%) based on existing (tested) replicas of the GNIRS master. Finally, the flat mirror used for the imaging mode and mounted back-to-back with the grating will have over-coated silver on the same substrate material used for the grating, OHARA Clearceram-Z.

The MOSFIRE filters, summarized in Figure 4 and Table 5, were selected primarily as order-sorting filters, but also to incorporate all regions of the 0.975-2.40 μm range over which the atmosphere is mostly transparent. The only part of the spectral region with relatively high atmospheric transparency that will not be accessible due to order sorting constraints is the region from 1.12-1.15 μm (between the Y and J bands) – see Figure 4. The spectroscopic K band filter is significantly wider than any standard photometric K filter in order to allow access to a larger wavelength range. If used for imaging this filter would not be ideal due to its long-wavelength cut-off that would increase the background unnecessarily. Furthermore, its short wavelength cut-on would make it more susceptible to rapidly changing atmospheric transparency. Because of this, a standard "K-short" filter will be provided, which may be used for either imaging or spectroscopy. All of the other bands are close enough to their photometric counterparts to play a dual role for both imaging and for order sorting.

Because of their primary importance as order-sorters, the filters must have very square bandpasses, very accurate cut-on and cut-off wavelengths and very good out of band blocking, while still maintaining high throughput. The filter substrates will be 10-mm thick N-BK7 for Y, J and H, and 10-mm thick Infrasil-302 for K and Ks for improved transmission beyond 2.2 μm. A purchase order for the 5 filters listed in Table 5 was submitted to Barr Associates in February, 2007, with an expected delivery in ~6 months.

#### 5.1.2.10 Guider Optics

We have developed an all-spherical construction design for our focal-reducing guider. It is Run No. 060506AE which operates at T= 2.0 C. The guider intercepts a (2.8' by 2.8') off-axis portion of the telescope field of view and images it on a (1024 x 1024 by 13 μm) frame-transfer CCD, the CCD47-20BT from E2V. The short-wavelength cutoff will be defined by an RG780 filter while the long-wavelength cutoff will be defined by the CCD's quantum efficiency. For an object whose spectral energy distribution is constant, the effective wavelength will be 0.85 μm. A passband of this style has been used successfully in the NIRSPEC guider.

The guider contains a 234.1-mm diameter contact doublet, which focuses the light with about 21.1% of the needed scale reduction and also forms a pupil image at a second, 83.3-mm diameter

contact doublet. This doublet is then followed by a thick singlet lens and a dome-shaped field flattener. The field flattener also serves as the vacuum window for the small guide camera dewar. A 79.24 μm/" final imaging scale is achieved. Pincushion distortion is only about 1.0% at the detector corners. The thick singlet will be translated along the optical axis for focusing, using a computer-controlled mechanism. No appreciable ghost images or ghost pupils appear in the guider design.

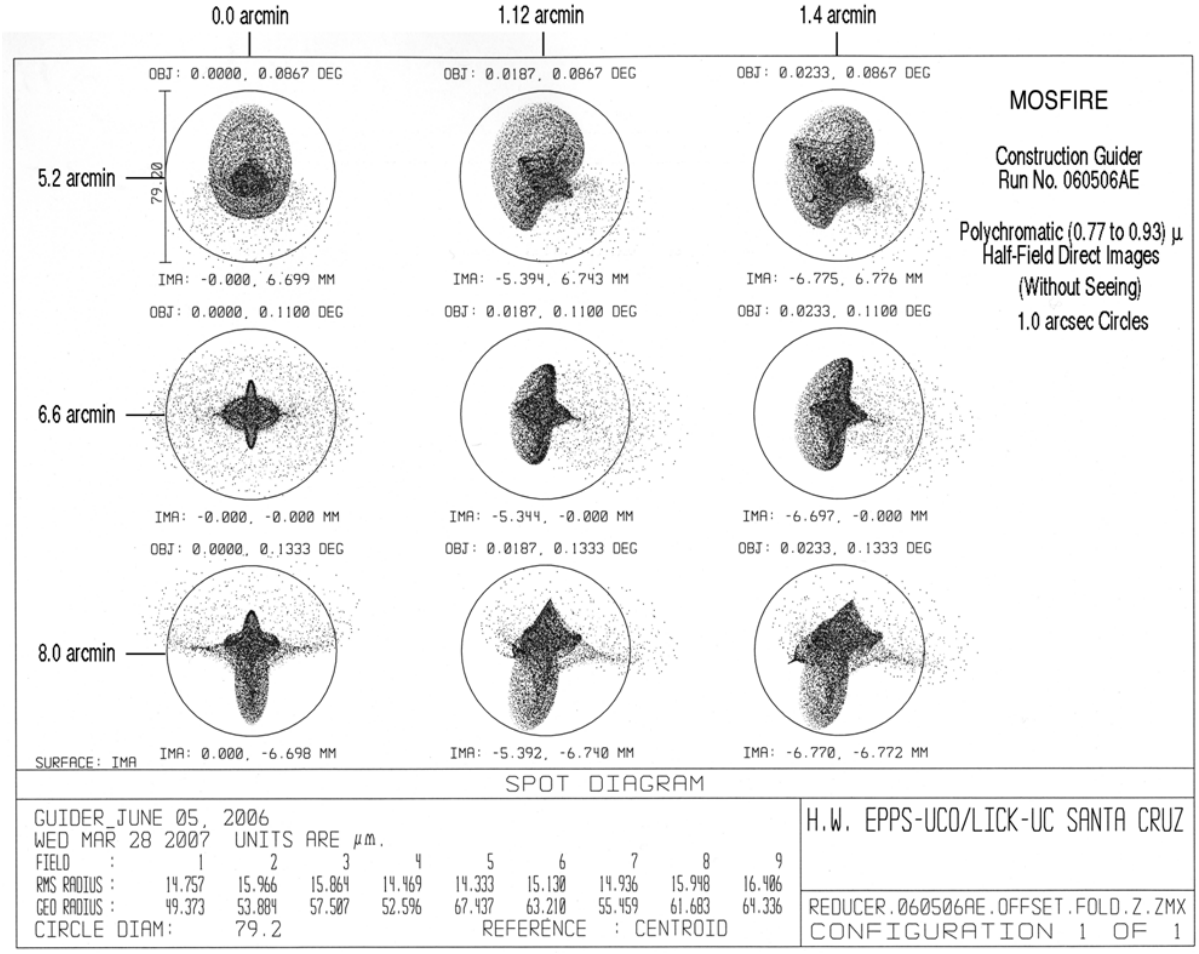


**Figure 19: Polychromatic Guider Images**
Spot images are shown over half of the (2.8′ by 2.8′) bilaterally symmetric off-axis field of view; the circles are 1.0" in diameter.

The guider's image quality is illustrated in Figure 19. The field of view is bilaterally symmetric about the X = 0.0 columns of images so only half of it is shown. Polychromatic rms image diameters are 0.39" ± 0.02" averaged over the full field of view, which should be excellent for the intended purpose.

The guider is located 6.6' off of the telescope's optical axis. It is folded with 2 flat mirrors into a compact "Z-shaped" geometry as shown in Figure 20. The current Zemax prescription for the construction guider is REDUCER.060506AE.OFFSET.FOLD.Z.ZMX. This file can be found on

the Team Web Page under "Documentation/Optical." The guider's passive (2.8' by 2.8') off-axis field of view is large enough to provide suitably bright guide stars in any part of the sky, and the folded geometry will enable its mechanical structure to be rigid relative to the CSU.

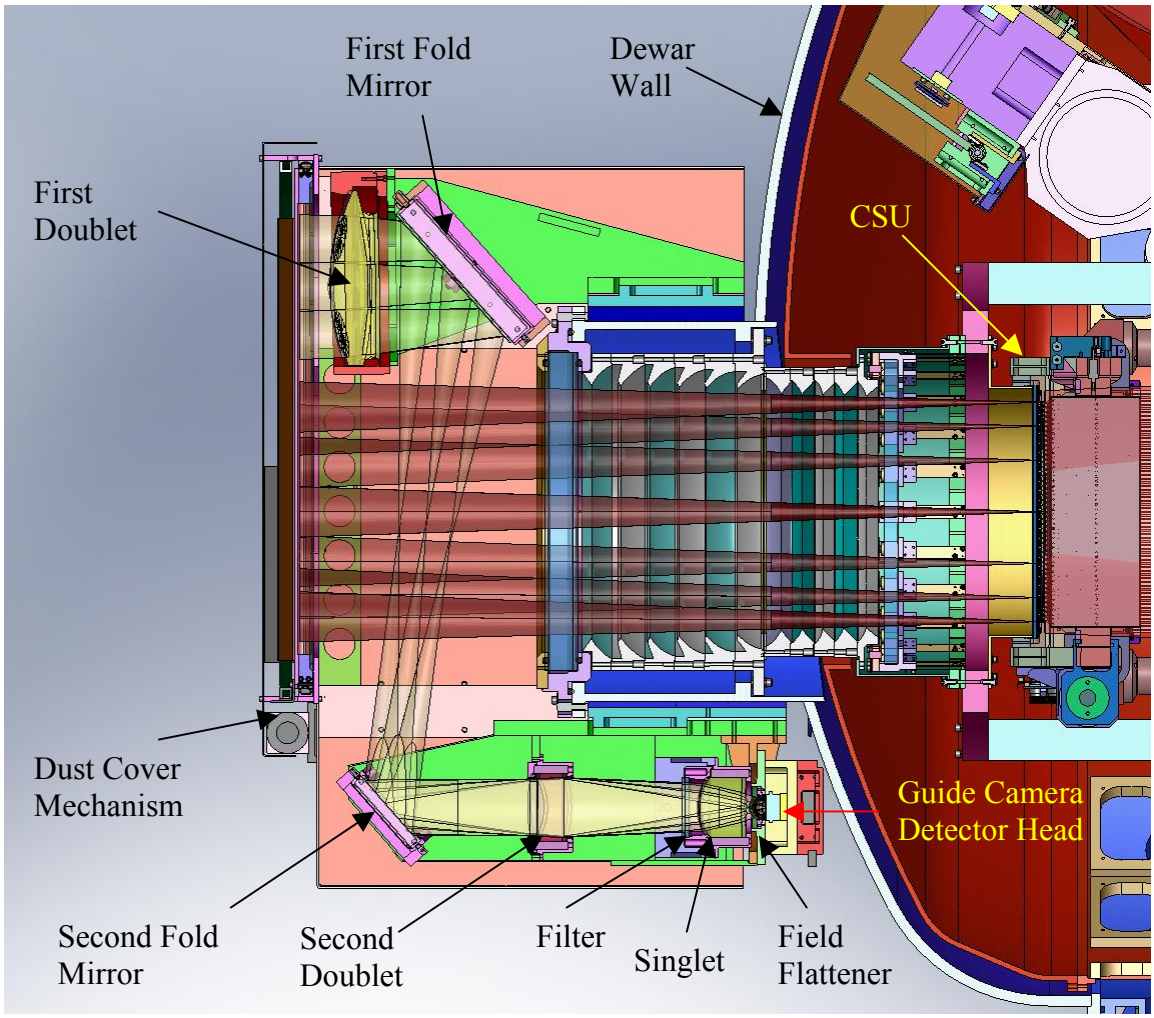


**Figure 20: MOSFIRE Guider Layout**

The flat mirrors for the guider have been polished and coated with protected gold by United Lens. Blanks for 3 RG780 filters were purchased from S.I. Howard Glass and 2 of them have been polished at UCO/Lick. Two copies of the quasi-hemispherical field flattener have been polished by TORC. All of the other guider lenses have been polished by UCO/Lick with the exception of the 1st S-FPL51 lens element. In that case, there was a thermal mishap during a heating/cooling procedure, which cracked the blank. Another blank has been ordered from Ohara and we expect delivery in early April 2007. We anticipate that all of the guider optics will be ready to be sent out for coating about one month after the replacement S-FPL51 blank arrives.

Two available lenses have been identified to use for bonding tests. One is about 200 mm in diameter with a convex radius of 291.9 mm, slightly more extreme than the 234-mm diameter and

408-mm convex radius on the bond surface of lens element #1. The other is about 75 mm in diameter with a convex radius of 68.8 mm, which matches the bond surface geometry of lens element #3 very nicely. We have made matching concave aluminum mates for these test lenses and we have ordered the Nyo-Gel OCK-451 bonding agent. When it arrives, we will bond the test samples and subject them to thermal excursions. We estimate that the (generic-glass/aluminum) doublets should have CTE differences of something like $(16 \times 10^{-6})\ C^{-1}$ whereas the CTE differences in the guider doublets are only about half that amount. Thus we should be able to subject the test bonds to more severe thermal stresses than they will ever encounter in operation.

### 5.1.3 Optics Sensitivity Analysis

A study of the imaging performance characteristics of the MOSFIRE *preconstruction* optical design was carried out with regard to "decenter" and "tilt" of its individual optical elements. The results of that study are reported in sections of PDR Report-v4.0 including:

5.1.2.1 Imaging Characteristics for the Collimated Preconstruction Design
5.1.2.2 Ray-Trace Sensitivities for the De-collimated Preconstruction Design
5.1.2.3 Initial-Alignment Error Parameters

The current Zemax prescription for the construction optical design in direct-imaging mode is DIFF21_DIRECT.IMAGING.ZMX as previously mentioned. For the purpose of sensitivity analysis, the construction collimator and camera designs that it contains are virtually identical to the preconstruction designs. Thus, no useful purpose would be served by repeating those labor intensive calculations and reporting them here at length. For all intents and purposes, the resulting information would be the same as we have already documented in PDR Report-v4.0.

#### 5.1.3.1 Practical Application

The results reported in section 5.1.2.3 of PDR Report-v4.0 do not constitute a "Tolerance Table" for MOSFIRE's alignment. Obviously, there will be a large number of other factors that will contribute to the so-called error budget, such as manufacturing errors, errors in axial lens-locations, "cross-talk" between the individual alignment errors, various systematic effects (such as a whole group of lenses being decentered and/or tilted as a unit). Moreover, if some lenses can be aligned more accurately than the parameters in PDR Report-v4.0 would suggest, then others can be aligned a bit less accurately. As in all prototype situations, we will polish and measure the lenses as carefully and accurately as possible, within the limitations imposed by practical technology. Likewise, we will machine and measure each and every mechanical part accurately, while we have it in the lathe or on the mill. Our goal is to fabricate and to assemble the opto-mechanical units such that they work as designed, without the need for adjustments.

#### 5.1.3.2 Flexure Compensation

In practice, MOSFIRE will flex under variable gravity loading. The sensitivity Table 8 shown in PDR Report-v4.0 can be used to assess the amount of image motion and additional rms image

diameter degradation that various flexure-induced decenters and tilts will cause. Image motion can be compensated by tilting the fold-mirror, which follows Col #1, by controlled amounts.

Detailed flexure compensation calculations for the *preconstruction* optical design are presented in section 5.1.2.5 of PDR Report-v4.0. For the purpose of flexure compensation analysis, the construction collimator and camera designs are still virtually identical to the preconstruction designs. Thus, again, no useful purpose would be served by repeating those calculations and reporting them here. For all intents and purposes, the resulting information would be the same as we have already documented in PDR Report-v4.0.

### 5.1.4 Modeling, Simulations and Prototyping

In addition to the ray tracing, sensitivity analysis and thermal modeling already mentioned, we have also undertaken the construction and evaluation of lens cells and various techniques for installing and aligning the optics. This activity is described in the mechanical section 5.2.1.7.

### 5.1.5 Performance Predictions

Spot diagrams have been produced for the most important instrument configurations. Image quality in imaging mode and in spectroscopic mode exceeds the requirements. In fact, the construction design allows for additional spectroscopic field, which will be made accessible through appropriate mechanical design and construction of the CSU.

### 5.1.6 Risk Identification and Risk Mitigation

A primary source of risk in the optical design has been mitigated by purchasing optical blanks in advance. With the exception of single-crystal CaF2 lens blanks for Col #1 and Cam #2, which are on order and will be delivered by Canon-Optron in early August 2007, we have two blanks on on hand for each lens element in the science optics except the Infrasil-302 blank for Col #4, the CaF2 blank for Cam #1 and the BaF2 blank for Cam #5. In each of those cases, we have one blank on hand.

There is a risk of schedule slippage if damage occurs during production of the science optics. A new Infrasil-302 blank for Col #4 could be obtained from Heraeus in about 2 months time. A CaF2 replacement for Cam #1 could be obtained from Schott in about 3 months time. However, it would contain 5 to 10 multiple grain boundaries and we have not been able to determine how those boundaries may (or may not) affect the opto-mechanical performance of the lens. A BaF2 replacement for Cam #5 could probably be obtained from Naked Optics in 2 to 3 months time but it would also contain multiple grain boundaries. Replacement material is not available from our primary supplier, Saint Gobain in Solon, Ohio as that company is no longer in business. The current MOSFIRE optics budget does not contain money for replacement blanks.

Coatings will also be a source of risk. Our 0.975 μm to 2.40 μm spectral range is nearly 2.5 octaves wide, which is similar to the familiar broad (0.39 μm to 1.0 μm) optical passband found in instruments such as ESI. Hardened, multi-layer dielectric coatings will be required to cover that

wavelength range. They should be applied with a sputtering, ion-assisted technology so as to avoid excessive heating of our crystalline lens materials and S-FPL51, where cracking can easily be caused by less than gentle *cooling* in particular. Properly equipped coating vendors are few in number and heavily scheduled. Pricing is astronomical in most cases as well. We intend to rely on the ability of our primary science optics production vendor to be able to muster the services of his regular coating sub-contractor(s) in order to get our coatings done in a safe, timely and cost-effective manner.

We are ready now to write our RFQ for the science optics production and tender it to 5 prospective vendors within the coming few weeks. Those are COSI, OSI, JANOS, ZYGO, and the UCO/Lick Optical Laboratory. We anticipate that we will have a production contract in place by mid-June 2007 such that it appears we are roughly 3 months ahead of schedule at the present time, relative to our mid-June 2008 delivery target date for the finished optics.

### 5.1.7 Open Issues

There are only a few open issues that will be addressed specifically in the near future as follows:

1. We need to decide upon reflective coatings for the flat science optics, which were polished by TORC and are ready now to be coated. This is not urgent but it needs to be done. Over-coated silver is the most likely choice.

2. We need to pursue possible ways to put pressure on NASA so as to get the CHARMS measured cryogenic index data for CaF2.

3. We need to receive the additional cryogenic index measurements from the M3 group, to evaluate them, and decide whether or not our present provisional construction optical design should be updated.

4. We need to execute a detailed ghost image and ghost pupil analysis for the "final" construction optical design and modify it (slightly), if necessary, to mitigate whatever ghosts (if any) are found. It is not anticipated that detector ghost images will be problematic as those are monitored and controlled on-the-fly by Oarsa during the optimization process. However ghost pupils off of the detector as well as double-bounce ghost images and ghost pupils could be present and must be mitigated if found.

5. We must consider coatings carefully during the solicitation and review of RFQ responses from potential science optics vendors. Coatings have been identified as a high-risk factor due to high cost, unavailability of suitable sub-contractors and the possibility of breakage of our thermally sensitive lens materials such as CaF2, BaF2 and S-FPL51.

6. We must decide whether or not to purchase spare CaF2 lens blanks for Col #1 and Cam #2 from Canon-Optron right away so as to avoid a potentially large schedule slippage should one or both of those blanks get damaged during the lens polishing and coating processes. If so, additional funding

will be needed as there is no money for that or for other replacement blank purchases in the current MOSFIRE optics budget.

7. We must come to some viable plan regarding the issue of "tolerances." We would all love to have an "error budget" with "slack" but in Epps' opinion, it is not productive to imagine that we can find such items for MOSFIRE with Monte Carlo techniques. It is Epps' opinion (perhaps not shared by everyone) that in his 40+ years of experience in designing and building one-of-a-kind optical instruments, he has found that 100% of the time when they fail, it is because of: 1) engineering errors of concept or execution, and/or 2) measurement errors that could and should have been avoided. The corollary to that experience is that 100% of the time they turn out to work acceptably well if they are: 1) designed creatively and correctly, and 2) manufactured to "machine shop" tolerances. Nothing else matters. It's as simple as that, although achieving the desired goal often takes a mountain of dedicated hard work and the willingness to endure years of "what if we did it wrong" anxiety.

## 5.2 Mechanical Design

All of the major mechanical elements of MOSFIRE now exist in detailed designs, including completed detailed analysis, that establish the mechanical performance (flexure and optical mounting tolerances), thermal behavior, and the weight and balance of the entire instrument. Approximately 50% of the shop drawings are completed. The remaining components and assemblies have completed detailed design CAD models of sufficient detail to obtain fabrication budgetary estimates and plan the fabrication schedule.

### 5.2.1 Description

A sectional side view of MOSFIRE is shown in Figure 21. MOSFIRE is designed for mounting at the Cassegrain position of the Keck I telescope. This focal station imposes strict space envelope limitations as well as requirements to cope with varying gravity vectors during operation. The instrument design must meet specific weight and balance requirements and provide definition points compatible with the existing defining points used for the Low Resolution Imaging Spectrometer (LRIS) instrument on Keck I.

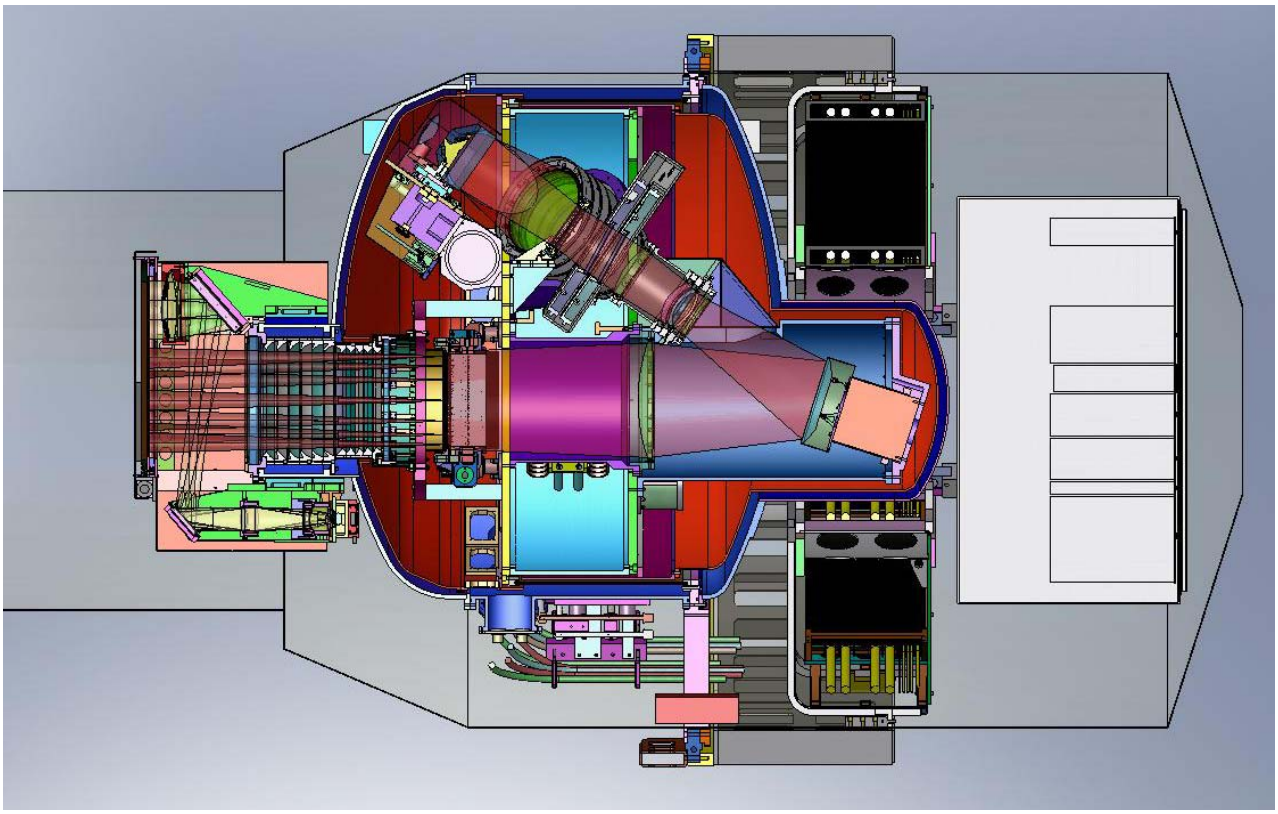

**Figure 21: Section View of MOSFIRE**
The thin black outline indicates the Keck I Cassegrain envelope limits.

#### 5.2.1.1 Overall Layout and Constraints

Our basic approach for MOSFIRE is to attach a cylindrical vacuum enclosure (the dewar) to a rotator module that is a copy of the one used for LRIS. The dewar is sized to encapsulate the folded optical design and to fit within the Cassegrain space envelope. Following the product structure shown in Figure 12, the dewar is divided into "cold" sub-systems which reside inside the vacuum enclosure, and "warm" sub-systems that are located on the outside. All of the cold sub-systems are mounted from a thermally isolated internal structure or frame.

The light path through MOSFIRE begins with the dewar window system that is comprised of an outer window that forms the pressure seal and a cooled, inner window located well inside the dewar. Heated baffles and cooled baffles are located between the pair of windows to keep the outer one close to ambient temperature while maintaining the thermal performance inside the instrument. Light then passes through a cryogenic configurable slit unit (CSU), which is located at the Keck I telescope focal plane. The beam expands towards a collimator that is split into two parts, a field lens and a five-element lens barrel assembly. Between these two parts within the collimator, the optical path is folded with an articulated mirror that can be utilized for flexure compensation. Light exits the collimator lens barrel and passes through the filter wheel before reaching the pupil wheel. After the pupil, the optical path is folded a second time by the grating/mirror exchange turret. Finally, light enters the camera optics and arrives at the H2-RG detector.

The warm sub-systems include a dust cover unit, guider unit, and a calibration lamp unit at the front of the instrument. Vacuum fittings are also located near the front of the instrument on the front cover of the dewar. At the rear, a large cable wrap assembly and a doublewide electronics cabinet are attached behind the dewar. Closed-cycle refrigerator heads and hermetic feed-through ports are positioned around the cylindrical body of the dewar.

As can be seen from Figure 21, MOSFIRE fits within the limits of the Keck I Cassegrain envelope. A weight budget has been established and Table 10 gives the current status of the design relative to the conceptual and preliminary design estimates. Our weight estimate for the final design is ~25% over the original goal of 4000 lbs, and ~14% over the current goal of 4400 lbs. This is due predominantly to an under-estimate of the shield weight during the conceptual design and the electronics cabinet weight during the preliminary design phase. Also, the window sub-system has grown in complexity and weight. Efforts made to balance the instrument with respect to the bearing axis with strategic component placements have not been completely successful and an additional 376 pounds of counter-balance weights will be required to position the CG on the bearing axis. The remaining axial CG offset, relative to the bearing plane, appears to be acceptable based on analysis and is comparable to the axial offset of LRIS.

The maximum allowable weight for MOSFIRE, assuming that MOSFIRE's module weight is comparable to previous versions, is 5051 lbs. Our current weight estimate of 5021 lbs is below this maximum. Currently, the MOSFIRE module weight estimate is 2200 lbs, which is ~270 lbs less than the module weight used to determine MOSFIRE's maximum limit. So there is a margin on the combined weight limit, but the module design is still being analyzed to determine whether it meets rigidity requirements for MOSFIRE. If it needs to be reinforced, this margin could go away. As a

contingency plan to further reduce MOSFIRE's weight if necessary, we have approached Physik Instrumente to shorten the length of the FCS tip-tilt stage. They have responded favorably that the unit can be shortened by 70 mm. Such a reduction in the length will allow the rear protrusion of the dewar to be shortened. The cable wrap width is also excessive and could be narrowed. With these two changes, the electronics cabinet could be moved within the cylindrical portion of the space envelope and offset in the direction of the imbalance to help shift the instrument CG. All of these changes should result in a significant weight reduction, if needed.

| Sub-System/Sub-Assembly | Conceptual Design Weight Estimate (lbs.) | Preliminary Design Weight Estimate (lbs.) | Current Design Weight Estimate (lbs.) | Difference (lbs) (Relative to Conceptual) | Difference (%) (Relative To Conceptual) | Comments |
|---|---|---|---|---|---|---|
| Vacuum System | 137 | 137 | 21.5 | -115.5 | -84.31 | No onboard pumps, model weight is 11.5 lbs |
| Cable Wrap | 315 | 325 | 270 | -45 | -14.29 | Includes space for extra pair of helium lines |
| Collimator Assembly | 80 | 61.5 | 40 | -40 | -50.00 | Glass=11.25 lbs. |
| Camera Assembly | 155 | 127 | 129.5 | -25.5 | -16.45 | Glass=66.7 lbs. |
| Internal Structure Assembly | 810 | 804 | 786 | -24 | -2.94 | |
| Detector Mount Support Assembly | 25 | 25 | 15 | -10 | -40.00 | model weight is 6.5 lbs |
| Field Lens Assembly | 35 | 32 | 32 | -3 | -8.57 | Glass= 21.3 lbs. |
| Filter Wheel Assembly | 95 | 85 | 93.8 | -1.2 | -1.26 | |
| Optical Baffle Assemblies | 30 | 30 | 30 | 0 | 0.00 | Collimator Barrel Baffle = 3 lbs. |
| Pupil Mechanism Assembly | 15 | 14 | 16 | 1 | 5.00 | |
| FCS Assembly | 32 | 37 | 34 | 2 | 5.62 | Mirror= 7.3 lbs; stage= 17 lbs |
| Guider System | 100 | 95 | 103 | 3 | 3.00 | Glass= 26.5 lbs |
| Getter | 0 | 0 | 5 | 5 | | Weight not inclded in conceptual budget |
| Thermal Strapping Assemblies | 75 | 75 | 87.9 | 12.9 | 17.20 | Thermal straps= 40 lbs; 48 straps/main CCR |
| CSU | 77 | 77 | 90.6 | 13.6 | 17.71 | |
| Calibration Lamps & Power Supplies | 0 | 0 | 30 | 30 | | Not designed yet, added after PDR |
| Grating/Mirror Exchange Assembly | 98 | 106 | 126.9 | 28.9 | 29.49 | Mechanism for second grating added after PDR |
| Dust Cover Assembly | 25 | 55 | 65 | 40 | 160.00 | Includes Guider Assembly Cover |
| Vacuum Chamber | 1260 | 1295 | 1306 | 46 | 3.62 | Includes port covers w/ connectors |
| Cold Head Assemblies | 80 | 148 | 226.4 | 146.4 | 183.00 | Inc: cold plate extensions, mounts, and 34 lbs. each of balance weight |
| Window Assembly | 30 | 60 | 185.5 | 155.5 | 518.33 | Glass= 29 lbs; includes heater & inner window mount |
| Electronic Cabinet & Cabling | 400 | 469 | 576.5 | 176.5 | 44.13 | Cabinet= 189 lbs; Electronics=289 lbs; plus cabling/hoses=100 lbs |
| Shield Assemblies | 125 | 450 | 374.9 | 249.9 | 199.92 | Initial shield weight under-estimated |
| Instrument Counterweights | 0 | 0 | 375.9 | 375.9 | | |
| **Total Weight** | 3999 | 4508 | 5021 | 1022 | 25.55 | Goal= <4400 lbs. |
| **Total Weight (w/out Counterweights)** | | | 4645 | 646 | 16.15 | |
| **Cold Weight** | | | 2047 | | | |
| **CG Location (relative to bearing CL):** | | | | | | Model weight used in CG calculation= 4487/4863 lbs. |
| *Nominal Wrap Position :* | *w/out Cweights* | *W/ Cweights* | | | | |
| X Position (in) | -0.7 | 0.2 | | | | |
| Y Position (in) | 2.9 | 0.0 | | | | |
| Z Position (in) | 5.1 | 4.6 | | | | |
| *Clockwise 260 Wrap Position:* | | | | | | |
| X Position (in) | 2.7 | -0.2 | | | | |
| Y Position (in) | -0.1 | -0.4 | | | | |
| Z Position (in) | 5.0 | 4.5 | | | | |
| *Counterclockwise 270 Wrap Position:* | | | | | | |
| X Position (in) | -3.2 | -0.3 | | | | |
| Y Position (in) | -0.6 | 0.3 | | | | |
| Z Position (in) | 5.0 | 4.5 | | | | |

**Table 10: MOSFIRE Weight Budget**

### 5.2.1.2 Dust Cover

Both the entrance window to the dewar and the guider optics must be protected from dust and damage when the instrument is not in use. The guider and the "snout tube" containing the window are enclosed in a lightweight enclosure of sheet metal. A motorized sliding door closes off this enclosure at the front of the instrument and guider optics. The door is fabricated from an aluminum honeycomb panel so that it is lightweight, yet strong and impact resistant. It is supported by a pair of roller slides and actuated by a magnetic hybrid step motor linear actuator (Figure 22). Industrial switches provide end of travel limits. To reduce the chance of injury to personnel, the drive speed and drive force are adjustable. In addition, a safety contact strip is attached to the leading edge of the door. When an object is in the door's path, the contact strip cuts power to the door actuator. The actuation force is 5 kg and the actuating distance is 4 mm. Both the leading edges of the door and the opposing doorframe have large surfaces to minimize pinching as the safety contact strip is actuated. Finally, the dust cover will be interlocked to prevent it from opening unless the

instrument is mounted on the telescope, but an override mode will also be provided to allow local control of the door for servicing.

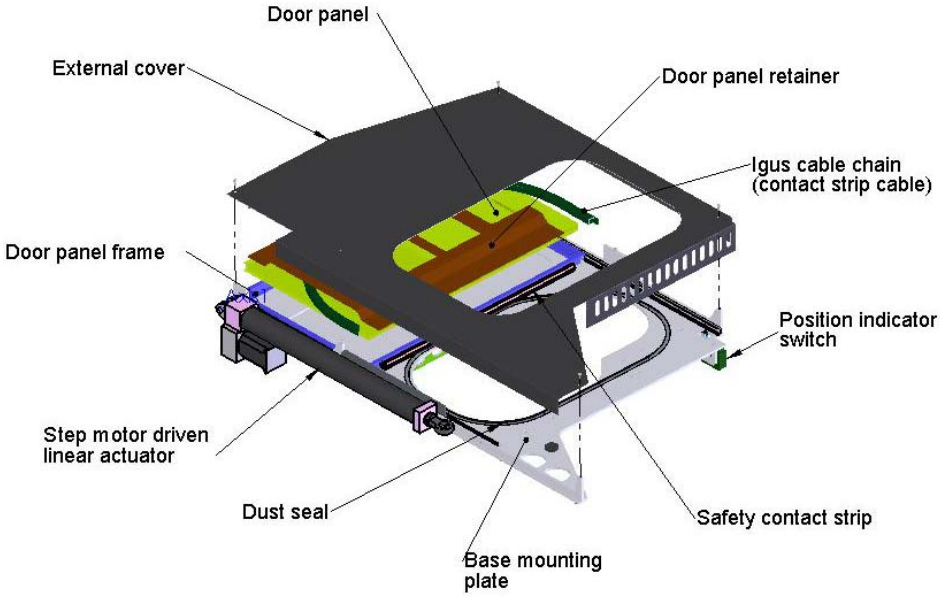


**Figure 22: Dust Cover Assembly Components**

A sample of the door panel material has been tested. It was supported in a similar fashion to the way the door will be mounted. A 3-m length of schedule 80 1-1/4 inch pipe was dropped on the panel to simulate WMKO's impact requirement in order to assess the strength of the panel. The test results indicate that the door panel can withstand an impact more that 6x the requirement before the pipe breaks all the way through the panel. Under the required impact, the outer panel skin was slightly dented (Figure 23), but the entire door panel remained flat and thus operable. Details of the complete test set-up and results are described in MMDN12.

**Figure 23: Pipe Impact Test Results**

Performance of the dust cover is considered nominal if it opens or closes in ~8 s, although faster transit times are possible. The actuation force will be adjusted such that a small margin exists over the force required to operate the door in all applicable gravity orientations. This is a redundant safety measure in order to minimize the chance of serious injury.

We will use the inside surface of the dust cover door as a screen for calibration arc lamp projection. Two pairs of "Penray" lamps (Argon & Neon) will be mounted on opposing sides of the snout aimed at the dust cover door as shown in Figure 24. The lamps and their power supplies will be contained in sheet metal enclosures that span between the dust cover and the front cover of the dewar.

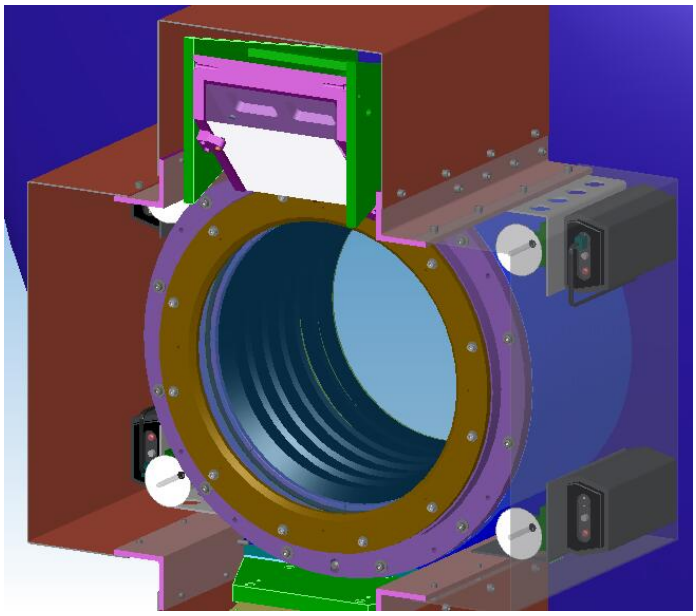

**Figure 24: Location of Four Calibration Arc Lamps**

Because the dust cover mechanism is at ambient temperature, the entire unit was not prototyped. It is constructed of mostly commercially available components and can be maintained and serviced easily. However, as the unit is intended to protect the dewar window from catastrophic damage, the strength of the door panel was thoroughly tested with a prototype. Due to its lower risk and priority, the manufacturing drawing package is not yet completed.

#### 5.2.1.3 Guider Unit

MOSFIRE's guider unit will be mounted on the front of the dewar along the snout tube that contains the window as shown already in Figure 21. The design of the dewar front shell and snout tube take into account the need to minimize motion of the guider field with respect to the CSU that is mounted on the dewar's internal structure. Utilizing the window snout as a strong-back for the guider components helps minimize instrument weight.

The guider is split into two sub-assemblies that are mounted on diametrically opposite sides of the vacuum window. To stay within the Cassegrain envelope, the optical design had to be folded into a Z-shape. This approach also keeps the guider components close to the snout, minimizing additional flexure within the guider assembly. The first sub-assembly in the guider contains a large doublet lens and the first fold mirror, whereas the second sub-assembly contains the second fold mirror, the

rest of the lenses, the filter, the focus mechanism, and the CCD detector package. Since PDR we have upgraded the focus mechanism to a precision, motorized unit to support WMKO's new guider requirements.

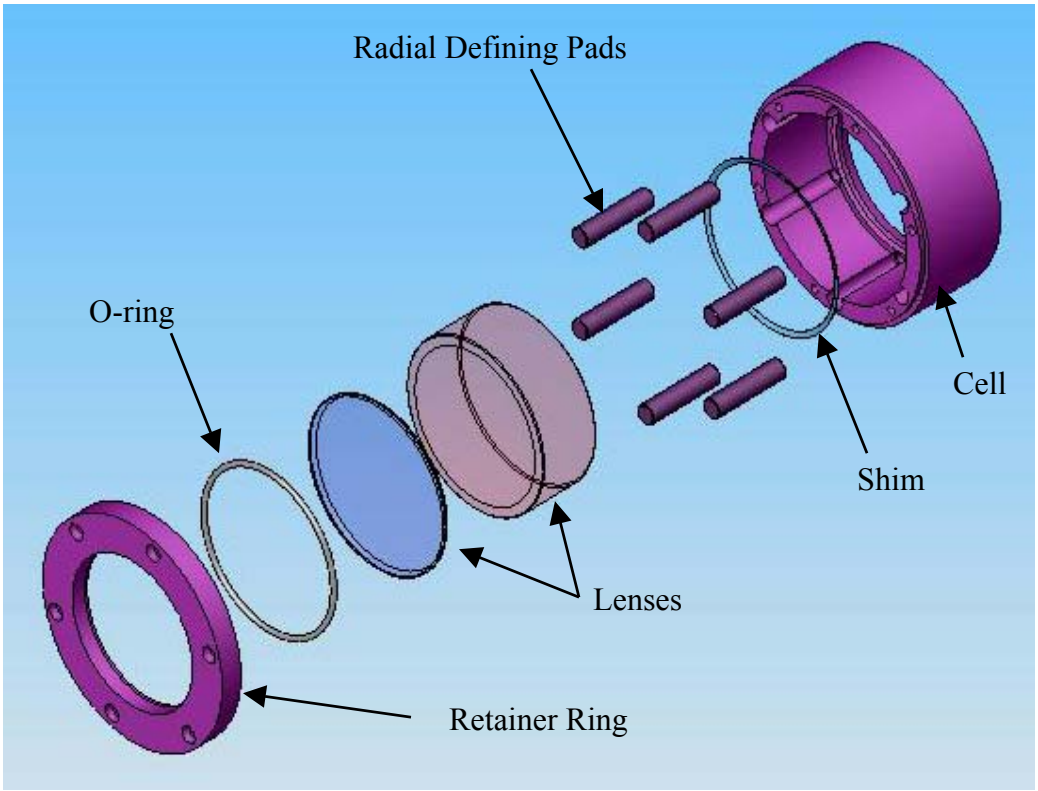


**Figure 25: Typical Guider Lens Cell Assembly**

Lens mounts for the Guider are based on designs utilized for the LRIS red and blue cameras. As shown in Figure 25 each lens will have radial support provided by a series of Delrin dowels that are installed in pockets in aluminum cells. The combination of material selection and dowel sizing results in essentially athermal radial support over the design temperature range and "spring-loading" of the lenses against Kapton washers with soft silicone o-rings provides axial support. MMDN27 describes the cell design, support calculations, and FEA in more detail.

For the fold mirrors, we utilize a six-point kinematic definition system designed for supporting and defining dichroics and grisms in LRIS. One of the guider fold mirror cells based on the LRIS design is shown in Figure 26. This design consists of spring-loading the optic against six adjustable hard-points. Polished tungsten-carbide reaction pads are bonded to the mirror substrates to prevent excessive contact stress in the substrate and to help reduce friction. The spring-plungers are Delrin-tipped to reduce friction. This kinematic mount design allows easy adjustment of the mirrors during integration. Force-balance equations needed to size the spring-plungers already existed from the LRIS work. Performance of the LRIS optics confirms the validity and accuracy of the design. This mount design ensures that the optics will maintain definition throughout the intended temperature range and will re-define their position if disrupted by accelerations. The force balance calculations and FEA results for the mirror mount design are given in MMDN27.

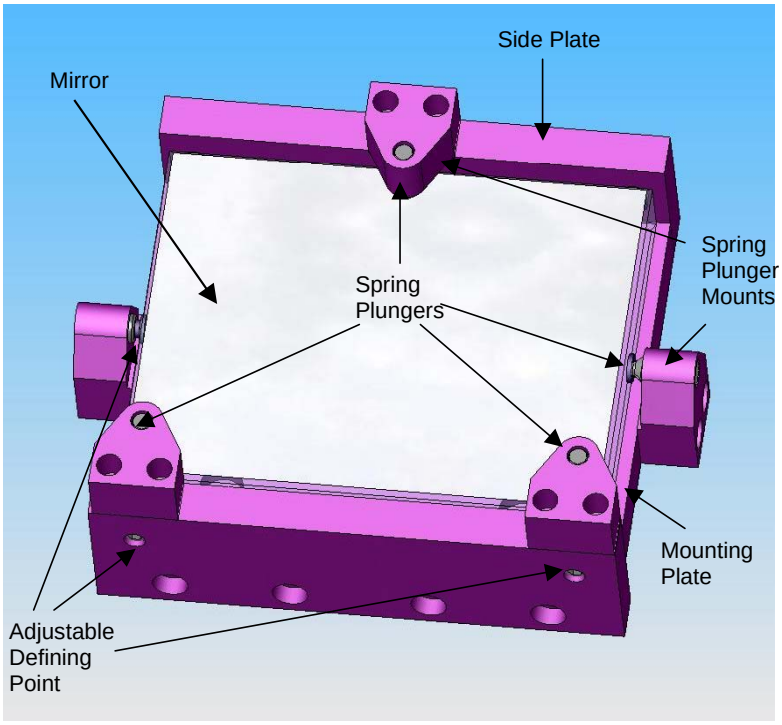


**Figure 26: Guider Fold Mirror Cell**

The optical prescription of the guider requires lens #5 to move back and forth along the optical axis to adjust the focus on the guider detector. Requirements for the focus mechanism performance were defined by WMKO such that MOSFIRE is compatible with the new facility guider program (MAGIQ). These requirements include a wavefront sensing cycle at a maximum rate of once every 5 to 7 minutes throughout the observing period. This requirement makes the focus mechanism wear and lifetime requirements more difficult to achieve. An appropriately robust stage and actuator were selected from Newport Corp. The items selected are the LTA-HL Motorized Actuator, and the UMR8.25 Linear Stage. These components are commercially available in case of the unlikely event of failure.

The CCD package selected for the guider is a CCD4720-BT from E2V Technologies. In the standard package for these detectors there is a window forming a hermetic package with an integral thermoelectric cooler (TEC). The guide camera head for MOSFIRE will be based on the standard SciMeasure Analytical Systems “Little Joe” camera, selected by WMKO for the MAGIQ program. SciMeasure will make a custom hermetic camera head so that a non-hermetic CCD4720-BT with TEC can be used, allowing the field flattener of the MOSFIRE guider optics to be mounted in the position defined by the optical prescription, very close to the detector focal plane. The MOSFIRE field flattener will form the front window of the hermetic camera head.

Since the guider optics mounts are based on previous successful designs by members of the MOSFIRE team the fabrication and assembly of the guider assembly is not considered a high risk item. Due to its lower priority, the drawing package for the guider assembly has not been

completed, but the CAD model in combination with the previous experience is sufficient to estimate fabrication costs.

#### 5.2.1.4 Dewar Window

A major challenge for an infrared instrument such as MOSFIRE with a large field of view is the presence of a large vacuum window that attracts condensation due to radiative cooling to the interior of the dewar. One solution that has been employed is to blow a continuous stream of dry $N_2$ over the vacuum window. However, as the size of the window increases, the $N_2$ becomes increasingly turbulent and much more likely to mix in moist air, affecting the image quality of the instrument. MOSFIRE will incorporate an alternative approach using a baffled internal radiator to keep the vacuum window at ambient temperature.

As illustrated in Figure 27, the dewar entrance window is actually a double window with a thicker outer window providing the vacuum seal, and a second inner window serving to help limit the thermal radiation that reaches the CSU masking bars. A snout tube extension of the dewar aids in thermal isolation of the instrument by increasing the separation between the windows and the CSU, thus reducing the viewing angles between the windows and the CSU. A heater element is located between the windows within the snout tube. This heater is constructed of coated aluminum rings with unique profiles to efficiently heat the window while minimizing the heat directed to the rear window and the CSU. The ring surfaces facing the window are coated with black paint and the surfaces facing the interior of the instrument are plated with gold. The heater baffle assembly consists of strip heaters attached to the outer wall and covered with MLI. Attachment of the heater baffle assembly to the snout is insulated to minimize heat transfer to the dewar walls, which therefore minimizes the heater power requirements as the heat is restricted to radiating to the window and snout interior rather than also trying to heat the dewar walls.

The inner window is in vacuum and acts as a radiation boundary with an intermediate temperature between ambient and the temperature of the internal optical components. Thermal studies indicate that the heat load on the CSU masking bars needs to be minimized. Consequently, the inner window is positioned at an optimized location further into the dewar interior and it is mounted from bulkhead A with columns fabricated from 1100 aluminum. The inner window mount is designed to pull as much heat from the inner window as possible and channel it to the cold head attachment locations on bulkhead A. A cold baffle, similar in design to the heater assembly, forms a shield along the optical path between the heater and the inner window. This assembly also has profiled aluminum rings to act as a cold baffle. These baffle profiles are reversed relative to the heater, as are the coatings, in order to reflect the incoming heat. The cold baffle assembly is firmly attached to the inner window support structure to channel incident heat around the window and CSU to the cold head attachment locations on bulkhead A.

Further details of the thermal aspects of the double-window design are discussed in §5.2.1.10 of this report.

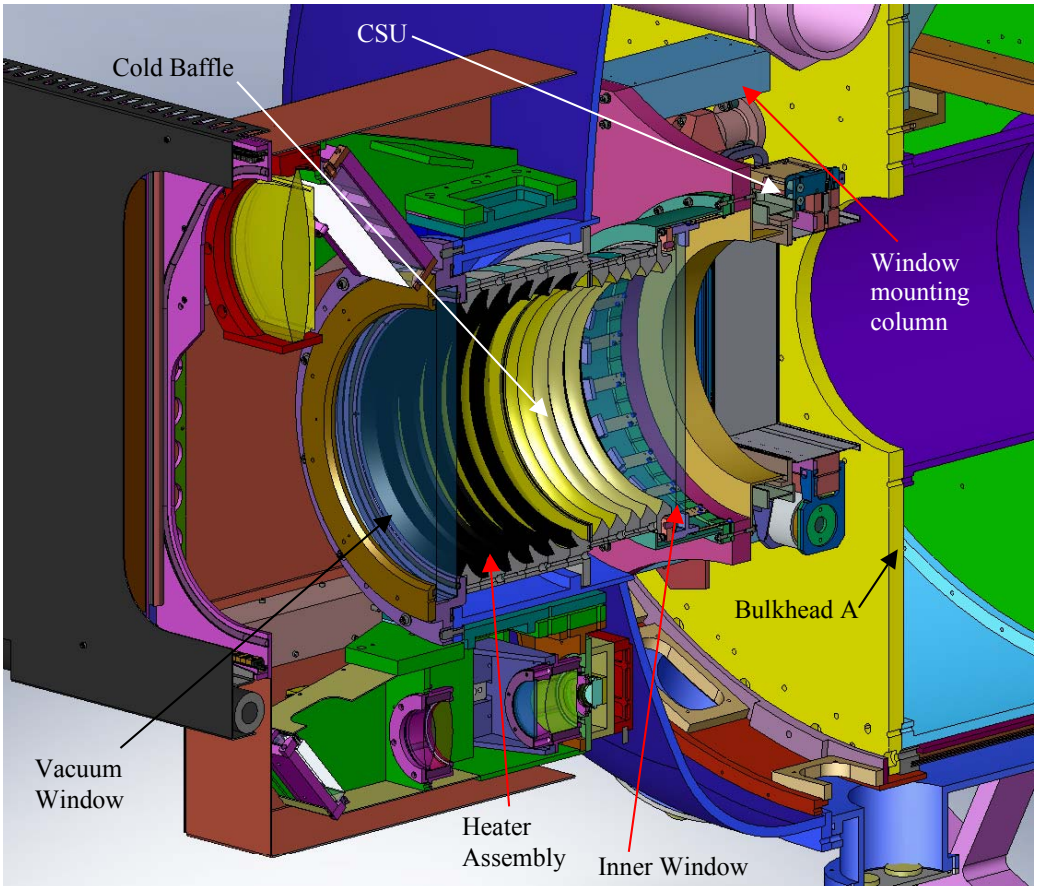


**Figure 27: Double Window Design**

The dewar window system can be broken down into three subassemblies: vacuum window mount, inner window mount, and heater assembly. Both the vacuum window mount and the heater assembly will attach directly to the snout. As described in the optics section, both of the windows will be fabricated from Infrasil. The diameter of the vacuum window is 388 mm in order to accommodate the 6.8′ diameter field of view and provide adequate room for the o-ring seal.

For the inner window the diameter is smaller at 372 mm and it is supported by 24 cantilever flexures constructed of 1100 aluminum. These flexures provide a conductive thermal path from the edge of the window while also compensating for the differential contraction between the window and the surrounding aluminum structure. The window is clamped to the flexures as shown in Figure 28 and it rests on aluminum supports. Indium washers are located between the window and the supports to provide maximum thermal conduction. Spring plungers provide a clamping force to the window and establish consistent thermal contact pressure. The plungers react on aluminum pads to minimize contact stresses on the window. An aluminum foil strip is placed between each retainer pad and the window. Each strip is also clamped to a window support flexure. The aluminum foil strip serves as a thermal path for the clamped face of the window.

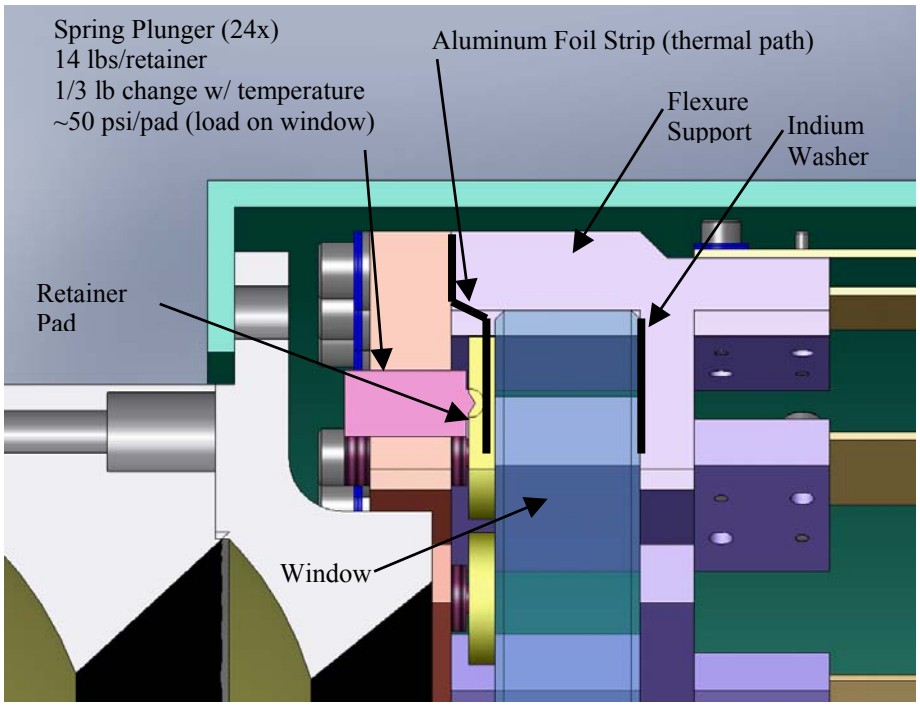


**Figure 28: Inner Window Mount**

Analytical and finite element methods were used to optimize the front window thickness. The thickness affects both vacuum-induced stress levels and temperature distributions. Analytic methods were used to determine a safe thickness for withstanding atmospheric pressure. The two cases of a clamped and a simply supported window were compared for completeness. Satisfactory performance was confirmed in terms of stress and flexure for a vacuum window thickness of ~35 mm. The goal was to keep the window stresses below 500 psi.

Thermal optimization was contracted to SDL during the detailed design phase. The goal of this study was to heat the window(s) by radiation to maintain a maximum 2 °C differential between the temperature of the center front surface of the vacuum window and the outside ambient. SDL's analysis indicates that a low power level (17.6 W) is all that is required to maintain the temperature above the Observatory dome ambient in order to prevent condensation from forming on the outer surface of the window. The inner surface of the inner window stabilizes at a temperature of ~165 K and the resulting heat load on the CSU is estimated to be ~0.3 W. The selected heater design provides additional margin since the heater power can be adjusted easily during integration and testing to compensate for any imperfections in the analysis. In addition, the radiative heater design has no moving parts and requires no service. Again, further details of the thermal analysis are described in §5.2.1.10 of this report.

Performance predictions are summarized as follows:

- Maximum vacuum window stress = 400 psi
- Maximum vacuum window deformation = 28 μm
- Maximum required heater power = 17.6 W

#### 5.2.1.5 Dewar Shell

MOSFIRE's optics must be maintained at low temperature to meet background requirements, which results in the majority of the instrument's components being housed within a cryogenically cooled vacuum enclosure referred to as the "dewar". Because MOSFIRE is a Cassegrain instrument, it will experience a varying gravity vector during operation. The instrument's guider unit will be located externally on the snout containing the entrance window to the dewar, and special attention must be given to minimizing relative motions between the guider and the CSU inside the dewar. The vacuum shell must safely resist the atmospheric pressure load in combination with the loads of external components and also have sufficient stiffness to keep the relative motion between internal components within acceptable limits.

To meet these requirements, a tubular vacuum shell was chosen based on its efficiency under vacuum loads combined with its uniform stiffness under radial bending loads. Likewise, the internal structure support is also tubular. The tubular-shaped shell efficiently fits the cylindrical envelope of the Cassegrain location on the telescope and accommodates the internal structure. The design is such that *both* the internal structural support tube and the external dewar barrel have one common end attached to an instrument mounting "ring" structure (Figure 29).

The instrument mounting ring is a machined steel structure that bridges between the instrument and the inner race of the instrument's rotator module. By having both the internal structural support tube and the vacuum shell barrel anchored at the same place, the two tubes sag consistently under radial gravity loads.

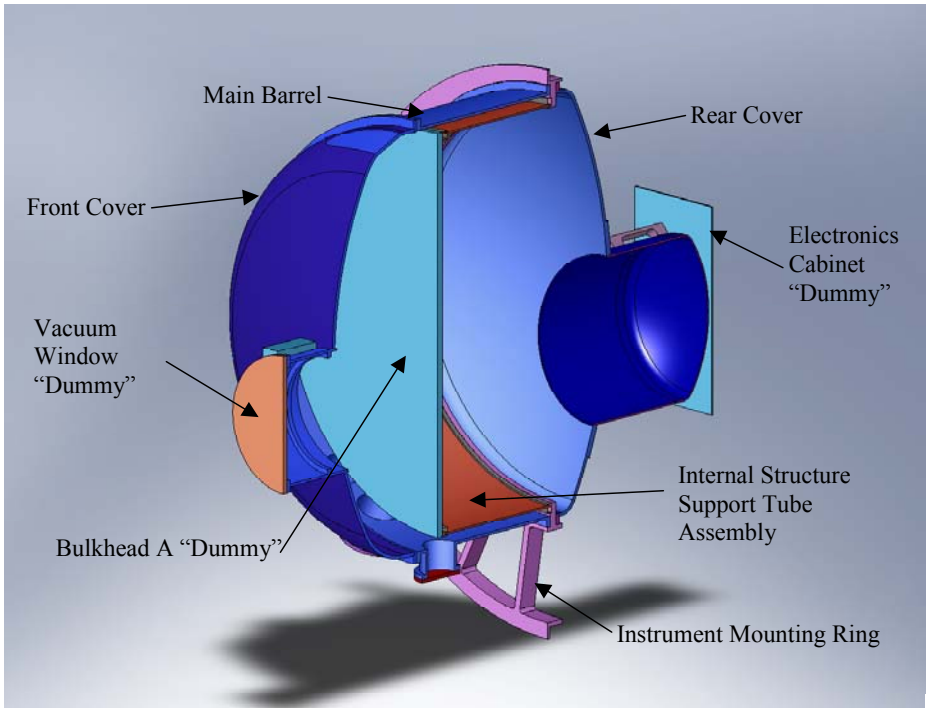


**Figure 29: Cross-section View of the Dewar Vacuum Shell Model used for Analysis**

The dewar has tori-spherical vacuum end-caps at both ends. Each end cap is removable for servicing, and the intent of the design is to make all of the mechanisms accessible for servicing after removal of either the front or the rear end cap. Both end caps are shaped for vacuum loading efficiency. This shape also helps to minimize the vacuum shell weight in order to fit within the Cassegrain focus weight budget. The front end cap has a cylindrical "snout", or protrusion, extending from it that contains the dewar's double entrance window. As mentioned above, the double window design is placed as far forward of the CSU as possible to minimize thermal loading on the slit mask. The design of the rear cap is similar. It is also tori-spherical in shape and has a cylindrical protrusion that houses the flexure compensation system (FCS). The cable wrap fills the space between the rear protrusion and the surrounding rotator module.

#### 5.2.1.5.1 Design Analysis

General results of the vacuum shell FEA studies are summarized in Table 11. This spreadsheet summarizes the maximum ranges of flexure that are due to changing gravity vectors. The spreadsheet also includes the maximum stresses for the vacuum chamber and the instrument mounting ring observed in the studies. Results are shown for load cases without vacuum and at atmospheric pressure. Most of the results are within the design goals, and all are within the requirements when certain limitations of the FEA model are taken into consideration. The chamber strain is clearly dominated by the load due to atmospheric pressure when the peak stresses in the electronic cabinet supports under gravity loads are rationalized. The FEA results indicate that, even with 5 g acceleration, the combined maximum stress would still remain safely below the material yield stress since the component due to gravity-induced loads is generally less than 1/3 of the stress due to the vacuum load. The vacuum load isn't influenced by instrument shocks during handling or earthquakes. Details of the analysis and results are included in MMDN11.

The maximum expected range of relative flexure between the guider assembly and the CSU mounting surface is indicated at the top of Table 11. Internal flexure within the guider assembly and the CSU is not included in this analysis or the tabulated results, but flexure of the instrument's internal structure is included. Guider and CSU flexure, evaluated separately, were estimated to be negligible relative to the vacuum chamber flexure. The CSU bar flexure is negligible in the X and Z directions, but the masking bars have been estimated to flex up to 160 μm with gravity in Y when a bar is fully extended (edge of field). The design goals in the table are equivalent to 0.1" of relative motion, while the requirement is equivalent to 0.3" of relative motion. In all cases but one, the relative flexure is predicted to be less than half of the goal. For the relative Y displacement, the estimate is approximately twice the goal, but still lower than the requirement, with margin. The maximum estimated stresses are displayed at the bottom of Table 11. Components whose failure could cause serious personnel or equipment damage are required to have safety factors of 10 on ultimate strength, per WMKO's guidelines. While most of the listed safety factors don't appear to meet this requirement, careful consideration of FEA model simplifications indicate that the maximum stresses will be lower in reality than predicted with the analysis tools. In addition, the FEA simulations used 15 psi atmospheric pressure, while the normal operating pressure will be ~ 60% of this.

While the relative flexure between the guider and CSU are important as previously explained, it is also important that the displacements and tilts of the guider and CSU don't deviate excessively from the instrument rotator axis (and the telescope axis) due to general sagging of the instrument under gravity loads. Analysis indicates that the instrument focal surface will have a maximum radial variation of ~ ±70 μm and a maximum axial variation of ~ ±80 μm. The pointing of the instrument is estimated to vary by a maximum of ~ ±92 μrad. Note that flexure within the CSU mechanism is not included in this assessment. Note also, that the predicted flexure of the rotator module was not available for this analysis and will surely increase these values. Additional FEA studies that include the module and bearing are in progress.

It should be noted that the vacuum chamber flexure due to atmospheric pressure is substantial. Radial flexure of the walls was up to 0.2mm and axial flexure was up to ~ 0.7 mm in certain regions. In general, this flexure is not important in terms of instrument performance. But, some displacements of the chamber are of interest in regards to guider assembly position. Some relative displacement of the axial spacing between the guider and the CSU would be expected due to the atmospheric pressure. The analysis predicts ~ 555 μm decrease in the spacing under vacuum. But due to the off-axis position of the chamber's window (and the guider) in the Y direction, the front cover also flexes in a way that results in –204 μm Y displacement and 131.5 μrad of pitch.

The vacuum chamber structure is loaded in a fashion that could cause buckling. Buckling analysis was completed for the six main features of the vacuum chamber using shell elastic stability equations from Roark & Young. All of the features have a wall thickness that will withstand more than 10 times the nominal pressure of 15 psi without buckling. In several cases, the safety margin is even greater since material is added to control flexure.

There were three main risks concerning the dewar design that were re-assessed during the detailed design phase. All three risks were interrelated. The risks were: 1) excessive flexure of the external guider, 2) excessive weight, and 3) fabrication difficulties/costs. The FEA addressed the first two risks and validated the dewar's cylindrical design. Guider flexure has remained at an acceptable level. The vacuum shell's weight was maintained within 4% of earlier predictions despite a slight lengthening of the structure and the addition of ports and other features. To address the third risk, potential fabricators have been consulted during the detailed design and RFQ process. Their ideas were incorporated into the design in several cases. The fabrication drawing package for the dewar has been completed and utilized in the RFQ and design refinement process. An example drawing from this package is shown in Figure 30.

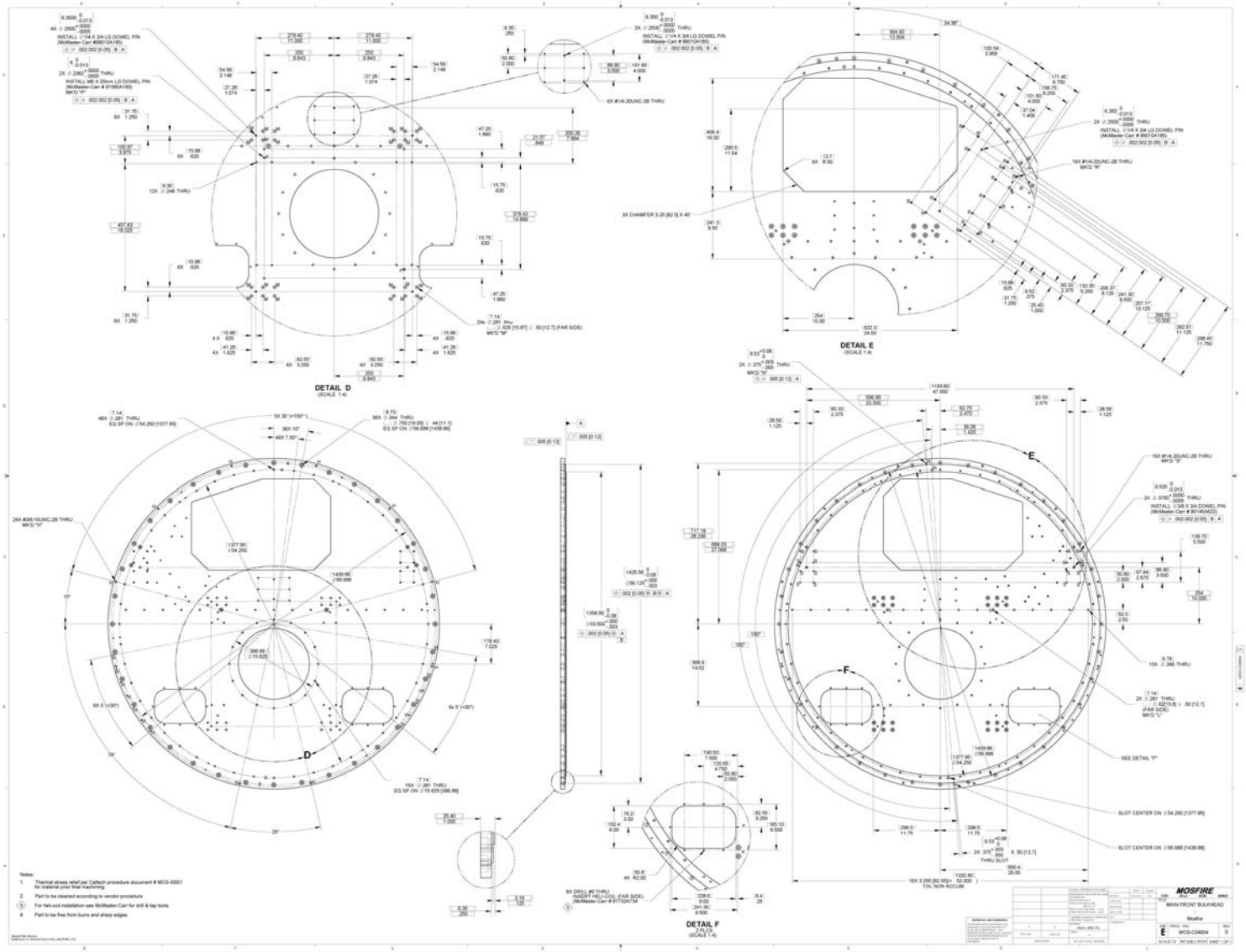


**Figure 30: Representative Fabrication Drawing of Internal Structure Component used for Vendor Quotations**

| Maximum Values | | | |
|---|---|---|---|
| **Parameter** | **Guider Relative to CSU W/ Instrument Structure Flexure** | **Design Goal (0.1")** | **Design Requirement (0.3")** |
| **Displacements:** | | | |
| X Displacement (± µm) | 17.6 | 36.3 | 108.8 |
| Y Displacement (± µm) | 76.7 | 36.3 | 108.8 |
| Z Displacement (± µm) | 14.1 | 36.3 | 108.8 |
| **Tilts:** | | | |
| Roll {about Z} (± µrad) | 6.1 | 96.7 | 290.0 |
| Pitch {about X} (± µrad) | 20.0 | 42.5 | 127.5 |
| Yaw {about Y} (± µrad) | 17.2 | 42.5 | 127.5 |

| **Stress:** | **Value** |
|---|---|
| Vacuum Chamber at Atmospheric Pressure | 4980 psi |
| Safety Factor on Ultimate (6061-T6 Al) | 8.4 |
| Vacuum Chamber Under Vacuum | 5601 psi |
| Safety Factor on Ultimate (5083-O Al) | 7.5 |
| Instrument Mount Ring at Atmospheric Pressure | 3255 psi |
| Safety Factor on Ultimate (A 36 Steel) | 17.8 |
| Instrument Mount Ring Under Vacuum | 10000 psi |
| Safety Factor on Ultimate (A 36 Steel) | 5.8 |

**Table 11: Summary of Vacuum Shell FEA Results**

#### 5.2.1.6 Internal Structure

The Internal Structure supports all of the internal sub-assemblies and mechanisms. It also serves as a thermal conduit for uniformly removing heat through the instrument's refrigerators. Cooled shields are firmly attached to the main bulkheads (or optical benches) at strategic locations surrounding the internal structure.

##### 5.2.1.6.1 Design Description

As with other Cassegrain instruments, the structural design of MOSFIRE must provide sufficiently uniform stiffness to maintain optical alignment through all possible gravity vectors. The MOSFIRE internal structure design primarily consists of two ~1500 mm diameter circular plates or optical benches, joined by a pair of nested, short tubes (Figure 31). This "stubby drum" assembly is suspended inside the cylindrical vacuum chamber by a concentric G-10 fiberglass cylinder that surrounds the internal structure. The thin G-10 cylinder serves as a thermal insulator between the cryogenic internal components and the vacuum shell at ambient temperature. Each of the optics assemblies and internal mechanisms are attached to one or other of the two optical benches. The tubular shape of the internal structure results in consistent radial flexure of the structure as the instrument is rolled about its cylindrical axis while it's horizontal. Also, the small length to diameter ratio of the structure results in relatively small radial displacements between the

two optical benches and between the internal structure and the vacuum chamber as the instrument is rotated and elevation is changed from zenith to the horizon.

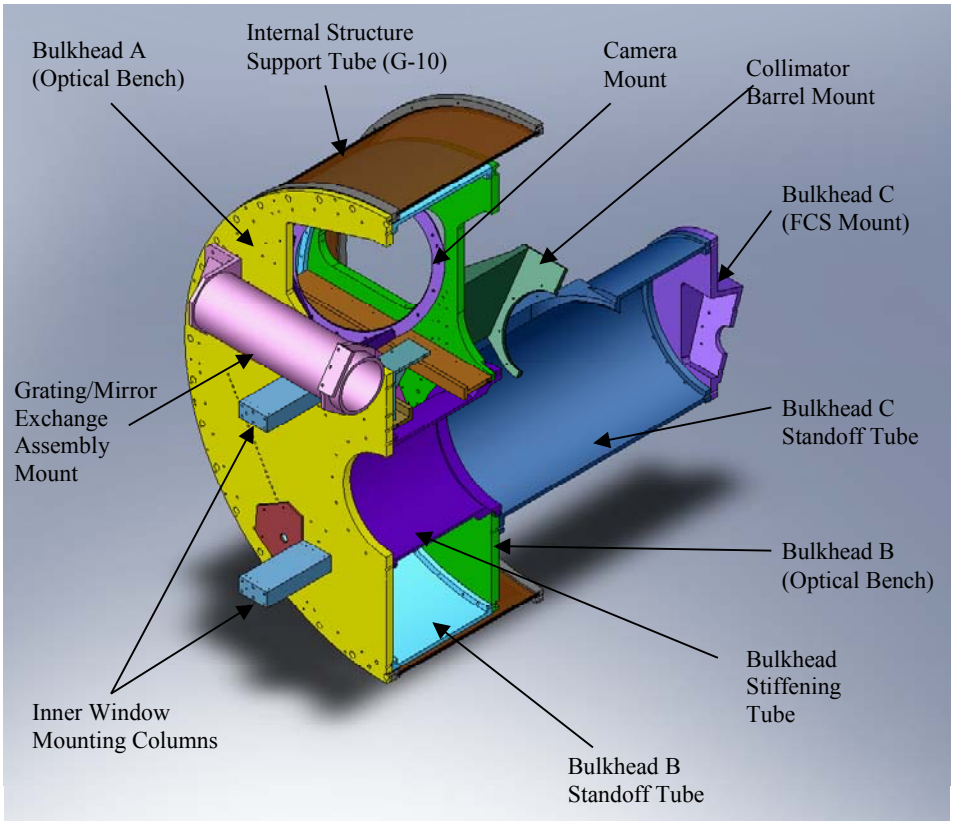


**Figure 31: Cross-Section View of the MOSFIRE Internal Structure Design**
All of the optic assemblies and mechanisms are mounted from one of the three bulkheads.

#### 5.2.1.6.2 Design Analysis

The internal structure was analyzed by FEA methods to estimate the stability of the structure under varying gravity loads (Figure 32). Flexure analysis shows that this structure is very rigid and exhibits generally consistent radial flexure as the instrument rotates about the optical axis. The small length to diameter ratio of the double cylinder construction serves to constrain displacements between the two optical benches and between the inner structure and the dewar. The results of the analysis are summarized in Table 12 and Table 13. The full analysis report is located in MMDN08.

The estimated maximum flexure-induced image motion is summarized in Table 12. Values listed in this table do not include the flexure estimates of the sub-assemblies attached to the structure. The values in Table 12 may be interpreted as follows. The first component listed is the CSU. This device is located at the telescope focal surface and is the reference point for all other motions, either directly or indirectly. The CSU does move and tilt as the instrument moves through the range of gravity orientations. The flexure estimates of the CSU are listed in red for reference. These motions are subtracted out in the table such that the other component's motions are all

relative to the CSU motions for a given load case. The next section of the table is for the field lens mount and the flexure compensation mount surface located along the optical axis between the CSU and the first fold mirror. Displacements listed (both axial & radial) are relative to the CSU. The tilts are relative to the instrument coordinate system with the CSU tilts subtracted out. Concerning the field lens position, for example, it is predicted to vary by a maximum of ±1.84 µm axial and ±3.74 µm radial from a nominal position relative to the CSU over the instrument's entire range of gravity orientations. Maximum predicted ± ranges for pitch, yaw, and roll are listed, as well.

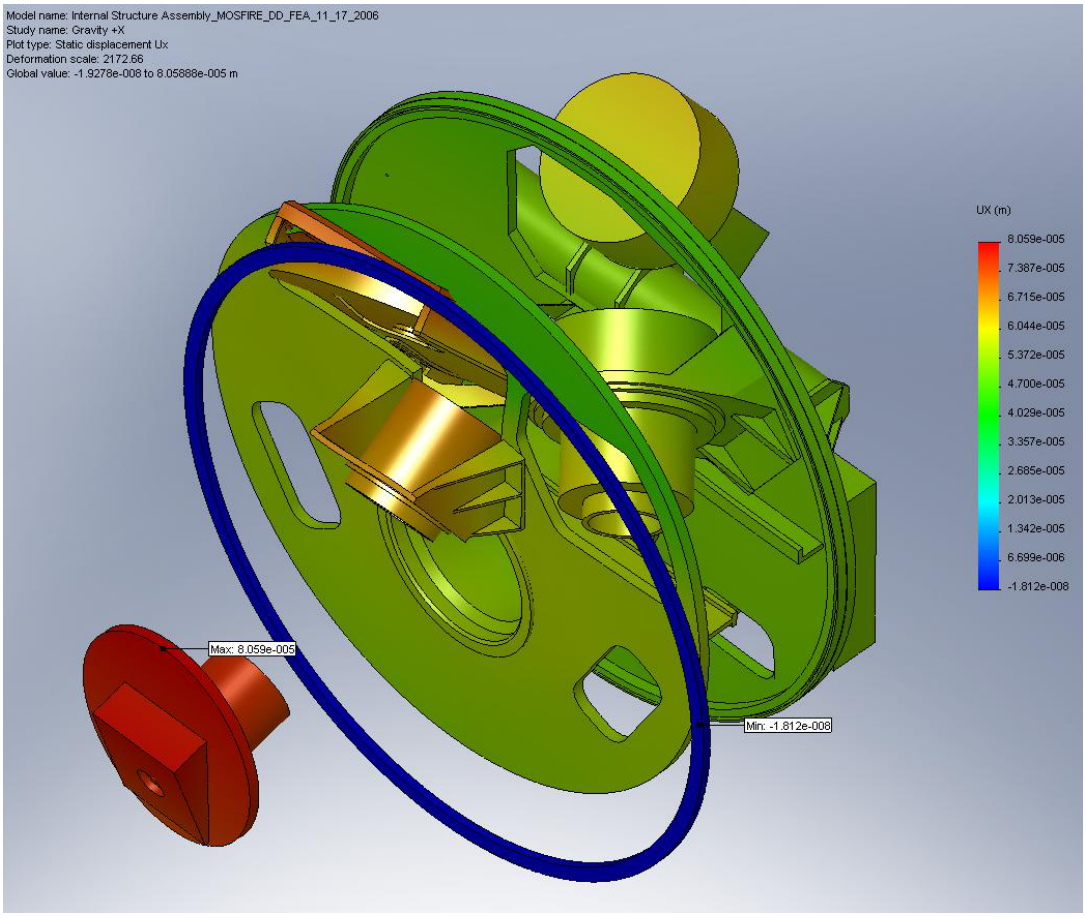


**Figure 32: Example of Internal Structure FEA Displacement Results Plot**
This image shows the X displacement estimate for gravity in X.

The third section of Table 12 lists the motions of the internal structure reference points for the optics/mechanisms between the first fold mirror and the grating. For these four items, the displacement reference coordinate system shifts from the CSU to the flexure compensation mount. The optic axis folds for these next four components, and a local coordinate system is created to follow the optic axis in order to calculate displacements and tilts that are relative to the folded optic axis. This coordinate change allows easier transfer of the data into optical simulations that can assess the impact of the component motions on image motion and image degradation. For these four components, the predicted displacement and tilt ranges are relative to the shifted position of the flexure compensation mount. Note that the shifted position of the flexure

compensation mount already has the CSU motion subtracted. Also, despite the convention in optical simulation software for the Z-axis to switch directions at folds (mirrors), the instrument and local coordinate systems maintain the same general direction (towards the telescope) on all segments of the folded optical axis.

| Maximum Values | | | | | | |
|---|---|---|---|---|---|---|
| | | | | | | |
| | Motions Relative to Gravity in Z (Instrument Axis Vertical) | | | | | |
| | Local Coordinate System {for ZEMAX input} | | | | | |
| Component | Axial Displacement (+/-um) | X Displacement (+/-um) | Y Displacement (+/-um) | Pitch (+/-urads) | Yaw (+/-urads) | Roll (+/-urads) |
| CSU: | 24.49 | 53.20 | 59.11 | 12.64 | 2.38 | 0.92 |
| | Motions Relative to CSU | | | | | |
| Field Lens Mount: | 1.84 | 3.74 | 1.95 | 11.90 | 14.97 | 2.88 |
| Flexure Comp Mount: | 1.83 | 20.69 | 13.97 | 10.88 | 12.45 | 16.66 |
| | Motions Relative to Flexure Comp Mount | | | | | |
| Collimator Barrel Dummy: | 3.83 | 10.29 | 12.64 | 16.13 | 13.77 | 2.32 |
| Filter Wheel Dummy: | 53.02 | 10.44 | 3.37 | 56.31 | 113.98 | 23.00 |
| Pupil Mechanism Mount: | 7.35 | 19.91 | 14.44 | 14.07 | 3.51 | 9.37 |
| Grating Mechanism Dummy: | 12.85 | 14.20 | 1.15 | 42.57 | 20.03 | 3.56 |
| | Motions Relative to Grating Mount | | | | | |
| Camera Barrel Dummy: | 2.18 | 8.94 | 13.18 | 29.43 | 31.28 | 29.60 |

**Table 12: General Results from the Internal Structure Flexure Analysis**

The final section of Table 12 lists the motion of the camera. Here, the displacement and tilts reference coordinate system is the shifted position of the grating mechanism dummy. The local coordinate system folds with the optic axis to follow through the camera to the detector. The detector is assumed to be rigidly attached to the exit of the camera barrel so the camera motion influences its motion. The table lists the maximum range of expected axial, radial, and tilt motion of the entrance to the camera relative to the shifted position of the grating mechanism.

| | Spectroscopic Mode | | | Imaging Mode | | |
|---|---|---|---|---|---|---|
| Gravity Vector | Y Motion (pixels) | X Motion (pixels) | Roll (pixels) | Y Motion (pixels) | X Motion (pixels) | Roll (pixels) |
| Gravity in +X (Relative to Zenith) | 1.734 | 1.561 | -0.117 | 1.839 | 2.337 | -0.073 |
| Gravity in -X (Relative to Zenith) | 1.876 | 0.472 | -0.058 | 1.923 | 0.814 | -0.094 |
| Gravity in +Y (Relative to Zenith) | 0.748 | 0.897 | -0.056 | 0.727 | 1.794 | -0.054 |
| Gravity in -Y (Relative to Zenith) | 2.866 | 1.137 | -0.119 | 3.036 | 1.357 | -0.113 |

**Table 13: Estimates of Uncorrected Image Motion From Flexure Accounting for Direction of Flexure**

Our requirement (goal) is ~0.3 (0.1) pixel flexure over 2 hours (Table 1). Assuming that we can reduce the flexure amplitude by 10:1 with a relatively simple tip/tilt mirror, the uncorrected flexure should not exceed 3 (1.0) pixels. The flexure analysis results were entered into spreadsheets that were used in combination with optic flexure sensitivities to predict resulting image motion. The spreadsheet calculations include internal flexure estimates for the grating/imaging mirror mechanism and the flexure compensation system (FCS) obtained in separate studies. Internal flexure within the collimator and camera barrels has not been included, since analysis of the bonded flexure supports indicates negligible flexure within the barrels (< 3 μm displacements, < 25 μrad tilts). Flexure of the detector mount was estimated and included.

Values in Table 13 may be interpreted as follows. Gravity induces significant flexure on this large structure no matter which gravity orientation is selected. The flexure analysis results for any given gravity orientations are relative to the absence of gravity. We will be assembling and adjusting the optical alignment of the instrument during integration with the instrument axis in the vertical direction (zenith). Therefore, the flexure analysis results indicate the relative flexure between

instances when the instrument axis is parallel to the horizon versus the case when the axis is vertical. In addition, there are slight variations in the predicted image motion depending on whether the grating or imaging mirror is deployed. Some of the variation is due to minor stiffness differences in the grating and mirror support. Some is due to the inclusion of the grating motion in some modes (i.e. roll) that affect image motion where similar mirror motions have no effect.

Roll induced motion is not correctible with the FCS, so the goal for roll induced motion is 0.1 pixels over 2 hours. The requirement is 0.3 pixels. Image motion estimates for roll are at the detector edge. To convert the 2 hour observing period into maximum gravity vector variation, it is assumed that 2 hours is less than a 30 degree instrument pointing change in all cases. As the motion estimates in the tables are for 90 degree gravity vector changes (zenith to horizon), a 2 hour equivalent (30 degrees) will be less than ½ the table value in all cases. The X and Y image motion predictions are due to the combination of tilts and decenters of optics.

These calculations indicate that the maximum correctible flexure-induced image motion will be ~3 pixels for full sky coverage. The maximum estimated correctible image motion over any 2 hour period is 1.5 pixels. These motions are due mostly to tilts of the grating turret and camera barrel, with only a small portion due to radial displacements of optics. The spreadsheet calculations indicate that the requirement (3 pixels/2 hours) will be satisfied with 10:1 compensation, but we didn't quite reach our design goal of 1 pixel per 2 hour period.

Uncorrectable image motion due to flexure-induced optic roll motions is estimated to be ~ ±0.06 pixels at the edge of the detector with full sky coverage. The requirement allows more than twice this (±0.15 pixels) over any 2 hour period. The roll flexure nearly meets our goal of ±0.05 pixels.

The flexure compensation system's tip/tilt stage has a specified range at 77 Kelvin of ±500 μrads, which is equivalent to ±6.2 pixels. The spreadsheet calculations indicate that this stage will have more than adequate range to compensate for flexure through the telescope's full range of motion.

The main risks associated with the MOSFIRE mechanical assembly are that it will be too flexible or that it will be too expensive or difficult to manufacture. Flexure performance has been addressed through extensive analysis. Manufacturability concerns have been addressed through interaction with potential fabricators throughout the design process. While the internal structure is large, the design doesn't include any features that are overly difficult to fabricate. A complete drawing package of the internal structure is completed and has been used in the RFQ process with potential vendors.

#### 5.2.1.7 Lens Mounts

Lens mounts must hold the lenses in place to the required mounting tolerances while allowing for differential expansion and contraction during cool down cycles. For large optics like those used in MOSFIRE, typical approaches based on compliant cells can easily result in excessive stress on the optics. A large optic mount based on tangential "flexures" has been refined, prototyped and tested during the detailed design phase. This mount has been shown to provide consistent radial and axial motions of the lens element with negligible hysteresis as the mount is rotated and tilted. The lenses

are separated into two groups, the Collimator group and the Camera group. The Camera group has an interface to the Detector Head and the Collimator is subdivided into the Field Lens assembly and the 5-element Collimator Barrel. The partial section in Figure 33 shows the relative locations of these lens groups.

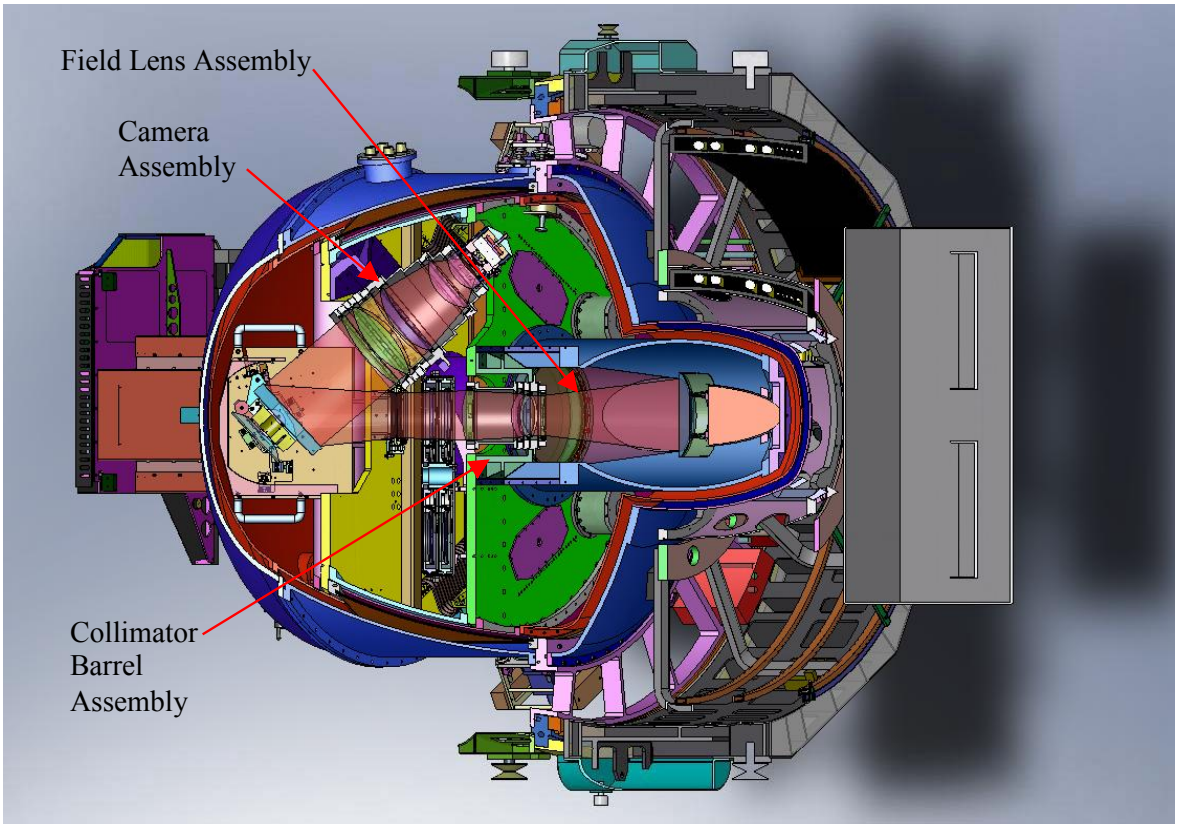


**Figure 33: Partial Section View of MOSFIRE Through the Collimator and Camera Barrels**

#### 5.2.1.7.1 Individual Lens Mounts

Each lens will be mounted in a sub-assembly or cell. A typical cell is shown in Figure 34. The lenses are supported by multiple flexures that are attached at one end to the lens cell ring and at the other to the lens itself. Figure 35 shows the basic components that form a flexure assembly. Attachment at the lens is through an epoxy bonded interface pad. The pad material for each lens is a metal that is closely matched in CTE to the lens material. Table 14 shows the final interface pad selections to match the MOSFIRE optical materials. Interface pads are attached with screws to flexure strips fabricated from beryllium copper sheet. The opposite ends of the flexure strips are attached to cylindrical copper inserts with more screws. Each copper insert fits into a pocket in the aluminum cell and is secured in place with screws during assembly.

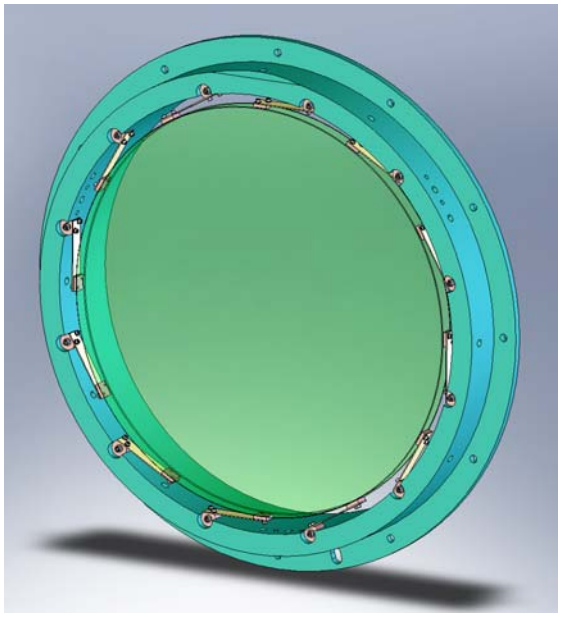

**Figure 34: A Representative Lens Cell Assembly with Multiple Bonded -Flexures and Mounting Ring**

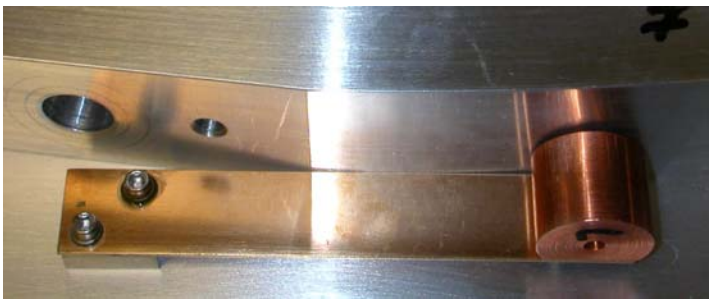

**Figure 35: Close Up View of a Typical Beryllium Copper Flexure**

| | Material | Weight (lbs) | Diameter (in) | Center Thickness (in) | Girdle Thickness (in) | Number of Lens Mounts | Lens Mount Size (in) | Avg Pad Load with 5G axial accel (lbs) | Mounting Pad Material |
|---|---|---|---|---|---|---|---|---|---|
| Collimator #1 | Calcium Fluoride | 21.26 | 13.90 | 1.85 | 0.51 | 12 | 7/16 x 1/2 | 8.86 | Copper, UNS C42500 |
| | | | | | | | | | |
| Collimator #2 | Calcium Fluoride | 1.28 | 5.46 | 0.32 | 0.57 | 6 | 1/2 x 1/2 | 1.07 | Copper, UNS C42500 |
| Collimator #3 | Zinc Selenide | 1.42 | 5.20 | 0.32 | 0.26 | 6 | 3/16 x 1/2 | 1.18 | Titanium Alloy Beta-21S |
| Collimator #4 | Fused Quartz | 0.86 | 5.35 | 0.32 | 0.47 | 6 | 5/16 x 1/2 | 0.72 | Allegheny Ludlum AL 36, UNS K93600 |
| Collimator #5 | Barium Fluoride | 3.20 | 5.83 | 0.79 | 0.38 | 6 | 1/4 x 1/2 | 2.67 | Copper, UNS C42500 |
| Collimator #6 | Calcium Fluoride | 4.42 | 6.54 | 1.40 | 0.76 | 6 | 1/2 x 1/2 | 3.68 | Copper, UNS C42500 |
| | | | | | | | | | |
| Camera #1 | Calcium Fluoride | 9.83 | 10.94 | 1.22 | 0.48 | 12 | 5/16 x 1/2 | 4.10 | Copper, UNS C42500 |
| Camera #2 | Calcium Fluoride | 18.4 | 10.83 | 2.95 | 0.38 | 12 | 5/16 x 1/2 | 7.67 | Copper, UNS C42500 |
| Camera #3 | S-FTM16 | 12.07 | 10.35 | 0.28 | 2.01 | 12 | 1/2 x 1/2 | 5.03 | Stainless Steel Type 430 |
| Camera #4 | I-FPL51 | 11.02 | 9.96 | 1.50 | 0.44 | 12 | 5/16 x 1/2 | 4.59 | Special Metals MONEL™ Alloy R-405 |
| Camera #5 | Barium Fluoride | 9.14 | 7.48 | 1.89 | 0.33 | 10 | 1/4 x 1/2 | 4.57 | Copper, UNS C42500 |
| Camera #6 | Barium Fluoride | 6.26 | 7.17 | 1.97 | 1.25 | 8 | 1/2 x 1/2 | 3.91 | Copper, UNS C42500 |

**Table 14: Final Lens Mount Design Parameters**

#### 5.2.1.7.2 Multiple Lens Cell Assemblies

As mentioned, there will be two sub-assemblies with multiple lens cells, the Collimator Barrel and the Camera Barrel. The alignment and interface methodology for these two units is the same. Figure 36 shows an exploded view of the Collimator Barrel and Figure 37 shows the Camera Barrel. Where distances between individual cells are relatively large, simple spacer tubes fill the gap. Axial positioning/alignment will be achieved through high tolerance interface surfaces on the lens cell "rings" and radial alignment through high tolerance overlapping steps in the rings. The cells are assembled together with a bolt pattern arrangement. Individual cells have adjustable spacer shims installed at each cell-to-cell interface and the spacer thickness can be altered at the last minute to account for as-built lens variations. In addition, these spacer shims have their internal diameters sized to serve as optical baffles within each barrel.

In most cases, the required tolerances for parallelism, concentricity and flatness needed to achieve the required performance are not much more stringent than standard machining tolerances. In a few cases, however, there are cell-to-cell tolerances that will require machining features of assembled and pinned parts as a unit. This level of accuracy is certainly achievable from precision machine shops. Prototypes of several cells have been fabricated during the detailed design phase. These prototypes have been utilized to practice the lens cell alignment, flexure bonding, and assembly procedures. Precision, "dummy" lenses made of aluminum were used for the prototype assemblies. Inspection and measurement of the assembled prototypes has confirmed that the necessary lens positioning tolerances can be consistently achieved with the MOSFIRE design.

Once assembled, the Collimator and Camera units will be light tight along their outer surfaces. However, stray light propagating through the optical system will need to be baffled. Several implementations of various forms of baffles will be used throughout the optical system. As mentioned, the collimator and camera barrels will include baffles as shown in the illustrations. Structures within the lens assemblies, such as the flexure assemblies, result in surfaces that can reflect stray light, leading to ghosting and/or an increase in general background radiation. Mounting baffle rings to mask these surfaces precludes this. The baffles as well as the internal surfaces of the lens cell "rings" will be painted infrared black using either Aeroglaze Z306 or WZ3301. These paints have been used successfully in NIRSPEC, NIRC2, and OSIRIS.

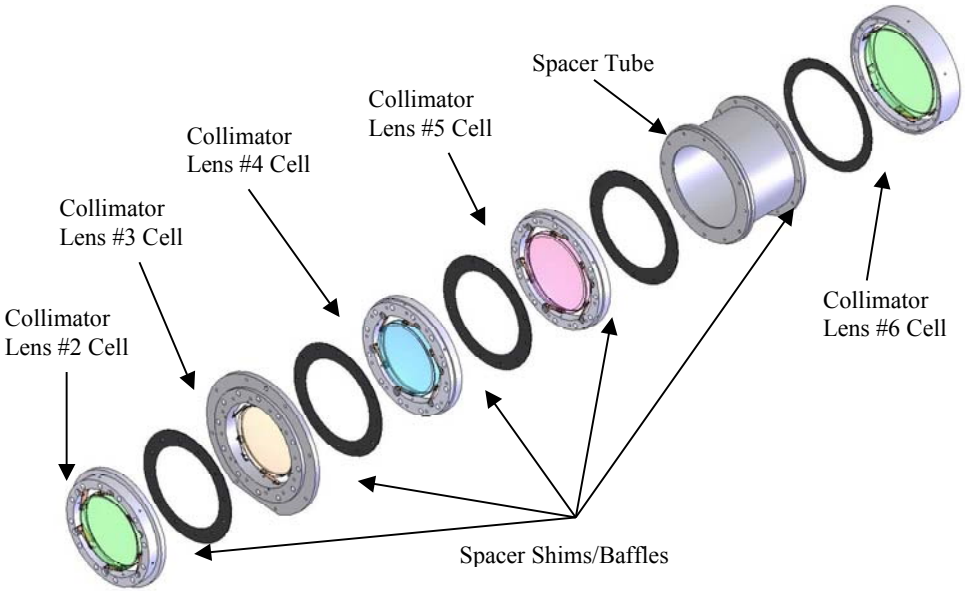


**Figure 36: Collimator Barrel Assembly**

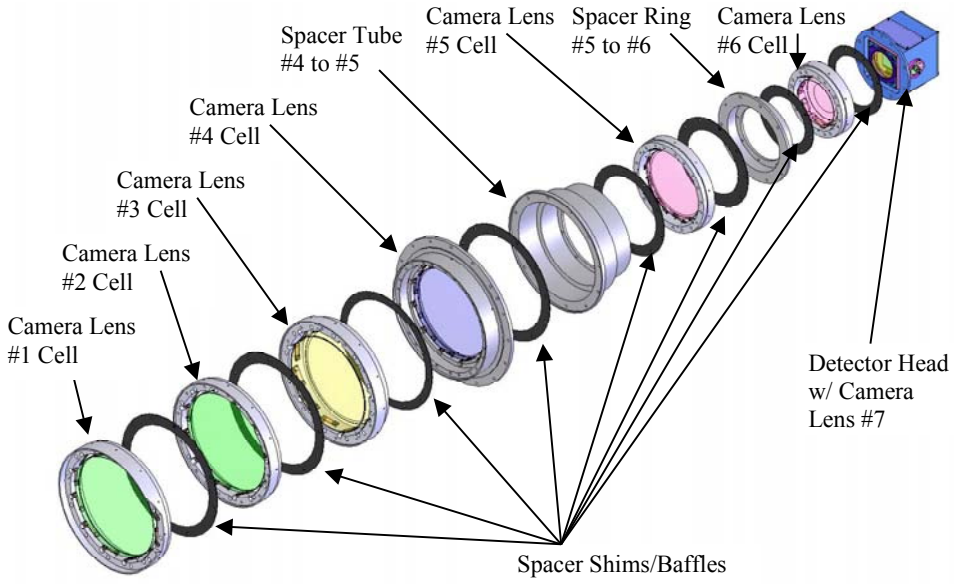


**Figure 37: Camera Assembly**

The Collimator and Camera barrels are attached to the instrument structure with mounting brackets (visible in Figure 33). These brackets have precision-machined features which properly align the lens assemblies during integration. Both the collimator barrel and camera assembly have precision, stepped flanges that interface with a precision bore in each mount bracket. This interlocking geometry determines centration and axial position of the optics with respect to the bracket. The base of each bracket has flat surfaces that define a plane and pins that define the position on the plane. These features correlate to machined regions on the main bulkheads of the structure.

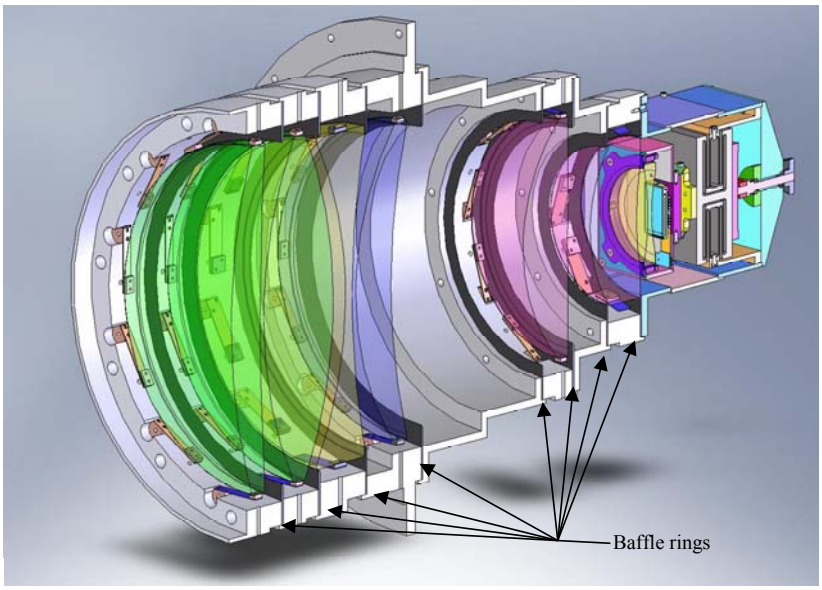


**Figure 38: Section View Showing Camera Barrel Assembly Light Baffles**

#### 5.2.1.7.3 Lens Mount Analysis

The proposed lens mounting method was analyzed extensively in the preliminary design phases of both MOSFIRE and its predecessor, KIRMOS. Analysis indicated that stresses in the lenses and flexure components were within acceptable limits and the flexure within each cell would be very low. But, the analysis results and limited bond testing performed earlier did not provide sufficient evidence of bond integrity in all cases. Therefore, during the detailed design phase of MOSFIRE, efforts were focused on bond strength testing, rather than analysis. Tests results were then compared to estimated bond-pad reaction forces from the earlier analysis to determine bond strength safety factors for each of the individual lens cells. Table 15 summarizes the estimated lens displacements and bond strength safety factors for each lens.

| Component | Radial Flexure Estimate (± µm) | Axial Flexure Estimate (± µm) | Tilt Flexure Estimate (± µrad) | Maximum Estimated 5g Bond Reaction Force (lbs) | Minimum Estimated Bond SF (5g load) |
|---|---|---|---|---|---|
| Collimator Lens #1 | 0.46 | 2.55 | 1.01 | 18.2 | 5.2 |
| Collimator Lens #2 | 0.42 | 3.40 | 7.46 | 4.6 | 20.7 |
| Collimator Lens #3 | 0.38 | 3.06 | 6.73 | 4.1 | 11.8 |
| Collimator Lens #4 | 0.28 | 2.21 | 6.05 | 3.6 | 10.6 |
| Collimator Lens #5 | 0.86 | 6.90 | 15.16 | 9.3 | 8.4 |
| Collimator Lens #6 | 1.19 | 9.53 | 20.94 | 12.9 | 7.4 |
| | | | | | |
| Camera Lens #1 | 0.25 | 1.22 | 0.08 | 8.2 | 11.6 |
| Camera Lens #2 | 0.47 | 2.29 | 0.15 | 15.4 | 6.2 |
| Camera Lens #3 | 0.31 | 1.50 | 0.10 | 10.1 | 3.1 |
| Camera Lens #4 | 0.28 | 1.37 | 0.09 | 9.2 | 7.2 |
| Camera Lens #5 | 0.28 | 1.37 | 0.09 | 9.2 | 8.5 |
| Camera Lens #6 | 0.24 | 1.17 | 0.08 | 7.9 | 9.9 |

**Table 15: Estimated Mounted Flexure and Bond Strength Results for the Collimator and Camera Lens Mounts**

#### 5.2.1.7.4 Prototype Testing

During the detailed design phase, we completed extensive adhesive bond strength tests. We also fabricated prototype lens cells and alignment and bonding fixtures to further evaluate the bonded flexure lens mount concept. These fixtures and prototypes are now being utilized to practice preparation and alignment of dummy aluminum lenses into the cells.

Adhesive bond tests are summarized in MMDN36. In these tests, Armstrong A-12 adhesive was used to bond metal blocks to various lens materials to create test samples. The dimensions of the sample bonds duplicate the MOSFIRE design dimensions. Test samples were then monitored as tensile and shear forces were applied. These tests were performed at room temperature and again at temperatures between 90 K and 77 K. The basic test set-up is shown in Figure 39. Test results for the cryogenic tests are summarized in Table 16. Generally, four samples of each material were tested both in shear and in tension at cryogenic temperatures. The lowest failure force has been used for comparison with the maximum predicted bond interface reaction forces for each lens mount (Table 15). In all cases, the minimum measured bond strength exceeded the estimated 5 g lens mount force often by substantial amounts. The minimum predicted safety factor is 3.1 over the 5 g design goal.

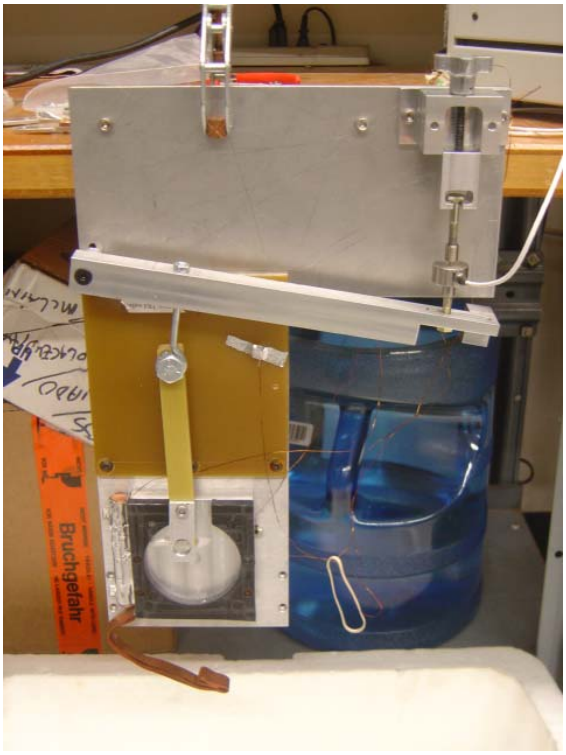


**Figure 39: Shear Test Set-up**
The copper strap at the bottom can be dipped in a bath of liquid nitrogen.

| Substrate Material | Min. Failure Force Shear (lbs.) | Max. Failure Force Shear (lbs.) | Min. Failure Force Tensile (lbs.) | Max. Failure Force Tensile (lbs.) |
|---|---|---|---|---|
| Clearceram-Z (for mirrors) | 158 | 215 | 90 | 138 |
| Calcium Flouride | 110 | 240 | 95 | 122 |
| Barium Flouride | 92 | 216 | 78 | 125 |
| S-FTM16 | 31 | 49 | 50 | 62 |
| I-FPL51 | 66 | 93 | 74 | 92 |
| Zinc Selenide | 49 | 62 | 52 | 78 |
| Fused Quartz | 38 | 52 | 55 | 80 |

**Table 16: Adhesive Bond Test Cryogenic Results Summary**

An aluminum dummy field lens has been repeatedly installed and aligned in a prototype cell during the detailed design phase. The assembly and alignment fixture to be used with the actual lens has been developed, manufactured, and used for these practice sessions. The dummy lens has a precision bore machined along the lens axis for use in measuring axis alignment with respect to the cell mounting features. Measurements obtained from three assembly and alignment attempts indicate alignment precisions of ±63.5 µm axial position, ±12.7 µm concentricity, and ±178.4 µrads. While these numbers are comparable to what is required for mounting the field lens, we have identified some changes to the fixture and process that will reduce the alignment errors even further, particularly the axial spacing and tilt. Figure 40 shows the lens cell prototype and the assembly fixtures. The dummy lens will be bonded into the cell in the near future to practice the bonding procedure and assess any affect on lens alignment.

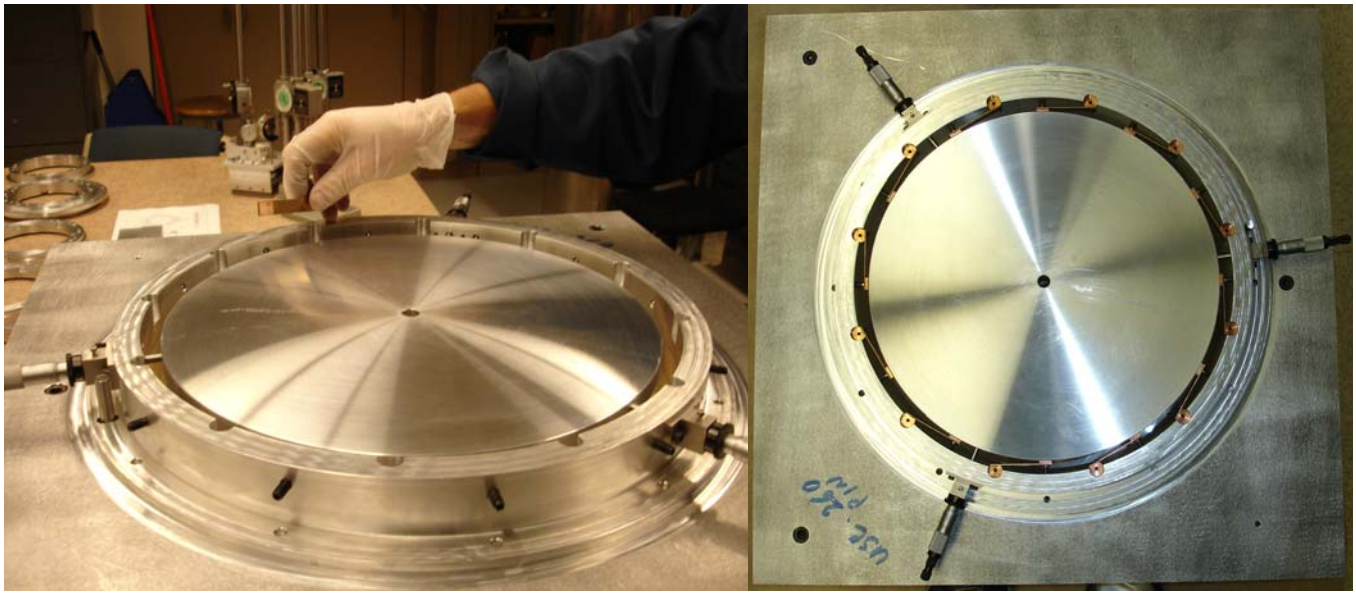

**Figure 40: Prototype Lens Cell and Assembly Fixture**

All of the collimator barrel lenses and cells have been prototyped and will be used to practice assembly, alignment, and bonding utilizing appropriate fixtures. Prototypes of the collimator lens mounts and dummy lenses are shown in Figure 41.


**Figure 41:Prototype Collimator Lens Mounts and Dummy Lenses**

#### 5.2.1.7.5 Lens Mount Assembly

Lens mount assembly and disassembly procedures have been developed during the detailed design phase. Jigs have been made to handle the installation of a lens into its cell and the bonding of flexures to the lens girdle. Figure 40 and Figure 41 in the previous section show the jigs and fixtures in use with dummy lenses. The basic assembly procedure is a nine-step process (Table 17). The first step is to assemble all of the flexure assemblies required for a particular lens. Flexure assemblies consist of a copper mount plug, beryllium copper flexure strip, and a CTE-matched metal mount block. These parts are screwed together utilizing an alignment jig. The mount blocks then have the lens girdle radius machined into them utilizing another fixture.

| MOSFIRE FIELD LENS ASSEMBLY PROCESS | |
|---|---|
| **STEP #** | |
| 1 | Assemble flexure subassemblies |
| 2 | Set-up lens assembly fixture |
| 3 | Set assembly fixture to proper position |
| 4 | Transfer lens to assembly fixture |
| 5 | Place lens cell in to assembly fixture |
| 6 | Align the lens |
| 7 | Install lens mount flexures |
| 8 | Bond lens mounts |
| 9 | Remove field lens assembly |

**Table 17: Summary of Field Lens Assembly Procedure**

The second step is to build up the lens assembly fixture, configured for the particular lens to be assembled. The alignment of the fixture is measured and adjusted to the specified accuracy.

The lens support is set to a height pre-determined to properly set the axial position of the lens within the cell. Proper support height is determined from the CAD model. Lens support level and

axial position are measured and confirmed. Next, the lens is carefully removed from its packaging and placed on the lens support, centered by eye. The lens cell is lowered into position on the fixture, located with the alignment features used to position it in the instrument, and secured. Extreme attention to cleanliness of all parts is needed at this stage.

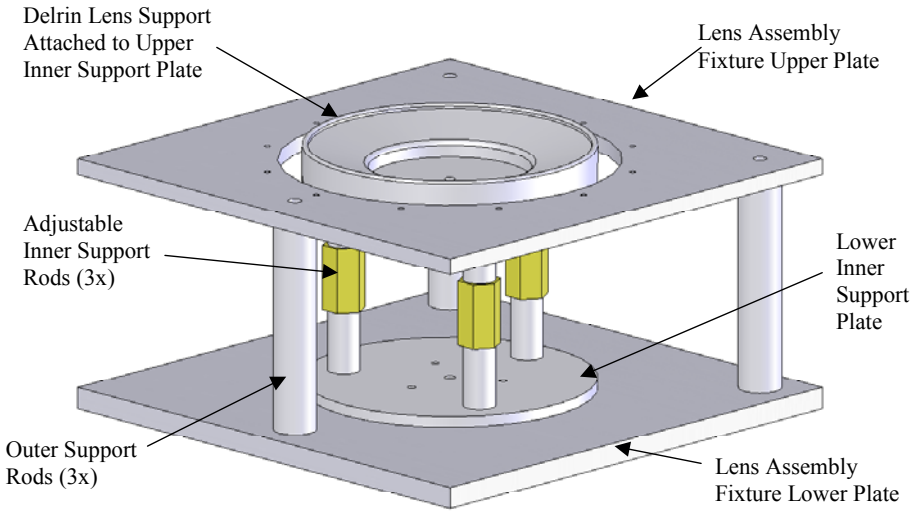


**Figure 42: Prototype Lens Assembly Fixture Configured for Field Lens Assembly**

Step 6 involves fine tuning the position of the lens relative to the cell. Three radial micrometers are used to gently center the lens within the precision cell. When the three micrometer readings are equal, the combination of the micrometers and the lens support define the lens in its proper position relative to the cell. At this point the pre-assembled lens mount flexure assemblies are inserted into their pockets in the cell around the perimeter of the lens and loosely restrained with hold-down screws. The flexures are each positioned backed away from the lens girdle in preparation for application of the adhesive. Adhesive is dispensed onto each pad utilizing a dispensing system. Each pad is the rotated into contact with the lens and each pad is clamped for curing by screwing radial spring plungers into contact with the pads and setting to the proper compression.

After the adhesive has fully cured for a week, the spring plungers and micrometers can be retracted and removed. The completed lens cell assembly can then be removed from the fixture and stored in an airtight container until the instrument is ready for installation of the lenses.

More details of the *evolving* assembly procedures can be found in MMDN35. The risk involved in handling the lenses during installation, alignment, and bonding is being reduced through the fabrication of prototypes and repeated practice with aluminum dummy lenses. This prototyping process should identify any problems with the fixtures, component designs, or procedures prior to fabrication of the final components and installation of the real lenses.

#### 5.2.1.8 Mechanisms

##### 5.2.1.8.1 Grating/Mirror Exchange Turret

MOSFIRE provides both imaging and spectroscopic observing modes and this is accommodated by interchanging a plane mirror and a reflective grating in the collimated portion of the MOSFIRE optical path. MOSFIRE is designed to use one of two "fixed" grating angles, so the method used to interchange the grating and mirror must be highly repeatable. This is achieved using a turret mechanism. During the detailed design phase, a new mechanism was added to provide a second grating angle. The two grating angles are determined by whether or not a simple shim is inserted at the deployed position of the grating. MMDN24 provides a detailed description of the grating/mirror exchange turret design and operation.

The grating/mirror exchange turret assembly is a worm-driven, cantilevered turret mechanism with three deployment positions within 157.39º of motion. Two grating positions are located at one end of the travel and have a relative angular position of 1.09º. Specifically, the three angular settings relative to the incoming beam are: 1) imaging mirror: 20º; 2) primary grating angle: 42.614235º; and 3) secondary grating angle: 41.523692º.

There are two parts to the grating/mirror exchange mechanism, a turret assembly and a drive assembly. The turret assembly contains the frame that supports the grating and mirror. The frame is attached to the end of a spindle, or shaft, which in turn is supported by a pair of cryogenically prepared deep-groove ball bearings (Champion CS6010BBRT-9 &CS6006BBRT-9). The bearings are retained in an aluminum hub structure while the spindle is constructed of stainless steel to match the bearing race construction. The bearings are pre-loaded with a pair of large spring washers to compensate for the ~ 218 μm axial thermal contraction differential of the materials. The bearing pockets in the aluminum hub are slightly over-sized at room temperature and contract to the proper fit at operating temperature. The drive end of the spindle is sized for a slip-fit on the bearing inner race to allow the axial thermal contraction. These bearings are substantially over-sized relative to the turret loads to allow for a thicker, stiffer shaft that minimizes turret flexure under varying gravity vector loads.

Layout of the turret assembly can be seen in Figure 43. This figure also shows the imaging mirror position stop-block and the grating tilt mechanism assembly, which define the deployed optic positions. Also shown is one of the two thermal straps which help cool the moving turret frame and the worm drive assembly. Thermal strap design is borrowed from an earlier instrument. The straps provide a conductive path to help cool the rotating components of the turret during instrument cool down.

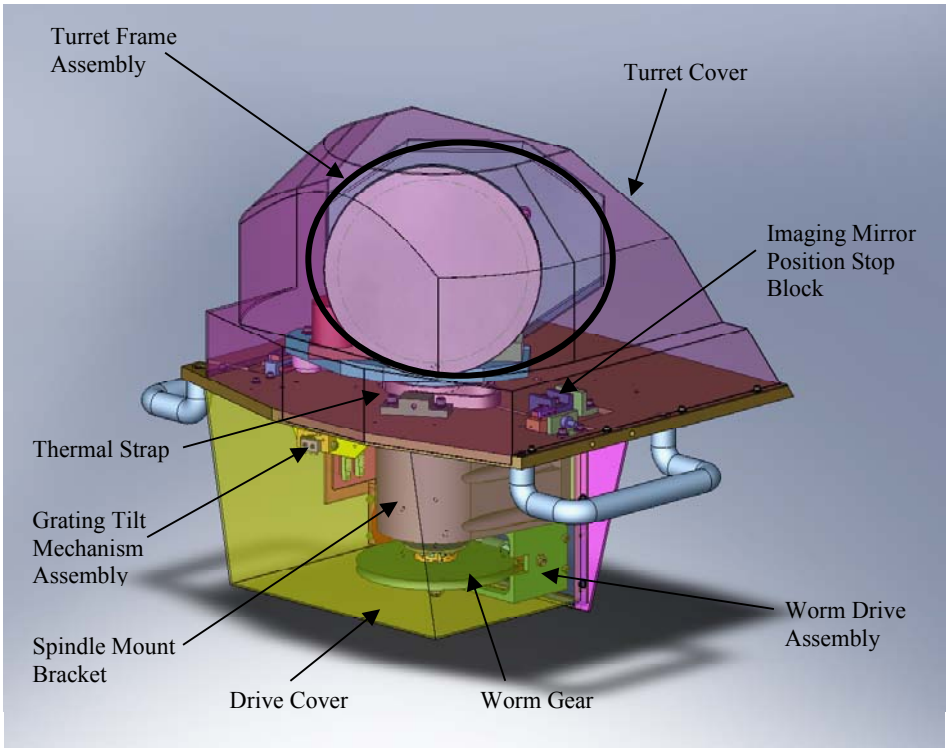


**Figure 43: Grating/mirror Exchange Mechanism**

The rotating turret frame assembly is shown in Figure 44. This assembly is an aluminum and invar structure that contains provisions for mounting the grating and the imaging mirror in a back-to-back configuration. The optics are mounted in a back-to-back configuration in order to help minimize turret space requirements. Each optic must be positioned at a unique angle to the optical axis while maintaining the same distance to the previous optic. This requires that the centerlines of each element be offset from one another and from the turret axis. This offset arrangement in combination with differing aperture sizes creates a slight out of balance condition for the turret. The turret frame position stop is located to help counteract this and an additional small counterweight mass is added to re-balance the turret frame assembly.

Bonded A-frame flexures configured in a tripod arrangement secure the grating and mirror to the turret frame. Each of the flexures is a two-piece assembly comprised of a sheet metal A-frame mechanically attached to cylindrical pads that form the bond interface. The frame and flexure components are constructed of Invar, a metal with a good CTE matched to the CLEARCERAM-Z substrate of the mirror and grating. Mount pads will be bonded to the optic with a 76 μm layer of Armstrong A-31 adhesive. Flexure performance of this design is reviewed in MMDN22. A fixture will be constructed to position a set of pre-assembled flexures relative to the grating or imaging mirror during bonding. The fixture will utilize the turret frame for setting the positions of the flexure assemblies. Bonding procedures and fixtures are described in MMDN32.

In the event that manufacturing and assembly tolerances don't achieve a high enough degree of parallelism between the fully assembled turret frame, then the relative "pitch" of the optics can be adjusted. The top-most flexure assembly for the imaging mirror can be slightly unclamped and reset with shims to adjust the ± pitch angle of the mirror relative to the grating. Slightly unclamping the two upper-most flexures and re-shimming can likewise adjust the pitch of the grating. These operations must be done with extreme care to prevent overstressing any of the flexure components or the bonds. The "yaw" angle of each optic can be adjusted either by adjusting the grating turret position stop blocks located on the fixed platform of the drive assembly or by re-setting the turret stop positions.

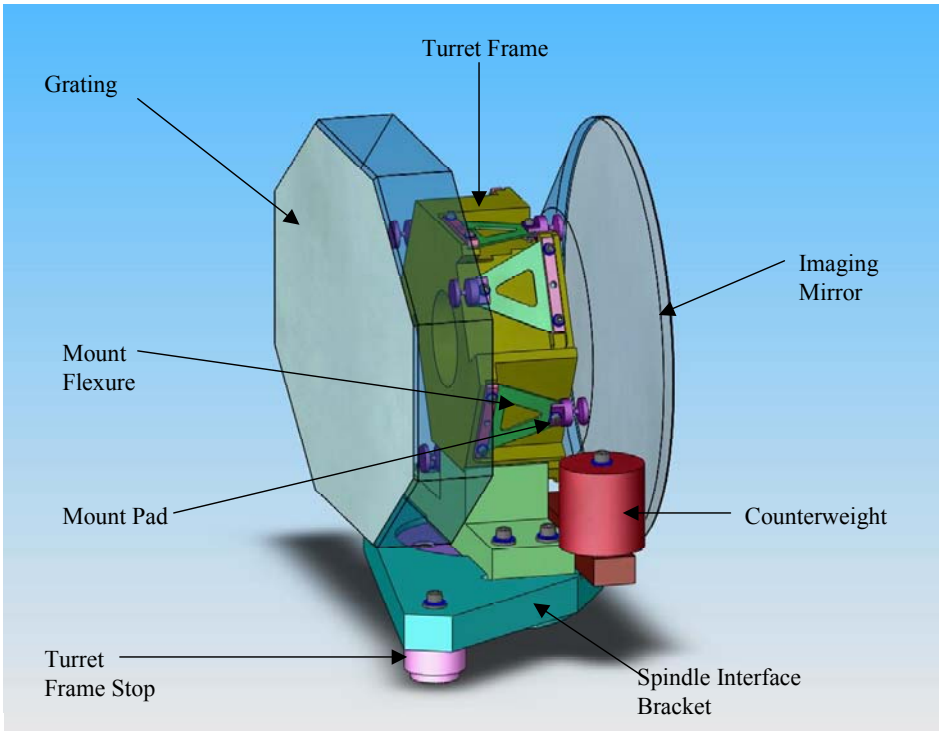


**Figure 44: Turret Frame Assembly Components**

The turret frame is attached to the drive assembly, shown in Figure 45. The drive assembly consists of a structure for supporting the spindle and all of the drive train components and switches necessary to accurately rotate the spindle. A worm drive assembly drives the spindle via a worm gear that is connected to the lower end of the spindle. The worm gear is 17-4 PH stainless steel with 16 pitch and 14.5 pressure angle. It has 100 teeth and a 159 mm pitch diameter. At the turret end of the spindle, a fixed platform is secured to the spindle mount bracket. This platform provides a structure for attaching the turret stop blocks, the grating tilt mechanism assembly, and the turret position switches. The imaging mirror has a single deployed position that is determined by an adjustable stop block. A micro switch activated by the turret stop cylinder senses when the turret is in the mirror deployed position.

The grating turret has two deployment positions. Using the tilt mechanism assembly, one can switch between the primary and secondary grating positions. A pair of micro switches is used for sensing whether the turret is in the primary or secondary grating angle position. Both switches are also activated by the turret stop cylinder, which has its diameter stepped-down at the lower end to ensure unique activation of each of the two grating position switches. In all cases, Honeywell Micro Switch 311SM6-T will be used.

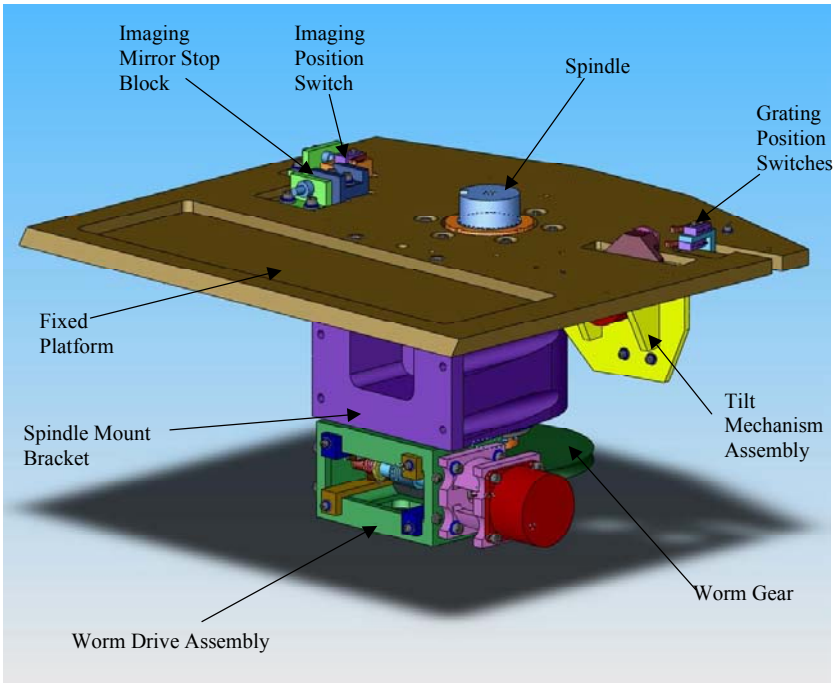


**Figure 45: Drive Assembly Components**

In this mechanism, the worm gear is driven by a tangentially floating worm. The worm is constructed of UHMW polyethylene and is mated to a 416 stainless steel shaft via a spline geometry. The spline interface allows the worm to be centered by compression springs. The compressions springs (Lee Spring LC-055G-2) allow the drive to "wind-up" when encountering one of the turret stops and create a uniform pre-load of the turret (~5 lb) prior to stopping the drive motor. Two pairs of symmetrically located micro-switches (for redundancy) are utilized to stop the drive motor after the worm has shifted from center by ~1mm. The worm shaft is supported by a pair of cryogenically prepared deep-groove ball bearings (Champion CSR3BBRT-9 & CSR6BBRT-9). The larger bearing is at the motor end and provides radial and axial support. The smaller bearing is located at the far end of the shaft and provides only radial support. It is sized to float in the structure's bearing pocket in order to compensate for differential thermal contraction of the shaft and the aluminum frame. The worm shaft is connected to a NEMA 23 ½ stack stepper motor, which is cryogenically prepared, via a flexible coupling (Berg C041A-2).

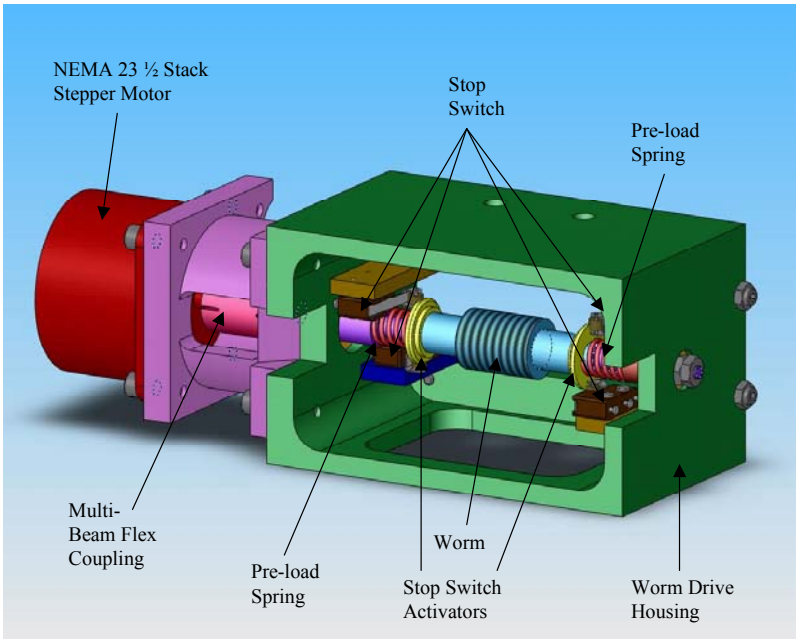


**Figure 46: Worm Drive Assembly Components**

The grating tilt mechanism is a simple rotary device which inserts and removes a "shim" between the turret frame stop and a fixed stop block in order to alter the grating tilt angle. A grating angle shifting shim is attached to a NEMA 17 ½ stack stepper motor shaft. The shape of the shifting shim is symmetrical with respect to the shaft for balance, so the mechanism can operate in 90º steps, or increments, between modes. The blades of the grating angle shifting shim add 2.76 mm of thickness to the fixed grating stop block when the shim is in one of the two deployed positions. Two micro switches provide the status information for the mechanism. One is activated when one of the blades of the shim is deployed. A second switch is activated when both of the blades are retracted. One of the switches can be used as a homing device for calibrating the mechanism. Motor steps are used to move through the 90º degree increments. The motor detent is sufficient to maintain position of the balanced shim, allowing the motor to be turned off at any position.

Ignoring the multiple grating angle positions (primary and secondary) for a moment, when the instrument operator wishes to switch between instrument modes (imaging/spectroscopy), the correct optic is selected (grating/mirror). If the incorrect optic is in position, based on the state of the grating exchange turret mechanism interlock switches, the mechanism's turret motor is driven in the proper direction for a pre-determined number of steps. The turret motor then decelerates and slowly creeps until the motor stop switch is actuated. Through this process, the motor is turning the worm, which in turn is driving the worm gear. The worm gear spins the turret through the ~160 degrees of rotation between the two optic deployment positions. As the turret slows down near the deployment position, the turret's stop engages one of the two fixed stop blocks that define the mirror or grating position. As the turret can no longer rotate in this direction, then the turret, spindle, and worm gear stop rotating. The worm and motor continue to turn, and this action causes the worm to translate tangential to the worm gear. The worm's motion is constrained to tangential

motion by the spline interface to the worm shaft. Tangential motion compresses the drive pre-load spring in that direction by approximately 1 mm. At that point, the redundant stop switches are activated- shutting off the turret motor. The worm drive won't back-drive, so the turret is loaded against a fixed definition block with consistent and sufficient force to accurately define the deployed optic.

The position of the turret is indicated by an interlock switch locate on the fixed platform which is actuated by the turret's stop cylinder. Position interlock switches are located right at the stop hardware and activated by them to ensure accuracy in sensing the actual position of the turret. The stop switches may disengage due to changing gravity vectors in between mode changes, but their job of stopping the motor has already been done and they are not used as interlocks. The pre-load springs are sized so that wear and variable flexure of the structure under changing gravity don't appreciably alter the amount of pre-load and, thus have negligible effect on the optic position.

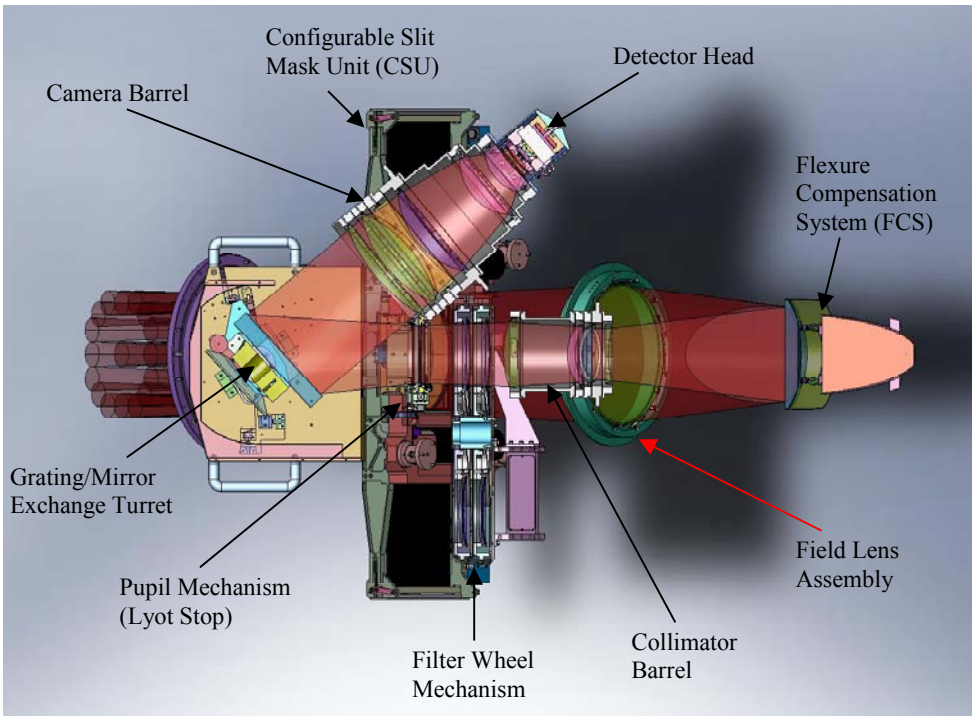


**Figure 47: Section View Of MOSFIRE's Optical System Components**
The Grating/Mirror turret mechanism is set for spectroscopic mode

The turret frame and spindle designs were refined during detailed design using FEA to predict the internal flexure within the structure. Detailed results of this analysis are summarized in MMDN22. The analysis first evaluated and sized the tripod mount flexures and pads to provide adequate support stiffness while minimizing substrate and bond stresses. Mirror and grating flatness was maintained at < 0.2 μm. The minimum safety factor of the flexure bond strength is estimated to be 21 based on comparison to bond pull test results. Analysis then refined the turret structure design to increase stiffness from the preliminary design, particularly in pitch motion. The estimated pitch

has been reduced to about half of the earlier design by increasing the section modulus of the spindle to turret frame interface.

Mechanism Performance Predictions:

- Exchange time: < 45 s
- Position accuracy: 0.25 μrad (< 0.1pixel)
- Position repeatability: 0.25 μrad (< 0.1 pixel)

The grating/mirror exchange turret design is comprised of many heritage components and mechanism concepts. The highest risk portion of the design is the bonded tripod flexure mirror support. Bond design was prototyped and failure tested, indicating that there is plenty of margin in the bond design for the FCS mirror. Fabrication drawings are approximately 10% complete.

#### 5.2.1.8.2 Double Filter Wheel

MOSFIRE's filter wheel design is based on the proven stepper motor driven filter wheels used in OSIRIS, scaled in diameter to accommodate the larger filters required. As shown in Figure 48 the design incorporates a double wheel. The volume available for the mechanism and the necessary filter size are the dominant drivers for the configuration. The design accommodates filters up to 170 mm in diameter, which provides ample area for the required clear aperture (~156 mm) and mounting requirements. Each filter will be mounted in an individual cell or mounting assembly that will provide the angular tilt (6°) with respect to the optical path and will facilitate the handling of the filters when not mounted to the wheel. Volume constraints dictate a wheel diameter no larger than 635 mm. This size can accommodate six (6) mounted filters. MOSFIRE will require at least five or six different filters as a bare minimum. To accommodate future requirements we have decided to have two filter wheels in a stacked configuration. Each wheel will have positions for 5 optical elements (filters, blanks, etc.) and one open position occupied by a counterweight.

The filter wheels will be edge driven. Custom gear teeth will be cut into the edge of each wheel and the wheels will be fabricated out of 6061-T6 aluminum with a black anodized finish. They will be driven by stepper motors and spur gears. Each spur gear is each fabricated from 303 stainless steel and they will be 20 pitch gears with a 20 degree pitch angle. The spur gear has a pitch diameter of 50.8 mm. With this ratio, any filter move should be accomplished in less than 20 seconds (probably much less).

The mechanism will use stepper motors that are modified for cryogenic use. One reason why we have decided on internal motors instead of external "warm" motors is that the size of the instrument and the placement of the wheel mechanism would require impractically long drive shafts. The motors are commercially available cryogenically rated motors from MRC. These motors have been tested at CIT and demonstrated a lifetime of at least 20 years.

Each wheel will be supported by and revolve around a central hub using a 440C stainless steel, 4 point contact ball bearing available from Kaydon Corp. Using a 4-point-contact bearing allows us to support both the radial and axial loads using a single bearing per wheel. The central axle will be fabricated from 416 stainless steel. The axle's coefficient of thermal expansion (CTE) is similar

enough to the ball bearing's CTE that no additional compensation for differential expansion is needed for the interface between the bearing's inner diameter and the axle's outer diameter. The bearings will be installed in a central well in the individual wheels. Since differential expansion between stainless steel and aluminum is an issue here the clearance between the bearings and the wheels will be slightly oversized for lab ambient temperature and optimized for operational temperature. Thin retaining rings constrain the bearings axially but will act as springs during cool down, again to compensate for differential CTE's.

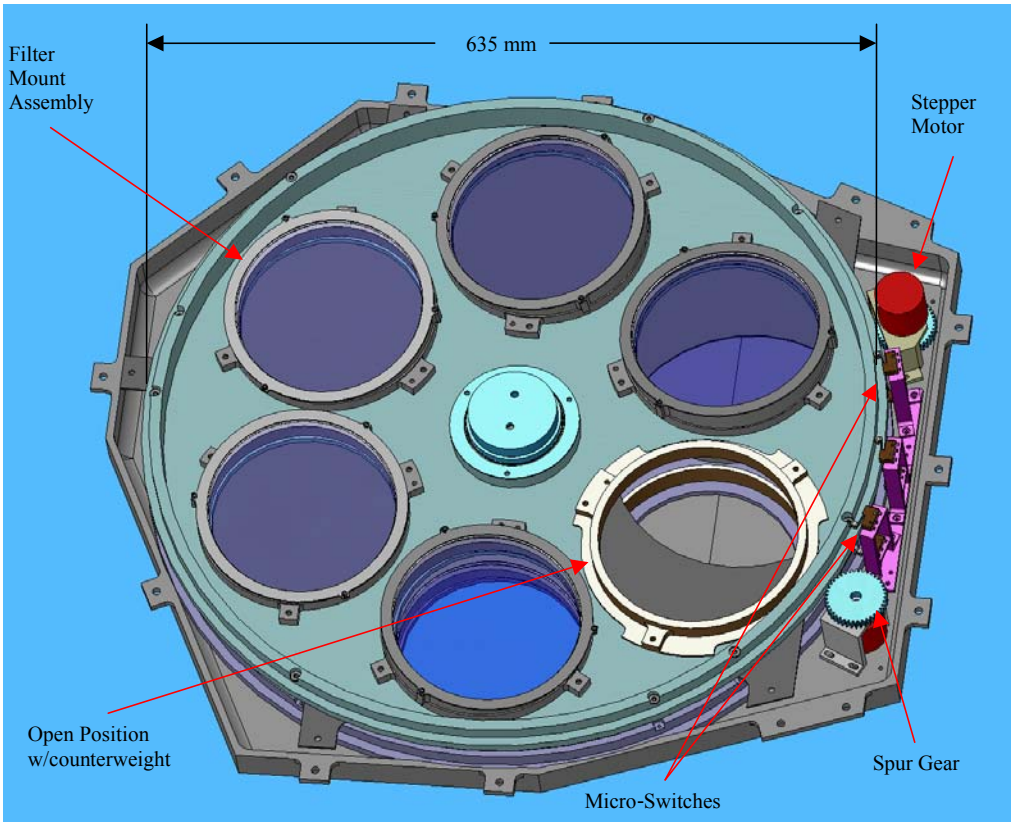


**Figure 48: Dual Filter Wheel with Cover Removed**

Positional accuracy and repeatability will be provided by detents. The gear pitch is relatively coarse to allow enough backlash for the detents to engage. The type of detent in the design is the type used in the UCLA OSIRIS instrument. They were also lifetime tested to greater than 10 years. The detents are simply small ball bearings mounted to leaf springs. When the wheel reaches a given position the bearing drops into a receptive V-groove that locates the filter. Positional feedback is achieved using three micro-switches for each wheel and a series of activators that give a simple, unique binary pattern for each individual position. This switch design was also tested and used in the OSIRIS instrument.

The case and cover are designed so the mechanism can be serviced while installed in MOSFIRE. Both the switches and motors can be accessed through the service cover. The filter mount

assemblies in the upper wheel are obviously accessible but also, once the counterweight in the upper wheel is removed, filter mount assemblies in the lower wheel are also accessible.

The large wheels have a fairly tenuous thermal connection to the static housing surrounding them. The only conductive path is through the ball bearings. Therefore, the wheels will cool down largely through radiation. In order to achieve the most efficient cool down we have made the interface from the wheel mechanism to the rest of the cryogenic system sufficiently robust to insure a very good conductive path to the wheel mechanism housing. In order to expedite the cooling of the wheels themselves there is a thin static plate mounted between the wheels and attached to the housing. This essentially doubles the "cold" surface area for the wheels to radiate onto and therefore almost halves the cool down time. Thermal analysis indicates that the filter wheels will reach operating temperature in the same period of time as the rest of the instrument.

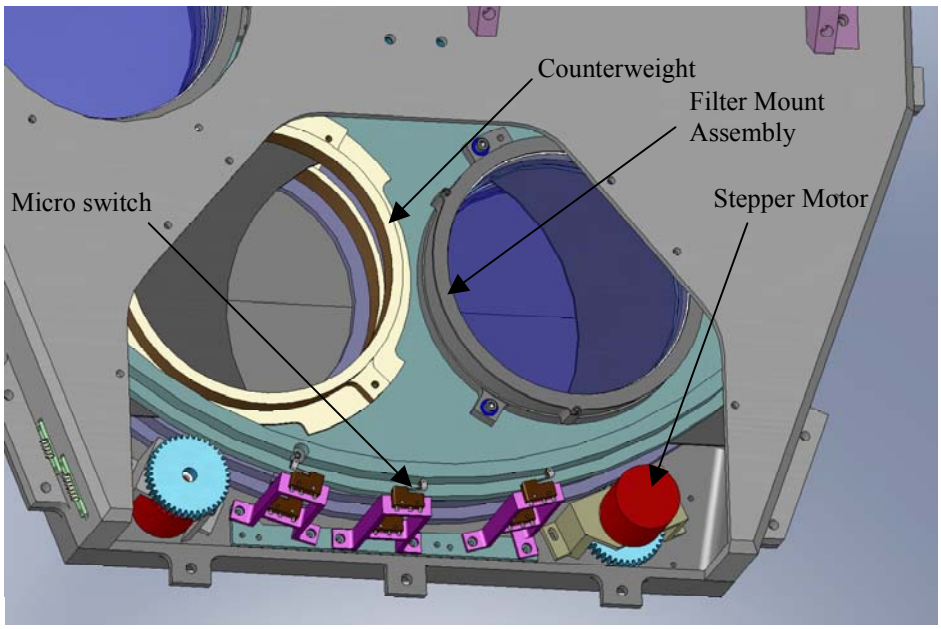


**Figure 49: Filter Wheel Service Access**

FEA was performed on the detailed design of the filter wheel case to assess flexure during the detailed design phase. The results of this analysis are described in MMDN28. These studies revealed that an earlier, cantilevered hub design allowed flexure that was large enough to effect operation of the position switches. Based on the analysis, the hub design was changed so that it is anchored in both halves of the case. This change will ensure that the position switch activation isn't affected by changing gravity orientations.

Based on its reliance on previously built and tested mechanisms, this mechanism is considered a low risk device. The fabrication drawing package has been completed for this assembly. Additional details about the design can be found in MMDN06.

#### 5.2.1.8.3 Pupil Wheel

For proper optical performance MOSFIRE will require a "stop" at a pupil position to prevent excess background signal from reaching the detector. This requirement is most critical at the longer wavelengths where thermal background is the problem. Because the optical field is rotating, this stop will be most effective if it rotates with the field. There is the added complication that the optimum stop position varies along the optical path (Z axis position) due to wavelength. To avoid an overly complex cryogenic mechanism, we compromise on the spatial position, size and shape of the stop and optimize for the K-band. The H-band positioning requirements are similar enough to include it with the K-band. The Y- and J-band require a larger field at this position. To accommodate these requirements the Pupil Stop Mechanism is designed to provide a rotating pupil stop for H- and K-band and a fixed baffle for Y- and J-band. A central obscuration will mask the central opening in the primary mirror. Adequate positional stability and feedback must be provided.

The MOSFIRE pupil wheel is shown in Figure 50. Two stop modes will be available using an adjustable iris. For the longer wavelengths, the iris will close to "K" band position and then the mechanism will rotate at the prescribed rate to track the hexagonal image of the primary. Figure 50 shows the mechanism with the iris closed to this configuration. The iris blades can be seen in detail in Figure 51. There are 6 blades based on a simple hexagon with a point-to-point size of 125 mm. The final aperture shape in Figure 51 results from overlaying a profile of the Keck primary. In this mode the mechanism can provide clockwise and counter clockwise rotation on the order of 300 degrees. A central obscuration is provided to mask the central opening in the Keck primary mirror. Because of image blur, a simple disk can be used instead of a hexagon. The diameter of the obscuration at operating temperature is 36 mm. To function properly as an optical baffle, the iris blades will be painted infrared black using something like Aeroglaze Z306 or WZ3301. These paints have been used successfully in NIRSPEC, NIRC2, and OSIRIS. For the shorter wavelengths the mechanism becomes a static pupil stop, the iris opens completely, and the mechanism travels to a home position.

Two 4-point-contact ball bearings available from Kaydon Corp. will be used as rotational bearings. This type of bearing has also been used in NIRC2. Because of the relatively large diameter of the bearings and the fact that they are of steel construction we have decided that the majority of the assembly will be fabricated from 416 Stainless Steel. The coefficient of thermal expansion (CTE) of this material is similar enough to the ball bearing's CTE that no additional compensation for differential expansion is needed for the interface between the bearings and housing.

As with the filter wheel, the pupil mechanism will be driven with a stepper motor that has been modified for cryogenic use. Once again, the location of the mechanism and heritage from OSIRIS were the key factors in selecting cryogenic motors.

We will use motors from MRC. These motors have been tested at CIT and demonstrated with a lifetime of at least 20 years. The mechanism will be edge driven using a worm and worm gear (see Figure 51). This drive train is very similar to the one used in the MOSFIRE grating turret mechanism and has been used several times in previous UCLA instruments (OSIRIS, NIRSPEC).

By setting the backlash between the worm and worm gear properly and by using accurate tolerancing techniques during fabrication, the positioning and stability requirements of the mechanism can be maintained without additional measures.

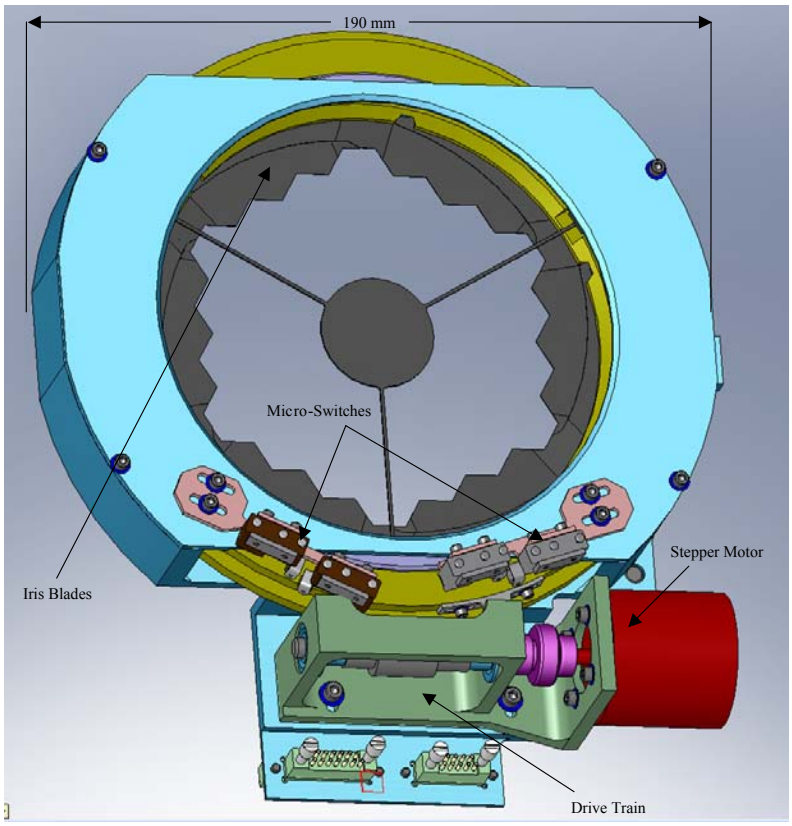


**Figure 50: Pupil Mechanism Components**

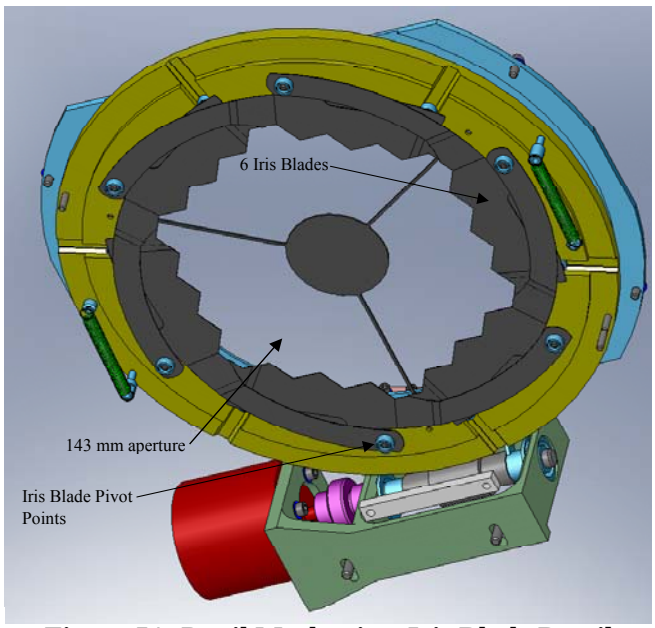


**Figure 51: Pupil Mechanism Iris Blade Detail**

The pupil mechanism will have a "home" position defined by a hard stop. In the home position the iris is open to the shorter wavelength mode. Positional feedback at the home position is achieved using a micro switch. There will also be a redundant micro switch for this position. Previous experience has shown that such a hard stop provides an adequate datum for positional calibration. The distance from the home position to the iris closed to the K-band position will need to be calibrated, but then the mechanism can then be rotated to the proper position in the field by simply counting steps. Another micro switch pair is located near the end of travel as a secondary datum.

In the long wavelength mode (iris closed for K-band and pupil rotating) the stepper motor will probably be running continuously. This will result in a heat source that will need to be attached to a heat sink. To avoid unacceptable heat transfer into the mechanism itself or other structure close to the optical path, the stepper motor will be connected with flexible copper straps to the nearest aluminum bulkhead of sizeable mass.

This mechanism design is based on previous mechanism designs, but contains some new features. Additional details about the design can be found in MMDN23. The fabrication drawing package has been completed and fabrication of some of the components has begun. In particular, prototype iris blades are being manufactured to perfect the stamping/forming process.

#### 5.2.1.8.4 Flexure Compensation System

In order to meet the MOSFIRE design goal of <0.1 pixel of residual image motion due to flexure, an active flexure compensation system (FCS) has been provided. This design utilizes a piezo actuator driven tip/tilt mirror mounted in a standoff tube attached to the rear optical bench as shown in Figure 21. Flexure correction will be implemented using a look up table based on telescope elevation and instrument rotator angle. Previous experience with similarly sized Cassegrain instruments (Kibrick et al. 2000, 2003) has shown that a 10:1 reduction in image motion is possible with such a system. For MOSFIRE, the instrument optics must be cooled to cryogenic temperatures (~120 K), so the flexure compensation system must be compatible with cryogenic conditions.

MOSFIRE's flexure compensation system is based on a custom version of a piezo tip/tilt platform to be designed and manufactured by a vendor named PI (Physik Instrumente). A similar system has recently been built for NIRES and has been successfully tested. The tests indicate that the PI stage to be used for MOSFIRE will have sufficient resolution over its range to provide 10:1 correction. Experience gained from the NIRES system will benefit the design of the MOSFIRE system. The layout of the flexure compensation system assembly is shown in Figure 52.

Basically, the tip/tilt platform, which has a 270 mm diameter mirror mounted from the platform's load plate, consists of three low-voltage piezoelectric linear drives which will support the load plate in a tripod fashion. The platform itself will operate closed loop with feedback from capacitive sensors. The tripod drive arrangement allows a level of redundancy in the system design since the platform could still operate through a portion of its range should one of the linear drives fail.

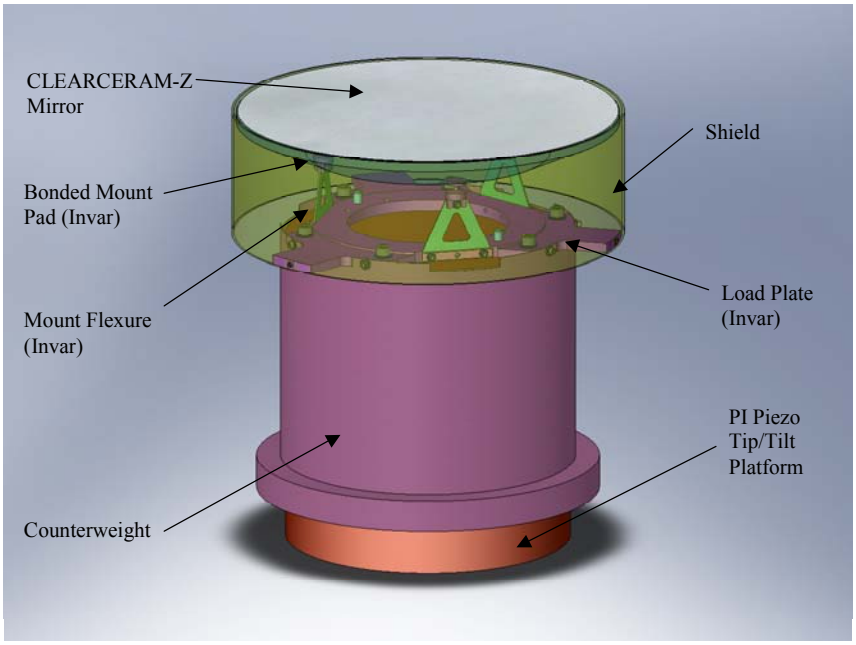


**Figure 52: Flexure Compensation System Assembly**
The shield is shown transparent so that the mirror mount components can be seen.

The mirror mount design is also based on a tripod layout. The FCS mirror will be fabricated from CLEARCERAM-Z, which is an ultra-low expansion glass-ceramic material. Attachment of the mirror to the load plate is accomplished with three flexure assemblies that form a tripod. These flexure assemblies consist of a cylindrical mirror pad that is bolted to an A-frame shaped flexure. The flexure components and the load plate will be constructed of invar so that their CTE closely matches the mirror substrate. The flexure assemblies are designed to allow for the relatively small differential radial contraction between the mirror substrate and the load plate without breakage of the mirror substrate. At the same time, they provide accurate location of the mirror with minimal flexure as the assembly experiences varying gravity vectors. Again, the mirror mount flexures are attached to the mirror substrate with bonded joints via approximately 14 mm diameter round CTE-matched invar pads bonded to the substrate with a 76 μm filled-epoxy joint (Armstrong A-12). This bonding approach has been prototyped and strength-tested to establish safety margins for various substrate/pad combinations.

The flexure compensation system assembly includes two additional components. First, there is an aluminum shield that surrounds the back side and edge of the mirror. This shield will help cool the mirror by radiation coupling to the exposed substrate surfaces. Also, the shield is designed to constrain the mirror from separating from the assembly in the unlikely event that any of the bond joints fail. The second additional component is a counterweight “sleeve” which is suspended from the load plate. This counterweight places the CG of the supported load at the pivot point of the tip/tilt platform.

Final analysis results indicate that the bonded, tripod mirror mount design provides sufficient rigidity to meet our flexure budget goals for this structure. Analytical results are summarized in Table 18. A full report of the analysis is contained in MMDN25. In addition, the design is estimated to safely withstand a minimum of 13 g of acceleration in all directions under cryogenic conditions.

| Summary of Extreme Values | | |
|---|---|---|
| **Parameter** | **Value** | **Unit** |
| **Maximum Axial Displacement** | **9.26** | **µm** |
| Maximum Axial Thermal Displacement | 8.98 | µm |
| Maximum Axial Gravity Displacement | 0.29 | µm |
| **Maximum Radial Displacement** | **2.89** | **µm** |
| Maximum Radial Thermal Displacement | 0.01 | µm |
| Maximum Radial Gravity Displacement | 2.89 | µm |
| **Maximum Roll** | | |
| Ambient Conditions (298 K) | 0.06 | µrad |
| Operating Conditions (120 K) | 0.03 | µrad |
| **Maximum Pitch** | | |
| Ambient Conditions (298 K) | 2.53 | µrad |
| Operating Conditions (120 K) | 2.25 | µrad |
| **Maximum Yaw** | | |
| Ambient Conditions (298 K) | 2.61 | µrad |
| Operating Conditions (120 K) | 1.82 | µrad |
| **Maximum Mirror Surface Deformation** | **0.26** | **µm** |
| **Minimum Bond Strength Safety Factor** | | |
| Shear Strength | 32 | |
| Tensile Strength | 36 | |
| **Minimum Support Component Safety Factors** | | |
| Flexure Stress | 13 | |
| Flexure Buckling | 27 | |

**Table 18: Summary of the FCS Static Analysis Results**

Estimates of mirror distortion under combined loads (thermal & gravity) shown in Table 18 indicate one extreme gravity orientation where the distortion may be marginal relative to the distortion goal. One edge of the mirror "curls" by ~ 0.26 µm while the goal is deformation < 0.25 µm (Figure 53). This deformation estimate is considered adequate for this mirror since it is only 4% greater than the goal and the optical footprint covers a small portion of the mirror. The tripod support design does not provide sufficient cooling paths to cool the mirror to operating temperature in the same time as the rest of the instrument through conduction alone. With proper surface finishes however, radiative coupling between the mirror substrate and the surrounding metal structure can reduce the mirror cool down time to match the rest of the instrument.

#### 5.2.1.8.5 Performance Predictions

- FCS correction range: +/-500 µrad (+/- 6.2 pixels) @ 77 K

As discussed in the instrument flexure section, the current conservative estimate of maximum image motion is ~3 pixels for complete sky coverage. Thus, the predicted FCS range is nearly twice the expected range.

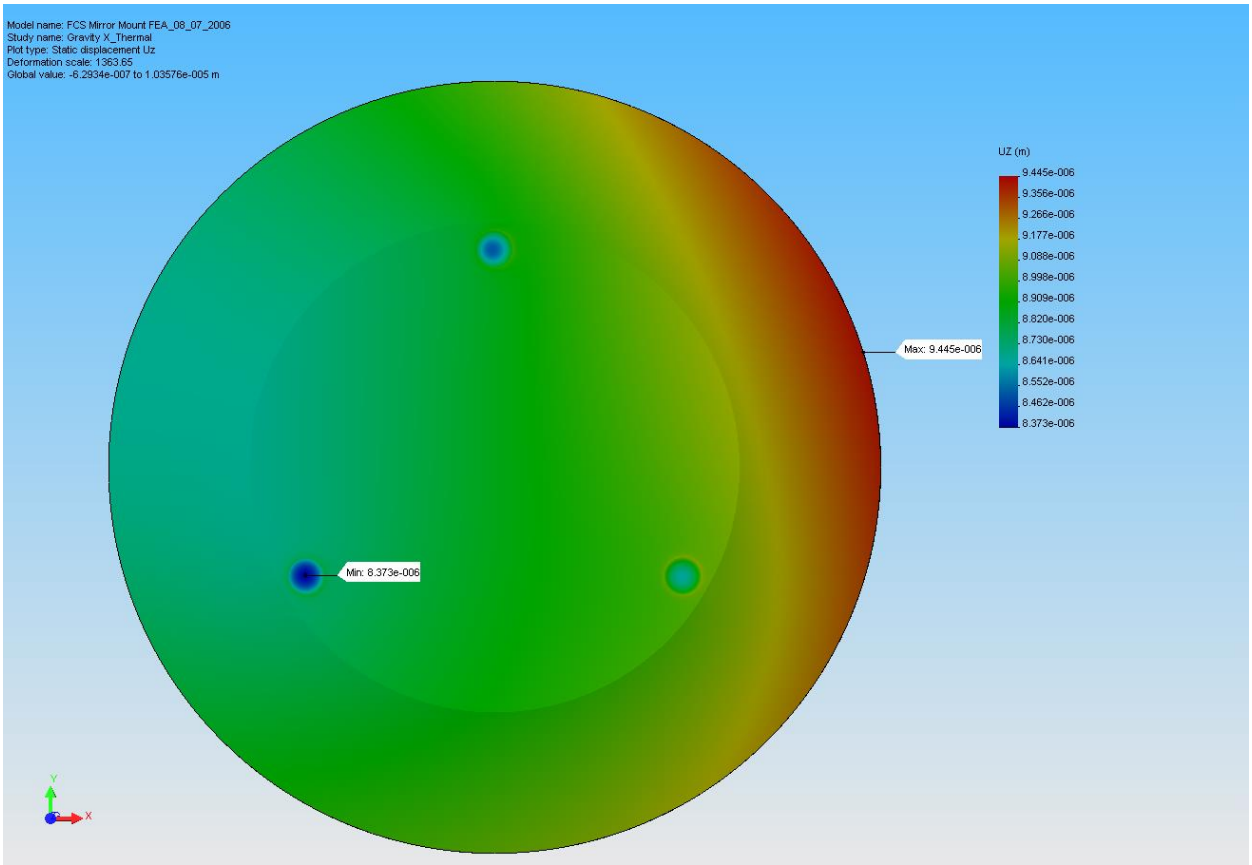


**Figure 53: Axial Displacement Plot from the Analysis Load Case Producing Maximum Surface Deformation (0.26 µm)**

The highest risk in the FCS system design is the bonded flexures that support the mirror. The same bonded tripod support system will be utilized for the grating and imaging mirrors. During the detailed design phase, pull tests were completed on prototype bonded pads. The results for all of the tested material combinations, including those used for the mirrors, was listed in Table 16 in the lens mount section. Procedures and fixtures for aligning and bonding the FCS mirror to its supports are described in MMDN32.

#### 5.2.1.8.6 Detector Head/Focus Assembly

The images and spectra produced by the MOSFIRE optics will be captured by a Teledyne Hawaii-2 RG detector. This detector is 2048 by 2048 pixels (physically 37 mm square), and is controlled by the SIDECAR ASIC mounted on a small cryogenic carrier board close to the detector. The ASIC is connected to an interface board outside the dewar, the Jade2 board, which in turn controls it and interfaces it to the detector readout computer. There will be a detector focus mechanism to

optimize focus in all wavelength ranges. The final lens of the camera optics, the field flattener, is located very close to the detector, so it will be mounted as part of the detector head.

The design is partially based on the detector head of the FLITECAM instrument, in which a vendor-supplied detector mount was enclosed in an outer shell, thermally isolated by G10 tabs, and cooled by a cold finger from a liquid Helium tank. In MOSFIRE we will provide a dedicated CCR head (CTI Cryogenics model 350) that will cool only the detector head. Figure 54 shows a cutaway view of the whole detector head assembly. The detector itself is supplied on a base made from molybdenum alloy, with threaded holes for three or four legs. The legs are threaded at both ends with spacers, in the form of thick molybdenum alloy washers, slipped over each leg and set the distance from the back of the detector base to the detector support block behind. The legs go through holes in the detector support block, which is made of the same molybdenum alloy material as the detector substrate avoiding thermal mismatch. After the legs go through these holes they are fixed by nuts on the back of the support block. A temperature sensor and heater are attached to the back of the support block to permit control of detector temperature by an external controller. The support block is attached to the focus mechanism via G10 A-frames. Attached to the front surface of the detector support block and enclosing the detector is a box structure. A plate holding the mount for the field flattener lens forms the front of this box, so that the field flattener lens moves with the detector during focus motion. The focus mechanism supports the detector, detector mounting plate and lens box, and in turn mounts to the rear of the outer enclosure. The outer enclosure is a rectangular box with a circular flange at the front; the circular flange attaches to the rear of the camera lens tube.

To allow detectors to be mounted closely butted against each other to form a larger detector mosaic, the detector's active area runs close to three of the edges of the base. Each of these three edges has a pattern of one tapped and two plain blind holes, allowing attachment of a handle to make it easier to manipulate and install the detector without risk of accidentally touching the delicate surface. On the fourth edge the connections to the detector's silicon multiplexer interface go to a ceramic block that is mostly underneath the detector base, with a slim extension wrapping up around the edge. Wire bonds from the detector go to pads on the top edge of the wrapped-around ceramic part. A flexible Kapton printed wiring cable connects to a grid pattern of pins on the underside of the ceramic block. All the necessary connections to the detector are brought out to a Hirose 92 pin connector on the other end of the Kapton cable. The detector and base are shown in Figure 55.

In the edge of the detector support block there is a similar hole pattern to that on the edge of the detector base, so that the same style of handle (with a larger screw size) can be used to handle the two parts when they are mated. The central hole of these patterns is also the attachment for the G-10 A-frames that stand the detector assembly off from the focus mechanism. To assemble the detector assembly to the A-frames, three of the A-frames are attached to the block on top of the focus mechanism, with the screws only finger tight. The handle is attached (firmly!) to the detector mounting block. The handle is used to position the detector assembly within the three A-frames. Each A-frame is attached to the mounting block, then the handle is removed and the fourth A-frame installed. At the suggestion of Bruce Bigelow we will use shoulder screws for this attachment so that the positioning is more reproducible.

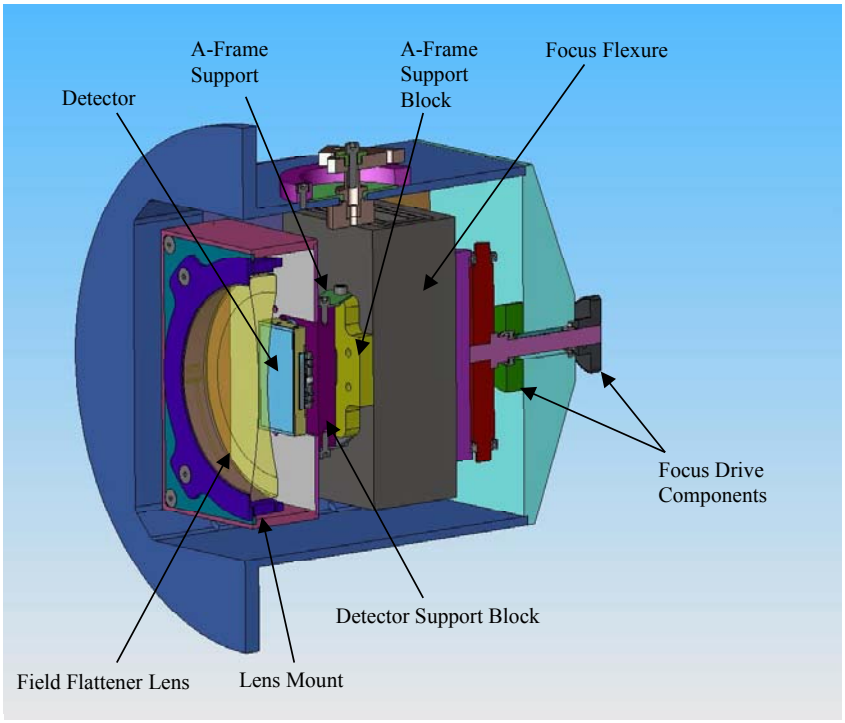


**Figure 54: Detector Head Cut-away View Showing the Field-flattening Lens and Focus Mechanism.**

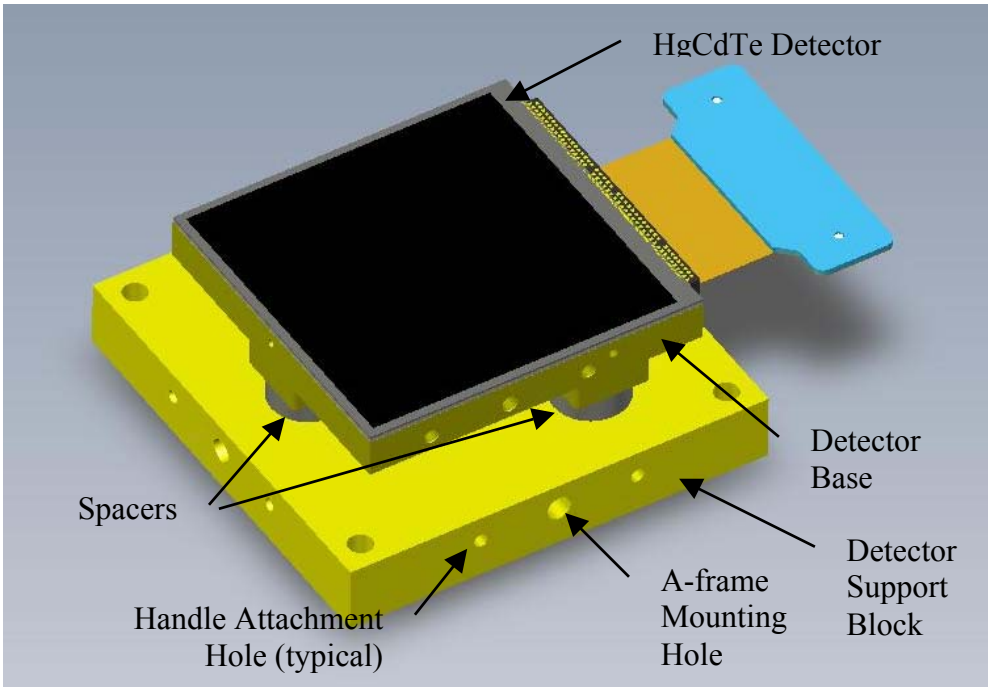


**Figure 55: The 2K x 2K Rockwell Detector Mount**

Other features of the interface block are a temperature sensor and heater on the back, and a tapped hole for the thermal strap connected to the auxiliary CCR head.

The base of the lens mounting box attaches to the top of the detector support block. At present this interface is drawn as a simple one of the box sitting on top of the block and four screws holding it down to the corners of the molybdenum block, but this will need to be improved to take care of CTE differential between the aluminum box and the molybdenum block, while keeping the whole assembly light-tight. A three-part box encloses the detector. The box base plate interfaces to the front of the detector support block, behind the detector. A square tube attaches to the base and extends forward of the detector. The front plate sets into a recess in the front of the square tube. The front plate in turn has a cutout and recess for the lens mount that carries the field flattener lens.

The box base plate is assembled to the detector support block *prior to installation of the detector* (it could be installed afterwards, but there is a risk of it making accidental contact with the detector surface). After the detector is installed on the block, the tube is attached, then the front plate installs to the front of the tube. The base plate and the edge of the square tube have mating cutouts to pass the Kapton printed flex cable. Earlier versions of the design had an interface between the short detector cable (as shown in the detector picture above) and an extender cable, but Teledyne recommended they fabricate a longer version of the cable to eliminate this intermediate connection.

The lens mount is a finger-type mount (Figure 56) as used in FLITECAM. It has a flange around the front which mates with the recess in the front plate of the lens tube, with four tabs for mounting screws. The lens itself then sits down inside the lens tube once the mount is installed. This means no light can enter the lens tube except through the lens. A cover is available which will protect the lens when the assembly is not installed in the instrument. This cover also forms a base for the detector/block/lens tube assembly once it is assembled. The assembly with the cover installed can be placed lens side down for attachment of the rest of the detector head.

**Figure 56: Field Flattener Lens and the Finger-style Lens Support Tabs**

The detector support block is mounted from the A-frame support block by four G-10 A-frames. The A-frames provide thermal isolation between the detector assembly at ~70 K and the rest of the system at ~120 K. This layout allows for a CTE differential between the molybdenum alloy detector support block and the aluminum alloy block. Each A-frame will flex equally as the detector assembly is cooled and contracts, maintaining the detector's location and center.

At PDR, the proposed focus mechanism was a piezo-driven flexure type actuator from Physik Instrumente (PI). However interaction with the PI representative uncovered a problem in that the side-to-side stability of the actuator might not be good enough. We looked for an alternate solution, and designed a new mechanism based on a titanium flexure. The basis of this design is the flexure used in the IMACS and NIRI instruments, originally described by R.V. Jones in the 1950s. The flexure is machined from a single piece of titanium alloy by wire EDM (Figure 57).

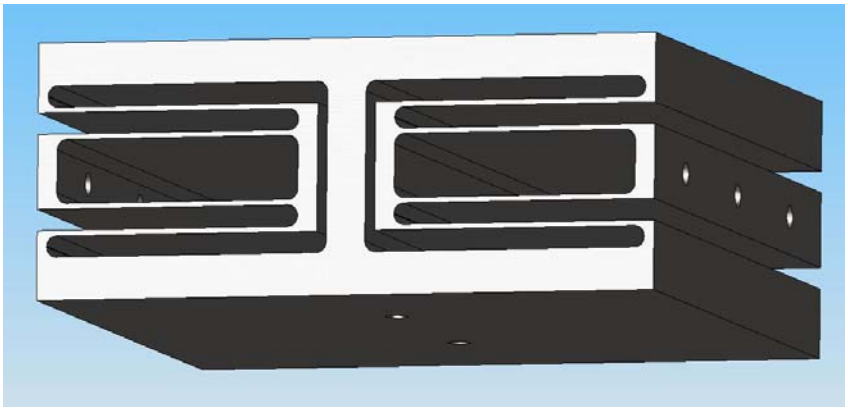

**Figure 57: Detector Focus Flexure Design**

The flexure is mounted to standoffs from the rear of the detector head outer shell, via the three tapped holes seen along each side. The "I" structure former by the top, bottom and the vertical bar through the middle of the flexure is the part that moves. The actuating mechanism pushes on the bottom surface, and the aluminum block and the A-frames supporting the detector/lens box assembly mount to a block on the top surface. The symmetrical design of flexible leaves on both sides makes the motion very rectilinear. A simple two-leaf flexure, for instance, exhibits a "parasitic" side-to-side motion as it moves in the required direction. In this design that "parasitic" motion is confined to the two vertical members next to the middle bar.

Since the camera feeds an extremely fast beam to the detector plane, tilt is of particular concern. FEA analysis of the motion of the flexure showed that this unwanted tilt is not significant, and that the flexure is in fact very resistant to transverse loads.

The outer shell of the assembly is an approximately cubic box (130 mm square by 127 mm high) with access hatches in two opposing faces, and a circular flange that attaches to the rear of the camera lens barrel. A thermal feed-through assembly is located on one of the sides of the shell without an access hatch. Electrical connection to the detector passes through one of the access hatches. Connections to the heater and temperature sensor still need to be located. The motor, worm gear and status switches for the focus drive mechanism are on the outside of the rear face of

the shell. The rear face of the cubic box is a separate plate from the four walls, which are machined from a single block to ensure a light-tight structure. The interface between plate and box has a lip to ensure a light-tight seal.

As shown in Figure 58, the thermal feed-thru structure has a thin G10 disk, which is only loosely clamped at its edge by a restraining ring attached to the outside of the outer shell. The disk has a two-part copper plug through its center, forming the cooling path through the outer shell. These components are flanged and mate so that they too only make loose contact and don't clamp the inner edge of the hole in the G10 disk. Thus the plug is isolated from thermal contact with the outer shell. The hole in the outer shell through which the plug passes is only just larger than the plug, so that it blocks most thermal radiation coming through the G10 disk. A thermal strap of braided copper connects the plug to the molybdenum block supporting the detector. This strap is curved so that it can flex as the focus mechanism moves the block, and also conform to thermal contraction of the molybdenum block without introducing stress.

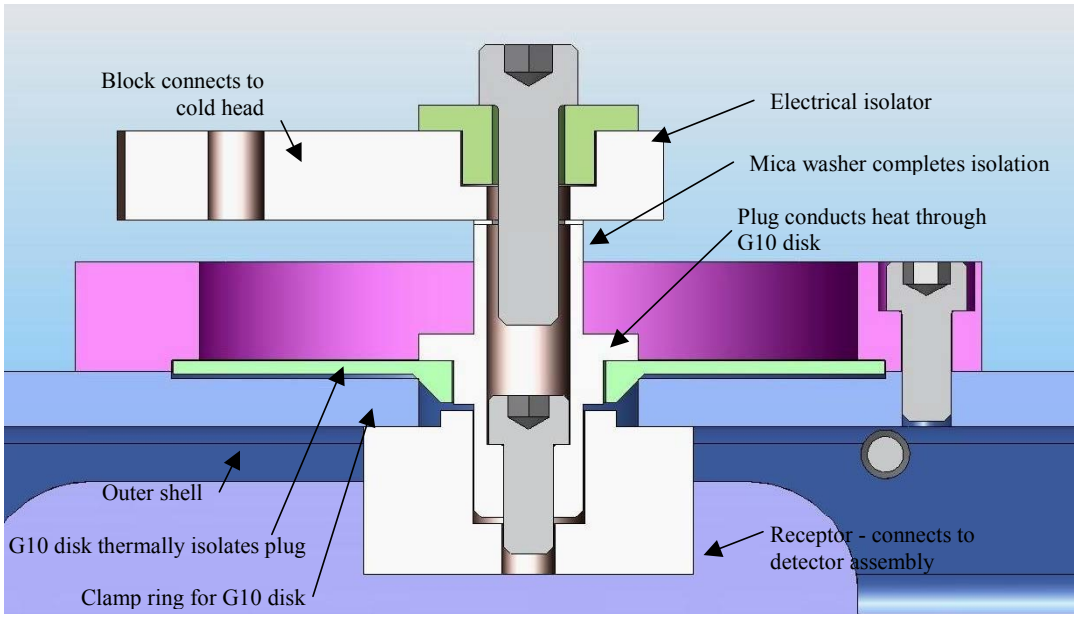


**Figure 58: Thermal Feed-thru Structure for Detector Head with Electrical Isolation**

As well as providing a thermal link for cooling but with thermal isolation from the detector head shell, this design incorporates electrical isolation, so that the cooling path doesn't interfere with the detector grounding scheme. The block on the outside that links to the cold head is connected to the copper plug by a #6 socket cap screw. This screw passes through a G10 isolator so it doesn't make electrical contact with the block. Between the block and the copper plug the screw passes through a thin (~0.001in) mica washer. This washer is so thin it makes little difference to the thermal conductivity of the assembly, but it is a very good electrical insulator.

Heat flow along the A-frames was calculated as 0.009 W per leg. This estimate is based on anticipated temperatures of 77 K for the detector and 120 K for the instrument structure. For four support legs, the total load is estimated to be 0.056 W. Additional thermal simulations of the

detector head are summarized in §5.2.1.10. More details of the detector head design can be found in MMDN07.

Prototypes of the detector mount and detector focus were fabricated during the detailed design phase. Detector focus mechanism tests are still in progress. Detector mount tests have been slowed due to a delay in establishing the detector contract with Teledyne. The fabrication drawing package for the detector head is approximately 90% complete.

### 5.2.1.9 Configurable Slit Unit

Our contract with CSEM for the Configurable Slit Unit (CSU) has progressed well, with a successful critical design review (CDR) recently completed. Since the MOSFIRE PDR, the design of the CSU has changed in only a small number of areas. In September 2006 ambient and cryogenic testing was completed on a prototype of the MOSFIRE CSU design. Based on the success of these tests CSEM was authorized to proceed with the detailed design of the deliverable CSU. This phase included the development of a detailed CAD model of the complete CSU and reached a successful conclusion at CDR last month. Production drawings are also nearing completion and full scale development of the CSU will begin shortly.

As discussed in the MOSFIRE preliminary design report, the MOSFIRE CSU is based on a prototype built for the European Space Agency (ESA) as a candidate for the slit mask on NIRSpec, an instrument to be installed on the James Webb Space Telescope (JWST). The prototype is shown in Figure 59

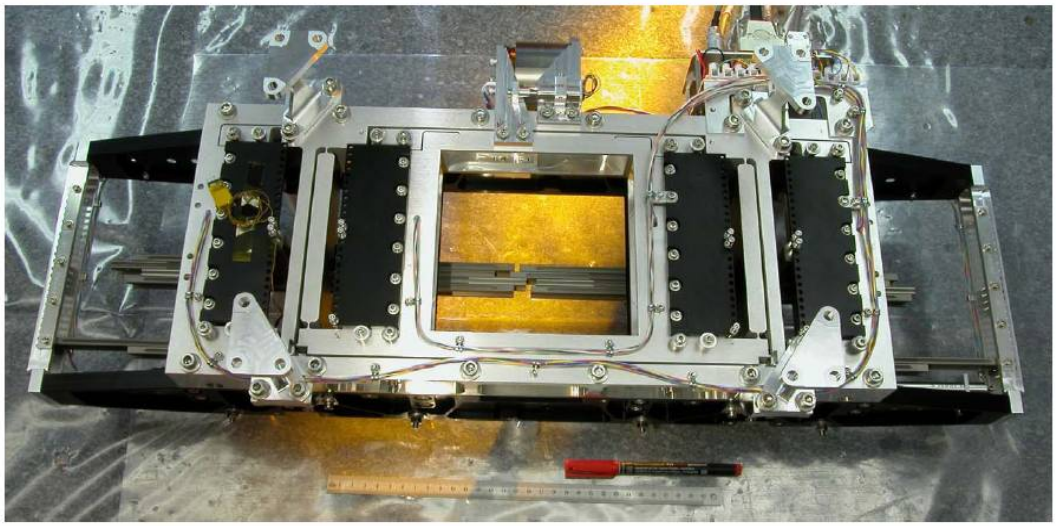

**Figure 59: Prototype CSU Developed by CSEM for ESA**
Only a few slit bars are installed.

The CSU is designed to simultaneously displace masking bars across the FOV to mask unwanted light. A slit is formed at a designated position within the FOV by positioning two opposing bars so as to create a rectangular slit. The end of each bar carries a slit jaw whose height is set to approximate the curvature of the Keck Telescope focal plane. A set of 46 bar pairs will be used to

form the MOSFIRE focal plane mask. The sides of the bars are convoluted so that light is prevented from passing between adjacent bars. Bars that form one side of the slit can be moved independently of those that form the other side, so that any width of slit can be formed, up to a completely open imaging field when the bars are fully retracted. Also, bars on one side form an identical assembly to those on the other.

The CSU consists of two major subassemblies, the indexing stage and the support frame. Figure 60 shows the full scale design of these two subassemblies in detail. It is the indexing stage that provides the mechanism for positioning the bars. Masking bars are displaced across the FOV using incremental steps (inchworm principle) where a number of oscillating steps are required to displace the masking bars. A voice-coil actuator on an indexing stage provides the motion to move the bars from opposite sides simultaneously. A common position sensor (LVDT) keeps track of all relative movement of bars with respect to the fixed reference frame. All bars can be displaced at the same time or individually, as is the case when final slit position is to be achieved.

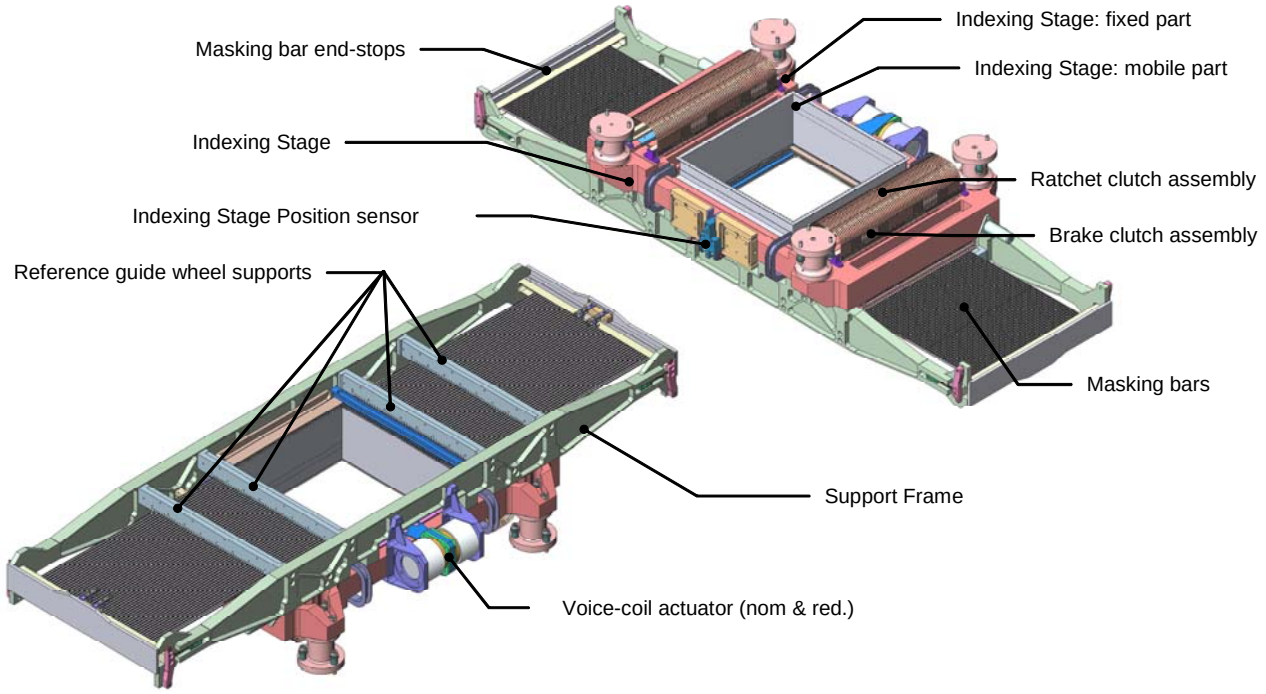


**Figure 60: Major CSU Sub-assemblies: the Indexing Stage (top) and Support Frame (bottom)**

The ratchet and brake clutch actuators are used to engage and block the masking bars during the incremental movement of the indexing stage. Clutches are assembled in a side-by-side array to create a sub-assembly capable of addressing all bars in parallel or individually. The masking bars are held within the support frame and are guided using rollers on bushings.

Some of the mechanism details are shown in Figure 61. The masking bars are guided using three pairs of crossed rollers; two rigid pairs and a spring-loaded pair that is compliant in the Z-direction

and pre-loads the sub-assembly. The rollers ride on a pair of angled surfaces machined along the top and bottom lengths of each bar. On the upper surface, the bars are machined to provide a tooth profile that engages with the ratchet clutch to provide motion. Tooth pitch is 1.2 mm.

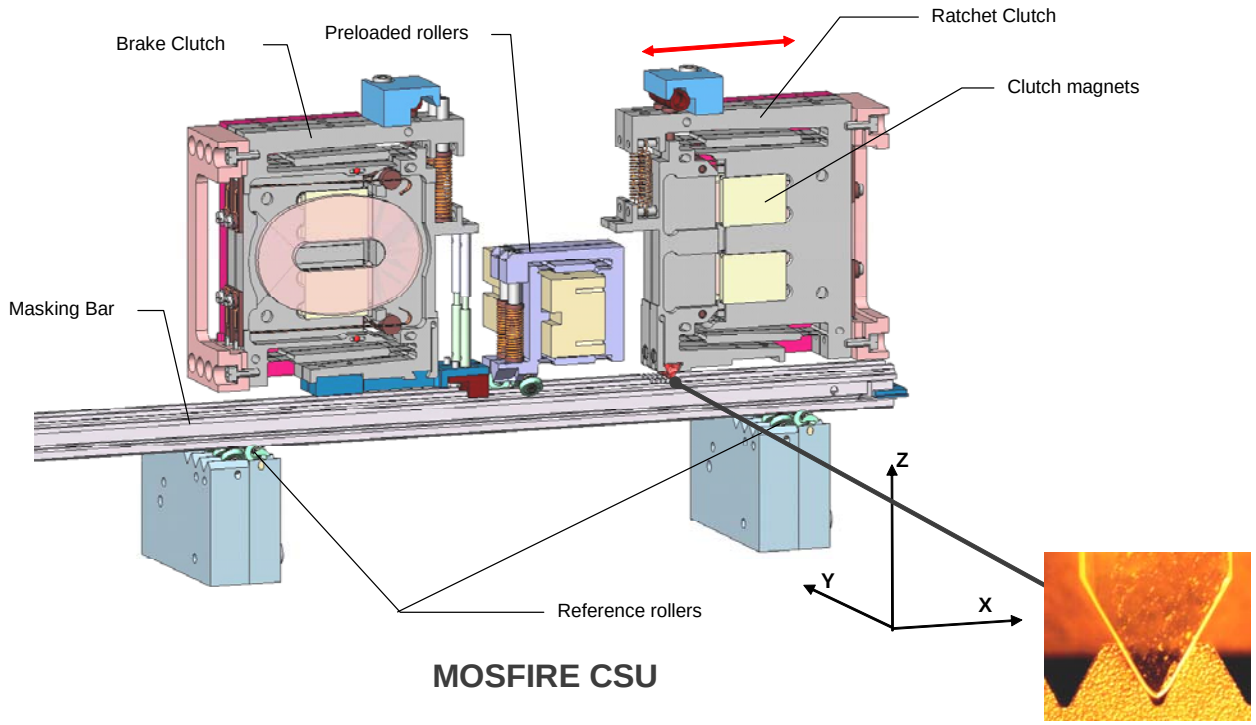


**Figure 61: MOSFIRE CSU Masking Bars and Guide Wheels**

There are two mechanisms associated with each bar: a brake which holds the bar's position by friction and a mover (called the ratchet clutch) which inserts a sapphire claw between the two teeth nearest it on the bar's edge. A coil of wire moving in a magnetic field actuates each of these mechanisms. By energizing a bar's brake coil, the brake for that particular bar can be released, and by energizing a bar's mover coil, the mover claw for that bar is inserted. With this design, any configuration of bars that have their mover ratchet clutches engaged and their brakes released can be moved by up to one tooth pitch. The configurations for each side are independent.

#### 5.2.1.9.1 Operating Modes

When all the bars are in-phase, any number of bars can be moved one step in any direction at each cycle. This is called mode 1, discrete in-phase group motion that allows the bars to move quickly to the vicinity of their exact target position. The bars can be moved within single steps only by individual actuation of one bar in mode 2, continuous out-of-phase individual motion. This continuous individual motion is how the slit position accuracy and slit width accuracy requirements of the mechanism are achieved. Figure 62 shows the sequential movement of one pair of bars: modes 1-2-1, and represents the state of the system after one consecutive cycle time (top to bottom).

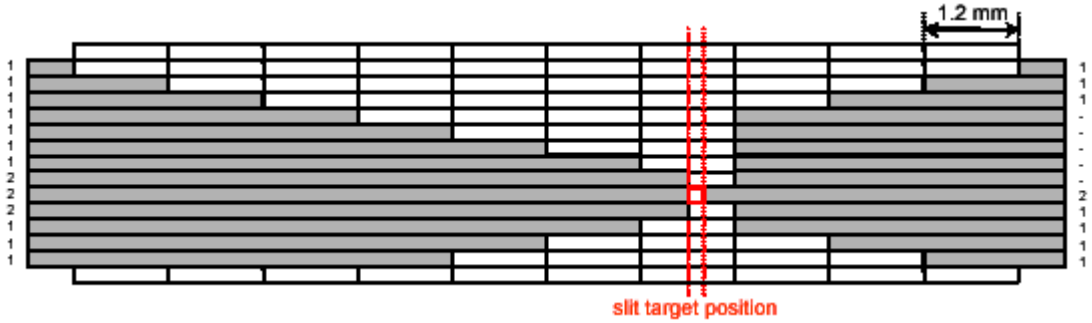


**Figure 62: Sequential Movement of One Pair of Bars: Modes 1-2-1**

There is also a masking bar initialization mode which is meant to retract all bars to the FOV open position in the case where total position information of the bar is lost (memory loss, power loss). In this mode each bar is activated individually and retracted to its end-stop position.

If all of the bars were retracted so the mask is open and it is desired to form a pattern of slitlets, the following efficient sequence of motion would be used:

1. All the ratchet clutches would be engaged and all the brakes released.
2. The frame for all the clutches would be moved one tooth pitch, the brakes engaged and the ratchet clutches disengaged.
3. The frame would then be moved again by one tooth pitch while the brakes hold all of the bars.
4. The three preceding steps are repeated until at least one bar is within one tooth pitch of its final destination.
5. The motion next cycle will engage the ratchet clutch and release the brake only for the bar (or bars) that are now less than one full tooth pitch of their final destination.
6. A motion of less than one full tooth pitch is then used to position the bar at the exact position.
7. Combinations of steps 1 to 4 and 5 to 7 are continued as required until all bars are at the final positions.

By moving groups of bars together by full tooth motions as much as possible, the time to configure all of the bars is less than the time needed to move one bar across the field. The worst case full reconfiguration is from a fully open FOV, to a set-up with all 46 bars all the way across to one side and then back to the fully open position. As discussed in section 3, to go from one slit configuration to another typically takes ~4.5 minutes, while going from image mode to or from a slit configuration takes ~3 minutes. The maximum reconfiguration time is within the requirement of 5 minutes.

The CSU development program consists of two phases. The first phase, which is complete, included the development of a prototype of the MOSFIRE CSU mechanism incorporating changes for the larger field of view and the needs of ground based operation such as a variable gravity orientation. CSEM refers to this prototype as the EUX model. As mentioned above, ambient and cryogenic testing of the EUX was completed during the MOSFIRE detailed design phase in

September 2006. Also part of this phase was a detailed thermal analysis of the temperature gradients in the bars and light leakage between the bars. Following a successful critical design review in mid-March 2007, CSEM is now ready to continue with the second phase, full scale production.

#### 5.2.1.9.2 Bar profiles and knife edges

The bar profile has been optimized to reduce mass and maintain lateral stiffness. Each aluminum bar is 10 mm by 445 mm. To reduce the mass of the masking bar a detailed trade-off study was carried out to find the preferred shape. The resulting bar profile, prototyped with the EUX, is shown in Figure 63. A knife-edge fitted to each bar defines the slit. Each knife-edge pair is tilted by 3 degrees to provide the required over-sampling. Light leakage between the bars is minimized by a masking shoulder that determines the fill factor of the mechanism as shown in Figure 64.

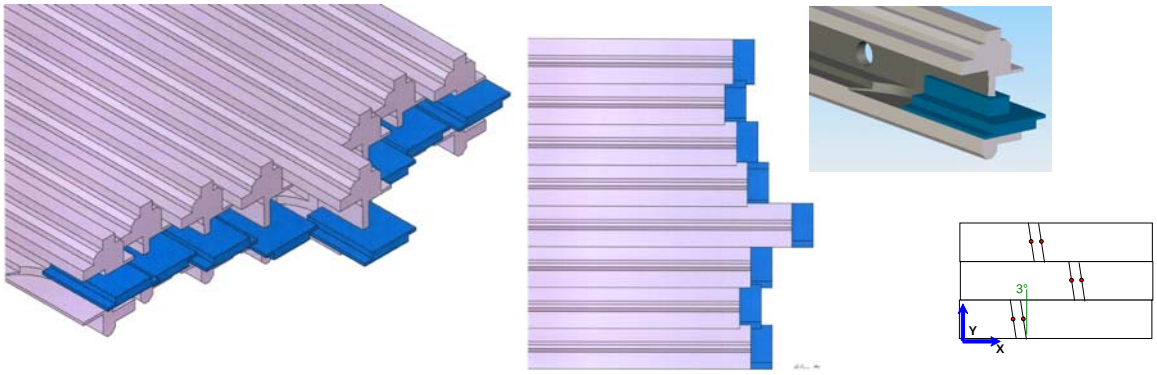


**Figure 63: Slit Bar Profiles and Tilted Knife-Edge**

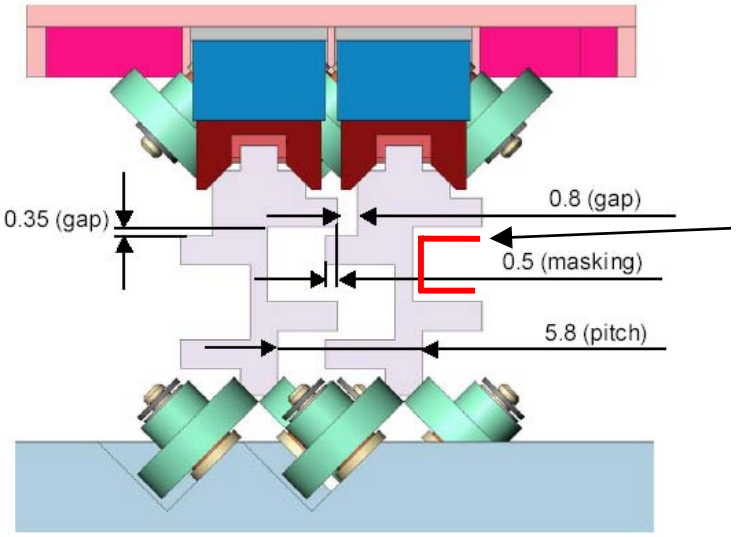


**Figure 64: Guide Wheel and Bar Detail**

A tribology surface coating of Ni-PTFE improves friction properties and is applied on all surfaces. This coating also limits the amount of light reflected between bars, but this has been deemed to be insufficient based on light-leakage tests carried out on a small set of test bars using an IR camera at UCLA. Transmission factors of about $10^{-6}$ were measured. An additional low reflectance coating will be applied to the sides of the bars to reduce the transmission to less than $10^{-7}$. The area where the coating will be applied is shown in Figure 64.

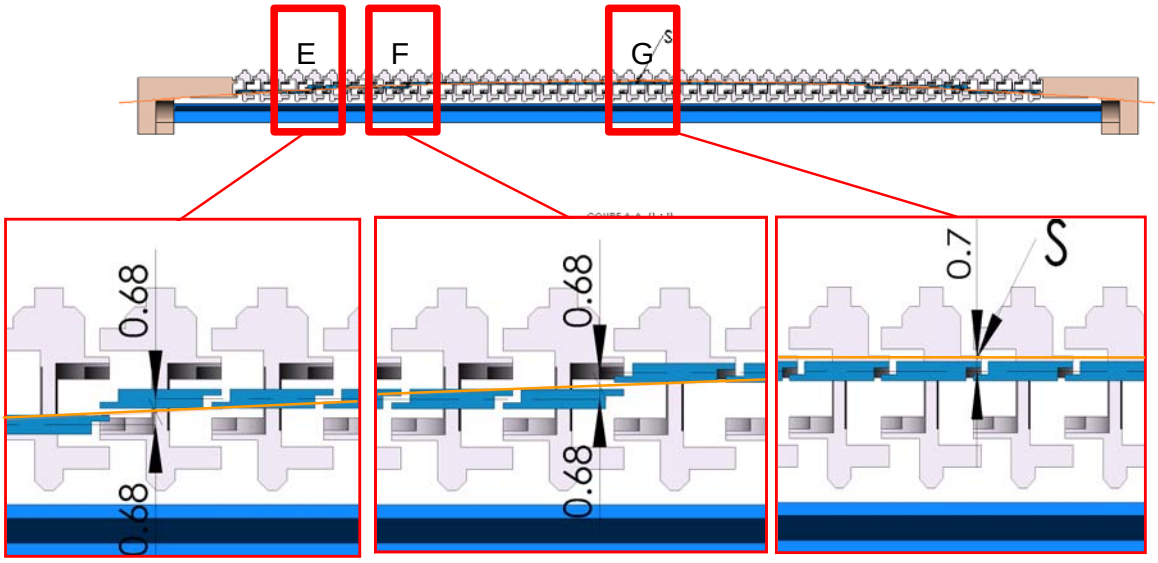


**Figure 65: Three-tiered Arrangement of Knife Edges to Compensate for Field Curvature**

Because of the field curvature of the Keck telescope, the MOSFIRE focal plane is not flat. An approximation of the spherical radius of curvature (2.124 m) by two flat planes with an angle of 176.47° was rejected because the knife edges were so far in front of the focal plane that the f/15 beam expansion unacceptably reduced the slitlet length. For this reason, a three level design with the knife edges interior to the range of the bar section was chosen. The change in height (Z) from one end of the MOSFIRE FOV to the center is 4.04 mm. The new design is shown in Figure 65.

#### 5.2.1.9.3 EUX Prototype

The EUX prototype mechanism shown in Figure 66 can index two bars across the field of view. The test campaign at both room temperature and cryogenic temperature has evaluated all critical parameters. This prototype is representative of all critical components (ratchet and brake clutches, guide rollers, limit switches, actuators and sensors) as well as interfacing with the control system and electronics. Lessons learned in these extensive tests included the following:

- LVDT calibration – error sources identified
    - Sensor core changed (larger diameter armature) to minimize sensitivity
    - Calibration and initialization procedure improved
- Clutch oscillations at cryogenic temperature operation

    - Error checking not functional – limits surpassed due to voltage transients from mechanical oscillations
- Brake Clutch pad support deformation greater than expected
    - Source of parasitic axial movement
    - Stiffening rod added
- Limit switches (2 reed-relay & 10 MyCom)
    - MyCom switches not reliable (1 failed open during cryogenic tests)
    - Thermal stability unpredictable $\Delta$ ~25 μm

All problems encountered during the testing were corrected successfully.

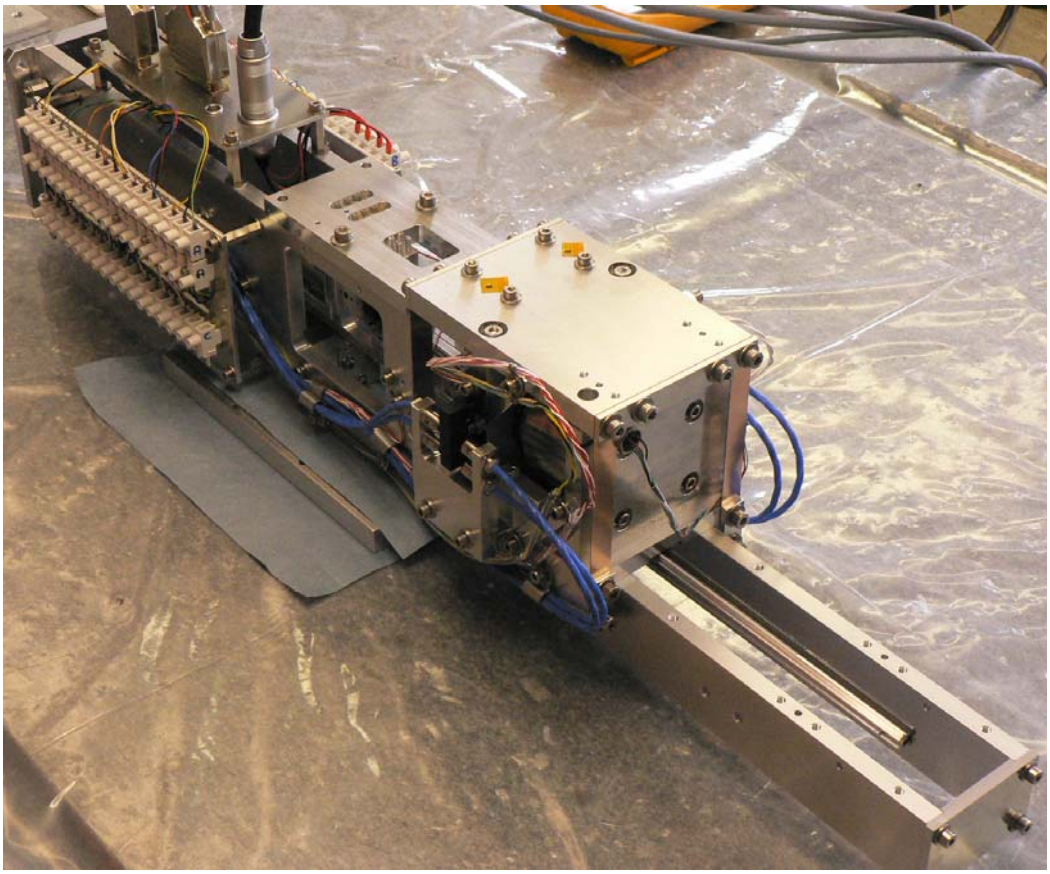

**Figure 66: EUX Prototype**

The EUX has evaluated all performance requirements with respect to bar positioning, initialization functions and operation in both horizontal and vertical positions. Cryogenic testing was carried out in a large chamber at CERN. An electronic system was developed for control of the CSU. The control software runs on a commercial off-the-shelf controller card purchased from dSpace. Electronic hardware is divided into two racks, a control rack including the intelligent motion control system, and an amplifier rack to drive the brake and ratchet clutches. The dSpace DS1104 card is mounted in a mini-PC with its own power supply. The prototype control electronics rack

used successfully during the EUX tests is shown in Figure 67. The control rack and amplifier rack will be mounted in the MOSFIRE electronics cabinet.

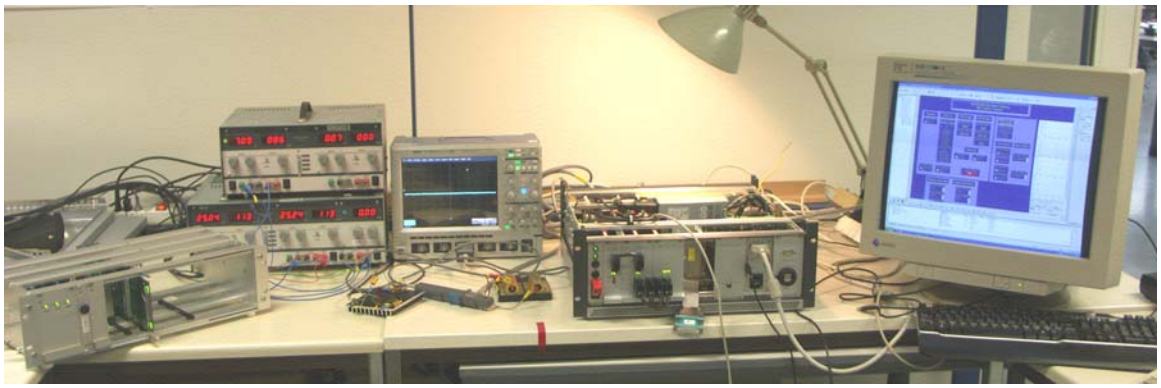

**Figure 67: Prototype Control Electronics Rack During Bench Tests**

Prior to CDR, CSEM carried out detailed thermal and finite element analyses of the CSU. In particular, the effect of radiative heating and cooling of the bars as they are moved in an out of the beam during observing cycles. The graph in Figure 68 illustrates the temperature distribution in the CSU and the thermal excursions experienced for an assumed radiation load of 1.2 W, 1800s observations and an emissivity of 0.35. Based on the thermal analysis of the double-window design the actual heat load should be ~4x smaller. Nevertheless, the bars never reach 130 K, which was our upper limit. Thermal effects therefore contribute a relatively small term (<15 μμm) to the error budget for the position of the masking bar tip and positional accuracy remains with specification.

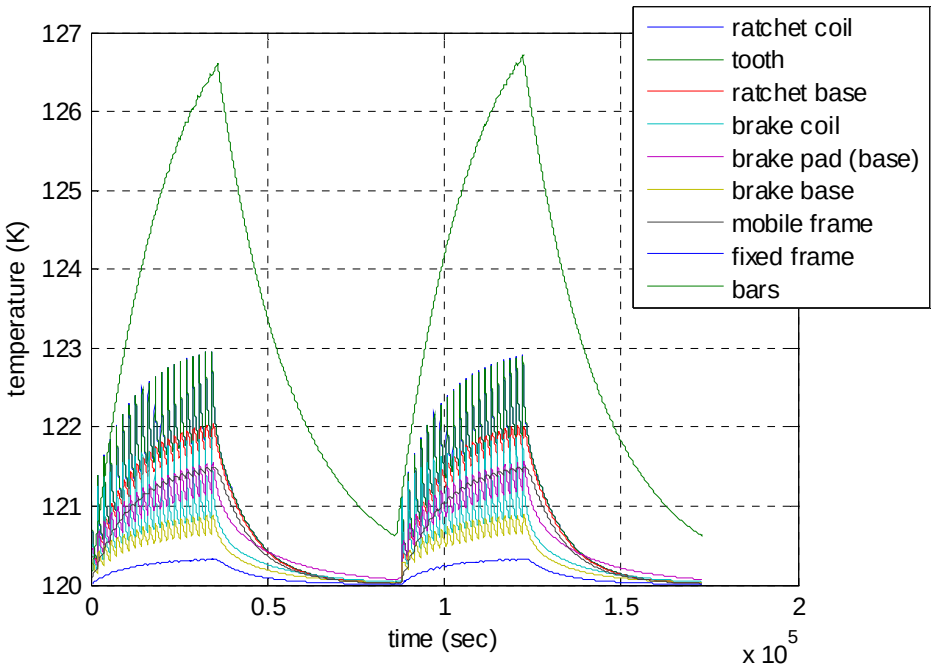


**Figure 68: Thermal Analysis and CSU Temperature Distribution**

During the initial study phase a specification was provided to CSEM and a detailed compliance matrix was developed. The compliance matrix was reviewed in detail at the CDR. It shows, with a few exceptions that are being worked, that all our requirements can be met. CSEM is working under a firm fixed price contract for the CSU that also includes control electronics and low-level software. There has been a small augmentation to the contract to add an additional bar pair to increase the original number from 45 to 46, vacuum impregnate the brake and clutch coils to reduce outgasing in the vacuum, and procure spares of long lead custom components. The delivery of the CSU continues to be as expected in mid 2008 for the complete 46-bar unit.

#### 5.2.1.10 The MOSFIRE Cryogenic System

For proper operation, MOSFIRE must be a cryogenic instrument. The instrument layout and internal structural design must be compatible with cryogenic conditions. Space, weight, and service restrictions at the intended Cassegrain mount location of Keck I also influence the instrument design. MOSFIRE's structural and thermal systems design achieves a balance of these considerations, while also meeting instrument stability (flexure) goals. The design for MOSFIRE has been refined so that it meets all of the objectives presented at the PDR. The main elements have not been greatly altered but there have been many refinements needed to meet requirements that have flowed down from other technical areas.

The layout of the internal structure still achieves a balance between structural flexure and thermal design considerations. The concept of two stout, circular bulkheads separated by a pair of concentric, stubby tubes has been shown to perform equally well in minimizing flexure and minimizing thermal gradients within the structure. The aluminum internal structure is supported inside the vacuum chamber by a thin-walled G-10 tube. This tube serves as an insulator, resisting thermal conduction between the internal structure and the vacuum chamber structure while also serving as an efficient, stiff support.

The entire internal structure is surrounded by a cooled, floating shield constructed of ~6 mm thick aluminum sheet. The shield is made of 1100 series aluminum whose high thermal conductivity minimizes thermal gradients. This shield, whose maximum temperature is kept below about 135 K and acts to minimizes the thermal load and gradients on and within the internal structure. The exterior of this shield is enshrouded with 40 layers of 0.25 mil MLI. The shield is connected to the interior optical bench near the attachment points of the cold strapping from the two CTI-Cryogenics Model 1050 single stage cold heads.

The cold heads penetrate the cylindrical portion of the vacuum chamber, the shields, the G-10 support tube, and the internal structure at a location between bulkheads A and B. Thermal conduction from the cold heads to the bulkheads is provided by flexible cold straps. These will be similar to cold straps used in previous instruments. For example, in Figure 69 a pair of spare NIRC2 straps is visible in this image of a test assembly. The straps consist of many layers of copper sheet, fused together at each end of the strap.

These straps are divided equally between A and B bulkheads. They are positioned ~120 degrees apart around the tube in order to provide equal cooling through both large bulkheads. These

bulkheads serve as conduits for removing heat uniformly from the structure's extremities. A speed controller will be used to extend the lifetime of the cold heads once the operating temperature is reached in 8 days or somewhat less if sub-cooling is allowed. The cold heads are sized for cool down; they have several times the capacity needed to maintain a bench temperature of 120 K.

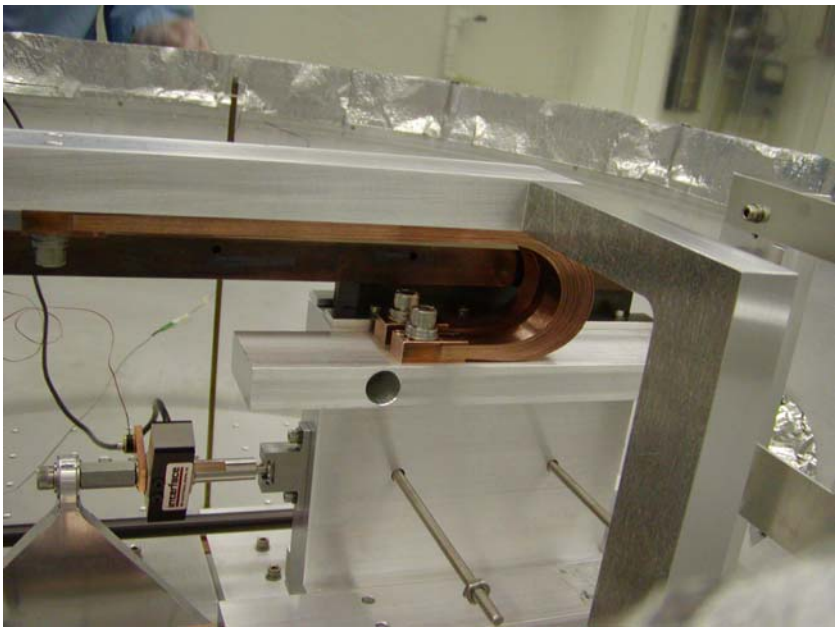

**Figure 69: NIRC2 Flexible Thermal Strap Design**

A third, smaller, two-stage CTI-Cryogenics Model 350 cold head is used to cool the detector as well as the getter container. This container will be insulated from the bulkhead and is cooled by the second stage of the cold head, so that the getter can be maintained at a very low temperature for optimal performance. This cold head will also be mounted to the cylindrical portion of the vacuum chamber immediately in front of the instrument's rotator bearing location. The cold head protrudes into the instrument just behind bulkhead B near the detector head.

Figure 70 depicts the general cold head mount design for MOSFIRE. The mount design is based on mounts utilized for both NIRC2 and OSIRIS (Figure 71). Since MOSFIRE is located at the Cassegrain position location, the previous cold head mount design must be modified to work in multiple gravity orientations. This is achieved by re-sizing the compression springs to handle lateral loads and by ensuring that the assembly's CG is centered between the springs.

The cold head spreader bar incorporates a heating arrangement controlled by the secondary temperature control loop of a Lake Shore 340 temperature controller. This provides a means to more precisely regulate the internal temperature of MOSFIRE that is possible just using adjustment of the cold head speed controls. More details on the cold head mount design can be found in MMDN17.

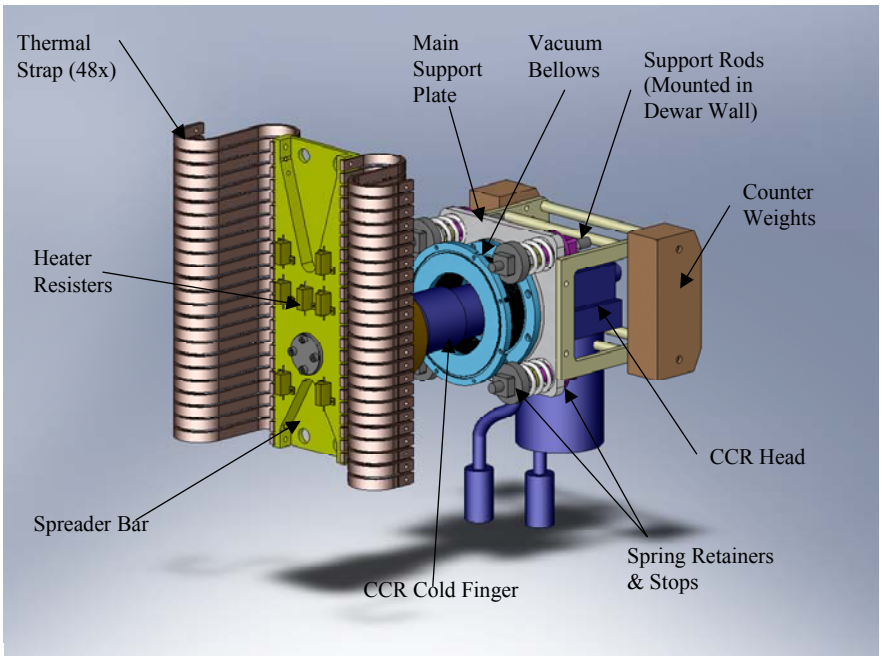


**Figure 70: CTI 1050 Cold Head, Thermal Strapping, and Low Vibration Mounting System**

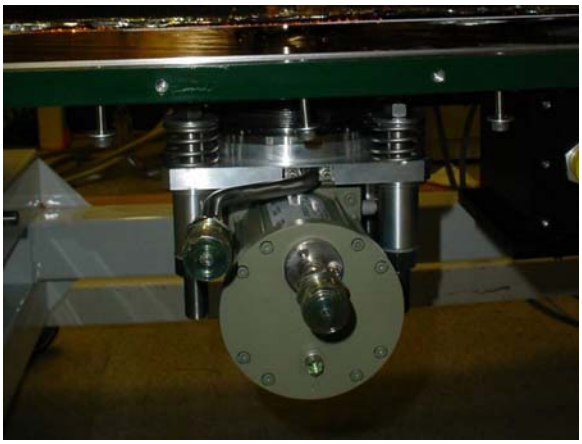

**Figure 71: CTI 1050 Cold Head Installed on OSIRIS**

A thermal analysis (MOSFIRE Thermal Analysis Report v4.0, Space Dynamics Lab, March 2007) includes both steady state and transient studies. A worst-case ambient temperature of 300 K was assumed. From the steady-state analysis the estimated temperature distribution within MOSFIRE under operating conditions was determined. We used this analysis to refine the thermal design to make the refractive optics as isothermal as possible and to reduce the power radiated on the masking bars of the CSU. These bars have a minimal conductive path to their supports. The former was done by redesigning the shield and making a very direct conducting path from it to the cold heads, while minimizing all other paths. The latter was accomplished by redesigning the heater and cold baffle for the window to make them much more efficient in minimizing radiation on the inner widow and also minimizing radiation from the vacuum window to the interior of the instrument,

while at the same time maximizing the efficiency of delivering radiant energy from the heater to the vacuum window.

The thermal gradient in the optical bench was reduced from 9 K at the PDR to about 2 K on those surfaces where the optics modules are mounted. The aluminum optical assemblies further reduce the gradients in the lenses. The total amount of thermal radiation on the CSU masking bars has been reduced from 2 W to less than 0.3 W in the final design, while still keeping the outside surface of the vacuum window at ambient. The steady state load on the cold-heads has also been reduced. It is now 47 W worst-case and 28 W nominal on each head. This will allow the heads to be run at a fraction of their full speed with an attendant increase in lifetime.

There was a concern about the equilibrium temperature distribution in the field-flattening lens and in the preceding barium fluoride lens in the camera barrel that has been addressed. The field flattener is attached to the detector assembly whose nominal temperature is 77 K, while the camera barrel is tightly thermally coupled to the optical bench, whose temperature is 120 K. The result is that the gradient in either lens is less than 0.1 K. The flattener is about 1.3 K hotter than the detector assembly while the barium fluoride lens is about 0.5 K colder than the rest of the camera barrel. The result is that the optical performance is not compromised in any way.

The dynamic analysis shows that the cool down time is 8 days if the cold head power is reduced when it reaches its nominal operating temperature. If the power is maintained so as to temporarily sub-cool part of the instrument, that time might be reduced somewhat.

It was determined that the field lens of the collimator was the most critical optic with respect to the adverse effects of thermal transients. It is the largest optic and is made of calcium fluoride, a crystal subject to fracture under thermal stress. The analysis shows that the maximum temperature difference from the center to the edge of the lens during the whole cool down sequence is 2 K.

The distribution of the temperature gradient is smooth and is shown in the thermal analysis report. Figure 72, Figure 73, Figure 74, Figure 75 and Figure 76 are examples of some of the results given in the thermal analysis report.

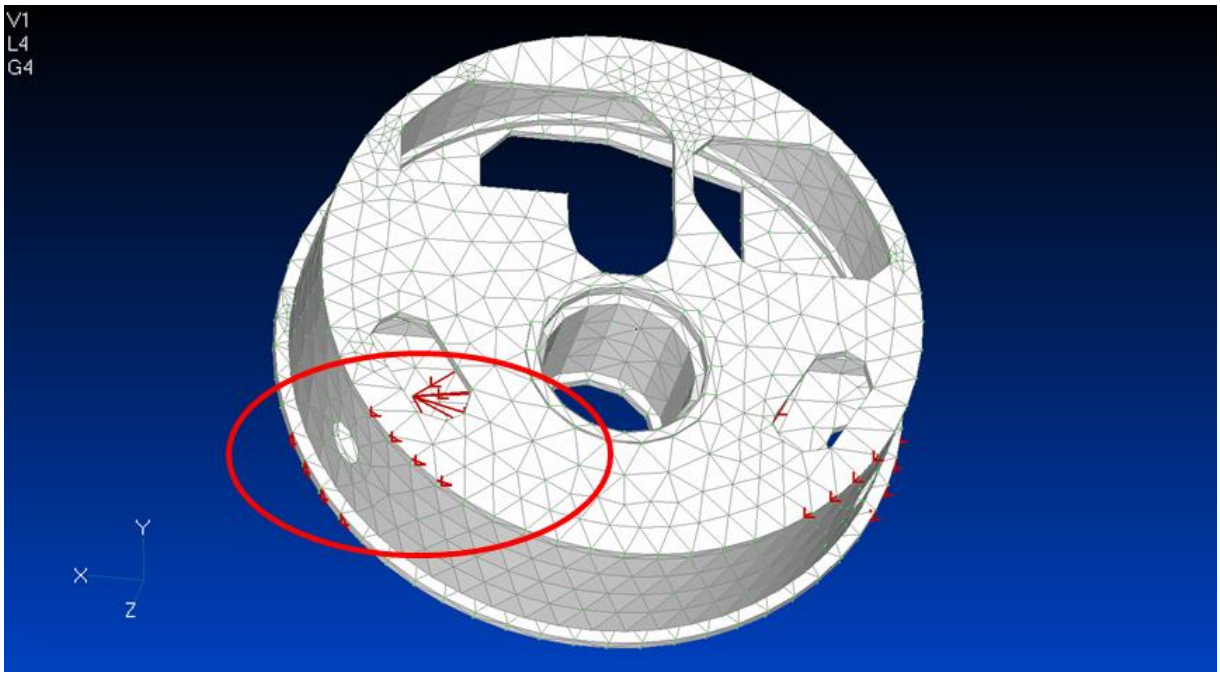


**Figure 72: Internal Structure Analysis Model**
The cold head attachments and cold shield attachments are indicated with the red arrows.

| Heat Source/Sink Description | Worst Case (Watts) | Nominal Case (Watts) |
|---|---|---|
| Cryo-cooler 1 | 46.9 | 28.3 |
| Cryo-cooler 2 | 46.9 | 28.3 |
| Dewar Window | 20.13 | 16.1 |
| Wiring | 2.5 | 2.0 |
| CSU | 1.5 | 1.32 |
| Radiation & G-10 Ring | 69.75 | 37.2 |
| TOTAL Heat Removed | 93.9 | 56.6 |

**Table 19: Thermal Analysis Predicted Heat Load**

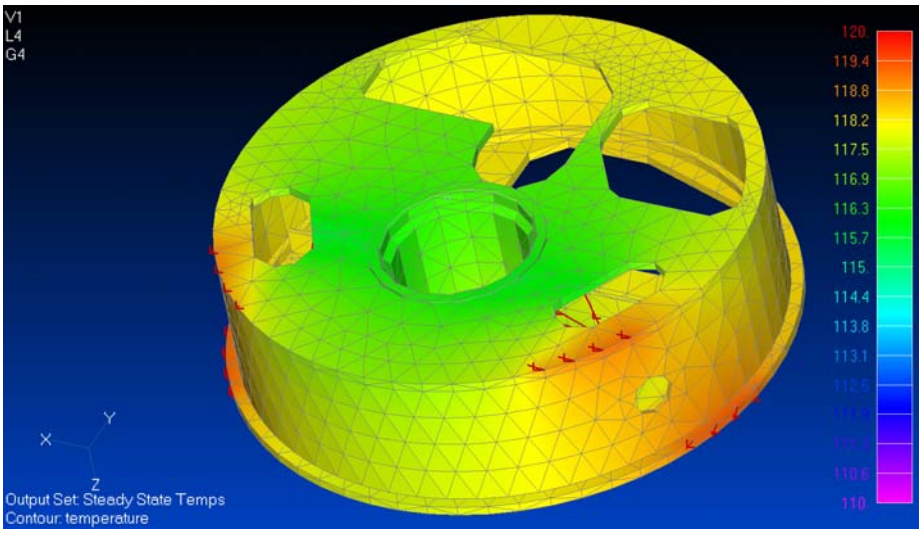


**Figure 73: Nominal Instrument Structure Temperature Plot**

The locations of the cooled shield attachments are apparent as the hottest regions. The cold head attachments are the coolest regions in this plot.

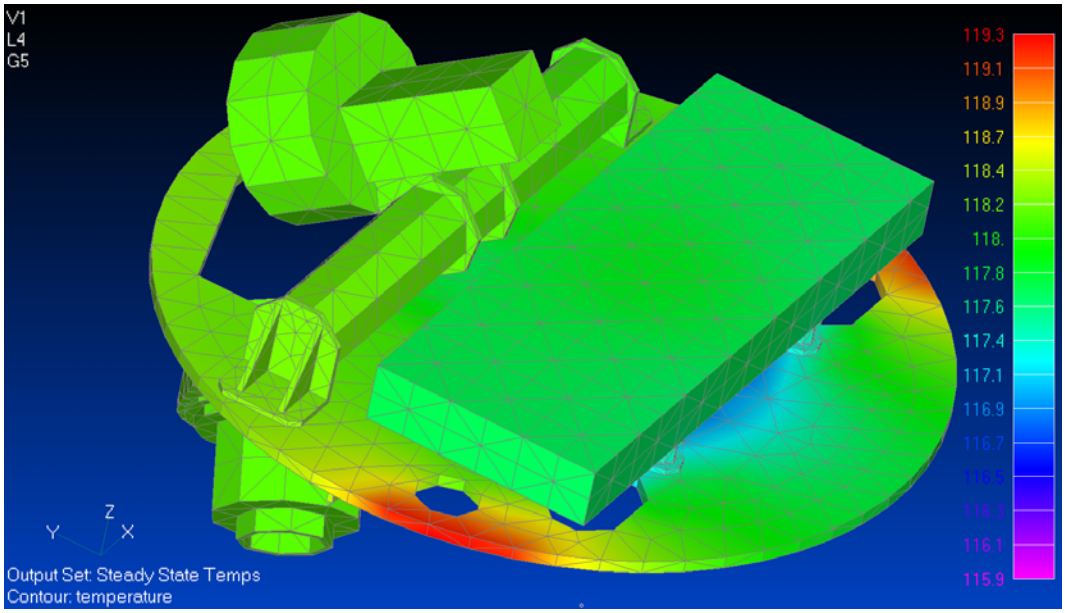


**Figure 74: Temperature Distribution in Components Attached to Bulkhead A (nominal load case)**

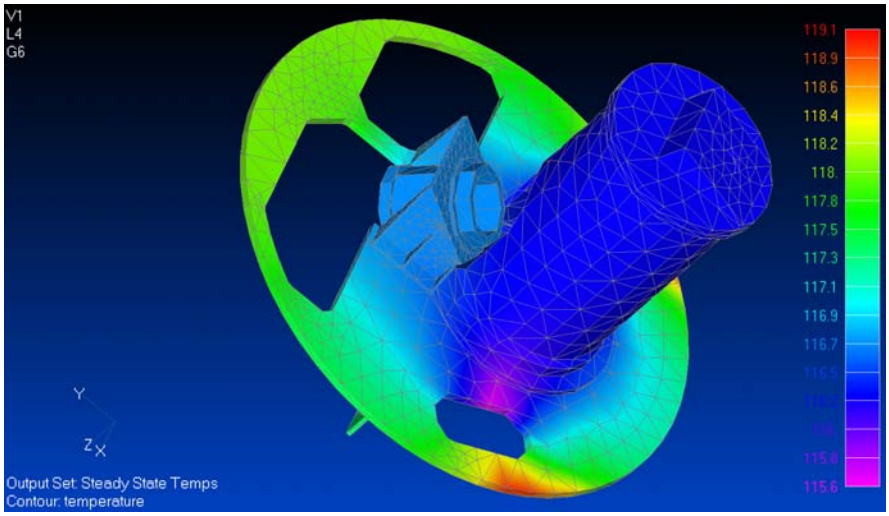


**Figure 75: Temperature Distribution in Components Attached to Bulkhead B (nominal load case)**

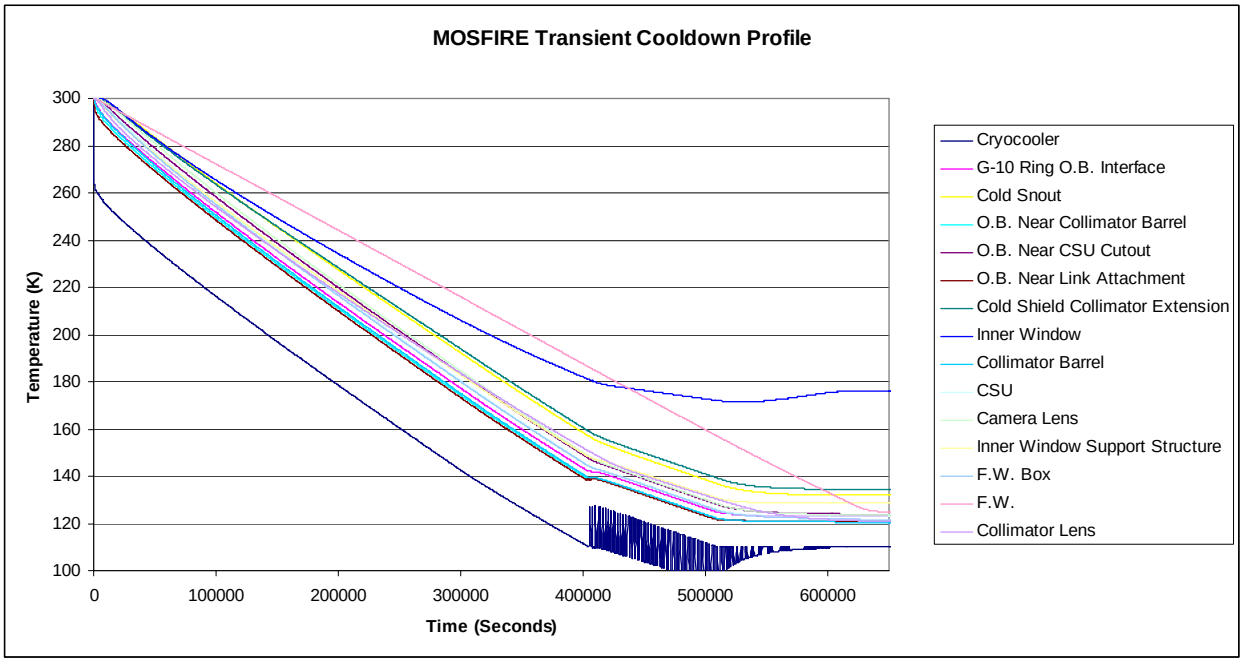


**Figure 76: Transient Cool Down Plot, 100000 s is 1.16 days**

### 5.2.1.10.1 Performance Predictions

- Steady-state cooling requirement: 57 W
- Cold head heat sink temperature: 110 K
- Cool down time: < 8 days to ~120 K
- Maximum structure temperature gradient: ~2 K
- Maximum optic component temperature gradient: 0.1 K
- Maximum optic sub-assembly temperature distribution: ~2 K
- Radiant power incident on CSU masking bars: < 0.3 W

#### 5.2.1.11 Cable Wrap and Rotator

The cable wrap (see Figure 77 and Figure 78) is the structure that safely manages the cables and hoses that connect between the instrument and the module as the instrument is rotated about the telescope axis during operation. The rotator is also shown in the figures. The rotator is a modular assembly containing the mechanisms required to rotate the instrument about the telescope's optical axis.

MOSFIRE's cable wrap design is based on a "serpentine" concept created in collaboration with engineers at IGUS, a manufacturer of cable wrap components. The design allows 530 degrees of instrument rotation (+260/-270). The cable wrap assembly basically consists of a plastic chain (carriage) that encases the required hoses and cables. The chain protects its contents and helps limit the direction and degree of bending that can occur. The end of the chain near the instrument's axis is attached to a drum-shaped guide (spindle) that rotates with the instrument. The other end of the chain is fixed to a stationary cylindrical drum (outer guide) that is secured to the rotator module. This outer guide constrains and helps support the chain as it moves through its range of motion. A carriage tray is also attached to the outer guide to help support the chain when the instrument's axis is vertical with respect to gravity.

The wrap's components were sized with extra capacity to allow for future contingencies. In order to eliminate repeated rubbing friction between the larger contents as the carriage reverses its bend during operation, all of the hoses contained in the wrap have been located aligned with the carriage neutral axis. This will minimize the chance for binding and wear damage to the carriage contents. The carriage is constructed of a low-friction plastic to minimize friction effects on the carriage's contents. The cross-section of the carriage was sized based on the largest cross-section of the contents. The cold head hoses are the largest items to be managed by the carriage and they have the largest minimum bend radius. A single pair of hoses will supply all three instrument cold heads. Manifolds on the instrument will split the supply and merge the returns.

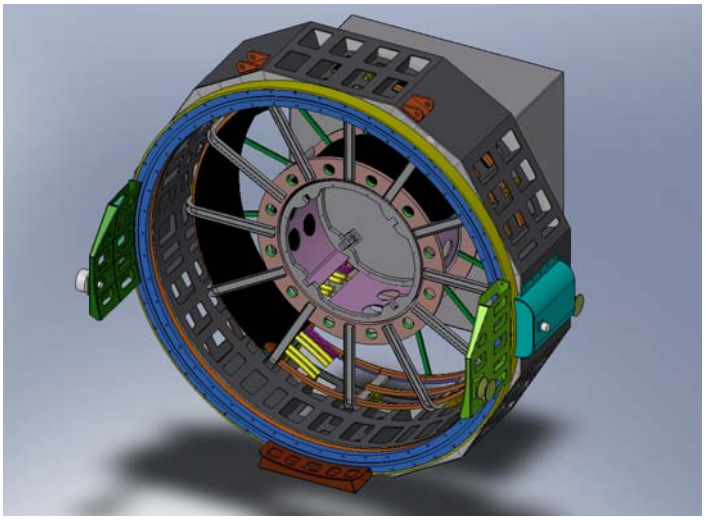

**Figure 77: Front ¾ view of the Rotator Module, Cable wrap and Electronics Cabinet Assemblies**

The hose carriage was selected with the assistance of IGUS. The interior of the carriage is separated into 9 compartments. Two compartments contain the cold head flexible hose pairs. Two compartments hold a pair of heat exchanger lines: supply and return. A heat exchanger will be required to remove any heat generated by the instrument electronics from the instrument so that it doesn't escape into the dome. The heat exchanger lines are assumed to be equivalent in size to the cold head return lines. One compartment will contain the power cable for the instrument. There is a compartment for fiber optic cabling and two compartments are currently spares. Figure 79 depicts the carriage cross-section layout.

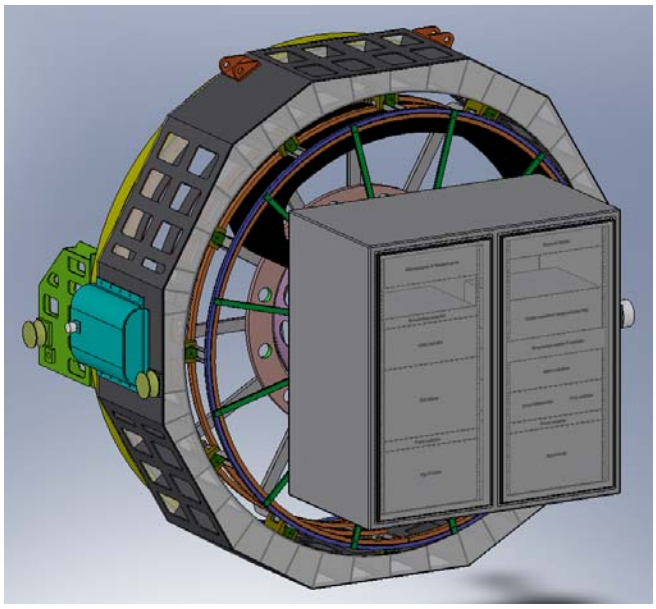

**Figure 78: Rear ¾ View of the Cable Wrap and Electronics Cabinet Assemblies**

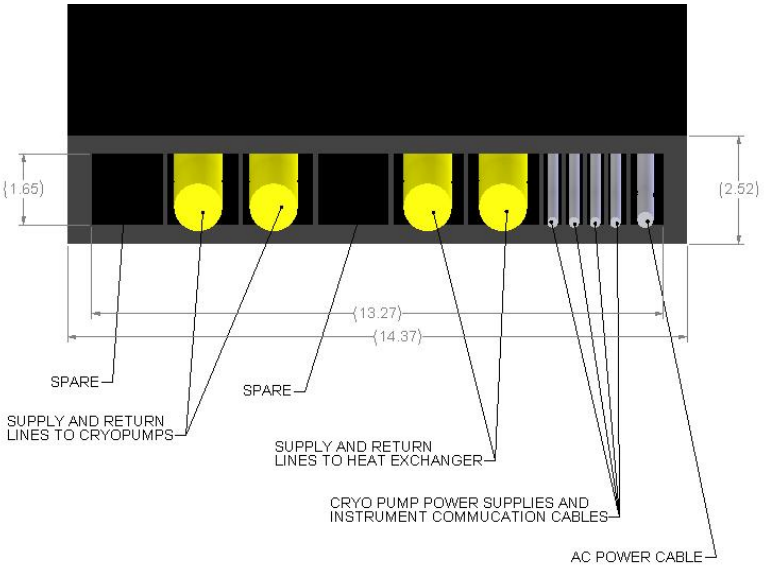


**Figure 79: Cross-section View of the Cable Wrap Carriage**

In order to provide access to the rear cover of the dewar, if necessary, the cable wrap and the electronics cabinet are designed to be removable with relative ease. The electronics cabinet assembly will be supported from support struts that reinforce the cylindrical protrusion of the rear dewar cover since the electronics cabinet must rotate with the instrument. The central hub of the wrap encases the cylindrical protrusion in the dewar's rear cover and the hub is also attached to the support bars. The hardware for attaching the electronics cabinet to the hub will be located so that it is accessible, as will all of the connections to the electronics cabinet. When access to the rear cover is required the electronics cabinet will be disconnected and removed first. This will provide access for disconnecting the cable wrap contents at both the instrument and the module. A temporary fixture will be attached to the cable wrap structure that will tie the rotating and fixed portions of the wrap together during removal so that the structure doesn't collapse. The hub can then be un-bolted from the support struts, and the stationary, outer guide structure for the wrap can be un-bolted from the rotator module. The size and weight of these structures will require special handling fixtures and procedures and both are described in MMDN20.

The instrument dewar mounts to a bearing in the rotator module. The rotator module also contains the mechanisms required to define the instrument at the telescope's Cassegrain focal station and it also provides an interface to the instrument handler. MOSFIRE's rotator module will essentially be a copy of the basic design used for LRIS and ESI. Some additional features will be required to interface with MOSFIRE. The module structure must be modified with the attachment points for the stationary portions of the cable wrap guides. Quick-disconnect panels must be integrated into the module structure at the proper locations for the cable wrap connections. The structural design of the original LRIS rotator is currently being assessed with FEA to predict the bearing loads and flexure performance with MOSFIRE attached. This analysis will determine whether MOSFIRE's module needs to be modified with additional bracing.

#### 5.2.1.11.1 Performance Predictions

- Instrument rotation range: 530 degrees (+260 / -270)

The wrap is considered to be a low risk assembly. A similar serpentine wrap design has been used successfully on IMACS. A small prototype was fabricated and tested during the KIRMOS preliminary design phase. The rotator was initially assumed to be a low risk item since it is based on a previous design. Locating a manufacturer who could provide a duplicate bearing in a reasonable time scale has been unsuccessful. But, a spare bearing in WMKO's possession can be refurbished in time to meet MOSFIRE's schedule. There are also concerns whether the existing module structure design is adequately stiff to support MOSFIRE and properly support the bearing outer race. UCO/Lick has been contracted to analyze the module and propose design changes, as necessary. This work is in progress.

### 5.2.1.12 Instrument Handler

The handler is an Observatory standard assembly that supports the instrument when it is not mounted on the telescope and provides for moving the instrument to and from its storage position.

MOSFIRE's instrument handler will be a copy of those previously designed and built for earlier Cassegrain instruments at WMKO (e.g. LRIS, ESI).

### 5.2.2 Integration and Testing

Instrument subassemblies will be integrated at the UCLA IR lab and at CIT. Where ever practicable subassemblies will be tested prior to beginning integration of the complete instrument.

System integration and testing of MOSFIRE will occur at CIT. Assembly will begin in the fall of 2007, with the first cool down cycle planned for February or March of 2008. We have reserved the High Bay Facility of the Downs-Lauritsen Laboratory on the CIT campus for the final phase of the project. This facility has an overhead crane that can easily handle the large structures.

All assembly operations will be performed within a clean room enclosure with a rating of class 100,000. A soft wall enclosure is to be installed in the high bay area at CIT to accommodate the assembly operations. UCLA already has a smaller, similar clean room for sub-assemblies produced there. The estimated dimensions of the Caltech enclosure and build areas are shown in Figure 80. Final details of the clean room enclosure will be refined in the next few months in collaboration with WMKO to achieve compatibility with proposed clean room facilities on the summit for maintenance and repair.

Much of the instrument assembly process will use two existing instrument assembly and test stands, with minor modifications. One of the stands is a flexure test stand originally assembled for another WMKO Cassegrain instrument, ESI, built by UCO/Lick. This stand will be used for mounting the entire Cassegrain module containing the fully assembled instrument (Figure 81). This stand allows the instrument to be placed in all of the gravity orientations that will be encountered at the Keck I Cassegrain position. Another smaller stand will be used for most of the early instrument integration for two reasons. First, the smaller stand is lower to the ground, making work on the instrument easier. Second, the ESI stand requires the rotator module. The rotator module has to go to the observatory for alignment to the telescope axis prior to being sent to CIT and this may limit the assembly process unless another frame is available. Planning to use the smaller stand during the early stages of assembly reduces the chance that delays affecting the module will affect the integration schedule. As the smaller stand is a build stand used for the LRIS instrument, it will be modified for use on MOSFIRE and designated as the instrument assembly stand.

Additionally, the team will design and fabricate simple laboratory assembly stands for all of the major sub-assemblies. Packing crates will also be built to enable components to be transported safely from UCSC and UCLA to CIT for final integration.

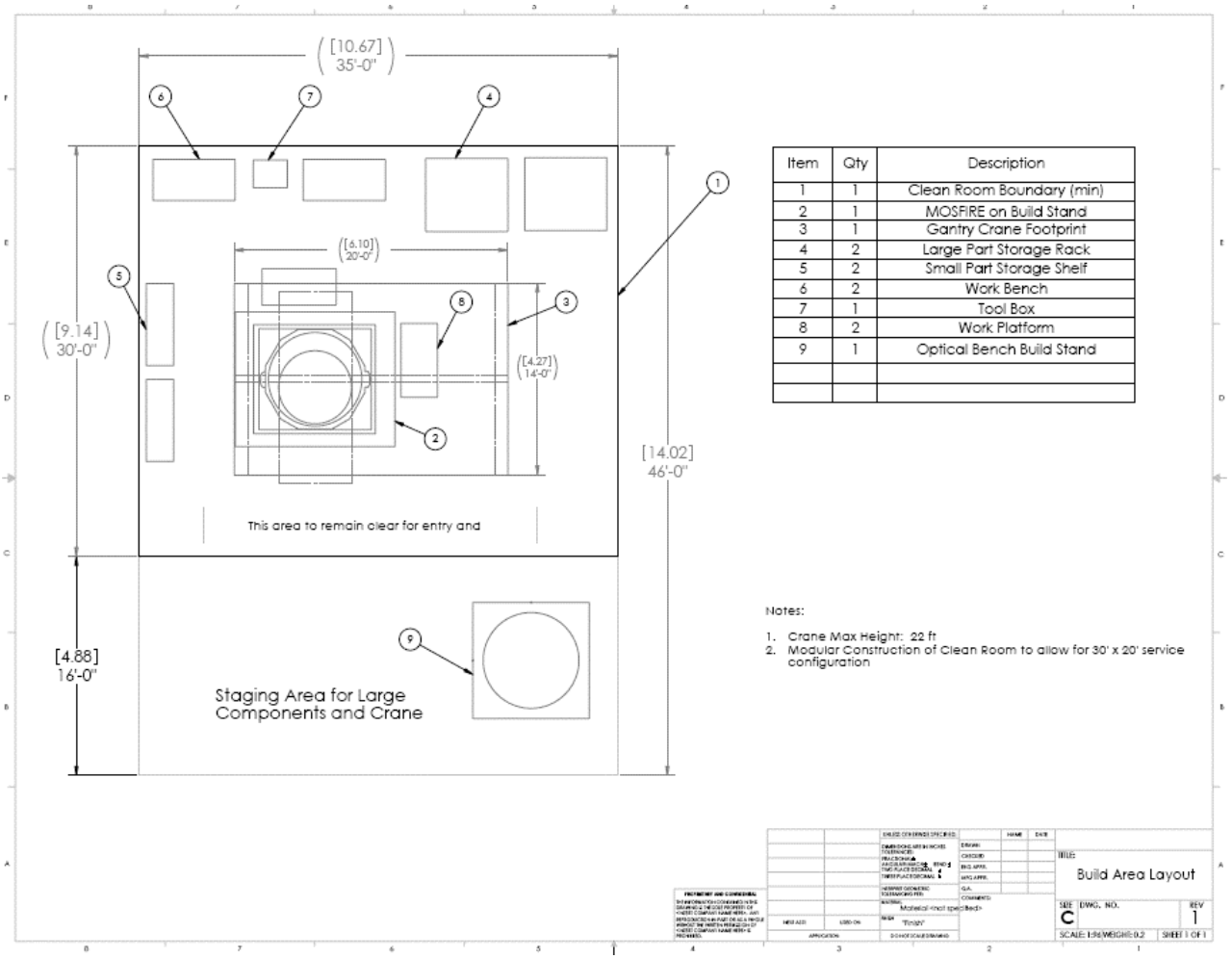


| Item | Qty | Description |
|---|---|---|
| 1 | 1 | Clean Room Boundary (min) |
| 2 | 1 | MOSFIRE on Build Stand |
| 3 | 1 | Gantry Crane Footprint |
| 4 | 2 | Large Part Storage Rack |
| 5 | 2 | Small Part Storage Shelf |
| 6 | 2 | Work Bench |
| 7 | 1 | Tool Box |
| 8 | 2 | Work Platform |
| 9 | 1 | Optical Bench Build Stand |
| | | |
| | | |

**Figure 80: Assembly Area Layout**

One of the challenges of the assembly of the instrument in the vertical orientation is the high overhead clearance that is required when the instrument is placed on the final assembly stand. Figure 81 shows the overhead clearance required in order to remove the Front End Cap while the instrument is placed on the ESI Test Stand. This requirement would drive the overhead clearance of the clean room enclosure to be at least 17 ft. It is also desirable to have overhead lift equipment enclosed within the clean room. Unfortunately, lift equipment that is high enough to provide the necessary clearance for all lifting operations would drive the clean room height to over 22 ft. As a compromise, it was decided to have a specific portion of the enclosure ceiling that could be opened to bring in an external lift hook from a facility crane for the brief time required to lift the few large parts that could not be lifted otherwise. We will also provide a smaller, portable gantry type crane that would reside inside the enclosure to facilitate all other lifting operations where high overhead clearance is not required.

As was our experience with NIRSPEC, NIRC2 and OSIRIS, these large cryogenic instruments typically require a 3-week cycle time for cool down, experiment and warm up. In general, we allow only one cool down per month. Time is allotted for up to 12 cool down and warm up cycles.

The first pump out of the dewar and first cool down occur soon after dewar fabrication is completed. We expect to install the CSU in time for the 3rd cool down (~May 2008). The science grade detector will be used on the 7th cool down.

An Acceptance Test Plan (ATP) will be drafted early in the full scale development phase and this plan will drive final testing of the instrument. The plan will be based on the ATP developed by WMKO for OSIRIS.

### 5.2.3 Instrument Assembly and Servicing Procedures

MOSFIRE is a large and heavy cryogenic instrument. Careful consideration has been given to assembly and potential servicing operations. The instrument and its contents have been arranged to provide reasonable access to the majority of the moving parts without requiring major disassembly of the instrument's structure. This section briefly describes the procedures and equipment required for initial integration of the instrument. It also includes descriptions and procedures for gaining access to the various components that might require access for service during the life of the instrument. A more detailed description of the procedures and hardware required to both assemble and service MOSFIRE is provided in MMDN20. It includes step-by-step images of the assembly process.

#### 5.2.3.1 Instrument Assembly

Some of the procedures and equipment utilized for instrument assembly at CIT will be unique to this process, whereas other equipment and procedures will also be used for servicing access, if necessary. Most of the assembly operations are performed with the instrument's optical axis in a vertical orientation. It was decided that this assembly orientation would allow for the most stable condition of the components while they are being lifted into position for assembly, as well as aiding the alignment and positioning of the components.

Attachment of lifting brackets or hoist rings will be performed using existing holes, or holes specifically placed for lifting purposes. Large diameter components are to be lifted at multiple points in order to spread the load and provide a more stable lifting configuration. A triangular lifting frame will be used for lifting large diameter components such as the front and rear end caps. Slings, straps or cables will be connected from the end points of the frames to hoist rings or lifting brackets at the component. Tapered alignment pins will be an additional assembly aid applied to more difficult assembly operations. The tapered pins would be threaded into the stationary component, and engaged into the mating holes of the component being lowered into place.

Warm instrument alignment will occur on the instrument assembly stand. Fixtures and procedures are being developed and are described in MMDN34. The instrument structure is predominantly aluminum and, despite the multiple folds, the alignment shouldn't vary a great deal between ambient and operating temperatures. The CAD model of the instrument is constructed with warm and cold configurations that simulate the dimensional changes that will occur. This model will be utilized to assist in determining warm alignment. Once the instrument is coupled to the module and installed on the ESI stand, the instrument axis can be properly aligned to the bearing axis. More

thorough warm and cold alignment checks can be completed with the instrument properly supported in the module on the ESI stand.

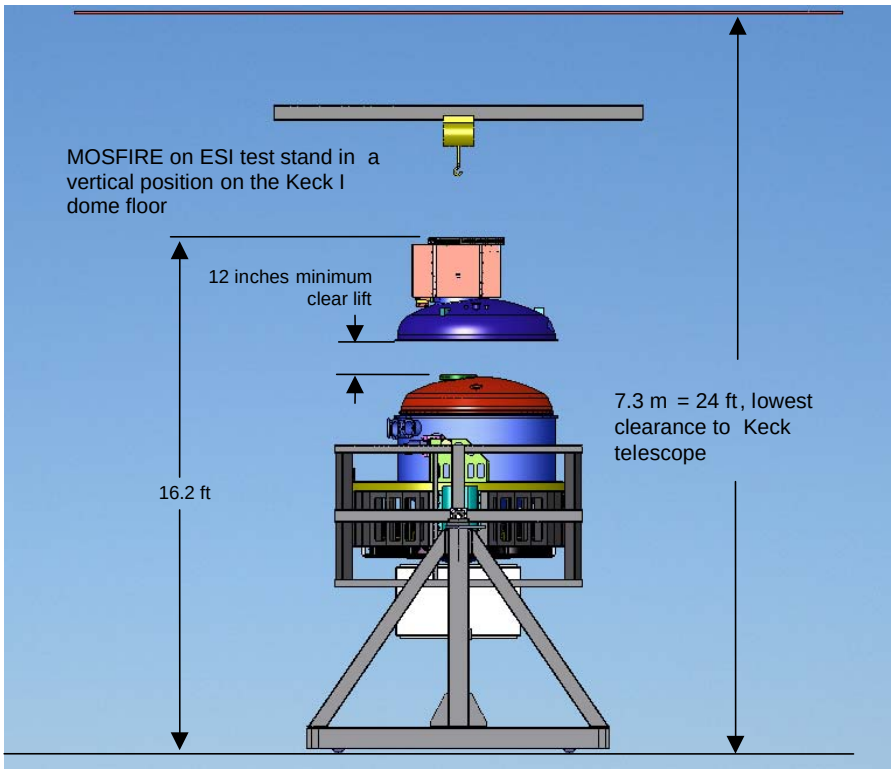


**Figure 81: MOSFIRE Attached to the ESI Test Stand**
This image shows the facility height requirements for front cover removal.

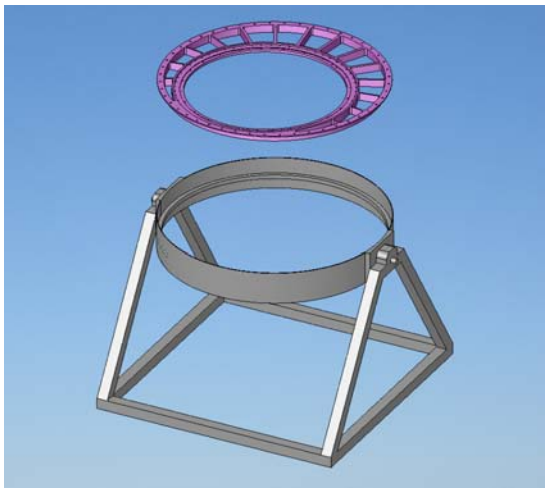

**Figure 82: The LRIS Build Stand**
This stand simulates the module bearing interface. The instrument mounting ring will bolt to this stand, which we refer to as the instrument assembly stand.

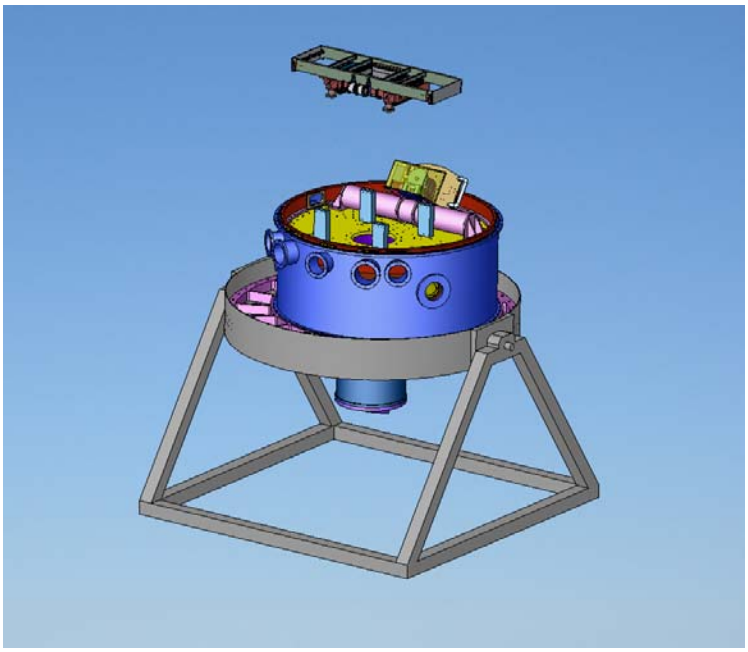

**Figure 83: Instrument Assembly**
Most of the instrument structure can be assembled and initial fit and alignment checked on the instrument assembly stand. Here, the CSU is lowered into position utilizing the small gantry build crane (not shown).

#### 5.2.3.2 Instrument Servicing

External instrument mechanisms have been located to provide adequate access should maintenance be required. Internal mechanisms have been designed with a goal of 10 years minimum service prior to maintenance. But, the layout of the instrument's internal structure has been designed to provide adequate access to internal mechanisms in the event that servicing is required. All of the moving parts within MOSFIRE can be accessed without removing the internal structure or the shielding that surrounds the cylindrical portion of the instrument. Access is provided from both the front and the rear of the instrument via the front and rear covers. Access to the rear is a bit more cumbersome due to the positions of the electronics cabinet and the cable wrap. But, since instrument warm-up will likely take about a week, there is time to remove these assemblies should rear access be required.

Although access to all of the internal mechanisms can be obtained through the vacuum chamber end caps, MOSFIRE is too large to be serviced on the Nasmyth deck (Figure 121). The safest, easiest, and most cost-effective way to remove the end caps is by vertical lift. And the instrument should be inside a clean room facility whenever the instrument is opened. Should MOSFIRE require internal service, it will be lowered to the dome floor where both the ESI stand and a temporary soft wall clean room structure can be erected.

#### 5.2.3.3 Front Cover Access

Removal of the front cover and shield provides immediate internal access to four sub-assemblies. The CSU, grating/mirror exchange assembly, window heater assembly, and inner window assembly can be accessed directly with the front cover removed (Figure 85). The left and right main refrigerator head thermal strap attachments can be accessed from the front through access holes on Bulkhead A. But access from the rear is better due to large access holes. A sixth assembly, the pupil mechanism, can be accessed and removed once the grating/mirror exchange assembly has been removed.

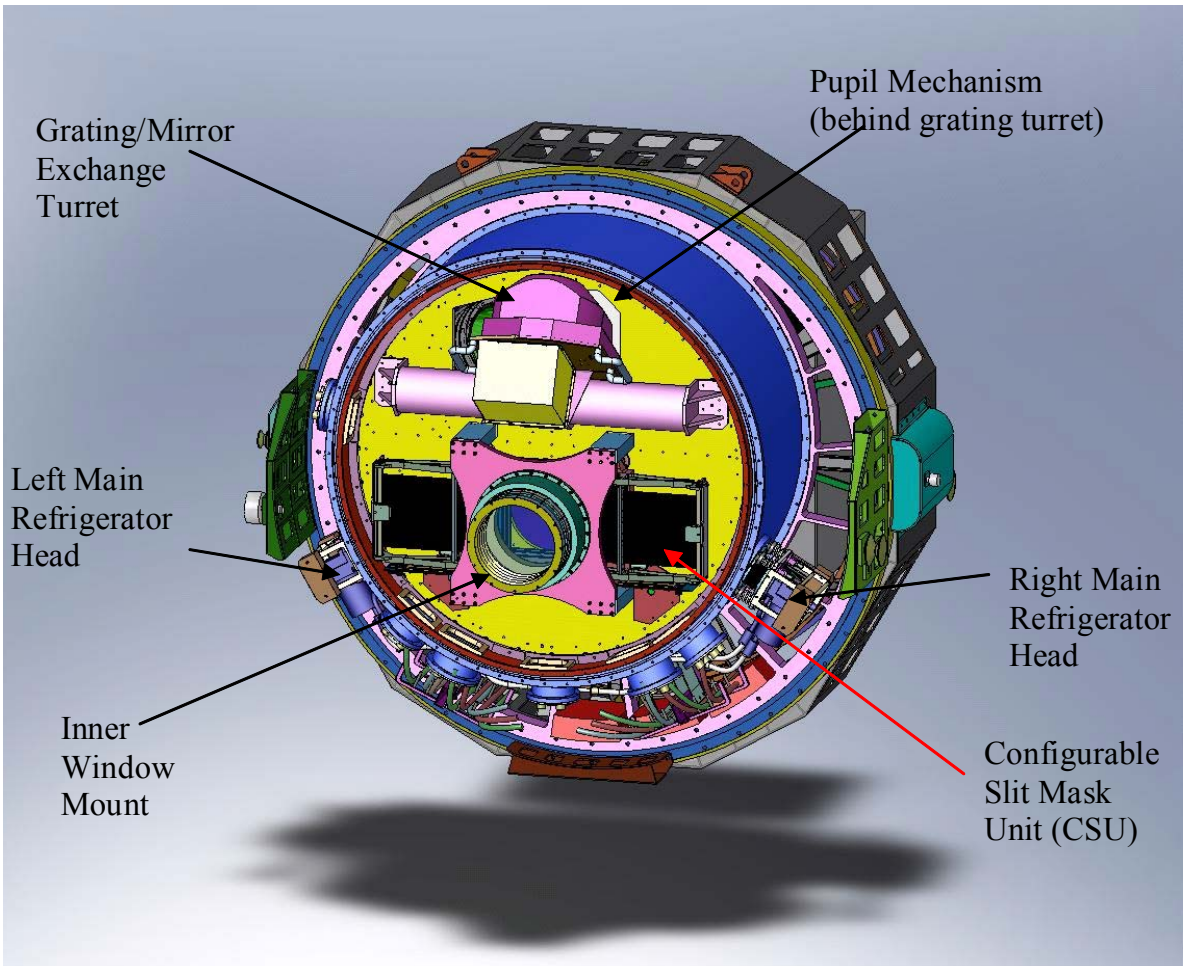


**Figure 84: MOSFIRE with the Front Cover and Shields Removed**
Accessible sub-assemblies are indicated.

#### 5.2.3.4 Rear Cover Access

Removal of the rear cover and shield provides immediate internal access to six sub-assemblies, as well (Figure 85). The flexure compensation system (FCS), detector head, collimator barrel, detector refrigerator head, getter assembly, and filter wheel assembly can be accessed directly with the rear cover removed. A seventh sub-assembly, the field lens assembly, can be accessed after the collimator barrel and the FCS supports are removed. Only the filter wheel assembly's drive and positioning hardware can be accessed with the unit installed in the instrument. The hub bearings cannot be accessed without further disassembly of the instrument structure, but failure of these bearings is considered very low risk based on past experience.

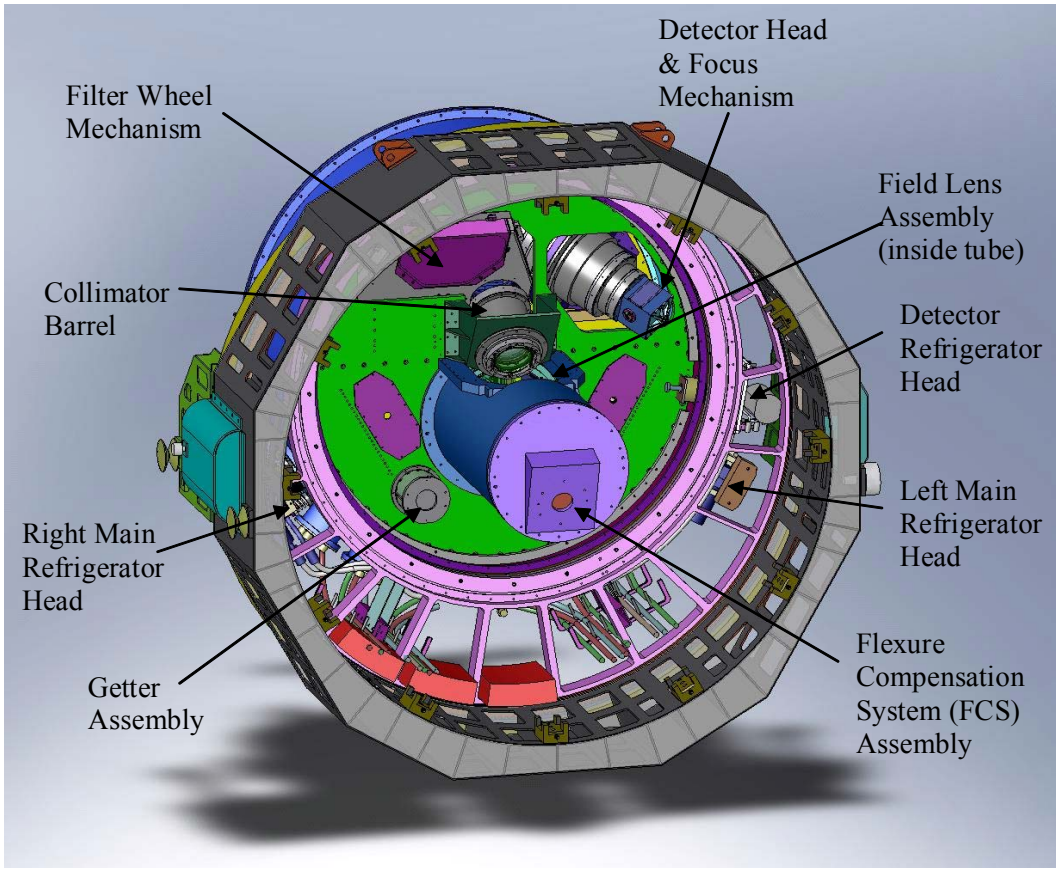


**Figure 85: MOSFIRE with Electronics Cabinet, Cable Wrap, and Rear Cover and Shields Removed**
Accessible sub-assemblies are indicated.

### 5.2.4 Responses to Issues Raised in the PDR Report

The report of the MOSFIRE preliminary design review (PDR) committee raised several issues related to the MOSFIRE mechanical design. The MOSFIRE mechanical team's responses to these issues are summarized here.

*The overall design and plan presented for the mechanical systems was excellent. The approach seemed generally sound and based on previous successful components and prototypes. Furthermore, the MOSFIRE design team seems aware that the dominant flexure in the grating system needs to be reduced. However, the committee did note with concern that the flexure compensation plan relies heavily on low hysteresis and smooth elastic behavior, but that the design philosophy did not reflect this reliance. We urge the team to consider kinematic connections between the instrument and telescope and between the inner and outer structure, for example. In general, the design should focus on repeatable deflections as much as possible so as to mitigate the risk of not meeting the flexure (or, more precisely, image motion of any type) specification at the focal plane.*

We agree that, in order for the flexure compensation plan to work most effectively, the instrument structure must provide smooth elastic behavior with minimal hysteresis. But in addition to this goal, the design also has to balance vacuum chamber and thermal performance considerations within tight space and weight constraints. We are confident that MOSFIRE's structural design efficiently balances these constraints while also providing the necessary levels of elastic flexure required by our FCS plan.

From the start of the project, we were concerned about proper support of the thin section rotator module bearing. Bearings of this type require rigid support for proper operation. We were concerned that the module structure design was not providing adequate support for the outer race of the bearing. Recent FEA studies show that the module, supported by the four-point, non-kinematic defining points needs help from the instrument structure to keep the bearing (and module) from becoming significantly warped under typical instrument loads. The MOSFIRE structure will provide the proper support for the inner race of the bearing, while simultaneously acting as an efficient vacuum chamber. The tubular portion of the chamber structure, in combination with the G-10 internal structure support tube, will minimize the "potato chip" warping of the bearing. And the tori-spherical end caps will act as diaphragms to help keep the bearing round.

Support of the internal structure is supplied by a thin G-10 tube in order to give maximum stiffness in the available space while controlling parasitic heat loads. The internal structure is isolated from significant radial deformations of the bearing mount by the thin section of the support tube. It is protected from significant distortions of the attaching front bulkhead due to the inherent combined stiffness of the short aspect ratio G-10 support and vacuum chamber tubes.

Slipping of joints will cause hysteresis, whether they are of kinematic design or not. The clamping forces at the joints must be sufficient that the joints can't slip, regardless of flexing of the joined components. Every joint included in the internal structure has bolts on a nominal 75 mm spacing, not only to ensure that the joints don't slip, but also to ensure that maximum thermal conduction is maintained as the instrument is cooled. The thermal performance of MOSFIRE relies on consistent thermal contact. All bolted structural joints include multiple spring washers sized to maintain clamping pressure throughout the possible temperature range. Attaching the optic sub-assemblies to the structure via truly kinematic interfaces would minimize the thermal contact with the instrument structure and require that additional thermal paths (and mass) be added to achieve the

required thermal performance. This added mass would do nothing to help the instrument stiffness, and could in fact increase flexure.

*The guide camera optical elements are mounted on the dewar such that pressure-induced flexure of the vacuum vessel may translate or misalign the optical system. The committee also believed that a calibration system would be a high-priority addition in the future. We suggest that both of these features might be facilitated by providing an annular optical bench in front of the instrument entrance window. On this bench, the guide optics could be folded such that the optical path remains in a single plane, perpendicular to the telescope optical axis. If the space is provided now, a calibration projector system could conceivably added later and mounted on the same optical bench, such that it illuminates the back surface of the dust cover or similar instrumental feature. A kinematic (hexapod arrangement) connection between the bench and the outer diameter of the vacuum vessel would provide stiff and repeatable support for the bench.*

The guide camera attachment to the front cover will be affected by the pressure-induced flexure of the vessel, and this has been simulated by FEA methods. Unless the attachments were moved to the front flange of the vessel barrel, the guider assembly will be affected by this regardless of whether the attachment is kinematic or not. Given space and weight limitations, we chose to use the vacuum window protrusion as a strong-back for the guider to minimize internal guider assembly flexure while adding minimal additional weight. The guider will have to be aligned to the telescope axis at the observatory during commissioning. We have an alignment strategy and fixtures planned for this task. The largest pressure-induced displacement is along the optical axis. Lateral and tilt motions are smaller. Normal variations in the observatory pressure will not be a concern.

*The plan to use a commercial vendor to provide a configurable slit unit seemed an excellent approach to a difficult problem for infrared spectrometers. The preliminary performance presented by CSEM representatives was impressive. Additional testing and development of the unit obviously is required (as plans presented at the PDR indicated). The committee urges a measurement of the light leaks through the bars under simulated observing conditions (near infrared light, appropriate beam and illumination pattern, etc.) and confirmation that these will not compromise science observations. Analysis of the thermal effects on the positioning of the bars should also be completed. Further, optical design and analysis of the tip/bar profiles should be done with the goal of understanding the vignetting caused by out-of-focus slit ends and general impact on potential observations. The committee also noted that the re-configuration of the bars seemed a significant cost to observing efficiency and urges any attempt at reducing that time, assuming this can be accomplished without compromising the positioning accuracy.*

CSEM has completed a thermal analysis of the slit bars. The estimated bar temperature rise is marginal with a conservative estimated incident heat load of 2W. In parallel, the instrument double window and entrance baffle design was refined and optimized using thermal design and analysis tools, reducing the estimated CSU incident load to 0.3W. With the final instrument entrance aperture design, the bars will remain well within acceptable temperatures.

The slit tips of the masking bars have been moved so that they are all located within the axial height dimension of the bars, rather than being attached on top of the bars. The masking bar design has also been changed so that the bars approximate the spherical image surface curvature with three height steps rather than two. These two changes minimize the vignetting caused by out of focus slit ends.

CSEM fabricated a small section of bars with different sizes of over-lapping shoulders and this module was tested for light leaks using an IR camera at UCLA. With the standard 0.5 mm overlap the attenuation was $\sim 10^{-6}$ which is very close to satisfactory. However, CSEM are now investigating adding a black coating to the interior of the bars to reduce the leakage by another factor of ten.

Finally, as already discussed in Section 3, tests have been carried out to fully understand the CSU timing issues and we are now confident of the slit reconfiguration times. Slight improvements are still possible but may not be worth the risk of mechanical damage or reduced reliability.

## 5.3 Electrical/Electronic Design

MOSFIRE's electronics design is based on the design heritage of recent WMKO instruments, in particular OSIRIS, NIRSPEC and NIRC2. Most of the electronics consist of commercial off the shelf (COTS) equipment with the required interconnections. There is a limited amount of custom equipment including, the CSU control system, the interface board for the science detector application specific integrated circuit (ASIC) and a few printed circuit boards used to simplify various high pin count interconnections.

### 5.3.1 Overall Configuration

The MOSFIRE electronics consists of three major component groups, the MOSFIRE instrument electronics located in the electronics cabinet mounted on the instrument, the MOSFIRE CCR compressor and controls located in the Keck I telescope mechanical equipment room, and the MOSFIRE computer rack containing the instrument host computer and data storage disks located in the Keck I Telescope computer room. A block diagram of the overall MOSFIRE electronics configuration is shown in Figure 86.

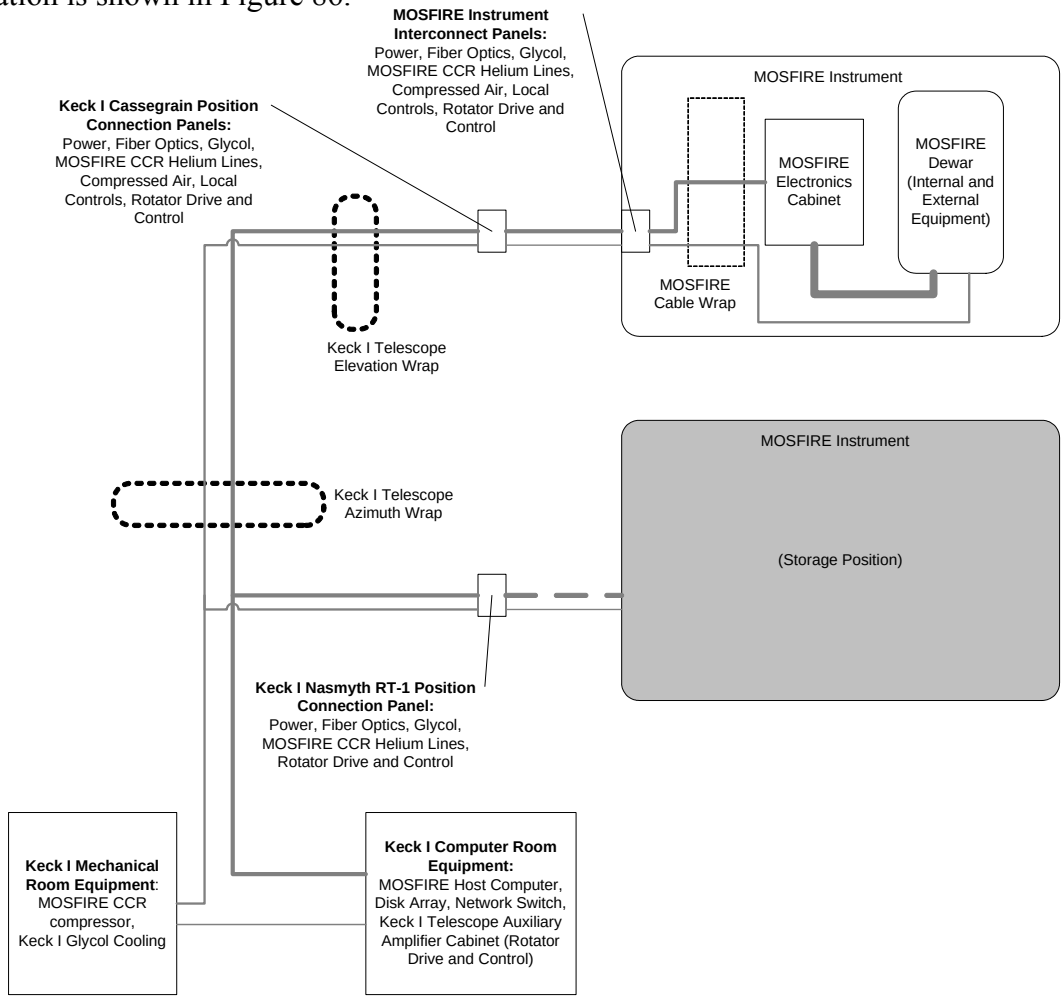


**Figure 86: MOSFIRE Electronics Overall Configuration**

In the lower left corner of Figure 86 is the Keck I mechanical equipment room where the MOSFIRE CCR compressor and variable speed control system will be located. The Keck I telescope and instrument glycol cooling system is also located in the mechanical equipment room. At the bottom center of Figure 86 is the Keck I computer room. The computer room is where an equipment rack is located that will contain the MOSFIRE host computer, network switch, disk array for data storage and the Keck I auxiliary amplifier cabinet which contains the drive and control system for the MOSFIRE rotator. This rotator drive and control system is shared with the LRIS instrument.

On the right middle portion of Figure 86 the Keck I Nasmyth RT-1 storage position is indicated. The MOSFIRE instrument is stored in this location. A full set of services for MOSFIRE is provided on a panel located between the RT-1 and RT-2 (LRIS storage) positions.

At the upper left of Figure 86 the telescope's two cable wraps (azimuth and elevation) are indicated, and all of the services required by MOSFIRE go through these two wraps to reach the Keck I telescope Cassegrain position. After passing through the telescope cable wraps the services reach the Cassegrain position connection panels. As discussed in §5.5, the various interconnections are divided among several connection panels due to the space constraints at the Cassegrain position.

The MOSFIRE instrument is shown at the upper right corner of Figure 86. Instrument connections are also made at several interconnect panels. The rotator drive and control connections, local controls, and compressed air for the rotator defining points are connected to the stationary portion of the instrument rotator. All the remaining connections proceed from the interconnect panels through a cable wrap mounted in the instrument and then connect to the MOSFIRE electronics cabinet and the CCR heads mounted on the instrument dewar. The MOSFIRE electronics cabinet connects to the dewar internal and external equipment and the electronics cabinet and instrument dewar rotate through a total angle of 530 degrees on the instrument rotator.

### 5.3.2 MOSFIRE Interfaces

A more detailed "one-line" diagram of interfaces between the MOSFIRE instrument and other equipment is shown in Figure 87.

#### 5.3.2.1 Keck I Mechanical Room

The CCR compressor, a CTI-Cryogenics 9600 will be located in the Keck I mechanical equipment room and will be cooled by the Keck I glycol cooling system. The compressor will supply high pressure Helium gas to three CCR cold heads (two CTI 1050 cold heads and one CTI 350 cold head) mounted on the MOSFIRE instrument dewar. Helium gas is distributed to the three cold heads by a manifold system located on the instrument.

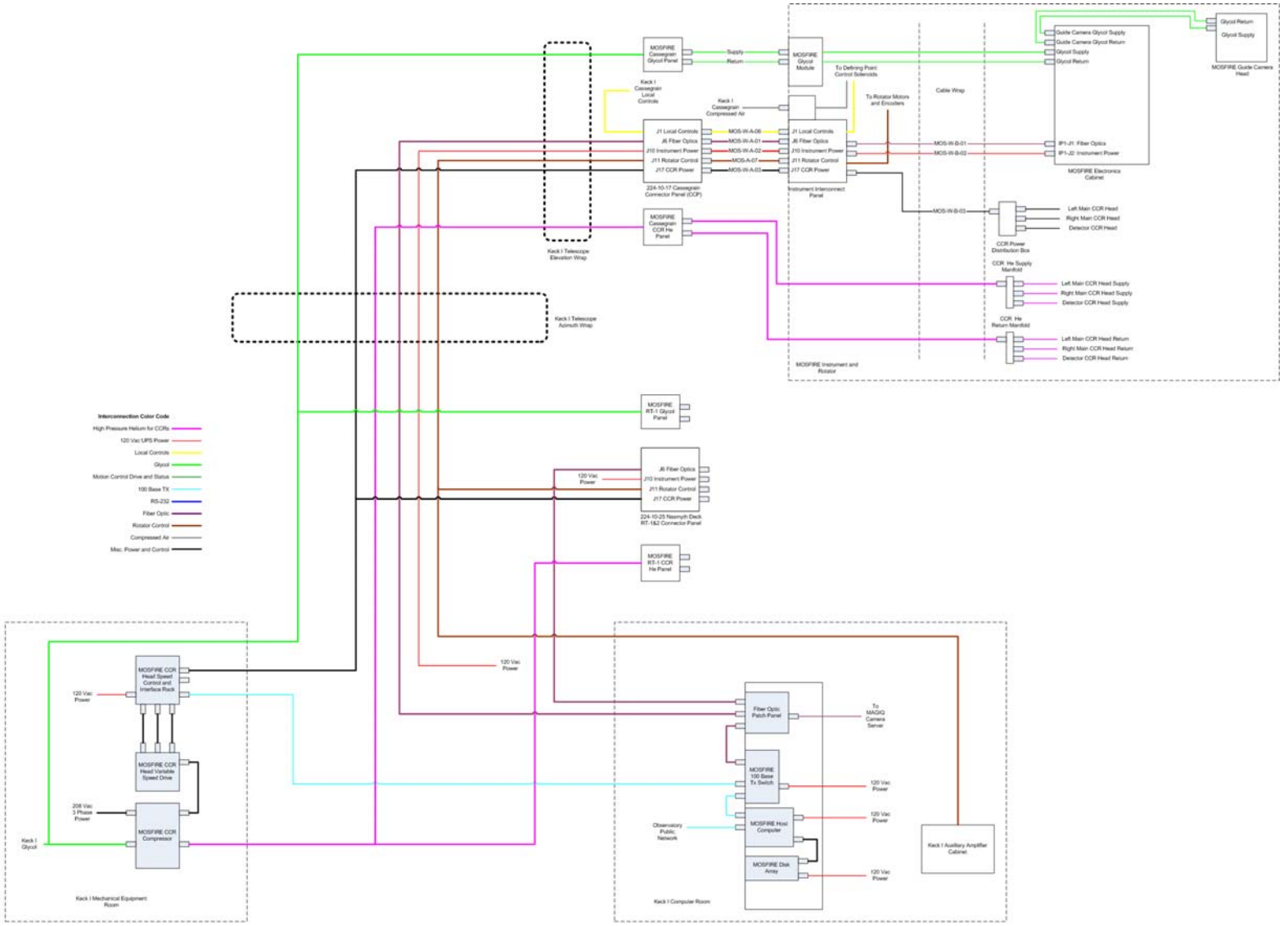


**Figure 87: MOSFIRE One-Line Diagram**

Our 1050 cold heads will be powered in parallel from a single channel variable speed drive. The 9600 compressor supplies power to the variable speed drive. Speed control is accomplished by a speed control and interface unit mounted in a small equipment rack in the Keck I mechanical room. This speed control and interface unit will be based on the design previously implemented for the NIRC2 instrument. NIRC2 has two separately controlled cold heads, so the design will be modified to control one cold head. Minor updates to the design will be made to replace obsolete components. The speed control and interface unit uses DGH Corporation RS-232/RS-485 controlled analog and digital interface modules to permit remote control of the variable speed drive. A Lantronix ET8PS terminal server will control the DGH modules via a 100Base-TX connection to the MOSFIRE private network.

The smaller cold head will be powered directly from the cold head power output of the 9600 compressor.

#### 5.3.2.2 Keck I Computer Room

The MOSFIRE host computer, a SunFire V245 server is located in an EIA 19 inch equipment rack in the Keck I computer room. Also located in this rack is a disk array for MOSFIRE science data storage. This disk array is interfaced to the host computer via an ATA interface. The host computer has two network interface controllers (NICs). One is connected to the Observatory 100 base-TX public network (intranet), and one is connected to the MOSFIRE private 1000Base-T/100Base-TX network.

A ProCurve 2824 networking switch is also located in the rack with the MOSFIRE host computer. This switch is connected to an identical switch in the MOSFIRE electronics cabinet via a 1000Base-SX transceiver and a fiber optic cable pair. The two 2824 switches form the MOSFIRE private network and allow 1000Base-T/100Base-TX communications between the MOSFIRE host computer and the MOSFIRE instrument electronics located at either the Keck I Cassegrain position or the Keck I Nasmyth Deck RT-1 position.

Because the fiber optic connection between the two 2824 switches is a point-to-point link, a patch panel is also provided in the equipment rack. This patch panel allows the selection of either the Keck I Cassegrain position or the Keck I Nasmyth Deck RT-1 position for connection to the 2512 switch in the computer rack, and also the selection of the corresponding fiber optic pair for the MOSFIRE guider.

The MOSFIRE rotator is also controlled by equipment located in the Keck I computer room. This is the Keck I auxiliary amplifier (AA) cabinet, controlled by the Keck I drive and control system (DCS). The servo amplifier in the AA cabinet is shared between the LRIS instrument and MOSFIRE, so provisions are also made for selection of the instrument rotator connections in the AA cabinet.

#### 5.3.2.3 Keck I Cassegrain Position

The Keck I Cassegrain position has four interface panels for MOSFIRE. Three of these are shared with the LRIS instrument, a glycol interface panel, the Cassegrain connector panel for the electrical and fiber optic interfaces, and a compressed air connection for the defining point motors on the MOSFIRE rotator. A fourth panel is added to provide the supply and return connections for the high pressure helium lines from the MOSFIRE CCR compressor to the MOSFIRE CCR manifolds located on the instrument.

#### 5.3.2.4 Keck I Nasmyth RT-1 Position

The Keck I Nasmyth RT-1 position interface panels are part of an interface panel assembly located on the Nasmyth deck between storage positions RT-1 and RT-2. The interface panel assembly is shared with LRIS, but separate connections are provided for all services to both instruments. The only exception is compressed air for the defining point motors. This is not required when the instrument is not installed in the telescope.

### 5.3.3 Instrument Electronics

The MOSFIRE Instrument electronics are housed in a welded aluminum cabinet meeting the NEMA-4 specifications (continuous hinges and clamped gasketed doors, interior protected from dripping water, sprayed water and ice formation on the exterior of the cabinet). The cabinet provides two bays equipped with EIA 19 inch rack mounting rails. Each bay has 25 U (43.75 inches) of rack panel space. The electronics cabinet is located at the rear of the MOSFIRE instrument behind the cable wrap as shown in Figure 88.

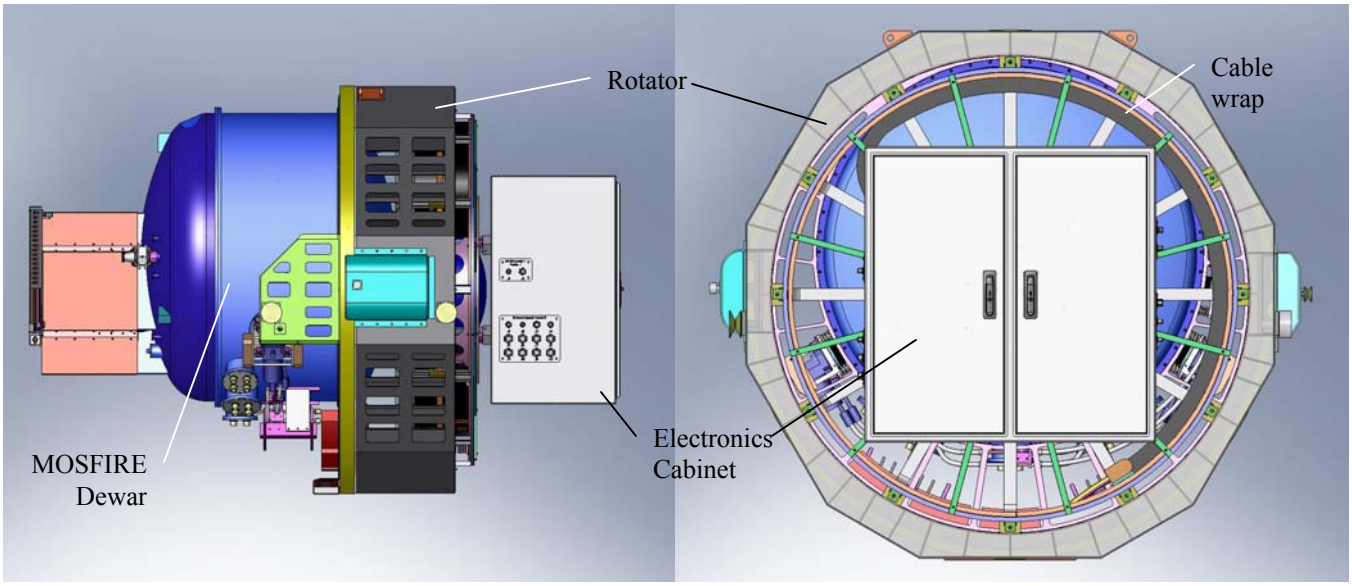


**Figure 88: MOSFIRE Electronics Cabinet**
The left side of the figure shows a side view of MOSFIRE with the electronics cabinet. The right side of the figure shows a rear view of MOSFIRE.

Connector panels are mounted on the left and right side of the electronics cabinet. These panels are designated instrument panel (IP) 1, IP2, IP3 and IP4. IP1 is used to connect the electronics cabinet to the instrument cable wrap. IP2, IP3and IP4 are used to connect the electronics cabinet to equipment inside the dewar and to equipment mounted on the outside of the dewar.

#### 5.3.3.1 Instrument Interconnect Panel

In the upper right corner of Figure 87 the connections are shown between the Cassegrain connector panels and the instrument interconnect panel (IIP), instrument glycol module, defining point motor air supply and the instrument high pressure helium lines. The connections through the cable wrap are also shown along with the instrument electronics cabinet, CCR head power distribution box and CCR helium manifolds.

At the stationary end of the instrument cable wrap the IIP is mounted to the stationary portion of the rotator. The cables between the IIP and IP1 are terminated in connectors at both ends so that the cables can remain captive in the wrap if instrument disassembly is required. In addition to the cables between the IIP and IP1 on the electronics cabinet, there are also glycol lines, power and high-pressure helium lines for the CCR cold heads that pass through the wrap.

The connections on the IIP are listed in Table 20.

| Connector Designation | Function |
|---|---|
| J1 | Local Controls Interface for Cassegrain Defining Points |
| J6 | Fiber Optics:<br>1000Base-SX 62.5/125 m multimode optical fiber (RX & TX)<br>Guider Camera Link optical fiber |
| J10 | Instrument Power |
| J11 | Rotator Control |
| J17 | CCR Power |

**Table 20: MOSFIRE IIP Connections**

Glycol cooling for the electronics cabinet and the guide camera is provided by the Observatory glycol system. A glycol module mounted on the stationary portion of the rotator is used to pressure regulate the glycol flow before it passes through the instrument cable wrap. The glycol lines that pass through the wrap are terminated in quick connects at both ends to allow these lines to remain captive in the cable wrap.

The high-pressure helium lines extend from the stationary end of the cable wrap with sufficient length to permit connection to either the Cassegrain CCR helium panel or the RT-1 helium connections. The other ends of the helium lines are connected to the CCR helium manifolds. High pressure disconnect fittings allow the helium lines to be uncoupled from the manifolds when the cable wrap is removed from the instrument.

The electrical and fiber optic connections between the Observatory and MOSFIRE and between the MOSFIRE electronics cabinet and dewar are shown in detail in Figure 89. At the upper left corner of Figure 89 the connections between the Cassegrain connector panels and the IIP are

shown. These connections are made via a group of cables designated the “A” series (MOS-W-A-XX, see MEDN02 for details).

Connected to the instrument side of the IIP are three cables in the “B” series (MOS-W-B-XX, see MEDN02 for details) that pass through the MOSFIRE cable wrap. The fiber optic connections for the MOSFIRE private network and guide camera are made via cable MOS-W-B-01, terminated in 38999 series connectors. The instrument 120 Vac power connection is made via cable MOS-W-B-02 also terminated in series 38999 connectors. After passing through the instrument cable wrap both of these cables connect to panel IP1 on the MOSFIRE electronics cabinet.

Power to the CCR cold heads is supplied via cable MOS-W-B-03, equipped with 38999 series connectors. After passing through the cable wrap this cable connects to a power distribution box that breaks out the three circuits in the CCR power cable for distribution to the three CCR cold heads, again using 38999 series connectors.

#### 5.3.3.2 Electronics Cabinet and Dewar Interconnections

All the electrical connections between the electronics cabinet and the internal and external dewar equipment are shown in Figure 89. The electronics cabinet is shown just to the left of center in the figure. The IP1 connector group is shown at the upper left of the cabinet and the IP2, IP3 and PI4 connector groups are shown along the right side of the cabinet. The connectors in each group are mounted on a connector panel. Each connector is gasketed and the panels are sealed with O-rings to preserve the NEMA-4 rating of the cabinet. The connectors are attached to the panels with hardware (external star washers) that ensure electrical continuity between the connector shells and the panel. The panels are attached to the cabinet in a similar manner.

Historically we have used MIL-C-26284 series connectors for electronic interconnections on instrumentation and other Observatory systems at WMKO. These connectors have some disadvantages that have been addressed with the more recent MIL-C-38999 series. The changes of interest to us are the provision of a spring loaded ground contact and improved EMI ratings and backshell designs. The 26284 series connectors do not have a spring loaded ground contact, so if they are subject to vibration or mechanical contact (like bumping into them) they will leak RF, creating EMI problems. The 38999 series connectors are rated under an EMI program called Tempest, which deals with the most mission critical level of EMI emissions control.

Cable shields need to be terminated over a full 360 degrees to the backshell, and the backshell has to provide full coverage of the unshielded portion of the cable connections to the connector contacts. The 38999 series connectors do not have a "default" backshell, so you always have to specify one, and this makes sure you get the proper EMI backshell for each connector. The 26284 series connectors come by default with a non-EMI, non-grounding backshell. The 38999 series connectors are designed so that their backshells make contact before any pins, providing an important level of static discharge protection and ground continuity for safety. Male pin configurations on 38999 series connectors are also “scoop proof” which protects the pins from damage if handled carelessly when not mated.

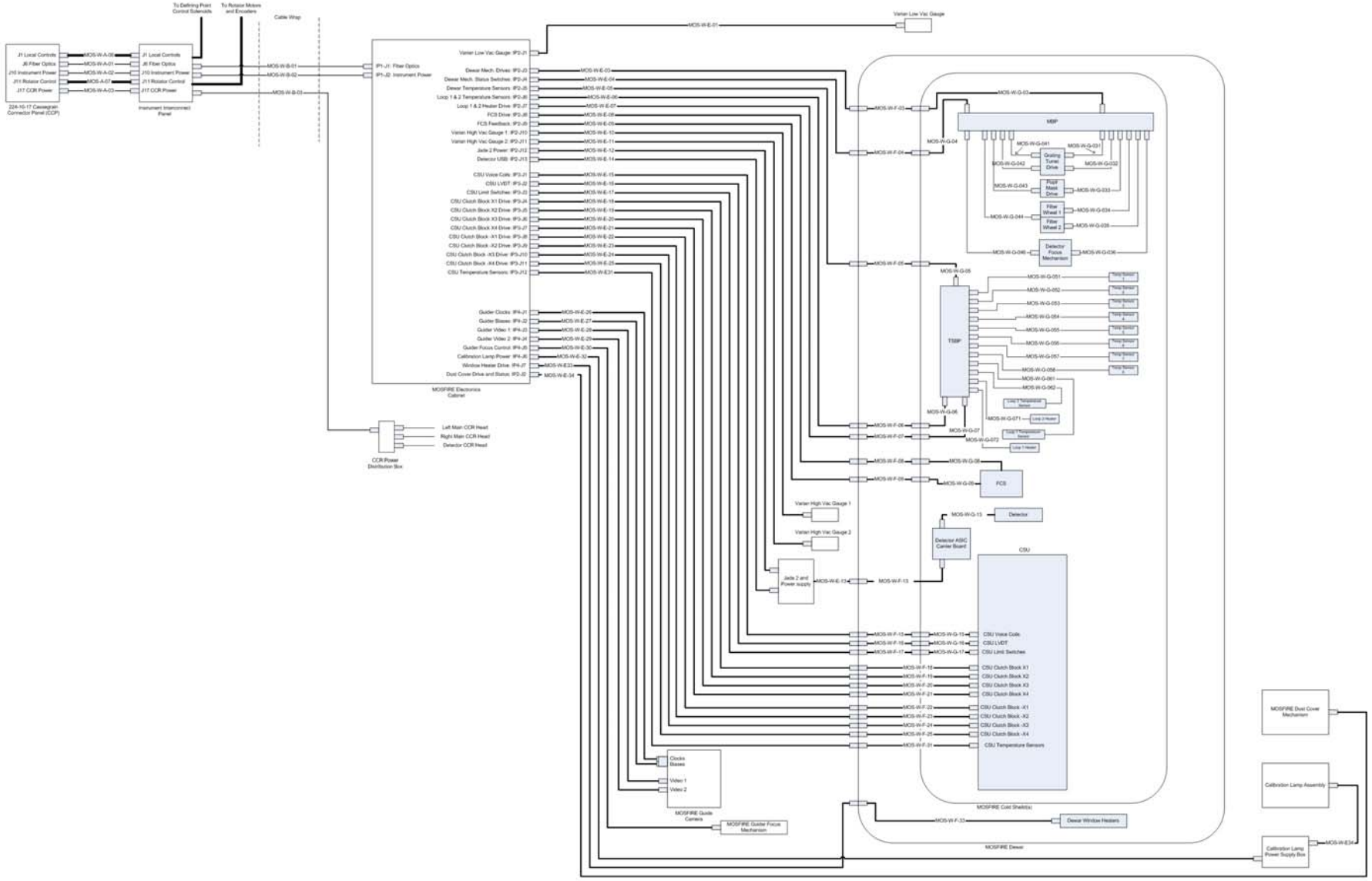

**Figure 89: MOSFIRE Instrument Interconnections**

The tooling and techniques to assemble 38999 series connectors are the same as the 26284 and much higher pin densities are available in the 38999 series. Examples of the 38999 series IV connectors are shown in Figure 90.

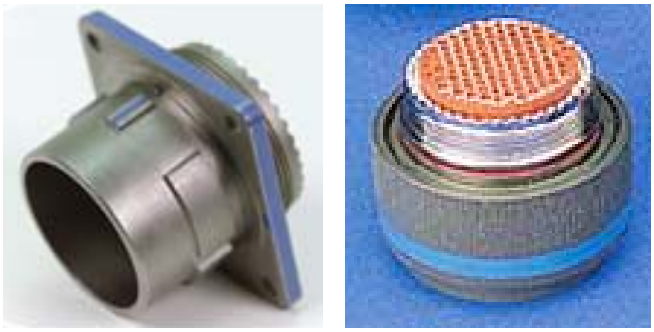

**Figure 90: MIL-C-38999 Series IV Connectors**

The MOSFIRE dewar is represented at the right side of Figure 89 along with the equipment mounted on the exterior of the dewar. Connections between the electronics cabinet and the dewar are made using a group of cables designated the "E" series (MOS-W-E-XX, see MEDN02 for details). These cables are shown proceeding from the cabinet to the various dewar feed thru connectors and to various pieces of equipment mounted on the exterior of the dewar.

Dewar feed thru connections are made via hermetic connectors mounted on six connector bulkheads located at the front of the main dewar shell section, just before the front cap. A view of MOSFIRE looking up at the bottom front of the dewar is shown in Figure 91.

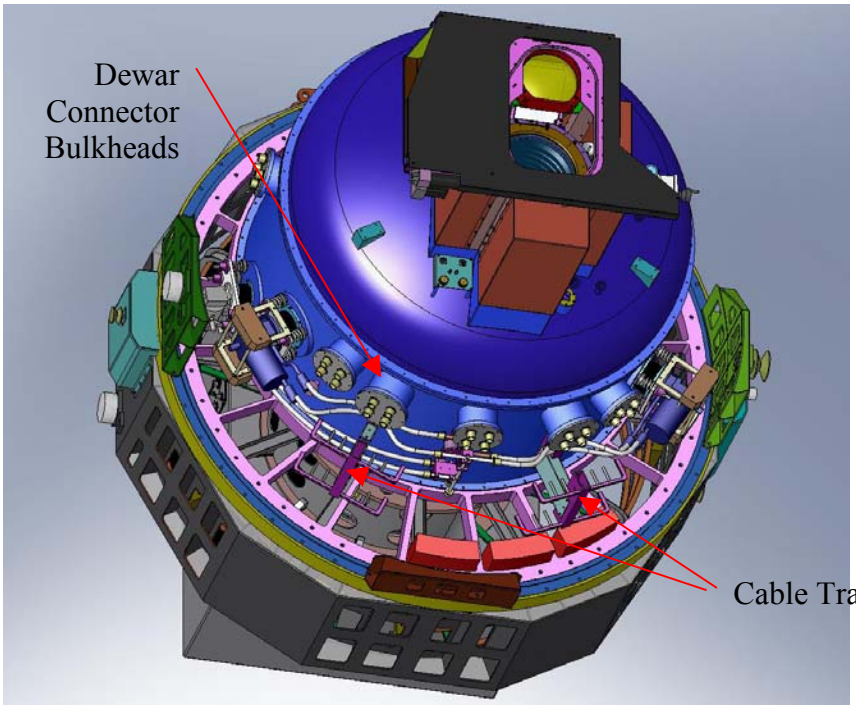


**Figure 91: MOSFIRE Bottom Front View Showing Connector Bulkheads**

Cables from the connector bulkheads are routed back to the electronics cabinet via cable trays, also shown in Figure 91. Each cable is individually secured into a cable tray using cable ties to prevent motion of the cables when the instrument rotates and when the telescope changes elevation. The cable trays will also be used to route cables from the electronics cabinet to the front of the instrument. Cable clamps will be used to secure the cables as they run up onto the front cover of the dewar.

There are 8 cables connecting the electronics cabinet to the dewar to carry the CSU clutch and brake coil signals. These cables are identical and terminate in identical connectors. To prevent damage due to a misconnection these cables are terminated in manner that ensures that accidental interchange will not short any of the clutch and brake coil amplifier outputs to ground. To prevent improper operation a pair of pins that would normally be used for signal return lines are used instead to create a connector-to-connector continuity signal. This signal has continuity only when all 8 connectors are connected in the right locations at both the dewar and the electronics cabinet.

Figure 89 also shows the equipment mounted on the outside of the dewar. This includes the low and high vacuum gauges, the MOSFIRE dust cover mechanism, the MOSFIRE guide camera head and focus mechanism, the calibration lamp assembly and the previously described Jade2 board and power supply.

The low vacuum gauge (a Varian ConvecTorr) is equipped with a HIROSE RM12 series connector and cable MOS-W-E-01 terminates in a mating connector at the gauge. The connector at the electronics cabinet is a 38999 series connector. The high vacuum gauges (Varian series IMG) have integral female SHV high voltage coaxial connectors. RG-58/U coaxial cable terminated with SHV male connectors at both ends connects the high vacuum gauges to female bulkhead feed thru connectors on electronics cabinet panel IP2. Each SHV bulkhead feed thru is connected to each IMG board in the Varian multi-gauge controlled via a second RG-58/U cable terminated in SHV male connectors.

38999 series connectors are used on the dust cover mechanism and the calibration lamp assembly. There are four “Penray” calibration lamps and each has its own power supply. For reliable operation the cable length from the lamp to the power supply must be kept short and this requires that the power supplies be mounted in the calibration lamp assembly. 120 Vac power is distributed to the four power supplies by a calibration lamp power supply box mounted on the dewar next to the calibration lamp assembly. This box contains distributes 120 Vac supplied from the electronics cabinet to the four lamp power supplies.

The guide camera head uses a hermetic 37 pin D series connector for clocks, biases and power. Hermetic female SMA connectors are used for the two video signals from the camera head. The camera head clocks, biases and power connection utilize two separate shielded cables that are terminated in a single 37 pin D connector at the camera head. The two cables terminate in separate 38999 connectors on panel IP4 at the electronics cabinet. The video signals are routed through RG-174/U coaxial cable with male SMA terminations at the camera head to male BNC terminations at the electronics cabinet. Female bulkhead feeds thru connectors are used to connect the video

signals on electronics panel IP4 via second coaxial cable to the guide camera controller in the electronics cabinet.

As described earlier, all of the external connectors and cables, with the exception of 120 Vac power wiring and the optical fiber connections utilize connectors that provide an RF tight 360 degree ground connection between the cable shield and the connector shell. Connectors and panels are mounted in a manner that ensures low impedance continuous grounding between the enclosures and connectors. The electronics cabinet is a completely sealed unit and will form a complete shield around the internal components due to the grounded connector panels and the use of an EMI gasket on each door. The dewar shell will likewise form a continuous shield around the dewar internal components with the exception of the double dewar window. The two windows are mounted on a "snout" with internal baffles, all of which will be grounded, so the entry of omni-directional RF energy should be minimized.

Externally mounted equipment is inherently shielded (vacuum gauges) or incorporates similar shielding provisions (guide camera head). The calibration lamps and the dust cover drive mechanism will incorporate shielding for all components have the potential for RF emissions or sensitivity.

#### 5.3.3.3 Dewar Internal Interconnections

As shown in Figure 91, feed thru connections to the inside of the dewar are made via hermetic connectors mounted on five connector bulkheads located at the front of the main dewar shell section, just before the front cap. These hermetic connectors are all printed circuit terminated connectors. A printed circuit board on the interior side makes the transition to the appropriate connector type for connection of the internal cables between the dewar wall and the cold shields. An example of this type of connector and printed circuit board arrangement is shown in Figure 92.

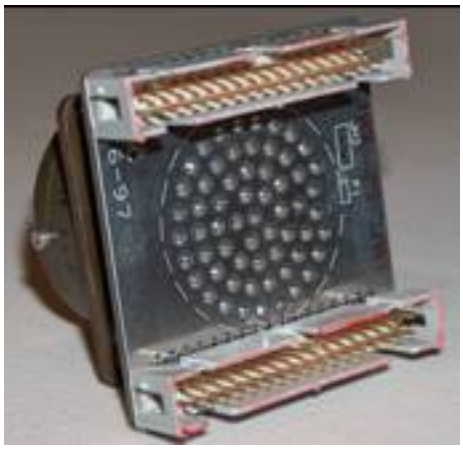

**Figure 92: Example Printed Circuit Board Transition Assembly**

The internal cables between the dewar feed thrus and the dewar cold shields are designated the "F" series (MOS-W-F-XX, also in MEDN02). With the exception of the high wire count cables to the CSU clutch blocks and the cable to the detector ASIC carrier board, all of these cables terminate

on bulkhead mount connectors attached to the cold shields. This is done to provide thermal insulation between the heat conducting exterior cables and the cold interior cables. The CSU clutch block cables and the cable to the ASIC carrier board pass through the cold shield and are clamped to the shield to shunt to the cold shield the heat conducted along the cable from the connection at the dewar connector bulkhead, preventing this heat from reaching the portion of the cable inside the cold shield.

On the inside of the cold shield "G" series cables (MOS-W-G-XXX, also in MEDN02) connect to the internal dewar equipment.

Within the dewar two breakout printed circuits are used to simplify the internal wiring. At the top right of figure one the motor breakout printed circuit (MBP) is used to connect the seven motor driven mechanisms to the motor drive and status switch cables. Just below the dewar mechanisms a second breakout, the temperature sensor breakout printed circuit (TSBP) is located. This board provides terminations for the various temperature sensors located inside the dewar. In addition to the sensors shown on this diagram additional redundant "backup" sensors are provided for critical locations. The backup sensors will also be cabled out of the dewar with sensor selection made in the electronics cabinet.

The Hawaii-2RG detector is controlled that ASIC performs all of the multiplexing control functions to read out the detector and incorporates 36 channels of analog to digital conversion to digitize the detector pixel values. Control and data communications with the ASIC uses a parallel interface with a low voltage differential signaling (LVDS) format.

In the middle right side of Figure 89 below the temperature sensor breakout printed circuit the FCS connections are shown and just below these the Hawaii-2RG detector is shown along with the ASIC carrier board. A flex circuit cable connects the Hawaii-2RG (designated MOS-W-G13) to the ASIC carrier board. The ASIC is mounted on this carrier board, and a second flex circuit cable (designated MOS-W-F-13) passes through the cold shield and connects the carrier board to a hermetic bulkhead connector mounted on a small feed thru plate on the dewar wall near the detector. This flex circuit is clamped to the cold shield.

The connector mounted on the dewar wall is in turn connected by a short length of shielded cable to the Jade2 interface board that is mounted in a shielding box attached to the outside of the dewar. The Jade2 interface board converts the ASIC LVDS format signals to universal serial bus (USB) signals. The Jade2 also conditions power supplied to the ASIC and the detector. The Jade2 USB is routed back to the electronics cabinet where it reaches the detector control computer. Power to the Jade2 is locally regulated by a dc-to-dc converter mounted with the Jade2 and supplied with dc power from a power supply mounted in the electronics cabinet.

The CSU is shown at the bottom right of Figure 89. The CSU voice coils, LVDT sensors and limit switches are connected to the CSU control rack in the electronics cabinet via cables from the electronics cabinet to dewar wall feed thrus ("E" series cables), then from the dewar wall to the cold shields ("F" series cables), and from the cold shields to the CSU ("G" series cables). The CSU clutch and brake coils (184 in total) are connected to the CSU amplifier rack in the electronics

cabinet via cables from the electronics cabinet to dewar wall feed thrus ("E" series cables) and then from the dewar wall directly to the CSU ("F" series cables). These cables pass through the cold shields and are clamped in place as described above.

The clutch and brake coil signal connections between the dewar feed thru connector printed circuit boards and the CSU are made with 3M series 3000 connectors and 24 AWG phosphor bronze ribbon cable. All of the other internal dewar connections ("G" series cables) and cold shield feed thrus are AirBorn series W connectors. The corresponding "F" series cables between the cold shield and the dewar feed thru printed circuit boards are also terminated in AirBorn series WTA connectors. AirBorn WTA printed circuit mounting connectors are used on the dewar feed thru connector transition printed circuit boards. Examples of cable and printed circuit board terminated AirBorn series WTA connectors are shown in Figure 93.

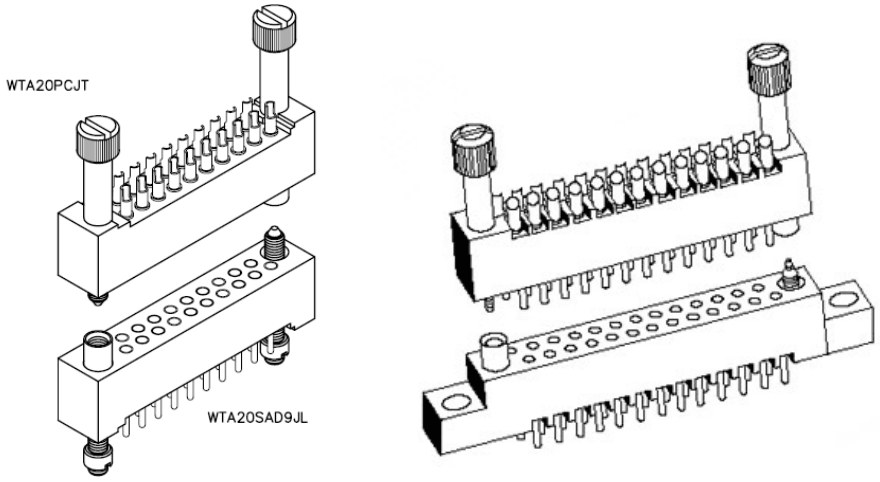


**Figure 93: AirBorn WTA Series Connectors**

### 5.3.3.4 Electronics Cabinet Layout

The MOSFIRE electronics cabinet layout is shown in Figure 94. This view shows the MOSFIRE rotator in the position that will be typical when MOSFIRE is stored on the Nasmyth deck. This rotator position defines a "normal" orientation where the equipment rack doors are vertical and the rack mounted equipment right side up.

All of the electronic equipment is mounted in the two EIA 19 inch rack bays inside the electronics cabinet. Components not supplied in a ready to rack mount form (such as the motion controllers) are mounted in 19 inch rack insert chassis. With the exception of the two glycol coolers all of the equipment in the two rack bays will be mounted on rack slides and provided with cable management hardware to maintain service loops. All rack slides will be specified to permit full extension of the slides to access rear panel mounted connections for installation and removal of the rack mounted equipment.

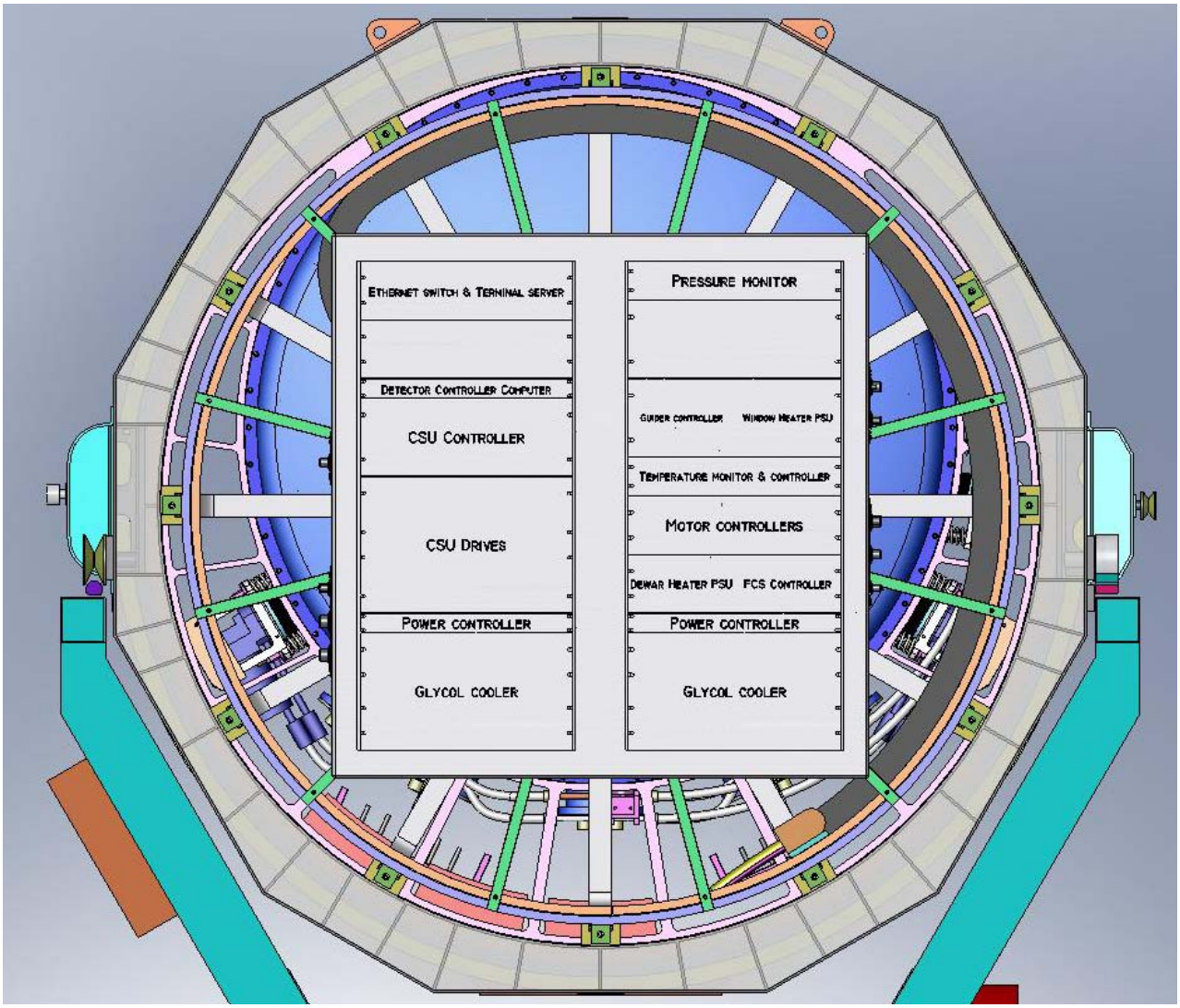


**Figure 94: MOSFIRE Electronics Cabinet Layout**

Two blank panels are shown in Figure 94 and these spaces can be subdivided and rearranged if airflow or cabling requirements dictate.

#### 5.3.3.5 Electronics Cabinet Internal Interconnections

With the exception of the science detector, the SIDECAR ASIC, Jade2 interface card and power supply, the guide camera head and the arc lamp power supplies all of the MOSFIRE electronics are rack mounted in two EIA 19 inch rack bays in the electronics cabinet. Each rack bay is cooled via a glycol cooled liquid to air heat exchanger equipped with fans to circulate the air within the cabinet. A block diagram of the electronics within the MOSFIRE electronics cabinet is shown in Figure 95.

At the upper left side of Figure 95 the fiber optic connection and the ac power input connections are shown. A fiber optic pair (Tx/Rx) is routed to the network switch for 1000Base-SX communications and a second fiber optic pair is routed to the guide camera controller for the Camera Link interface.

Input power to the electronics cabinet is 120 Vac/60 Hz, which is supplied by the Observatory "clean" UPS, power, a regulated and filters 120 Vac power source. Power is distributed directly to the network switch and the two Pulizzi IPC3402-NET Power Controllers.

The network switch provides 100Base-TX communications to the power controllers and to a pair of terminal servers. The terminal servers provide an interface between 100Base-TX network communications and RS-232 devices. Each terminal server supports 8 independent RS-232 connections. 1000Base-T (gigabit Ethernet) is provided for communications with the detector control computer to maximize science data transfer performance.

The various units of electronic equipment shown in Figure 95 are color coded with respect to the rack bay in which they are mounted, and with the exception of one terminal server and the glycol cooling module fans, power to all of the equipment in each bay is controlled by the power controller located in the same bay.

At the top center of Figure 95 the ambient temperature and contact closure interface is shown. This interface uses two DGH D1451 thermistor input modules and a DGH D1701 digital I/O module. One thermistor will be used to monitor the rack internal temperature in each bay. Two digital inputs will be used to monitor switches that will indicate if the electronics cabinet doors are closed. This monitoring is provided to ensure that the when the instrument is on the telescope that the doors are closed prior to moving the telescope from the horizon lock position. Two additional digital inputs will be used to monitor flow switches on the electronics cabinet glycol supply and return lines.

Just below the ambient temperature and contact closure interface is a power supply for the Jade2 board and just below that is the detector control computer. The Jade2 power supply provides 13.8 Vdc to a dc-to-dc converter located next to the Jade2 in the shielding box on the outside of the dewar. The detector control computer is a flash disk equipped Augmentix A+860 server. This computer provides a USB 2.0 interface to the Jade2 card and a Microsoft Windows environment to run the Teledyne supplied hardware abstraction layer interface to USB and a COM DLL for external interfaces. Java software will run on this computer and communicate via 1000Base-T to the MOSFIRE detector target computer (located in the Keck I computer room) via the network switch and 1000Base-SX fiber optic link. A RS-232 connection is used to provide a console for maintenance and configuration of the detector control computer. The detector control computer will normally be configured to automatically start the detector control software at power on.

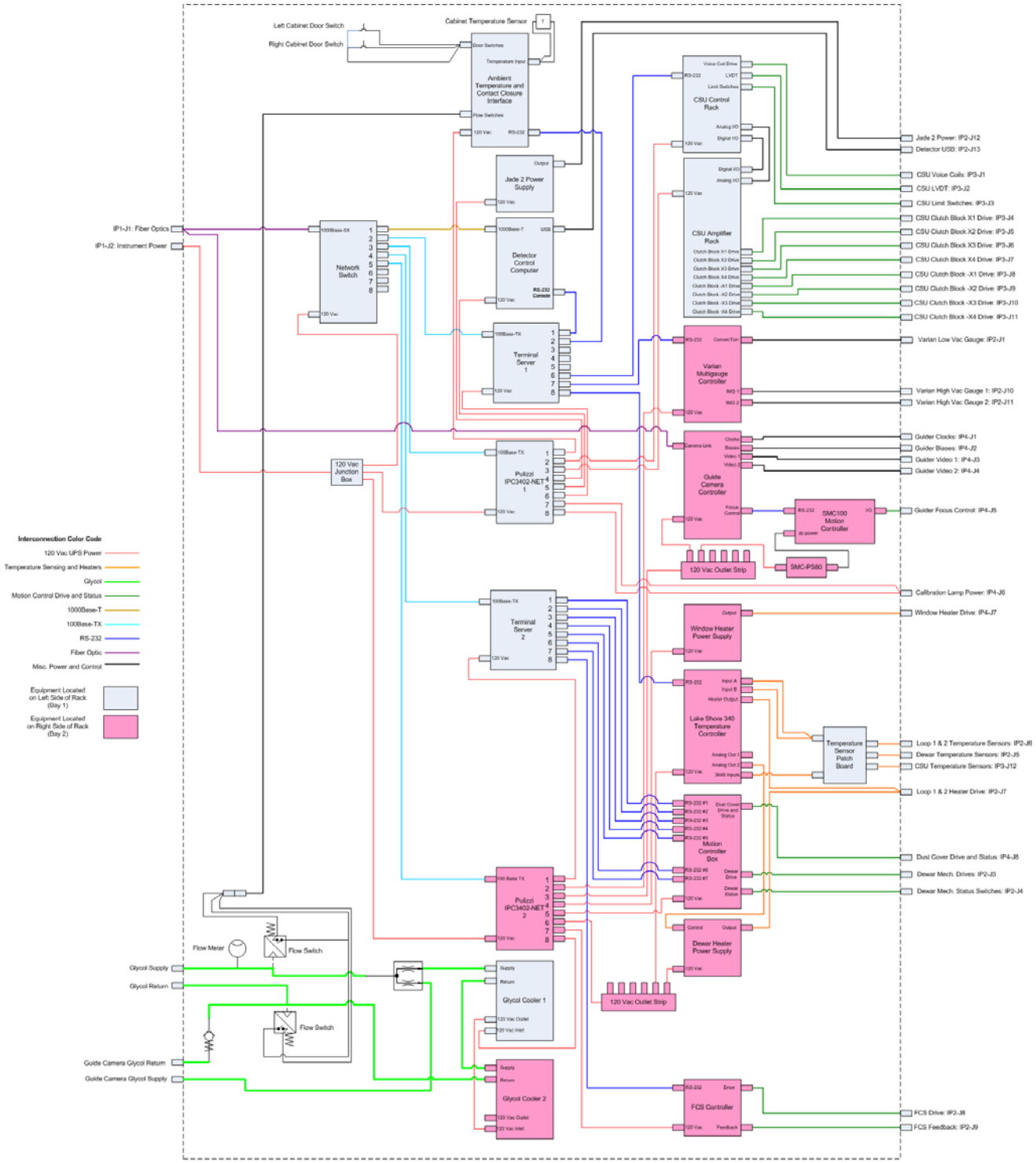


**Figure 95: MOSFIRE Electronics Block Diagram**

At the bottom center of Figure 95 the two glycol coolers are shown. Each cooler is equipped with fans to circulate the air inside the cabinet through the liquid to air heat exchanger. The fans are controlled by an outlet on the power controller in the right hand bay of the electronics cabinet. Glycol is supplied by the Observatory glycol cooling system. The pressure of this supply is regulated in the instrument glycol module mounted on the stationary portion of the rotator. As shown in Figure 95 the glycol supply to the electronics cabinet will be monitored with a flow indicating meter and a flow switch. An adjustable diverter will be used to provide an adjustable flow to a parallel circuit to provide cooling for the guide camera head. The glycol return line is also monitored with a flow switch and the guide camera return flow is merged with the return flow from the electronics cabinet coolers with a check valve. While the flow switches will not detect small leaks they do provide protection for loss of coolant flow, disconnection of either the supply or the return, and for a substantial difference in supply and return pressure due to a larger glycol leak. The flow switches are monitored by the ambient temperature and contact closure interface described above.

The remaining electronic equipment is found starting at the top right side of Figure 95. At the very top is the CSU control rack and amplifier rack. The CSU control rack communicates with the MOSFIRE host computer, which runs the MOSFIRE CSU server, via RS-232. The control rack incorporates the hardware interfaces for the voice coil used to drive for the CSU indexing frame. The control rack also monitors the LVDT and limit switches used to monitor the CSU motions. The control rack supplies analog and digital control signals to the CSU amplifier rack that provides the drive to the ratchet clutch and brake coils. The clutch and brake coils are assembled into modules referred to as “clutch blocks”. There are 46 pairs of masking bars that can be moved by the CSU to form slitlets in the FOV, with one bar in each par located on either side of the CSU FOV. The direction of motion for the masking bars is along the CSU x-axis. There are two clutch blocks, one on each side of the CSU x-axis, and these blocks are referred to as the X and -X blocks. Each block contains 92 coils, with a ratchet clutch and a brake coil for each masking bar. Because of the relatively high signal count and the need to provide adequate common returns for the clutch drive power, multiple connector and cable assemblies are used. The 184 clutch drive signals are divided among eight 40 pin ribbon cables in the dewar, and these connect as described in §5.3.3.2 to eight connectors on panel IP3 on the electronics cabinet.

Shown immediately below the CSU amplifier rack in Figure 95 is the Varian Multigauge controller. This unit controls the high and low pressure vacuum gauges and communicates with the MOSFIRE host computer via RS-232.

Immediately below the Varian Multigauge controller is the detector controller for the MOSFIRE guider. This unit is housed in the MOSFIRE electronics cabinet, but it is controlled by one of the Observatory’s MAGIQ software and the MAGIQ camera servers via a Camera Link fiber optic interface. Power to the guide camera controller is controlled by one of the MOSFIRE power controllers, but the MAGIQ software will have access to this power control function via the MOSFIRE power control server. The guide camera controller also provides focus control for the MOSFIRE guider. This is via an RS-232 interface controlled through the Camera Link connection by the MAGIQ software. The RS-232 connection controls a Newport SMC100 motion controller mounted next to the guide camera controller. The guide camera controller and the power supply

for the SMC100 (a Newport SMC-PS80) are supplied with 120 Vac power via a standard power strip that is used to connect these two units to one outlet on the power controller in bay 2. Control and drive signals to the guider focus stage are provided by connector J5 on panel IP4 of the electronics cabinet.

Shown below the guide camera controller in Figure 95 is an adjustable output low voltage dc power supply that will be used to control the dewar window heaters. The normal thermal condition will be steady state and open loop control is used for the dewar window heaters. 120 Vac power to the window heater power supply is controlled by the power controller in bay 2 of the electronics cabinet.

Just above the window heater drive connector (IP4-J7) a connector is shown for power to the calibration lamps (IP4-J6). This connector is supplied with two circuits of 120 Vac power from power controller 1.

Shown immediately below the window heater power supply is the Lake Shore 340 temperature controller. The 340 is controlled via RS-232. The 340 operates two temperature control loops. Loop 1 is a high performance control loop used for control of the MOSFIRE science detector temperature. Loop 2 is a lower performance control loop used to regulate the internal temperature of MOSFIRE by heating the cold head spreader bar on each of the two main MOSFIRE CCR cold heads. The analog output from loop 2 on the 340 is used to drive an adjustable output power supply, the dewar heater power supply, shown immediately below the 340 in Figure 95. This power supply is required because the second 340 heater output is limited. The 340 is provided with complete software capabilities for temperature control, requiring only the programming of set points and control loop servo parameters.

The 340 is also used to monitor temperatures inside the MOSFIRE dewar. An eight channel option board (3468) is used to interface to temperature sensing diodes (Lake Shore DT-470-CU-13) located at various points in the dewar. For testing purposes more than eight temperature sensors will be installed in the dewar, including back up sensors for each of the temperature control loops. There are also 10 temperature sensors provided on the CSU, again these are used for monitoring during CSU cryogenic testing by CSEM, and will also be available for use by MOSFIRE.

During testing these various sensors will be independently interfaced to a Lake Shore 218 temperature monitor. However, eight channels of temperature monitoring are considered sufficient for normal operation. To permit selection of the desired sensors a printed circuit board patch panel will be mounted on a rack insert chassis behind one of the blank panels in the electronics cabinet. This will provide jumpers to select which of the temperature sensors in the dewar and on the CSU are monitored by the eight channel 3468 board in the 340 temperature controller. It will also allow selection of the primary or back up sensor for each of the two temperature control loops.

120 Vac power to the 340 and the dewar heater power supply is controlled by the bay 2 power controller. A standard power strip is used to connect these two units to one outlet on the power controller.

Finally, at the bottom right corner of Figure 95 the FCS controller is shown. This is a self contained control and servo amplifier unit that drives the piezo actuators on the FCS tip/tilt mirror stage. Capacitance sensors are used to provide position feedback. The FCS is programmed and controlled via an RS-232 interface.

### 5.3.4 MOSFIRE Electronics Components

As previously noted most of the MOSFIRE instrument electronics are COTS items. Many of these items are very similar or identical to those used in the OSIRIS instrument. The temperature controller/monitor, vacuum gauge controller, network switch, and terminal servers are components standardized by WMKO, and the instrument's network architecture and motion control systems are very similar to those used on OSIRIS.

All of the major MOSFIRE electronics components are listed in Table 21. With the exception of the CSU controller, all of these hardware components are commercial off-the-shelf products, and each component requiring software control comes complete with firmware and a documented API.

| Function | Instrument Electronics Component | Control/Data Interface |
|---|---|---|
| **Science Detector** | | |
| Detector | Teledyne HAWAII-2RG 2048×2048 HgCdTe Infrared Array | Discrete digital + analog I/O |
| Detector Controller ASIC | Teledyne SIDECAR ASIC and Jade2 interface card | Discrete digital + analog I/O, LVDS |
| Detector ASIC to USB Interface | Teledyne Jade2 interface card | LVDS, USB 2.0 |
| Jade2 Power Supply | 13.8 Vdc Regulated Power Supply and dc-to-dc converter (located at Jade2) | Not required |
| Detector Target | 1U rack mount Windows XP server | 100Base-TX CAT-5e & USB 2.0 |
| **Motion Control** | | |
| Rotary Mechanisms (5) | Pacific Scientific PD2400 Motion Controller | Serial RS-232 |
| Flexure Compensation System | Physik Instrumente Two-Axis Piezo Controller | Serial RS-232 |
| Detector Focus Mechanism | Pacific Scientific PD2400 Motion Controller | Serial RS-232 |
| Dust cover actuator | Pacific Scientific PD2400 Motion Controller | |
| Cryogenic Slit Unit | CSEM Custom CSU Controller | Serial RS-232 |
| Guider Focus Control | Newport SMC100 Motion Controller | Serial RS-232 |
| **Thermal Management and Control** | | |
| Temperature Control | Lake Shore 340 Temperature Controller | Serial RS-232 |
| Detector Temperature Control | 340 Control Loop 1 | |
| Dewar Temperature Control | 340 Control Loop 2 | |
| Dewar Temperature Monitoring | 8-input option card (model 3468) in 340 | |
| Dewar Temperature Heater Power | Kepco ATE 100-2.5M power supply | Analog input |
| Window Heater Power Supply | Adjustable low voltage dc supply | None required |
| Ambient Temperature and Contact Closure Interface | 2 DGH 1451 2252 Ohm Thermistor Input Modules | RS-232 |
| | 1 DGH 1701 Digital Input/Output Module | RS-232 |
| | 13.8 VDC Power Supply | None required |
| **Housekeeping** | | |
| Pressure Monitor | Varian Multi-Gauge Controller | Serial RS-232 |
| Power Control | 2 Pulizzi IPC3402-NET Power Controllers | 100Base-TX CAT-5e |
| **Data Communications** | | |
| Network Switch | HP ProCurve 2824 Switch | 1000Base-T/100Base-TX CAT-5e UTP & 1000Base SX optical fiber |
| RS-232 Terminal Servers (2) | Lantronix ETS8PS Terminal Servers | 100Base-TX CAT-5 & RS-232 |
| **Guider** | | |
| Guide Camera Controller | SciMeasure Little Joe Controller | Camera Link optical fiber |

**Table 21: MOSFIRE Instrument Electronics Components**

#### 5.3.4.1 Science Detector and Detector Controller

As presented at PDR, the MOSFIRE team selected the HAWAII-2 RG 2K x 2K HgCdTe array from Teledyne Imaging Sensors (formerly Rockwell Scientific). This detector, which has 18 μm pixels and a 2.5 μm cut-off wavelength, is the same device architecture being developed for JWST and many ground-based users. Consequently, we stand to benefit from the considerable development work undertaken to solve many difficult detector issues such as charge persistence, QE, noise, dark current and delamination. Recent proprietary data presented to us by Teledyne suggests that excellent progress has been made in all these factors and that our performance goals will be achieved. Dark currents of <0.005 $e^-$/s have been measured in devices operated at 35 K; our goal is < 0.01 $e^-$/s at 77 K. Teledyne will provide MOSFIRE with H2-RG arrays with the lowest read noise possible. Currently, Teledyne is measuring between 17 and 22 e- CDS over the temperature range of 35 K to 80 K for SWIR arrays. R&D efforts are underway to improve read noise, and any improvements available to support the MOSFIRE deliverable focal plane arrays will be incorporated in the devices. Multiple sampling (16 Fowler reads or Up-the-Ramp samples) can achieve ~5-6 electrons rms according to tests of devices for JWST and other groups. The MOSFIRE device will be substrate-removed and AR-coated to yield QE > 80% across our spectral range.

Teledyne is now offering H2-RG devices with an ASIC that implements all of the detector readout functions. The ASIC, called "SIDECAR", provides clocks and bias voltages to the detector and digitizes the detector outputs. The SIDECAR ASIC is packaged separately on a small board that is located inside the dewar next to the detector head. Just outside the dewar wall is another board, the Jade2, which provides the interface between the ASIC and USB 2.0. To enable our team to become familiar with the operation of these devices we obtained a prototype ASIC mounted on a development (non-cryogenic) board, plus a Jade2 interface card and software (as shown on the left side of Figure 96). We have been operating this device since February 2006, and we are working closely with Teledyne staff to develop software compatible with the MOSFIRE server architecture to control the ASIC.

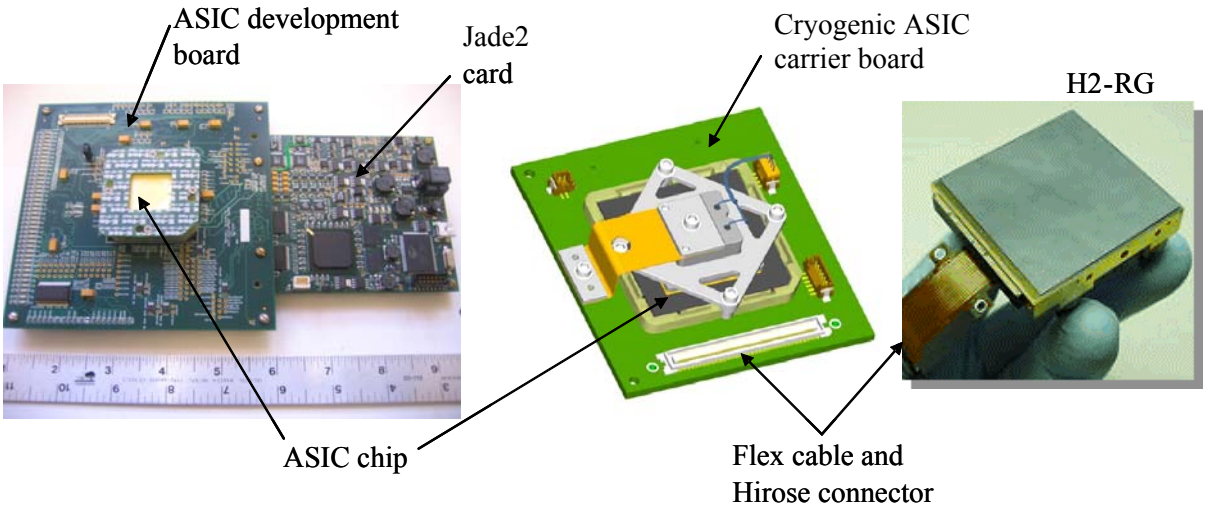


**Figure 96: The ASIC Development Board and Cryogenic ASIC Carrier Board**

We are expecting to receive the cryogenic ASIC carrier board (shown in the center of Figure 96) and an engineering grade H2-RG detector very soon. A prototype of the MOSFIRE detector head has already been built and will be installed with the ASIC and carrier board in a $LN_2$ cooled dewar to gain experience using the ASIC to control and readout the detector array.

Detector temperature control will be provided a standard Lake Shore 340 temperature controller in an implementation similar to that used in OSIRIS.

Figure 97 is a block diagram of the hardware and software components of the MOSFIRE detector system. This system consists of the detector, detector controller, interface components, two computer systems (the MOSFIRE host and the detector target) and the software modules required to control and read out the science detector.

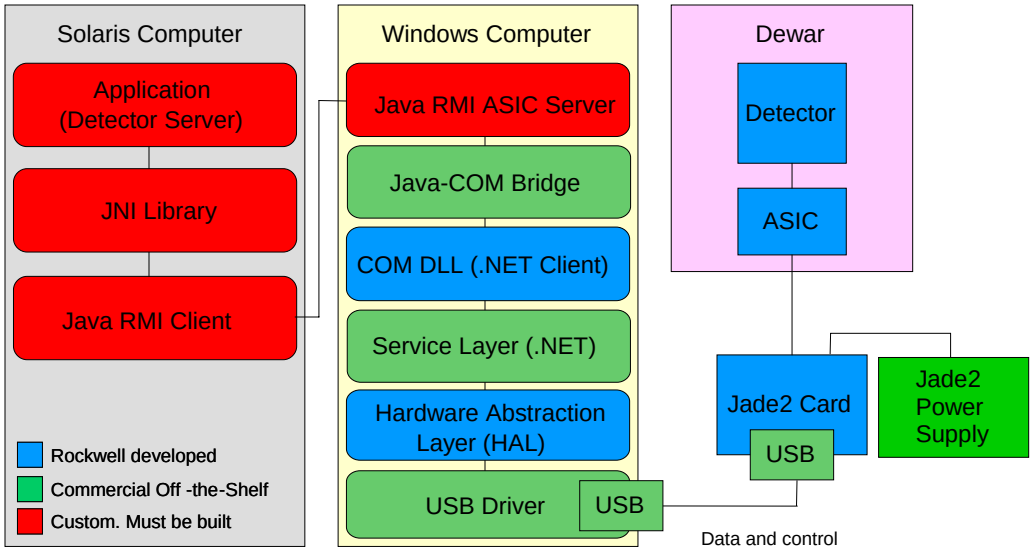


**Figure 97: MOSFIRE Detector System**

The Teledyne SIDECAR ASIC uses a proprietary interface to a module called the "Jade2", also supplied by Teledyne. The Jade2 provides power conditioning for the H2-RG and the ASIC and a USB 2.0 compliant interface to the detector target computer. All of the detector control communications and read out data are transferred over the USB 2.0 interface.

Teledyne uses a third party USB driver (Bitwise Systems QuickUSB) and their own hardware abstraction layer (HAL), which translates application commands into driver specific commands, hiding USB-specific driver detail from a higher-level application layer. The HAL in turn uses a second Teledyne-supplied software component called the "COM DLL" to communicate with the HAL using the Microsoft .NET web service The COM DLL application allows third party software to interface to the HAL and in turn to the ASIC via USB and the Jade2.

A computer running Windows XP is required to run the USB driver, HAL software and COM DLL. This computer, which is equipped with a flash drive and rack-mounted in one of the MOSFIRE electronics cabinets, will function as the detector control computer. This computer will

be located on a private network within the instrument and it will not be accessible via network communications except through the MOSFIRE host computer. The system will not require the use of less secure applications such as web browsers, reducing the need to implement frequent security updates.

Tests at Teledyne have confirmed that the noise performance of the H2-RG detector is better if the Jade2 board is powered by a clean 5 Vdc power supply, rather than the 5 Vdc line in the USB connection (which derives its power from the computer's noisy switched-mode power supply). A low noise instrumentation grade dc-to-dc converter located in the shielding box where the Jade2 is mounted will provide separate power to the Jade2. Power to the dc-to-dc converter is supplied from the electronics cabinet as described in §5.3.3.5.

#### 5.3.4.2 Motion Control

MOSFIRE has 7 motion axes driven by two-phase bipolar stepper motors. Five of the mechanisms are rotary and two are linear. Each of the mechanisms is equipped with limit switches that are interfaced with the corresponding motion controller. A Pacific Scientific PD2400 indexing motion controller controls each motion axis.

The PD2400 motion controllers are mounted in an EIA 19 inch rack mount chassis with a dedicated DC power supply. Fan cooling will be provided to ensure adequate air circulation within the chassis. Each of the motion controllers will operate with low duty cycles so power dissipation will be minimal.

The Physik Instrumente (PI) piezo controller for the Flexure Compensation System is a self contained rack mount unit. The CSEM controller consists of two rack mount units, one for the controller and one for the clutch amplifiers.

Table 22 describes the Motion control requirements for MOSFIRE in greater detail.

| Mechanism | Description |
|---|---|
| **Rotary Motion** | |
| Dust Cover | A linear stage that slides a cover over the window when instrument is not in use, two positions (open/closed) |
| Filter Wheel 1 | Edge-driven wheel with 6 positions, including an open position |
| Filter Wheel 2 | Same as filter wheel 1, the two wheels provide for a total of 10 filters |
| Pupil Rotator Wheel | Used for imaging and spectroscopy in the H- and K-band. A hexagonal mask serves as a Lyot stop, and rotates to match the rotation of the telescope pupil as an object is tracked across the sky. The mask is formed using an iris that is open for the Y- and J-bands. |
| Grating-Mirror Exchange | The spectrometer diffraction grating and imaging fold mirror are mounted back-to-back on a turret. The mechanism rotates approximately 157 degrees between the imaging position and two grating tilt positions |
| Grating Tilt | Rotates a grating angle shim between deployed and retracted, continuous rotation in 90º steps |
| Detector Focus | Single-axis piston stage that adjusts the detector focus based on filter selection |
| **Piezo Controllers** | |
| Flexure Compensation System | Piezo actuator driven tip/tilt mirror that compensates for flexure in the instrument due to a varying gravity vector. Uses a lookup table based on positioning information from the telescope drive system. |
| **Cryogenic Slit Unit** | Cryogenic adjustable slit mask, comprised of a set of 46 pairs of bars |

**Table 22: MOSFIRE Motion Control Requirements**

### 5.3.4.3 Thermal Management and Control

The science detector operating temperature is controlled by a closed loop temperature control system using a Lake Shore Cryotronics, Inc. model 340 temperature controller, a diode temperature sensor and a resistive heater located on the detector mounting block.

The overall temperature of the dewar's internal structure is controlled by the second control loop of the 340, which drives heaters via a Kepco model ATE 100-2.5M power supply.

The snout tube heaters are resistance type cartridge heaters driven open loop from an adjustable low voltage power supply

### 5.3.4.4 Housekeeping

The MOSFIRE instrument housekeeping functions include electronics cabinet, dewar and ambient temperature monitoring, dewar pressure monitoring and instrument power control. Dewar temperature monitoring is provided by a Lake Shore Cryotronics, Inc. model 3468 8-input option card added to the model 340 controller. Silicon diode temperature sensors will be deployed at various locations in the dewar. Temperature sensors are also provided in each equipment rack. Pressure monitoring is provided by a Varian Multi-Gauge controller. This controller is equipped with two high vacuum gauges (Varian IMG-100), one as the primary high vacuum gauge and one as a backup. A low vacuum gauge (Varian ConvecTorr gauge tube) is also provided.

AC power comes in via an interconnect panel on electronics cabinet 1 and then distributed to the AC power controllers. AC power control for the MOSFIRE electronics is performed by 2 Pulizzi IPC3402-NET power controllers. Each distribution unit provides 8 outlets, and these are assigned

as shown in Table 23. The network switch and terminal servers are directly powered from the input connector without going through the power controllers. As long as the instrument has power, the switch is powered up, providing network services, particularly to the power controllers that supply power to everything else.

| **Pulizzi IPC3402-NET Power Controller Circuit #** | **Load** | |
|---|---|---|
| **Electronics Cabinet Bay 1** | **Description** | **Typical Wattage** |
| 1 | Communications crate | 60 |
| 2 | Detector Target Computer | 550 (max.) |
| 3 | CSU Controller | 265 (max.) |
| 4 | CSU Drives crate | 50 |
| 5 | Detector Control Computer | 345 (max.) |
| 6 | Terminal Server 1 | 12 |
| 7 | Calibration Lamp 1 | 30 |
| 8 | Calibration Lamp 2 | 30 |
| **Electronics Cabinet Bay 2** | **Load** | |
| 1 | Terminal Server 2 | 12 |
| 2 | Varian Multi-Gauge Controller | 120 |
| 3 | Guide Camera Controller | 60 |
| 4 | Window Heater Power Supply | 15 |
| 5 | Motion Controller Box | 75 |
| 6 | Lake Shore 340 Temperature Controller and Dewar Heater Power Supply | 190 |
| 7 | FCS controller | 80 |
| 8 | Glycol Coolers 1 & 2 Heat Exchanger Fans | 32 |

**Table 23: MOSFIRE AC Power Distribution**

#### 5.3.4.5 Data Communications

A Hewlett Packard ProCurve 2824 switch equipped with a 1000Base-SX transceiver is used to provide TCP/IP communications for the instrument electronics. The 1000Base-SX transceiver provides a gigabit link to a second ProCurve 2824 located in the MOSFIRE computer rack in the Keck I telescope computer room. The two switches form a single private 1000Base-T/100Base-TX network for the instrument.

One switch located in the left bay of the electronics cabinet on the instrument communicates with the detector target computer, two Lantronix ET8PS terminal servers housed with it in the same crate, and two Pulizzi IPC3402-NET power controllers (one in each rack).

The other switch located in the MOSFIRE computer rack communicates with the MOSFIRE host computer, detector target computer and the terminal server in the MOSFIRE CCR head speed control and interface rack located in the Keck I telescope mechanical equipment room.

RS-232 communications is used for control and monitoring of the other MOSFIRE electronics components and the two terminal servers allow control of these devices via the MOSFIRE private network using TCP/IP.

### 5.3.5 Guider

The MOSFIRE guide camera will be operated as part of the Observatory's new acquisition and guide camera system called MAGIQ, the Multi-function Acquisition, Guiding and Image Quality monitoring system. This project is developing an integrated system for acquisition, guiding and image quality measurement for the Keck telescopes. This system will replace the acquisition and guiding hardware and software for existing WMKO seeing limited (i.e. non-adaptive optics) facility instruments and the acquisition cameras on the Observatory's adaptive optics systems. The MAGIQ system will also become the observatory standard for acquisition and guide cameras and software for new seeing limited instruments

The SciMeasure Analytical Systems, Inc. "Little Joe" camera has been selected as the standard observatory guide camera. It is well matched to the E2V Technologies CCD47-20, and delivers nearly detector-limited performance, highlighted by low read noise and high frame rate. The Little Joe camera consists of a camera head and a 3U high half rack or full rack camera controller. A typical configuration is shown in Figure 98. The camera head is of small size, which will simplifies integration of this camera into existing WMKO facility instruments. The standard cable length between the controller and head is 3 m, and 6 m has been proven with a slight ($1e^-$) increase in noise. This allows flexibility in the mounting position of the controller inside existing instruments. Furthermore, the controller and power supply are available as separate units, connected by a 1 m cable, giving additional flexibility in mounting this equipment.

**Figure 98: SciMeasure Little Joe Camera Head and Controller**

The Little Joe camera controller is equipped with the Camera Link interface that can use copper connections for short distances or fiber optic connections for long distance runs. Additionally, the detector controller incorporates a separate RS-232 serial port, which can be used for troubleshooting and low-level commands. The controller consists of four 3U Eurocard format boards, a command module, output module, input module and support module, all mounted in a rack enclosure. These board sets are readily accessible and interchangeable, greatly increasing serviceability of the systems. This arrangement also allows for easy upgrades and improvements during the life of the camera systems. The manufacturer, SciMeasure, is willing to guarantee a minimum 10 year service life and is also willing to escrow all intellectual property at time of build

for these cameras, including schematics and source listings, for delivery to WMKO if or when SciMeasure discontinues this line of cameras. With this information, WMKO will be in a good position to support these cameras for many years and the long-term risk of camera system obsolesce is mitigated.

The guide camera head for MOSFIRE will be based on the standard SciMeasure Analytical Systems Little Joe camera. SciMeasure will make a custom hermetic camera head so that a non-hermetic CCD4720-BT with TEC can be used, allowing the field flattener of the MOSFIRE guider optics to be mounted in the position defined by the optical prescription, very close to the detector focal plane. The MOSFIRE field flattener will form the front window of the hermetic camera head.

The Little Joe camera controller incorporates an $I^2C$ control interface on its backplane. Remote command and data transactions can be performed with backplane connected $I^2C$ devices using the Camera Link interface. The MOSFIRE guider optics focus will be controlled using a Newport SMC100. The RS-232 interface on the SMC100 will be interfaced to the $I^2C$ bus in the backplane using an $I^2C$ to RS-232 converter. The SMC100 and its SMC-PS80 power supply will be mounted next to the guide camera controller along with the dewar window heater power supply.

### 5.3.6 MOSFIRE Instrument Computers Overview

WMKO has standardized on computers running the Sun Solaris operating system as the primary platform for instrument host computers. The final selection of server computer will not be made until the third year of the project, so it is possible that the model number and feature set will change when the computer is actually purchased.

The MOSFIRE computer architecture consists of three main computers and two switches: an instrument host computer, a detector target computer, and a detector control computer. The detector control computer's responsibility is to run the MOSFIRE ASIC Server and SIDECAR ASIC control software. This system will run Windows XP Professional and will reside in the instrument electronics cabinet. The detector target computer will run the Detector Server and connect to a storage array for data. The instrument host computer will run everything else. These latter two systems will run Solaris and reside in the Keck computer room. All network devices are connected through two private network switches: one at the instrument, one in the Keck computer room. The MOSFIRE computer network is illustrated in Figure 99.

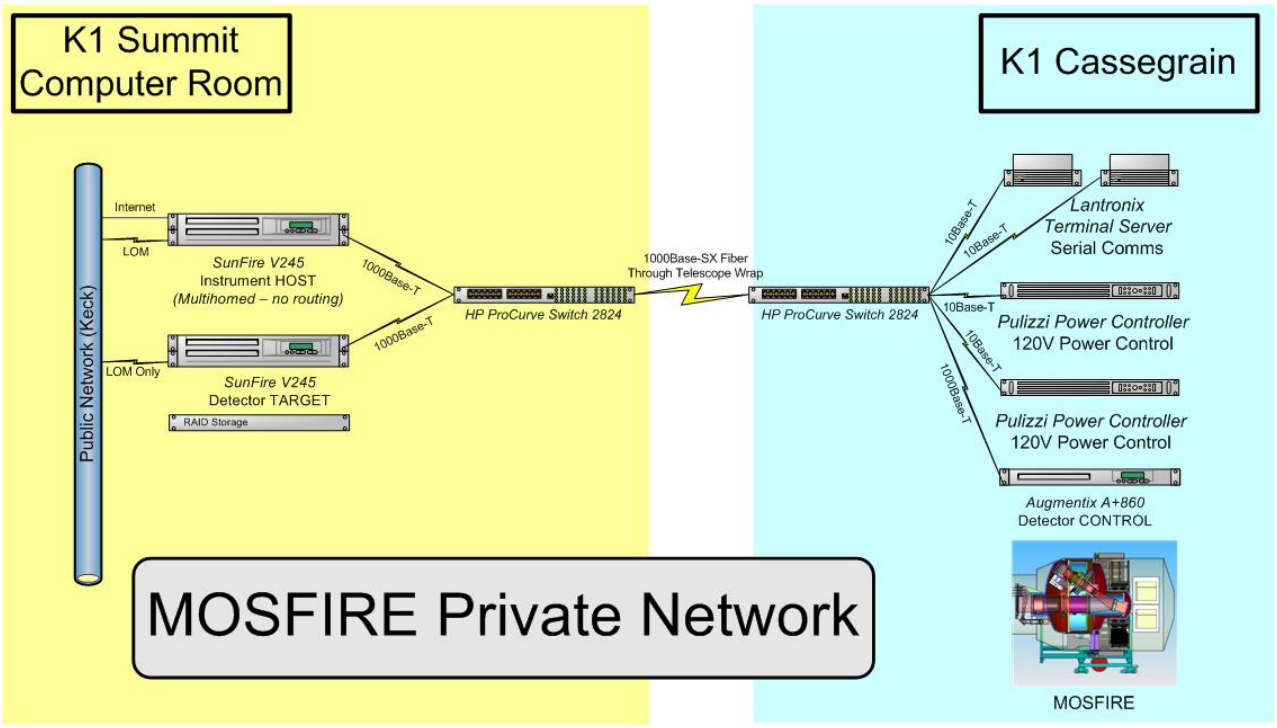


**Figure 99: MOSFIRE Computer Network**

### 5.3.7 Major changes since PDR

The main changes to the electronics system are:

- The addition of arc lamps for wavelength calibration of the instrument. These lamps are located in the guider enclosure at the front of the instrument and turned on and off via one of the Pulizzi power controllers.
- Consideration of the Leach controller as a fallback choice for detector control has been dropped.
- The on-instrument vacuum pump has been dropped, along with the requirement for a contactor to control power to it.
- All of the details of the connections between the MOSFIRE electronics and dewar have been defined.
- All of the internal wiring details for the MOSFIRE dewar have been defined.

## 5.4 Software

MOSFIRE is a third generation WMKO instrument and therefore inherits a wealth of existing software infrastructure, and benefits from previous experience in designing and implementing instrument control software and user interfaces. Most significantly, MOSFIRE will benefit from a polished and robust client-server architecture, which facilitates distributed processing and remote observing. This framework, which began with NIRSPEC and NIRC2, and was most recently refined in the implementation of the OSIRIS instrument software. This server architecture offers many features that have become standard practice for infrared instruments at WMKO. Each instrument server is compliant with the Keck Task Library (KTL), which uses remote-procedure calls (RPCs) in a WMKO standard framework for network communications. Standard WMKO keywords are used as the main applications programming interface (API), and simple clients, such as "`show`" and "`modify`" facilitate easy access and scripting. By using existing KTL interfaces to other popular languages such as Java, IDL and Tcl, a diverse range of user interfaces can be implemented.

MOSFIRE will make extensive use of software developed for OSIRIS, delivered to WMKO in 2005, including server frameworks, GUI components, and client-server interface tools. In addition, the pressure monitor, power control, and rotary motor servers will be identical to the servers implemented for OSIRIS, with the temperature control server needing only slight modification. The flexure compensation system (FCS) server will also be reused, in this case from another instrument in development, NIRES, which is using a flexure correction approach very similar to the MOSFIRE design.

The only completely new software components are the interface to the Hawaii-2RG ASIC and the server for the CSU. Both of these components will require significant development effort, but overall the software for MOSFIRE does not present any major technical or schedule risks.

Software effort will be distributed among three programming groups, the COO group at CIT, the IR Lab group at UCLA and the software development group at WMKO. Collectively, this team brings many years of experience in developing instrumentation software at WMKO.

In the sections that follow, references are made to MOSFIRE Software Design Notes (MSDN). These documents may be found in the software documentation section of the MOSFIRE project team web page. This is a password protected web site.

### 5.4.1 Changes from PDR

This section summarizes the changes in the software design since PDR.

#### 5.4.1.1 MSCGUI

The MOSFIRE Slit Control Graphical User Interface (MSCGUI, described in detail in MSDN17) will now serve as a front end GUI to the MOSFIRE Automatic Slit Configuration Generator (MASCGEN, described in detail in MSDN19). MASCGEN is responsible for determining the best

slit configuration for a given list of prioritized targets in a given patch of sky. In this case "best" means the configuration that yields the highest cumulative total of target priorities, based on priorities preassigned to the targets by the user.

At the PDR MASCGEN was a stand alone program. The user provided a target list and a few other parameters and MASCGEN would generate an Extensible Markup Language (XML) formatted slit configuration or MOSFIRE Slit Configuration (MSC) file (described in detail in MSDN18). The MOSFIRE Slit Control GUI would then use the MSC file to configure the MOSFIRE CSU.

We have decided that an interactive front end to MASCGEN will allow the user to be more efficient in field selection. The MSCGUI will be used as the UI for MASCGEN, taking in the target list and providing text areas and dropdown menus for specifying the position and rotation of the field and determining wavelength coverage. Objects on the target list are then plotted in a dedicated dialog that also displays a suitable patch of sky around the specified center of the field. The user can then drag a box, representing the CSU field of view across the patch of sky, selecting the desired region for slit placement. When the desired region is selected, the MSCGUI will pass the field position parameters to MASCGEN, which will then optimize the slit configuration, and return the slit placement parameters to the MSCGUI. The MSCGUI will then present the configuration to the user for further adjustment, execution, or saving to a file for later retrieval.

It should be noted that while it is not a requirement, it would be relatively simple to create wrapper Java classes to make MASCGEN work in a standalone mode. This functionality could be potentially added in the future.

#### 5.4.1.2 GUI Builder

The GUI Builder is a new software tool developed to automate the design and implementation of simple GUIs. In MOSFIRE, many of the GUIs are relatively simple. For example, status GUIs present keyword values to the user, such as a temperature reading, or the sampling mode of the current exposure. Control GUIs often simply set a keyword value, such as the controlled temperature setpoint of the detector. The code that monitors or modifies keyword values and displays their values on the screen is very similar regardless of the keyword type, widget type, or encasing GUI. Therefore, it is possible to create a system that can create such GUIs only by specifying the keywords of interest and the widgets that represent their values.

The GUI Builder (described in detail in MSDN35) does just that, taking a set of widgets defined in an XML file, realizing them, laying them out, and associating the widgets with instrument properties. Eight of the twelve MOSFIRE GUIs (described in MSDN36) will be built this way.

#### 5.4.1.3 Refinement of Operational Modes and Use Cases

The refinement of the operational modes and use cases described in MSDN03 has led to a corresponding refinement in the approach to the design of slit configurations as noted above with the addition of the MSCGUI. Field acquisition will be done in a similar manner to DEIMOS and LRIS, using fine alignment software (MSAlign, see below) to determine the offsets to align the

mask. The use of MOSFIRE imaging frames to create on-the-fly slit masks has been descoped to a possible upgrade option because it requires an accurate mapping from the MOSFIRE detector plane to RA and Dec, which could be complex in cases where mosaiced MOSFIRE frames would be required to obtain images that are deep enough (the mapping will be straightforward for single MOSFIRE imaging frames). The feasibility of providing on the fly mask design without astrometrically calibrated images will be investigated during commissioning.

#### 5.4.1.4 Fine Alignment Software

In refining the operational modes and use cases, we identified a role for software to aid in the alignment of each slit mask configuration on the sky. This new MOSFIRE fine alignment software is called MSAlign (described in detail in MSDN64). This software will be modeled after the *xbox* software for DEIMOS and LRIS. To use MSAlign, the slit mask is initially configured with alignment boxes, openings in the mask that are large enough to permit imaging of alignment stars. The user takes an image through the slit mask, and MSAlign will find the alignment boxes, measure the position of the star in each alignment box, and determine how to move the telescope and/or rotate the instrument in order to center the alignment stars in each alignment box.

#### 5.4.1.5 Grating Tilt Mechanism

The addition of a second grating tilt to optimize spectral coverage in the various wavebands has resulted in the addition of a second mechanism to the MOSFIRE grating turret. A rotary mechanism is used to position a retractable shim at the grating turret hard stop to define the second grating position (this mechanism is described in detail in MSDN06). This mechanism will be controlled by another instance of the MOSFIRE Rotary Mechanism Server (MRMS).

#### 5.4.1.6 Lake Shore 218 Replaced

The Lake Shore 218 temperature monitor will be replaced with a card inserted into the Lake Shore 340 temperature controller that performs the same functionality. The MOSFIRE Temperature Monitor Server (MTMS) will be removed, and its functionality will be implemented in the MOSFIRE Temperature Control Server (MTCS). The new eight temperature sensors in the temperature controller are read out the same way the existing two sensors are. This presents no change to the existing GUI design.

#### 5.4.1.7 Slit and Target Information FITS Extensions

In order to provide consistency between MOSFIRE and existing multi-object spectrographs at WMKO, the FITS file format for MOSFIRE now includes two FITS table extensions, one for the slit mask configuration and the second for the target list. The slit mask configuration table identifies the location of each slit and the target within each slit. The target list table contains the target list associated with the slit configuration. The format of this target list is identical to the target list used in the slit mask generation process (MASCGEN), which is identical to the format used for LRIS and DEIMOS without the columns related to proper motion.

The two extensions will be created by the MSCGUI whenever a slit configuration is executed. When exposures are taken, the detector server will append these FITS extensions to new frames written to disk.

#### 5.4.1.8 Other Minor Changes

- The MOSFIRE CSU Server has been renamed from MSUS to MCSUS (described in MSDN14).
- The detector focus mechanism now uses a rotary drive and as a result the MOSFIRE Detector Focus Server will now be another instance of the MRMS.
- A three-axis piezo-driven tip-tilt stage will be used for the Flexure Control System instead of a two-axis stage (described in MSDN07).
- The motion controllers used for rotary mechanisms are now Pacific Scientific PD2400 series motor controllers (identical to OSIRIS) instead of Danaher motion motor controllers
- The MOSFIRE ASIC Server (MAS) will now write frames to disk, instead of passing them through RMI and JNI (described in MSDN34). The detector server will reopen each frame to append FITS header information (described in MSDN05). Since the MAS will write frames to disk, it will also be responsible for de-interlacing, byte-swapping, and sampling arithmetic.

### 5.4.2 Software Architecture

The MOSFIRE software is based on three software layers, a low-level server layer, the KTL layer, and a user interface layer, which provides the graphical user interfaces (GUIs). The block diagram shown in Figure 100 illustrates these three layers.

The low-level server layer consists of a generic server module configured by a hardware dependent function library to control each MOSFIRE hardware subsystem though a variety of hardware interfaces (Ethernet, RS-232, etc.).

The KTL layer is a standard WMKO software component that is used in every instrument at the Observatory. This layer is implemented as a set of library routines to provide keyword control of the servers. Instrument specific keywords are defined in a keyword list. Common practices and standards exist for the development of keyword lists, and the keyword lists for MOSFIRE are based on existing keyword lists. An important feature of this architecture is that the MOSFIRE hardware can be controlled and tested using keywords and keyword scripts once the servers are complete. This avoids many of the interdependencies between hardware assembly/test and user interface development that often lead to development schedule problems.

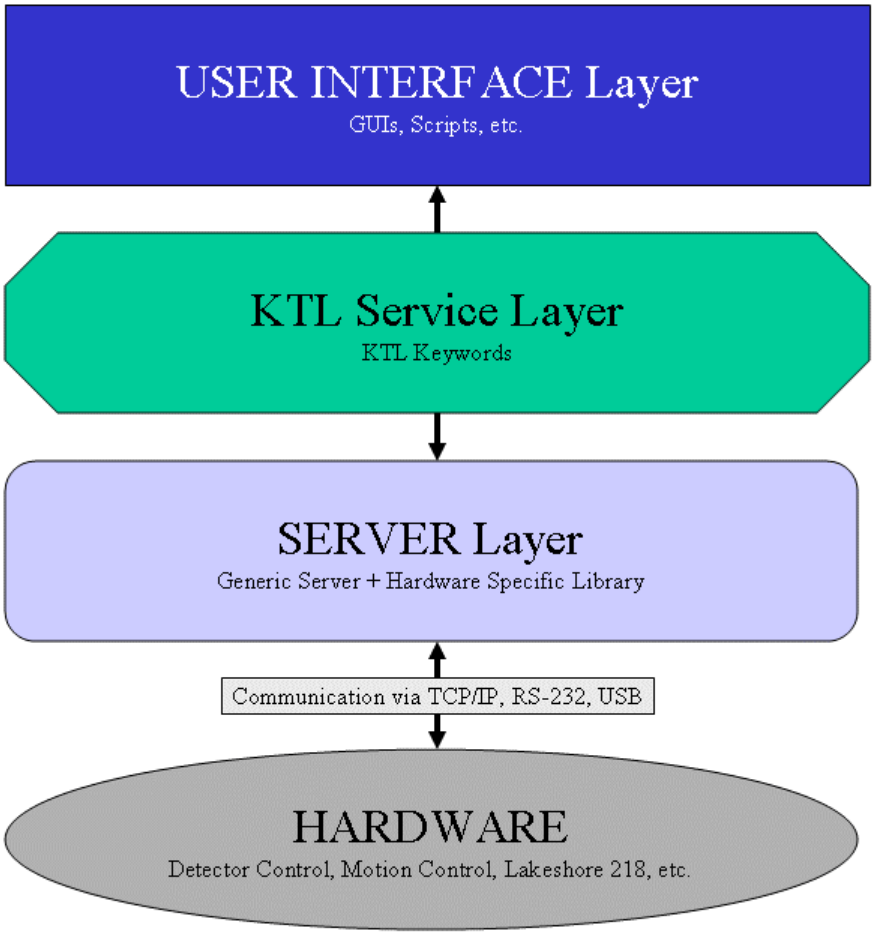


**Figure 100: MOSFIRE Software Layers**

### 5.4.3 MOSFIRE Software Modules

The MOSFIRE software is made up of three kinds of software modules. Two of these correspond to the server and user interface layers shown in Figure 100. The third kind of modules encompasses the related applications, including the CSU configuration software, alignment software, the image viewing software, and the data reduction pipeline. The complete set of MOSFIRE software modules are shown in Figure 101.

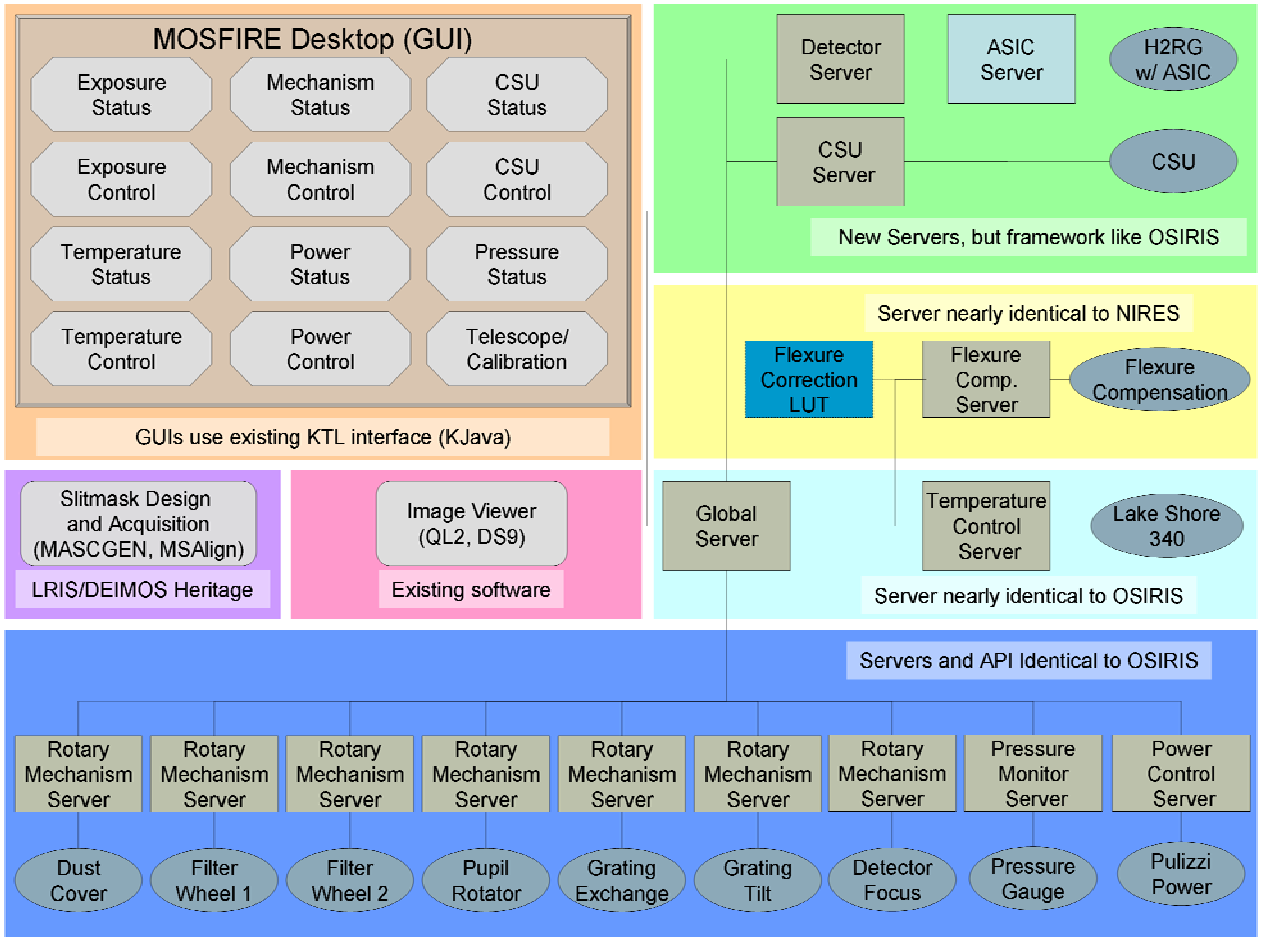


**Figure 101: MOSFIRE Software Modules**

#### 5.4.3.1 Servers

The MOSFIRE servers are based on the WMKO KTL layer (see MSDN04). Included in KTL is a methodology for implementing keyword servers. These keyword servers maintain a list of keyword-value pairs. Some keywords are status keywords, updated as a hardware dependent value changes (e.g. a temperature reading); some keywords are functional keywords that execute some action when set to appropriate values (e.g. setting a "go" keyword to 1 to start an exposure); and some keywords are utility keywords used to define system parameters or information (e.g. location of temperature sensor 1).

All servers (except the ASIC server) use a common KTL server framework called `rpcKey_server`, a distributed, RPC-based, client-server infrastructure written in C. This framework isolates all details associated with the RPC communications scheme and the network and transport layers below it from the developer. The developer is responsible only for the application code loaded via shareable libraries and configuration files, which together define the behavior of the server.

The server framework features the creation of iterative forked processes, each of which iterate at a constant, keyword-defined rate. These processes are used for checking the status of hardware, polling hardware for current values (e.g. temperatures), or probing another server. Each component of the MOSFIRE instrument electronics that requires software control will have a server instance, referred to as a hardware server. For each MOSFIRE hardware server, the MOSFIRE software team then only needs to implement the hardware specific library that handles the actions of the keywords and bind it to the framework server process.

#### 5.4.3.1.1 Hardware Servers

The MOSFIRE hardware servers are listed in Table 24.

| Acronym | Name | Description |
|---|---|---|
| MDS | MOSFIRE Detector Server | Provides controls to configure, start, and abort exposures through the ASIC Server. |
| MAS | MOSFIRE ASIC Server | Controls the Rockwell ASIC, and through the ASIC controls the science detector. Runs on Windows machine. Based on RMI, not KTL. |
| MRMS | MOSFIRE Rotary Mechanism Server | Controls mechanisms that use one-axis spinning motors, such as wheels, slides, and turrets. For MOSFIRE, the rotary mechanisms are the filter wheels, the deployable rotating pupil mask, the dust cover, the grating-mirror exchange, the grating tilt, and the detector focus. |
| MFCS | MOSFIRE Flexure Compensation Server | Controls the Tip/Tilt Mechanism Controller. |
| MCSUS | MOSFIRE CSU Server | Controls the CSU. |
| MTCS | MOSFIRE Temperature Control Server | Controls a Lake Shore 340 temperature controller. |
| MPRS | MOSFIRE Pressure Monitor Server | Monitors vacuum gauge(s) via Varian Multigauge Controller. |
| MPWS | MOSFIRE Power Control Server | Controls a Pulizzi power controller. |

**Table 24: MOSFIRE Hardware Servers**

#### 5.4.3.1.2 Housekeeping Servers

There are the three housekeeping servers. All use an instance of the generic RPC server and all three will be copied directly from OSIRIS, with a slight modification to MTCS.

#### 5.4.3.1.2.1 Power Control Server

Two power control servers (described in MSDN10) will be necessary to control the two Pulizzi IPC3402-NET network power controllers. Each server is required to provide a means of switching power on and off, report power status, and to provide a safety system that prevents power from accidentally being switched off to the associated instrument subsystems. The outlets will be used for power to each electrical component in the electronics cabinet, except the network switch. The calibration lamps will also be controlled by the power controller, so that they may be turned on and off remotely.

#### 5.4.3.1.2.2 Pressure Server

The MOSFIRE Pressure Server (described in MSDN11) monitors the pressure of the instrument dewar using a Varian MultiGauge controller with ConvecTorr (high-pressure) and IMG (low-pressure) gauges. It is required to initialize the hardware, provide a polling capability with a keyword-defined polling interval, to provide error information, and to provide time-stamped data logging. It is also required to provide the capability to define operational limits for the pressure sensors and to provide warnings when those limits are exceeded.

#### 5.4.3.1.2.3 Temperature Control Server

The MOSFIRE Temperature Control Server (described in MSDN12) will interface to a Lake Shore 340 temperature controller and operate two temperature control loops – one for the detector and one for the instrument dewar. It must provide for initializing the hardware and establishing temperature setpoints. It also will provide the capability to set the controller's PID temperature loop tuning parameters and the ability to switch temperature control on and off.

The Lake Shore 218 temperature monitor will no longer be used because the same functionality can be obtained by using an internal card in the Lake Shore 340. The MTMS will therefore be removed, and the MTCS will also be responsible for reading out the eight temperature sensors available through the daughter card. For this reason, this server is no longer identical to OSIRIS. However, the changes will be modest, mostly involving the addition of temperature keywords and the reading of eight more inputs in addition to the existing two.

### 5.4.3.1.3 Mechanism Servers

MOSFIRE will use nine mechanism servers: seven instances of the MRMS, the flexure compensation server, and the CSU server.

#### 5.4.3.1.3.1 Rotary Motors

The MOSFIRE Rotary Motor Server (MRMS, described in MSDN06) will interface to the Pacific Scientific PD2400 series drives to provide control of the rotary motors used throughout the instrument. The server must initialize and configure the drive, send motor-move commands, both absolute and relative, and keep track of the motor position. The PD2400 drive is identical to the

one used by OSIRIS and the OSIRIS motor server can be used as is. An initial version of the server has been compiled, linked and installed on a test machine at CIT.

The keyword configurable drive parameters are: motor acceleration, velocity, deceleration, time-to-power on and off, motor current and power. Additionally, the following parameters will be keyword controlled: backlash, current loop gain, current loop midband compensation gain, third-harmonic compensation, acceleration, velocity and deceleration. The server will also report drive fault information.

Seven instances of the MRMS will be deployed, one each for the following mechanisms:

- Dust cover: a rack-and-pinion sliding door system that is either open or closed.
- Filter wheel 1: a six-position, edge-driven wheel used to select one of five filters or the clear position.
- Filter wheel 2: identical to filter wheel 1. Note that to select a given filter, coordinated keywords must be used through the global server. The global server will be responsible for determining the positions of both wheels as needed to select the requested filter.
- Pupil mask mechanism: a mechanism that controls the shape and position angle of a deployable, rotating hexagonal pupil mask. At one rotation limit, the mask is retracted from the beam and does not need to counter rotate with respect to the instrument position angle. By moving off the rotation limit the mask is deployed into the beam to form a hexagonal shape that provides an optimum mask for the Keck telescope pupil. The supplementary task `watch_keywords` (described in MSDN08) will coordinate this rotation by getting values for the rotator position from the DCS and sending the appropriate rotation commands to the pupil mask server through the standard RPC keyword interface.
- Grating-mirror exchange mechanism: a two-position rotary mechanism which places either the grating or the mirror in the MOSFIRE optical path.
- Grating tilt mechanism: a two-position, lead-screw-driven, slide that inserts and removes a shim at the grating stop to switch its tilt between two values: 41.525 degrees for J- and Y-band filters, and 42.614 degrees for H- and K-band filters.
- Detector focus mechanism: a rotary mechanism that drives a flexure to adjust the focus of the science detector.

#### 5.4.3.1.3.2 Flexure Compensation Server

The MOSFIRE Flexure Compensation Server (MFCS, described in detail in MSDN07) controls the position of a fold mirror mounted on a tip/tilt stage that is used to keep the image stable on the detector despite instrument flexure with changes in instrument position angle and telescope elevation. The fold mirror is controlled by three actuators with built-in linear voltage differential transformer (LVDT) position sensing, connected to a Physik Instrumente (PI) servo amplifier system and controlled by a PI E-516 computer interface and display module. The MFCS is required to initialize and configure the various parameters associated with the PI computer interface and servo system, and to move the actuators and read back their positions.

When flexure compensation is enabled, a separate task associated with the RPC server package, `watch_keywords` (see MSDN08), becomes active. This process monitors selected keyword services and associates a callback function with each keyword. It will establish communications to the DCS and to the MFCS using the standard RPC keyword interface. It will then command the MFCS to adjust the fold mirror position in response to keyword values it receives from the DCS. The flexure compensation procedure will be open loop. Actuator positions will be obtained from a lookup table based on the telescope elevation and rotator position angle and applied via the MFCS. These actuator positions, a function of elevation and rotator position angle, must be determined experimentally just before or during commissioning.

#### 5.4.3.1.3.3 CSU Server

The MOSFIRE Configurable Slit Unit Server (MCSUS, described in detail in MSDN14) connects to the control electronics (via RS-232) of the mechanical slit mechanism and will control all aspects of slit-mask setup. This mechanism accurately and repeatably controls of 46 pairs of movable bars that are moved opposite one another to create slitlets. Each bar is constrained to move in a straight line, across the FOV. Each bar can travel completely across the FOV and no light can leak between bars. Each bar has two mechanisms associated with it: a brake which holds the bar in position and a clutch which inserts a claw into the teeth that are cut along the edge of each bar. All clutches for both sides of the bars are mounted to a single indexing stage (IS) so that when the stage moves one step, engaged bars can be moved in parallel. A voice-coil actuator moves the IS one step at a time. A LVDT provides feedback for fine positioning when bars must be located between steps. Step sizes are adjustable.

The MCSUS will be an instance of the standard RPC keyword server. It is required to both move individual bars and to define groups of bars and move those bars in parallel. The MCSUS will provide keyword access to the various parameters that control the mechanism's operation – voltages, currents, LVDT values and various status and error messages. It will responsible for initializing and configuring all parameters associated with the mechanism and its control system. Bars can be moved by keyword or entire multi-slit setups can be defined by keywords and then executed by a single keyword. The server will also provide keyword control of individual slits, their positions and widths. The MCSUS will keep a state file containing the position and status of each bar. This will allow for quicker restoration should the server need to be restarted.

In close collaboration with CSEM staff, work was done to estimate the reconfiguration times. The timing for multiple configurations of 5 basic reconfigurations were simulated and calculated. The results are summarized in Table 2.

A worst case scenario was also considered, in which at least one pair of bars is moved from a half-tooth position on the far left to a half-tooth position on the far right, and the rest of the pairs of bars are similarly moved from the right to the left. The timing in this case would be 406 seconds. These results have been documented in MSDN63.

#### 5.4.3.1.4 ASIC and Detector Servers

The MOSFIRE ASIC Server (MAS, described in detail in MSDN34) is unlike the other servers in that it is not built upon the KTL framework. This server runs on a Windows machine, and is responsible for providing a translation layer between the legacy C code inherited from OSIRIS and reused for the MDS and the Teledyne proprietary ASIC control software. It does so using a set of Java technologies, including Java Native Interface (JNI) and Remote Method Invocation (RMI). More information can be found in the interfaces section below.

The functionality of the detector server is very similar to OSIRIS. The same exposure parameters are available, with the addition of Fowler sampling. The main difference is that instead of binding in the API of the SDSU controller, it binds in the JNI library with access to the MAS. Another primary difference is that the MAS will perform sampling reduction and then write the exposures to disk in a simple FITS format. The MDS will reopen the FITS file when it is written, and insert the FITS header, append the slit and target table extensions.

#### 5.4.3.1.5 Global Server

The MOSFIRE Global Server (MGS, described in detail in MSDN15) is the central conduit to all other MOSFIRE servers. It controls no hardware but provides a single-point connection between all clients and all other servers. It services various generic keywords, provides special processing for some keywords and allows the capability of servicing "coordinated" keywords for instances where multiple servers for different mechanisms must be accessed from a single keyword. The MGS will use keywords to keep track of the health of the other servers, and it will provide the capability of executing a one-shot collection of keyword-value pairs for inclusion in a FITS-file header. All instrument keywords will be gathered this way for recording in the FITS files.

### 5.4.3.2 User Interfaces

User interfaces for MOSFIRE consist of GUIs, scripts, and KTL clients. KTL RPC clients are the simplest of user interfaces to the servers. There are five clients that are commonly used to access server keywords: `show`, which can get the value of a keyword from a server; `modify`, which can set the value of keyword; `cshow`, which watches a keyword and prints out the new value when it changes; `xshow`, which is like `cshow`, but is displayed in a Motif dialog; and `waitfor`, which pauses command-line or script execution until a keyword becomes a specified value. KTL clients are part of the KTL library, and are reliable engineering tools that quickly and directly interface with any server.

Scripts (described in MSDN20) are built using these KTL clients. They are C-shell scripts that use `show`, `modify`, `waitfor`, and other tools to automate a sequence of actions. Scripts are broken down into three categories:

- Control scripts: These scripts are used to control the instrument, such as configuring the mechanisms and automating exposure sequences.

- Operations scripts: These scripts are used by the observatory staff to prepare the instrument and user environment for observing. Scripts are also used to automate initial software installation and configuration.
- Run scripts: These scripts do not manipulate server keywords but instead they are used to start and stop the various server and GUI components of the system.

While the KTL clients and scripts can be used to fully control the instrument, this approach can be clumsy and non-intuitive for new users. Therefore, a set of GUIs (described in MSDN16) will serve as the primary user interface for the instrument. GUIs will provide visual status information and interactive dialogs to control the instrument and take exposures.

The GUIs will run in a virtual desktop. The MOSFIRE Desktop (described in MSDN62) will allow the selection of which GUIs are visible and their locations to be saved for recreation of the screen configuration at a later time. This will not only allow frequent users of the instrument to quickly set up their working space, but will also provide a unique customizable setup for support engineers. In our case, the desktop will also provide the connection to the server; GUIs will access keywords through the desktop as child processes, rather than directly accessing the servers, reducing the number of lines of communication.

The MOSFIRE GUIs will be written in Java. This is primarily for commonality with the OSIRIS software package, allowing MOSFIRE to take advantage of the OSIRIS heritage and development experience. A Java KTL interface, called `KJava`, was created for OSIRIS to allow access to the servers, and MOSFIRE will use this interface as well.

MOSFIRE GUIs are designed using the Model-View-Controller (MVC) framework. The MVC separates the data model of a program, the user interface (the view), and the communication between them (the controller) into logical components. The model encapsulates all of the properties of the program, and handles the interaction between them. This is the core of the program, and is usually quite stable. The view, on the other hand, often undergoes changes to suit the end user's preferences. The MVC allows the view to change quite significantly, yet the core logic of the program, stored in the model, remains the same. It also allows for multiple views to represent the same model.

The MVC implemented for MOSFIRE is event-driven. Events are usually triggered in one of two ways, user interaction with the GUI such as pressing a button, and when a keyword value changes. The model registers itself to the server as a listener of keyword value change events. Events are propagated from the server to the model using `KJava`. When the model itself changes the usual method for notification of the change is to trigger an event to notify the view of the change.

Many of the GUIs are used to simply display a keyword value, or to provide a control to change a keyword value, and there is significant commonality in the underlying methods. For example, the propagation of a `KJava` broadcasted keyword change event through the GUI model to the displaying widget is identically implemented for nearly all keywords. Therefore, a system was developed to create a GUI simply by defining the keywords of interest and the widgets that display

their values. This system is called the GUI Builder (described in MSDN35). The GUI Builder will be folded into the MOSFIRE Desktop, and will be able to create GUIs on the fly based on XML GUI description files. Eight of the twelve MOSFIRE GUIs will be built with this way. In addition, by using the GUI Builder, custom GUIs tailored to liking of an astronomer, engineer, or instrument specialist can be rapidly developed and deployed.

The MOSFIRE GUIs are listed in Table 25.

#### 5.4.3.2.1 GUI Screen Layout

In the Keck 1 Remote Operations Room three computers named Haleiwa, Onemea and Pupukea are typically used for observing. Haleiwa is equipped with three displays, and is used for primary instrument control. Onemea is also equipped with three displays and is typically used for image viewing, observation planning, and data reduction. Pupukea has a single display is typically used to display observatory (FACSUM) and environmental (XMET) information.

Figure 102, Figure 103, Figure 91, and Figure 92 depict the arrangement of the three displays used for Haleiwa. The first screen is for control of the instrument, with the MSCGUI, the MECGUI, the MMCGUI, the MCGUI, and the MTGUI. It will also offer an `xterm` for direct keyword and script access. The second screen is a status screen, with the MESGUI, MMSGUI, MTSGUI, MPRGUI, MPSGUI, and MSSGUI. It also shows the MTCGUI, although modification of controlled temperature setpoints is considered an engineering level command. The third screen is used for data viewing, containing the *DS9* image display software and the guider software.

| Acronym | Name | Description |
|---|---|---|
| MECGUI | MOSFIRE Exposure Control GUI | Sets up exposures (integration time, coadds, etc.) and starts and aborts them. |
| MESGUI* | MOSFIRE Exposure Status GUI | Tracks the progress of an exposure, showing parameters of current exposure and remaining integration time. |
| MMCGUI* | MOSFIRE Mechanism Control GUI | Controls the mechanisms of the instrument. Only filter and observing mode (imaging or spectroscopy) options are provided, and the two filter wheels, pupil mask mechanism, grating turret, and focus mechanisms are moved according to those two parameters. |
| MMSGUI* | MOSFIRE Mechanism Status GUI | Shows the status of each MOSFIRE mechanism, except the CSU. |
| MSCGUI | MOSFIRE CSU Control GUI | Provides controls to configure the CSU. |
| MSSGUI | MOSFIRE CSU Status GUI | Shows current position of bars in CSU. |
| MTCGUI* | MOSFIRE Temperature Control GUI | Provides controls to set MOSFIRE dewar and science detector operating temperature. |
| MTSGUI* | MOSFIRE Temperature Status GUI | Shows current temperatures at various locations in the instrument. |
| MPRGUI* | MOSFIRE Pressure Status GUI | Shows current dewar pressure. |
| MPCGUI* | MOSFIRE Power Control GUI | Provides controls to turn on and off power of selected components. |
| MPSGUI* | MOSFIRE Power Status GUI | Displays power status of selected components. |
| MTGUI | MOSFIRE Telescope GUI | Provides controls to the telescope drive and control system, such as offsetting and control of the instrument rotator. |
| MCGUI* | MOSFIRE Calibration GUI | Provides controls for the calibration lamps. |

**Table 25: MOSFIRE GUIs**

*An asterisk (*) denotes GUIs built with the GUI Builder.*

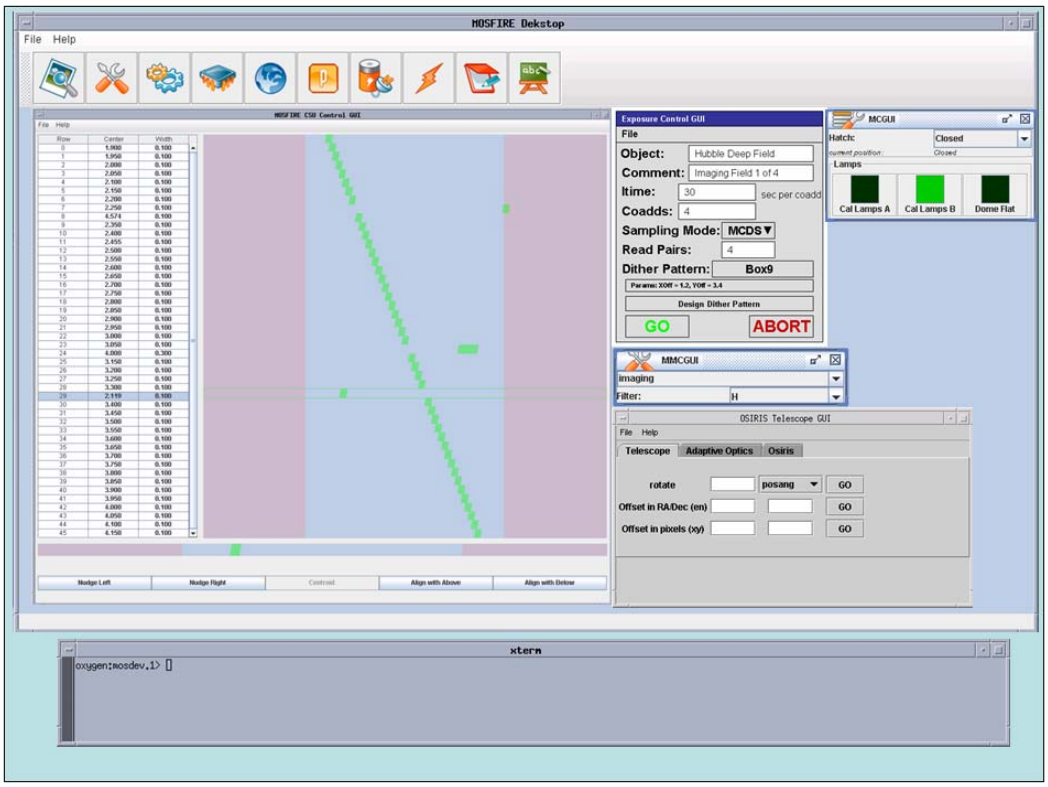


**Figure 102: Instrument Control Screen on Haleiwa**

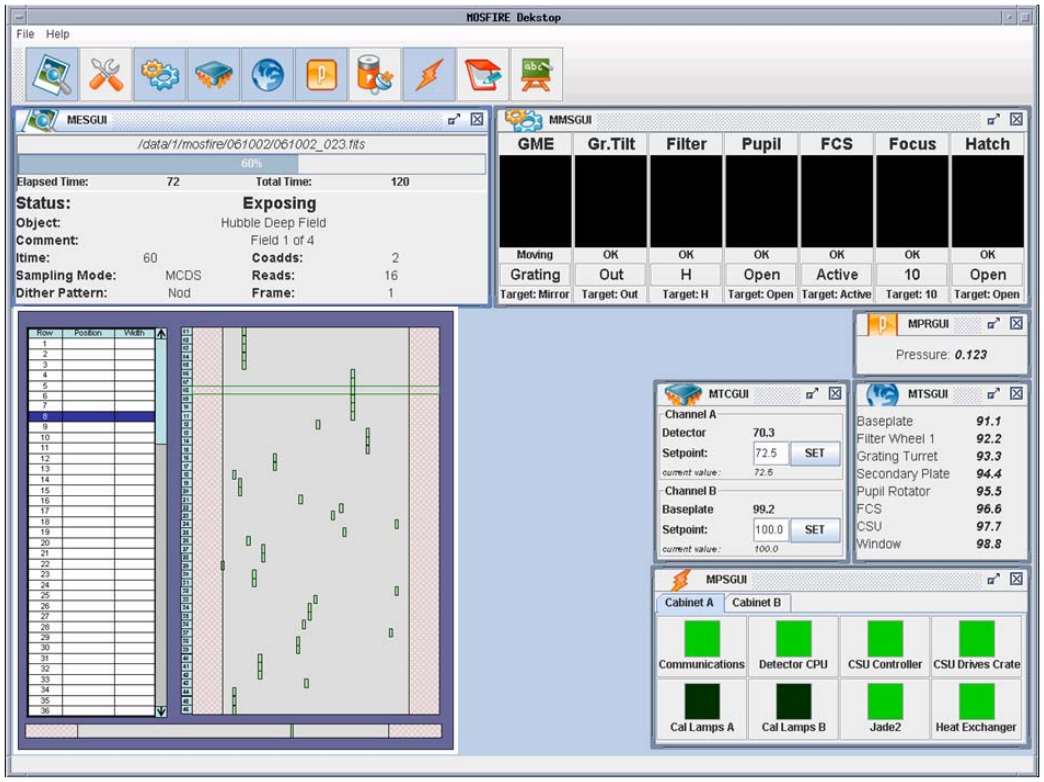


**Figure 103: Instrument Status Screen on Haleiwa**

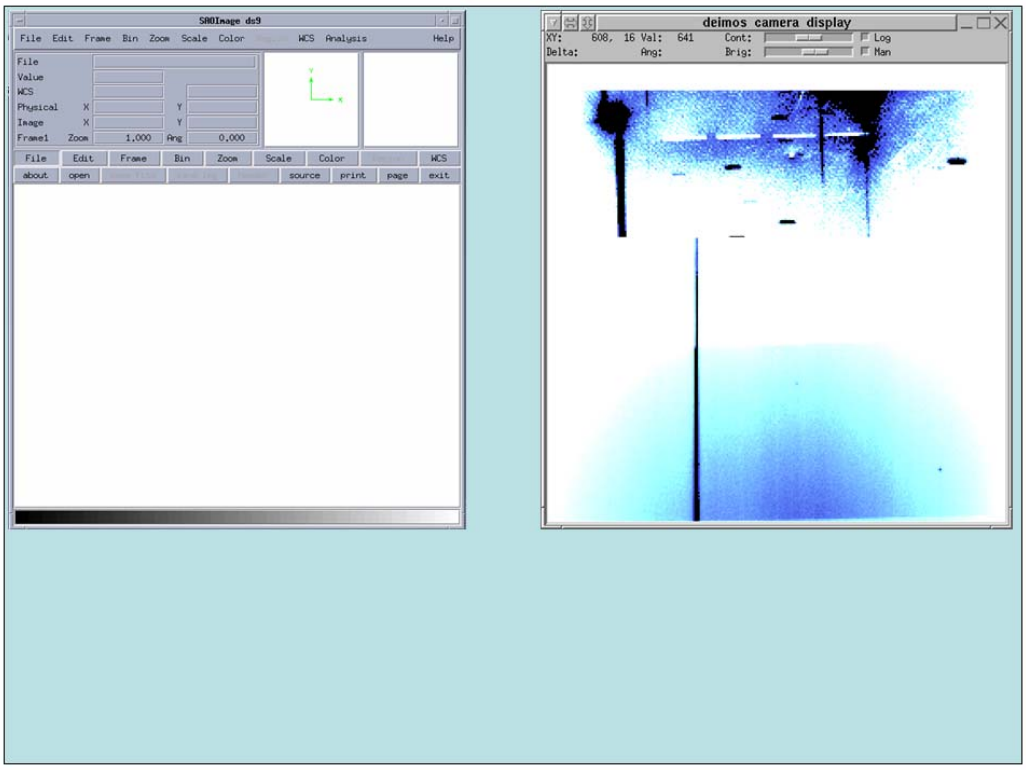


**Figure 104: Data Viewing Screen on Haleiwa**


**Figure 105: Observatory Status Screen on Pupukea**

The layout of the GUIs on Onemea will depend on the GUIs being used; these are likely to be additional instances of DS9 or the MSCGUI.

#### 5.4.3.2.2 The MOSFIRE Desktop

The MOSFIRE GUIs will run within a desktop environment called the MOSFIRE Desktop (described in MSDN62). The MOSFIRE Desktop is a virtual desktop consisting of an empty dialog or frame to contain the MOSFIRE GUIs. Figure 106 shows the empty desktop. In Figure 102 and Figure 103 above the desk top is shown with child GUIs that comprise the various parts of the MOSFIRE user interface. The desktop will manage the creation and destruction of the child GUIs, and provide a toolbar for launching them. The visible GUIs and their position can be saved to disk in an XML file for later restoration of the desktop.

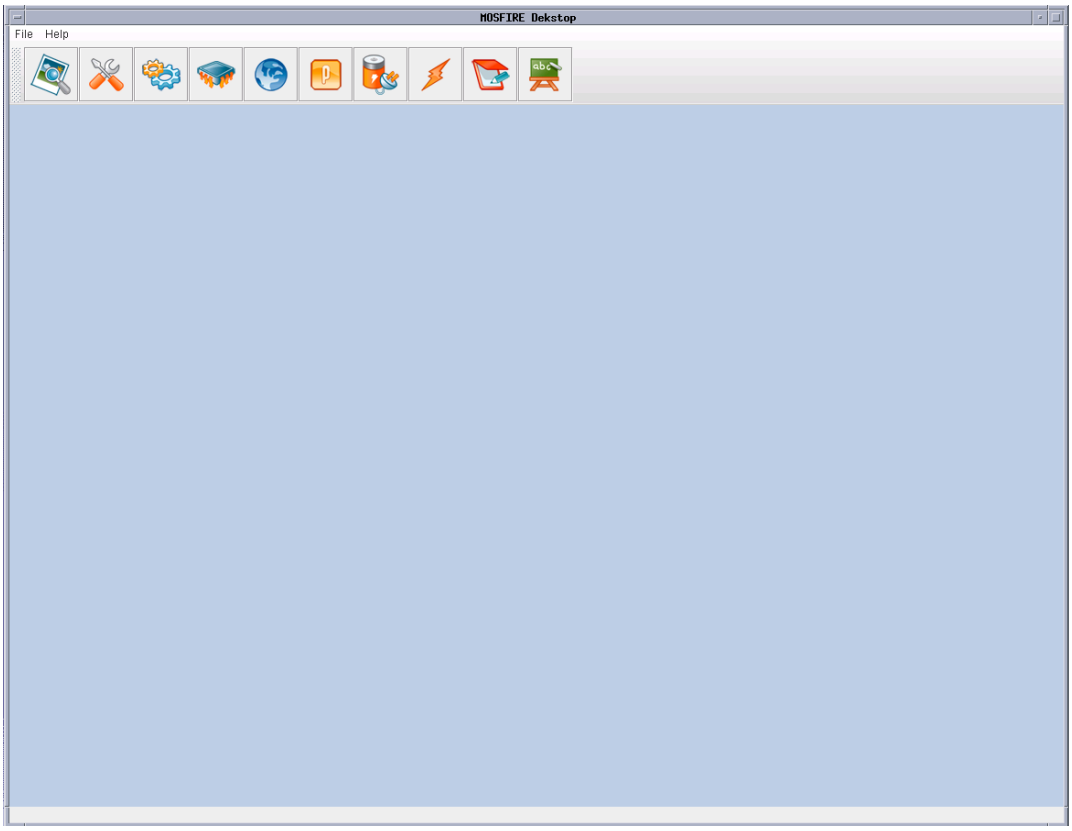


**Figure 106: MOSFIRE Desktop.**

The desktop will also have the responsibility of connecting to the instrument servers via a `KJava` connection to the MOSFIRE Global Server. The desktop will receive updates as global server keyword values change. The desktop maintains its own list of these values and broadcasts them to the child GUIs. These local desktop values are called properties, and the desktop will have a `PropertyList` class to handle them. Properties are described in MSDN62. A property is any single value that represents a piece of information about a system. For MOSFIRE, and other KTL systems, most properties will be linked to server keywords, so that modifying a keyword value also modifies the linked property, and vice versa. However, this is not a necessity.

Property definition and keyword linkage is represented in an XML configuration file. Through the use of their own `PropertyList`, a child GUI of the desktop can have the ability to make their own connection to a server, so that they can be run, fully featured and independent outside of the MOSFIRE Desktop environment. This will not be the default method of use, but may be used during development or for engineering.

#### 5.4.3.2.3 GUI Builder

The GUI Builder (described in MSDN35) is used to create simple GUIs that monitor and control properties. The properties are generic and are defined in an XML file. The GUI Builder will be part of the MOSFIRE desktop, which performs the linkage between properties and keywords. The GUI Builder GUIs will register themselves as interested in the MOSFIRE desktop properties, rather than server keywords.

The GUI Builder uses an XML GUI layout specification to dynamically create widgets and link them to properties in order to visualize the current values of those properties. A widget can also be assigned to modify a property value. Widgets can be any `JComponent`. When the value of a property is changed, the `setValue()` method of the `JComponent` is called. Property-setter widgets can be specified as "setcontrol" widgets; these widgets have a "Set" button next to it to perform a modify call on the property. Typically, this is done in conjunction with a `JTextField`.

#### 5.4.3.2.4 Status GUIs

MOSFIRE will use one set of GUIs to monitor the status of the instrument. Each status GUI is read-only. The status GUIs monitor keyword values, receiving `KJava` callbacks whenever a keyword value changes. For most items, the value is simply displayed as text or numbers. Some items can also be displayed graphically. Regardless of the visualization, the underlying model which handles the actions taken when a keyword changes is the same. This is the power of the MVC architecture.

As an example, consider displaying the status of a power outlet on a Pulizzi power controller using the power status GUI, MPSGUI. When the power is turned on via the power control server, the keyword representing the power status, say `pwrstat1`, changes value from 0 to 1. The keyword in the power control server is reflected as a meta-keyword in the global server. When the meta-keyword changes value, an event is triggered to all registered listeners. For MOSFIRE, the MOSFIRE desktop will have registered as a listener. The `KJavaCShowCallback` function is called, saying that `pwrstat1` has a new value of 1. The MOSFIRE desktop will link the `pwrstat1` keyword to its own internal property, `CabinetAPowerStatus1`. MPSGUI will have registered with the desktop as being interested in the `CabinetPowerStatus1` property, and will be notified of the change. The model of the MVC based MPSGUI will set its internal member variable representing the status of the first outlet to "on" or "true" (since it is a boolean state). The controller of the MVC based MPSGUI has registered itself as interested in a change of the value of the member variable (not the keyword) of the model, and it is notified using Java `PropertyEvents` which, as an inner class member of the MVC based view, tells the view that the value has changed. The view then decides how to visually represent the change to the user. One

view could simply be a text label saying "On" or "Off". Another, used in OSIRIS, is a button that turns bright green when on, and a dark green color when off, resembling a light.

MPSGUI is one of the GUIs constructed by the GUI Builder. In its XML specification, the widget to use in its view is specified to be a light button as described above. The button is specified to be linked to the `CabinetAPowerStatus1` property. When the GUI is constructed, the GUI Builder creates the model, view, controller, and all necessary code for the keyword value propagation as described above; the method for keyword value propagation in GUIs created by the GUI Builder is identical to those not created by the GUI Builder.

#### 5.4.3.2.5 Exposure Status GUI

The MOSFIRE Exposure Status GUI (Figure 107), a GUI Builder GUI (see MSDN36 for details), is responsible for displaying information about the current or last exposure taken with the instrument.

It will show the following information:

- Integration time (per coadd)
- Number of coadds
- Sampling mode
- Number of reads / read pairs
- Filename
- Object name
- Frame comment
- Exposure progress (percentage complete, time remaining)
- Dither pattern progress (frames complete/remaining)

A progress bar will be used to graphically show exposure progress.

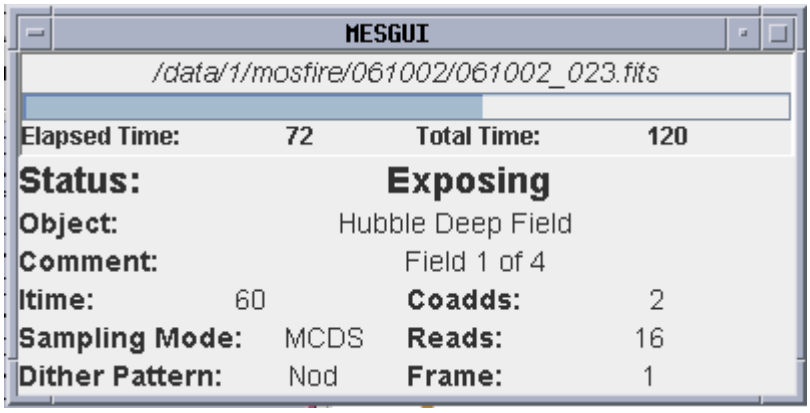


**Figure 107: MOSFIRE Exposure Status GUI**

#### 5.4.3.2.6 MOSFIRE Mechanism Status GUI

A Mechanism Status GUI (Figure 108), another GUI Builder GUI (described in MSDN36), will be used to show status information for a mechanism. An instance of this GUI will be used for each mechanism in the instrument. It will give the current mechanism status (moving, lost, error, etc.), current position, and target position. A graphical representation of the mechanism will also be displayed, and animated to reflect the motion of the mechanism when appropriate. Detailed information, such as switch status, will be available via a menu option or as another engineering level GUI.

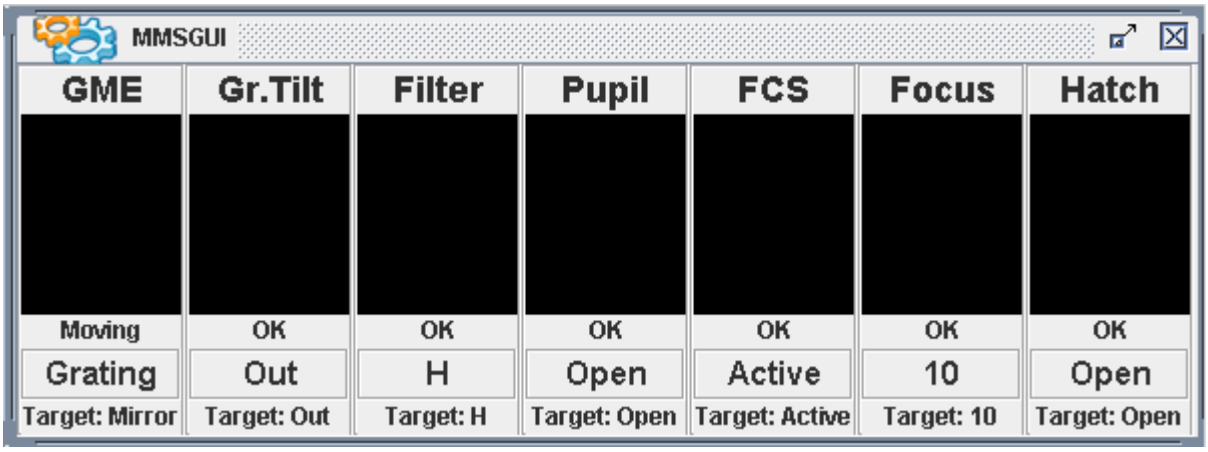


**Figure 108: MOSFIRE Mechanism Status GUI**

#### 5.4.3.2.7 Temperature Status GUI

This GUI (Figure 109), another GUI Builder GUI (described in MSDN36), shows the temperatures monitored by the MOSFIRE Temperature Control Server. It will simply display the values as text to the screen, with the sensor location prefacing the value.

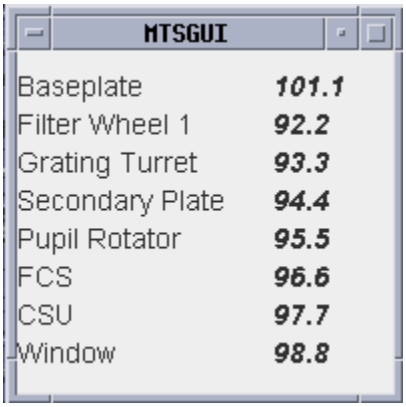


**Figure 109: MOSFIRE Temperature Status GUI**

#### 5.4.3.2.8 Pressure Status GUI

This GUI (Figure 110), another GUI Builder GUI (described in MSDN36), will show the current pressure of the dewar, monitored by the MOSFIRE Pressure Server. Like the MTSGUI, it will display the value as text.

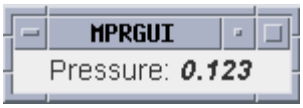


**Figure 110: MOSFIRE Pressure Status GUI**

#### 5.4.3.2.9 Power Status GUI

This GUI (Figure 111), another GUI Builder GUI (described in MSDN36), will show the status of each of the outlets in the power controller controlled by the Power Servers. It will use a set of lights, as described in the example above, each labeled with the function of the outlet.

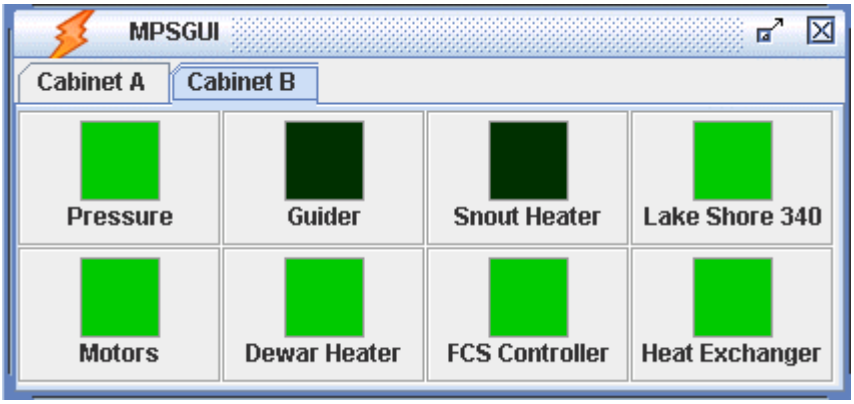


**Figure 111: MOSFIRE Power Status GUI**

#### 5.4.3.2.10 CSU Status GUI

The MOSFIRE CSU Status GUI (MSSGUI, Figure 112) is responsible for reporting the positions of the slits in the CSU. The MSSGUI displays the slit configuration in two forms. One way is as a simple list of positions and widths for each mask bar position shown as a table in a scrollable viewport. The other method is graphical, showing the field of view and each slit. This will be displayed in an extension of a `JPanel` called the `SlitConfigurationPanel`. The sides of the field of view will be colored differently to depict the regions where slits will not get full spectral coverage. The slits may be exaggerated in width in order to make their locations more noticeable. There will be a zoomed in drawing of a single row available, so that when a user clicks on a row, that row is visualized in a larger view, showing the true width of the slit.

This GUI is not a GUI Builder GUI. It will have custom MVC components, with the connection to the `PropertyList` class of the desktop in its model. As properties of the instrument change, the desktop forwards events to the model, and the controller class notifies the view to update. The

CSU server will have keywords that specify the location and width of each slit. When one of these values updates, both the table and `SlitConfigurationPanel` will update.

The `SlitConfigurationPanel` uses the Java Graphics2D package to draw the slits, as does the zoomed row panel. The slit table will be a typical `JTable`, with a custom extension of an `ArrayListTableModel`, a table model coded for OSIRIS that handles `ArrayList` data.

More information can be found in MSDN17.

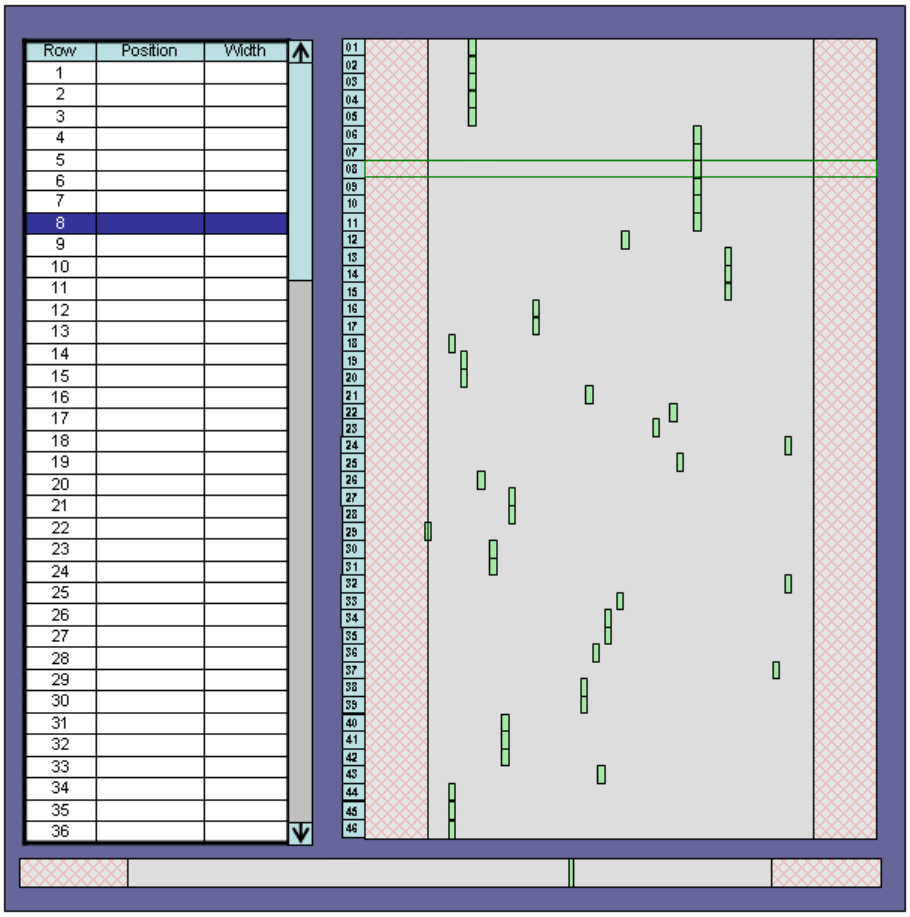


**Figure 112: MOSFIRE CSU Status GUI**

### 5.4.3.2.11 Control GUIs

Control GUIs are used to control the instrument, switching on power, moving mechanisms and taking exposures. They will use `KJava modify` calls to set keywords in the Global Server. These calls will be routed through the MOSFIRE desktop. As the instrument changes configuration, the status GUIs will update to reflect this new information, leaving the control GUIs free to set up the next setting. The control GUIs know very little about the current state of the instrument, except what is needed to present the proper options to the user.

For GUI Builder GUIs, the widgets that modify properties are specified as either a "control" or "setcontrol" widget. When the user activates the widget to set the value (e.g. hitting a set button), the value of the widget is obtained and the GUI will try to set the value of the property. Properties can have a `ValueValidator` assigned to it for range checking on the new value. See MSDN35 for more information on `ValueValidators`. Once the new value is approved, the MOSFIRE desktop will find the associated keyword in its `PropertyList`, and then, using its `KJava` connection, perform a modify call on the keyword. When the value is changed, it is reported in the same way as described for the status GUIs.

#### 5.4.3.2.12 Exposure Control GUI

The MOSFIRE Exposure Control GUI (MECGUI, described in MSDN61and shown in Figure 77) provides controls to the user to set up and take an exposure. This includes the following controls:

- Integration time
- Number of coadds
- Sampling mode
- Number of reads
- Object name
- Frame comment
- Filename controls (including data directory)
- Dither pattern

A filename will automatically be generated for the user, but this GUI will provide controls to alter the filename and set the output directory for raw files. This GUI will also provide buttons to start and abort an exposure or dither pattern sequence. A dither pattern sequence is a set of frames that are combined together during data reduction to increase field of view or reduce noise. The MECGUI will provide controls to define a dither pattern and execute it. Selecting a dither pattern from the dither pattern dropdown will bring up another dialog to set the dither pattern parameters. When the user presses the OK button on the dialog, it is dismissed, and the description box is updated.

No keyword modify calls are made until the GO button is hit. When it is, the values are obtained from the GUI widgets, and a script is called to execute the dither pattern (even for stare dither patterns of one frame). Script execution for Java GUIs is detailed in MSDN67. This method of script execution is used for OSIRIS in the Dataset Execution Client and Telescope GUI. Once executed, progress through the dither pattern can be monitored in the Exposure Status GUI. Hitting the Abort button calls a script to stop the exposure. More information can be found in MSDN61.

The supported dither patterns are listed in Table 26.


**Figure 113: MOSFIRE Exposure Control GUI**

| Dither Pattern | Number of Frames | Description | Parameters |
|---|---|---|---|
| Single | 1 | A single frame taken without moving telescope. | None |
| Object+Sky | 2 | First frame taken, then telescope is offset by a user specified amount, and then second frame is taken. | XOffset, YOffset |
| Sky+Object | 2 | Telescope is offset by a user specified amount, first frame taken, then telescope is offset back to the starting position and a second frame is taken. | XOffset, YOffset |
| Nod on Slit | 2 | Frame taken at evenly distributed positions on slit. Positions are 1/3 and 2/3 from the top of the slit | None |
| User Nod on Slit | 2 | Frames are taken at distributed positions on slit Positions taken ½ YOffset above center, and ½ YOffset below | YOffset |
| Box | 4,5,9 | Frames are taken in an overlapping box pattern. | XOverlap, YOverlap |

**Table 26: Supported Dither Patterns**

#### 5.4.3.2.13 Mechanism Control GUI

This GUI (Figure 114), another GUI Builder GUI (described in MSDN61), will allow the user to set the mechanisms as required for each observation. Even though MOSFIRE will have eight software controlled mechanisms, the options presented to the user for instrument setup for an observation is reduced to two options: exposure mode (imaging or spectroscopy) and filter selection. The exposure mode sets the position of the grating-mirror exchange mechanism, and filter sets the positions of the dual filter wheel, the pupil mask, grating-tilt, and detector focus.

Flexure compensation is performed without user interaction. Science detector focus control is used only for engineering adjustments and tests. The dust cover is only used when storing the instrument, and will be controlled by observatory staff using scripts. The Cryogenic Slit Unit (CSU) will be controlled with its own dedicated GUI (see below).


**Figure 114: MOSFIRE Mechanism Control GUI**

#### 5.4.3.2.14 Temperature Control GUI

This GUI (Figure 115), another GUI Builder GUI (described in MSDN36), is used to set the target temperature of the temperatures regulated by the temperature controller. It also displays the locations of the temperature control loops. Temperature set points are only adjusted in engineering procedures.

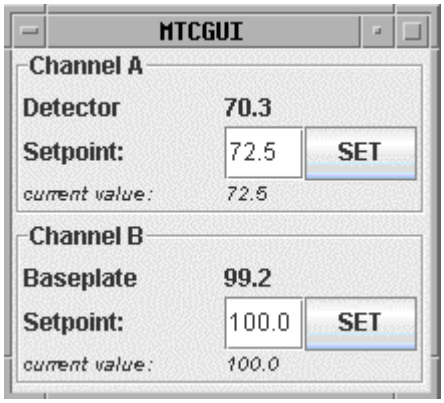


**Figure 115: MOSFIRE Temperature Control GUI**

#### 5.4.3.2.15 Power Control GUI

This GUI (Figure 116), another GUI Builder GUI (MSDN36), is used to switch power on and off to various instrument subsystems. This GUI looks very similar to the Power Status GUI, but the buttons are clickable. Clicking on a button switches the power of the outlet represented by the button to the opposite state. Calibration lamps, plugged into the power control strip, will be turned on and off using the switches on this GUI.

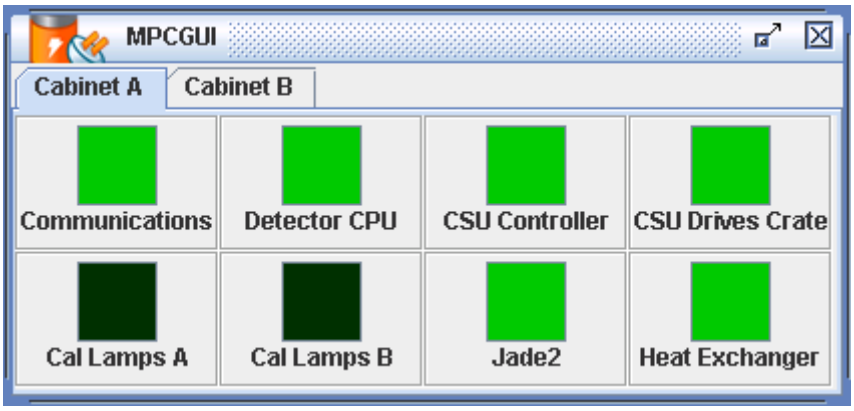


**Figure 116: MOSFIRE Power Control GUI**

#### 5.4.3.2.16 CSU Control GUI and MASCGEN

The MOSFIRE CSU Control GUI (MSCGUI, described in MSDN17 and shown in Figure 119) is used to define and adjust CSU configurations. Configurations defining the positions and widths of the slits are stored in files called MOSFIRE Slit Configuration (MSC) files. The MSCGUI can save and load CSU configurations using these files. The format of these files is described in MSDN18.

The MSCGUI will look very similar to the MSSGUI (Figure 112) and will have the same display modes (a table mode and a graphical mode) to display slit positions. Using the table mode the positions and widths of slits can be manually entered into the cells in the table. In the graphical representation slits can be dragged to the desired position. The zoomed view of the selected row can be used for fine adjustment. Fields will also be provided for selecting the position on the sky and the desired wavelength coverage.

The MSCGUI will incorporate the MOSFIRE Automatic Slit Configuration Generator (MASCGEN). MASCGEN will enable a user to determine the best slit mask for a given field and range of spatial positions.

##### 5.4.3.2.16.1 Operation of MSCGUI and MASCGEN

The user will specify a filter and the horizontal region where slits can be placed. If the user is interested in a particular spectral feature, the user must make sure the wavelength is within the range of the limiting wavelengths defined by the selected horizontal region. The filter will be set using a dropdown combo box. The X-range limits would be set with a pair of text fields. This working field of view is graphically displayed by appropriately sizing the hatched region of the `SlitConfigurationPanel`.

The user would also load in a target list for the field. The target list would be a list of all objects the user is interested in that lie within a patch of sky, in which the field would lie. Targets are listed with an identifier, the coordinates, and a priority score. The target positions would be listed

in sky coordinates. The MSCGUI would be responsible for making the transformation from sky coordinates to CSU coordinates.

The user would then determine the positioning of the field on the sky. This would be done in one of two ways. The first way is simply entering the coordinates in right ascension (RA) and declination (Dec) and the position angle (PA) into text fields at the top of the GUI.

The second method is by using an interactive region selector, a separate window called the field selection panel. The main area of the field selection panel represents the area of the sky the user is interested in. The targets from the target list are plotted in the display area with the identifier and a graphical representation of the priority (either color or size of icon). A background sky image could be obtained from an archive, such as 2MASS or SDSS. The user could also supply an image that includes the desired field. FITS file format would be supported, with other image formats (JPG, GIF, PNG, etc.) being potential upgrades. In order to properly place targets in the field, FITS header information including a World Coordinate System (WCS) transform would be required. The CSU FOV would then be overlaid on this area. The user could move the overlay by dragging it with the mouse. The coordinates would be displayed on the field selection panel, and would update there as well as on the main MSCGUI. The PA would be set using a text field, although interactive mouse control, such as holding down the right button and dragging, could be a possible upgrade.

When the user presses the "Done" button, the position of the field is considered selected and MASCGEN then optimizes the slit configuration to maximize the priority score. If this optimization is quick enough, it can be automatically performed on mouse button release events.

The slit-assignment function will use a three-pass algorithm to assign slits to target objects:

1. For each CSU slitlet, scan its accessible zone and assign it to the object within the zone with the highest priority. It is possible the slitlet will not be assigned.
2. On the second pass, check each zone "between" bars for objects. Assign two slitlets to any object if such an assignment would increase total priority.
3. On the final pass, assign any unassigned slitlet to the adjacent slit with the highest priority to lengthen an already-assigned slit and use any unassigned slitlets.

The main MSCGUI is then updated to reflect this optimized slit configuration. The table and slit configuration panel are updated with the correct slit positions. The user could then tweak the configuration, if desired, by moving the positions of the slits by dragging them onto the desired objects. Simple tools such as centroiding will be provided to help with positioning the slits on objects. Buttons will be provided to help align adjacent slits. Automatic optimization can be disabled to allow the user to create a slit configuration manually using these tools.

Dithering is a common technique used for sky subtraction. To support dithering, the optimization must make sure that the targets stay in the slits for all dither positions. This is accomplished by specifying the minimum distance a target can be from the edge of a slit in a field on the main MSCGUI. This value would put constraints on how close an object could be to the top or bottom

of a slit, even if the user did not dither. Multiple slits could be joined together, if this improves the overall priority score.

To help understand the spectral coverage for each target, a dialog will be available via a button on the GUI. This dialog shows a depiction of where each spectrum will lie relative to the detector area. The limiting wavelengths at the edge of the detector would also be given for each row. Once again, the MSCGUI is responsible for a transformation, this time from CSU coordinates to detector coordinates.

The user would then submit the mask to the CSU server (normally via the MOSFIRE desktop and MGS) to configure the CSU. To describe the MSC to the server, a series of keywords defining the position of each slit and the associated width would be set. Then, a final keyword is set to command the CSU server to send the configuration to the CSU controller.

When a mask is submitted, the MSCGUI will also create the binary FITS table extensions that describe the slit configuration and target list. The extensions will be written to a directory specified by a keyword, with a name that includes the time and date of the CSU configuration. The name of the extensions will be written to a keyword, and the detector server will read this keyword to obtain the extensions to append to the detector data. See MSDN18, MSDN22, and MSDN05 for more information.

The MSCGUI will also provide the ability to create a guide star map. This feature will use the current position and position angle defined in the GUI to predict what the sky will look like in the guider. This option is started from the MSCGUI menu. When selected, a new dialog is created with a window for displaying images. Based on the FOV of the guider an image of the sky is obtained from an archive that fills the field of view. Using a star catalog, the MSCGUI will then determine what bright stars are available in the selected field, and plot them on the display. The user will select the desired guide stars by clicking on them, and save the coordinates as a guider map. The map will be saved to disk, with notations that indicate what pixels on the guider detector each star will fall on. This information will be then used for coarse alignment during observing. See MSDN03for information on how this image will be used.

Guide star information will also be written to the MSC file. See MSDN17for more information. When saving an MSC, if a guide map has not been created since changing the position or position angle, the MSCGUI will prompt the user to create one.

#### 5.4.3.2.17 Calibration GUI

The Calibration GUI will be used to configure the instrument for taking data used for calibration. This includes the taking of arc lamp spectra and flat field images. In order to take calibration lamp spectra, the dust cover must be closed and a calibration lamp source must be turned on. This GUI provides controls to open and close the dust cover hatch, as well as turn on and off the various calibration lamp sources, including the dome flat lamp.

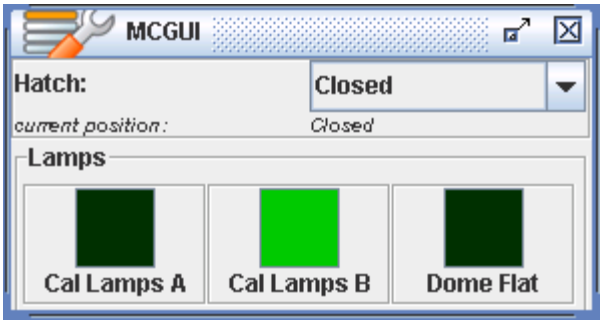


**Figure 117: MOSFIRE Calibration GUI**

#### 5.4.3.2.18 Telescope GUI

The MOSFIRE Telescope GUI is used to perform common telescope operations during observing, such as rotating and offsetting. These moves are usually performed via scripts at WMKO, and these will also be available for MOSFIRE. However, the MTGUI will provide a simple graphical tool to use as in interface to these scripts. The MTGUI will be similar to the OSIRIS Telescope GUI, used for the same purpose.

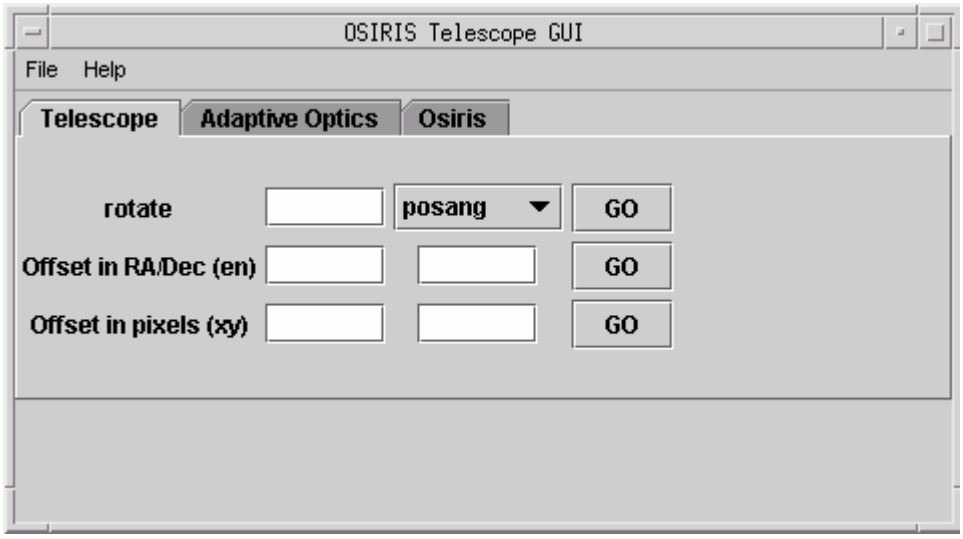


**Figure 118: OSIRIS Telescope GUI**

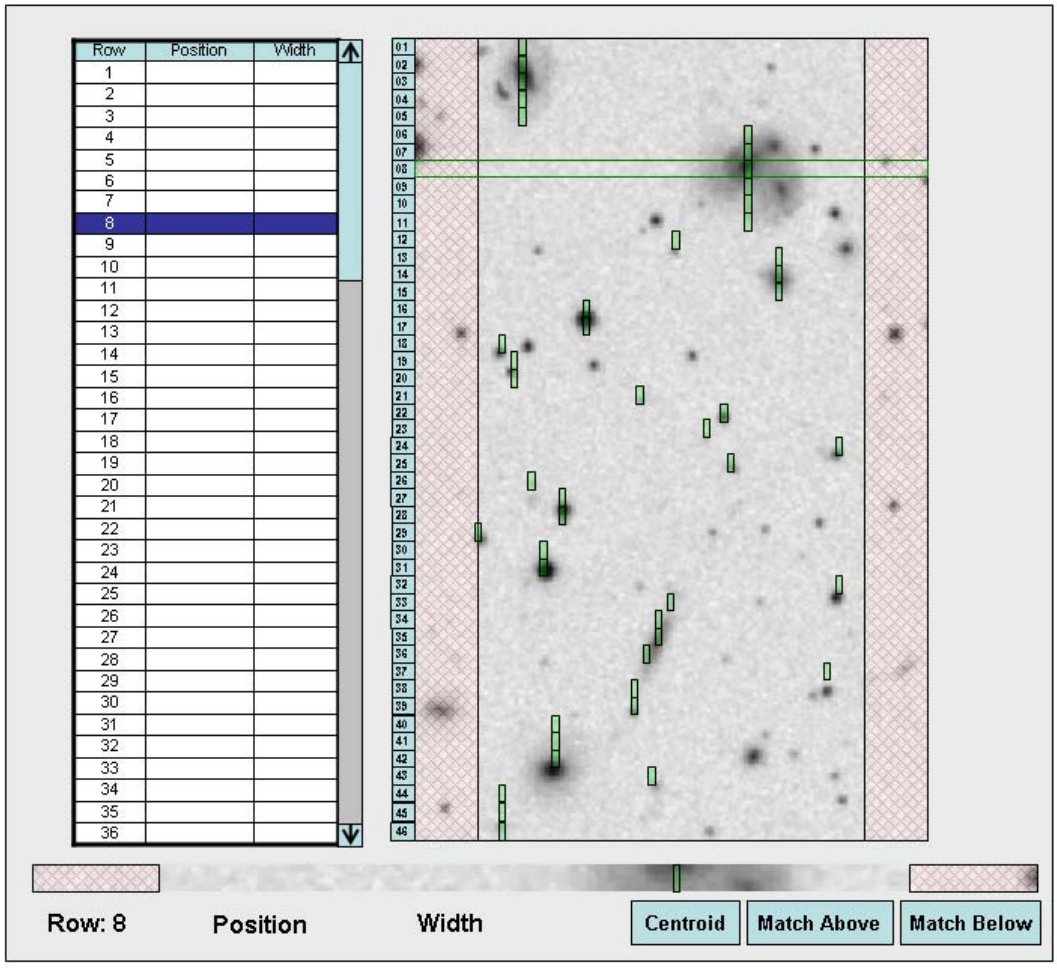


**Figure 119: MOSFIRE CSU Control GUI**

### 5.4.3.3 Image Viewing Software

MOSFIRE will use existing programs for image display. MOSFIRE data will be written to disk in the standard FITS format. Therefore, programs such as *DS9* and *Quicklook v2* (written as part of the OSIRIS project) can be used with little or no modification.

### 5.4.3.4 Data reduction

Data reduction for MOSFIRE will be very similar to the data reduction for any near-IR spectrograph. Though MOSFIRE will have multiple spectra on the detector, the spectra will be well separated, and once isolated, each one can be reduced using standard infrared spectroscopic techniques. These techniques include flat fielding, bad pixel masking, cosmic ray rejection, and wavelength calibration. MOSFIRE will take advantage of the *DEEP2* pipeline, developed for the reduction of DEIMOS data by a team at UC Berkeley. Because of the similarities between the instruments, the level of effort to convert the *DEEP2* package into one that can reduce MOSFIRE data is expected to be modest.

An important element of the data reduction pipeline will be an accurate optical model of both the f/15 Cassegrain focal plane of Keck I and the resulting spatial and spectral mapping to the MOSFIRE focal plane. Given the position of a slit in the focal plane, and which order sorting filter is in the beam, it will be possible to accurately predict the wavelength versus detector X-position, and the Y-positions of both of the slit edges and the location of the targeted object within each slit. This information provides the observer with a good knowledge of the spectral coverage provided by each slit (for planning purposes) and provides the data reduction pipeline with first guesses that allow quick convergence on the full 2-D wavelength solution for each slitlet. For more information, see MSDN23.

### 5.4.4 Interfaces

#### 5.4.4.1 Hardware-Server Interfaces

##### 5.4.4.1.1 ASIC

The hardware interface to the SIDECAR ASIC is a standard USB 2.0 compliant interface, provided by a Teledyne engineered interface board called the Jade2 card. To manage the USB port, Teledyne has created a Hardware Abstraction Layer (HAL), built upon the Microsoft .NET framework. The detector server MDS is built upon the WMKO legacy framework KTL. This server runs only in the Solaris environment. This presents the challenge of interfacing the COM DLL, running in a Windows environment, with the detector server, running in the Solaris environment (described in MSDN28). A common technology that can bind with a COM component and a legacy C component, yet provide inter-platform communication, is needed. Our chosen technology for this is Java (see MSDN29 for details).

Java can bind with legacy C code using the Java Native Interface, or JNI, as is used in `KJava`, the Java-KTL interface (see below). Java Remote Method Invocation (RMI) would provide the necessary inter-platform operability, allowing Java code to be called across a network and even across operating systems.

Third party Java-to-COM bridges are available that allow a Java object to bind to an object in a COM library. Evaluation of some of these Java-to-COM bridges has been performed during the detailed design phase. Open-source projects JACOB and JCOM proved inadequate because of the lack of support for unsigned data types (Java does not implement unsigned types). The commercial product *ComfyJ* was determined to have most of the required functionality, but problems occurred when attempting to obtain data from an array passed to the COM object by reference. Another open-source project, *J-Interop*, recently developed support for unsigned types, but also has a problem with passing an array by reference. However, being open source, this option is attractive as it can be modified at will by the MOSFIRE software team. In addition, the primary programmer and manager for the project has been extremely supportive, since he is eager to improve the product. We will continue to pursue this option as our baseline. Discussions with WMKO staff have led to two fallback strategies. The first is to create a C interface to the COM object, and develop a custom JNI package to access this interface. The second is to abandon RMI and use cross-platform RPC, again connecting a C interface to the COM object.

To summarize, the interface from detector server to detector is comprised of the following items:

- Detector server running on a Solaris machine, using legacy KTL code.
- Java JNI library, which translates C code to Java code, and invokes a Java Virtual Machine to execute.
- Within the JNI library, an RMI client is created to access the Windows machine.
- On the Windows machine, an RMI server is run to handle requests from RMI client in Solaris.
- RMI server uses a Java-to-COM bridge to bind to the Teledyne COM DLL.
- COM DLL uses Microsoft .NET services to interface with HAL.
- HAL interfaces with the off-the-shelf USB device driver that interfaces with the Jade2 ASIC interface card.
- The Jade2 passes commands from the USB to the SIDECAR ASIC.
- The SIDECAR ASIC controls the Hawaii-2RG detector.

#### 5.4.4.1.2 Serial RS-232

Most of the components in the MOSFIRE instrument are accessed through an RS-232 serial connection. These components are the Lake Shore 340 temperature controller, the pressure gauges through the Varian Multigauge controller, the mechanism controllers, and the CSU.

There is nothing special about the serial communication required for these components. The housekeeping components are identical to the ones used in OSIRIS, and the communication protocol will be reused. This protocol consists of a set of utility functions that open, configure, read, and write to a standard serial device. The mechanism controllers and CSU will be able to use these functions as well.

Table 27 details the supported connection configuration for each device. The bold items specify our implementation.

| Device | Baud Rate | Data Bits | Parity | Stop Bits |
|---|---|---|---|---|
| Lake Shore 340 Temperature Controller | 300, 1200, 2400, 4800, **9600**, 19200 | **7**, 8 | **Odd**, Even, None | **1** |
| Varian Multi-Gauge Controller | 1200, 2400, 4800, 9600, **19200** | 7, **8** | Odd, Even, **None** | **1** |
| PD2400 Motion Controller | **19200** | **8** | **Even** | **1** |
| Flexure Compensation | 9600 - **115200** | **8** | **None** | **1** |
| CSEM CSU | **115200** | **8** | **None** | **1** |

**Table 27: Configurations for Serial Devices**

MOSFIRE will use two Lantronix ETS8P terminal servers to handle communication with the serial devices. A terminal server is a device that transmits and receives serial data over an Ethernet network, providing conversion between TCP/IP and one or more serial I/O ports. The reasons for using a terminal server are:

- Allows for control of multiple devices from one host computer.
- Since the protocol is TCP/IP, the terminal server allows remote control from any computer on the network.
- Ethernet extends cable lengths beyond the typical ~15 m maximum cable length recommended for high-speed RS-232.
- Ethernet can be implemented with fiber optic data links, providing for electrical isolation of the instrument electronics from the telescope and observatory systems.
- The same Ethernet connection can be used for communication to the Windows machine controlling the SIDECAR ASIC, reducing the number of cables in the instrument cable wrap.

Network communications with the terminal server are in the TCP/IP format, and software level serial device communications must be converted to packets to be sent over the network to the terminal server. WMKO has developed a small service called *tnet* to provide this function. This service was used very successfully for OSIRIS and will be used again for MOSFIRE.

#### 5.4.4.1.3 Ethernet

In order to power cycle the terminal server, the power controllers were selected with an Ethernet interface; if they had serial interfaces, powering off the terminal server would eliminate the communication path to the power controller. A set of utility functions similar to that used for serial communication is used for Ethernet communication over a socket. The power controllers and the communication method used to control them will be identical to the implementation used for OSIRIS.

#### 5.4.4.2 UI-Server Interfaces

This section describes the methods used by GUIs and scripts to interface with the hardware servers.

##### 5.4.4.2.1 KTL

When the Keck Telescopes were being built, the WMKO software group, led by William Lupton, Al Conrad, and Hilton Lewis developed a set of functions called the Keck Task Library (KTL) to provide a standardized library for event-driven applications. These functions have become the core of the RPC functions supported by Keck instrument servers and clients. MOSFIRE will continue this practice. By use of KTL, we can build our servers on the same framework that has evolved over the lifetime of the Observatory, ensuring that both servers and clients will be stable and maintainable by the WMKO programming staff.

As mentioned above, MOSFIRE will build its servers on a KTL framework called `rpcKey_server` (described in MSDN04). This server allows the relatively quick creation of hardware servers with a built-in KTL compliant interface. With this approach any KTL compliant client, such as `show` and `modify` is available for immediate use at the command line or in scripts.

##### 5.4.4.2.2 KJava

`KJava` is a package written by UCLA Software Engineer Jason Weiss as part of the OSIRIS project that allows programs written in Java to interact with a KTL server. It uses the Java Native Interface (JNI), a specification that allows communication between Java objects and native C code stored in a sharable object library. `KJava` is comprised of a set of C code that implements the `show`, `modify`, and `cshow` capabilities of the standard KTL clients, an additional method for gathering all of the keywords and their properties from a server, and the corresponding Java code, supplied in a Java Archive (JAR) file, to be added to the client application. The C code mirrors the code for standard KTL clients, and handles all RPC communication.

A client that wishes to monitor server keyword changes starts a `KJava` "`CShow`", and registers a listener to watch for keyword change events. The listener must implement the `KJavaCShowListener` interface, providing an implementation of the `KJavaCShowCallback` method that will handle the event triggered when the value of a keyword changes asynchronously. See MSDN16 for more information.

#### 5.4.4.3 Server-Server Interfaces

The section describes the necessary communications between a server and another server.

##### 5.4.4.3.1 Hardware Server-Global Server

The hardware server to global server interface is similar to the UI server interface: RPC-based, keyword services over Ethernet. The observatory-developed, generic, RPC-based client-server

software includes a number of functions and tasks for server-to-server keyword communications based on the functions in the Keck Task Library.

At its lowest level, the communications consists of RPC functions. Above that are the KTL keyword functions `ktl_open`, `ktl_read`, `ktl_write`, `ktl_ioctl`, `ktl_close`. Above this level are an application's tasks and libraries.

The MGS (described in MSDN15) registers itself as a listener of the subservice keywords that it maps as meta-keywords. Its own keyword list is updated much in the same way a `cshow` is performed, via KTL callbacks. The MGS, when it starts up, reads keyword configuration files for all the services it needs to contact for keyword information. It starts keyword monitors for all keywords that are not local to it, using the `ktl_ioctl KTL_CONTINUOUS` option so that it has current values for all specified keywords. Any server can then contact the MGS for a current value for any keyword.

#### 5.4.4.3.2 Detector Server FITS Header Keyword Gathering

The MOSFIRE Detector Server (MDS, described in MSDN05) is responsible for creating the FITS file for each exposure that contains header keyword data and the image data. The header data not only comes from the instrument servers, but also from the telescope ACS and DCS servers.

The MDS obtains detector keywords from itself and all of the other servers with "oneshot" calls to the various servers. The interface is the same as described above – standard KTL keyword calls on top of RPC network communications. When a server receives the "oneshot" request from the MDS it replies with a list of keyword-value pairs, predefined for that particular service.

This interface quickly supplies a timely snapshot of the entire system's status, as reflected in keywords, for the MDS FITS writer to add to the header data for the FITS file.

#### 5.4.4.3.3 Server to Telescope

The server to telescope interface is also implemented using RPC-based keyword services as described above for the server to server interface. In this case, the top-level application's code consists of procedures for coordinating mechanism movements with telescope and/or rotator positions.

A task called `watch_keywords` (described in MSDN08) was created for NIRC2 that watches specific keywords and takes action according to how their value changes. It uses the KTL interface to connect to servers and act on its list of specified keywords, each one of which can have a callback function associated with it. This task will be used to monitor DCS keywords and send commands to MOSFIRE servers to facilitate coordinated operation. It also serves to insulate instrument servers from possible DCS problems. Instances of `watch_keywords` will be used by the MOSFIRE FCS and pupil mask servers to coordinate their movements.

## 5.5 Interfaces with the Keck I Telescope and Observatory Facilities

The mechanical configuration of MOSFIRE is based on the Keck I telescope Cassegrain focus envelope as used for the LRIS instrument. The following constraints are being used in the mechanical design of MOSFIRE:

1. Envelope size compatible with the LRIS envelope
2. Weight not more than LRIS including the weight of the Cassegrain ADC
3. Rotator design similar to LRIS
4. Instrument dewar center of gravity located on the rotator bearing axis
5. Handler design similar to LRIS
6. Same defining points as LRIS

MOSFIRE creates a storage problem at the Keck I telescope; there are no more Nasmyth deck positions available unless an instrument is retired. Given the time frame for MOSFIRE delivery (mid-2009) it seems likely that either the Forward Cassegrain Module will be retired by that time, or a re-allocation of instruments will take place. If the Forward Cassegrain Module is still in use we propose moving it to a "campaign" mode of operation and storing it on the Keck I dome floor. With these considerations in mind we have identified the space currently used to store the Forward Cassegrain Module on the Keck I Nasmyth deck as the storage position for MOSFIRE.

The instrument will use three (two large and one small) CCR cold heads. These will be supplied from a single compressor. This will require the installation of helium lines on the Keck I telescope and the installation of a compressor in the Keck I mechanical room. The instrument requires a glycol cooling supply for the instrument electronics and an air supply for the defining point drive motors.

WMKO will be responsible for the instrument rotator, instrument handler, and the usual interfaces (glycol, helium, etc.). New interface panels will be installed at the Keck I Cassegrain position to provide the additional connections required for MOSFIRE. The Keck I Cassegrain position and the current interfaces are shown in Figure 120.

The Keck I Nasmyth deck storage position RT1 will be used for storage of MOSFIRE as shown in Figure 121 and Figure 122. A new connection panel, shared between MOSFIRE and LRIS will be installed between RT1 and RT2 as shown in Figure 123. As indicated in Figure 87 this panel will provide a full set of services for MOSFIRE at the storage position.

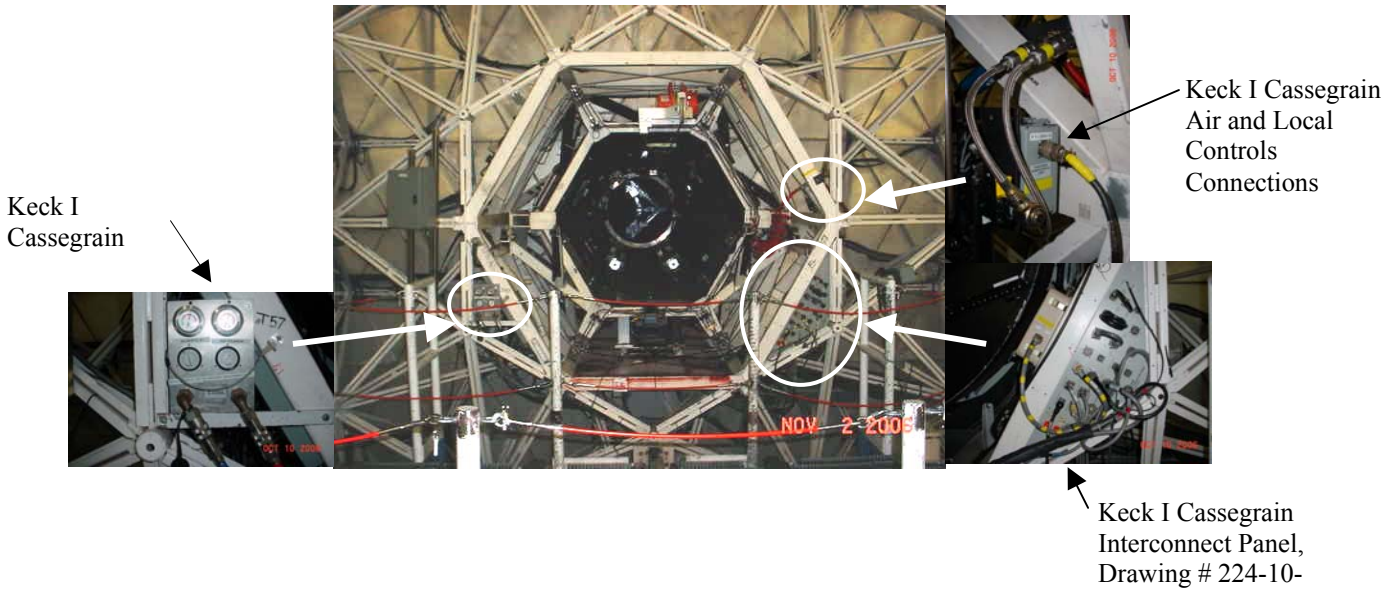


**Figure 120: Keck I Cassegrain Focal Station**
Viewed from the Cassegrain platform, telescope at horizon.

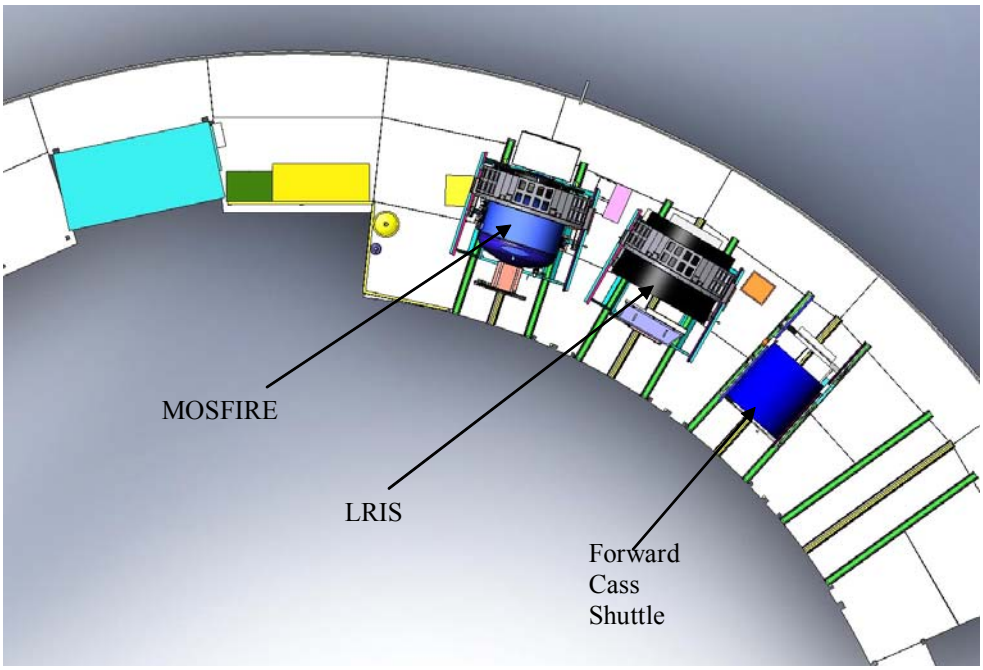


**Figure 121: Plan View of MOSFIRE on the Keck I Nasmyth Deck**

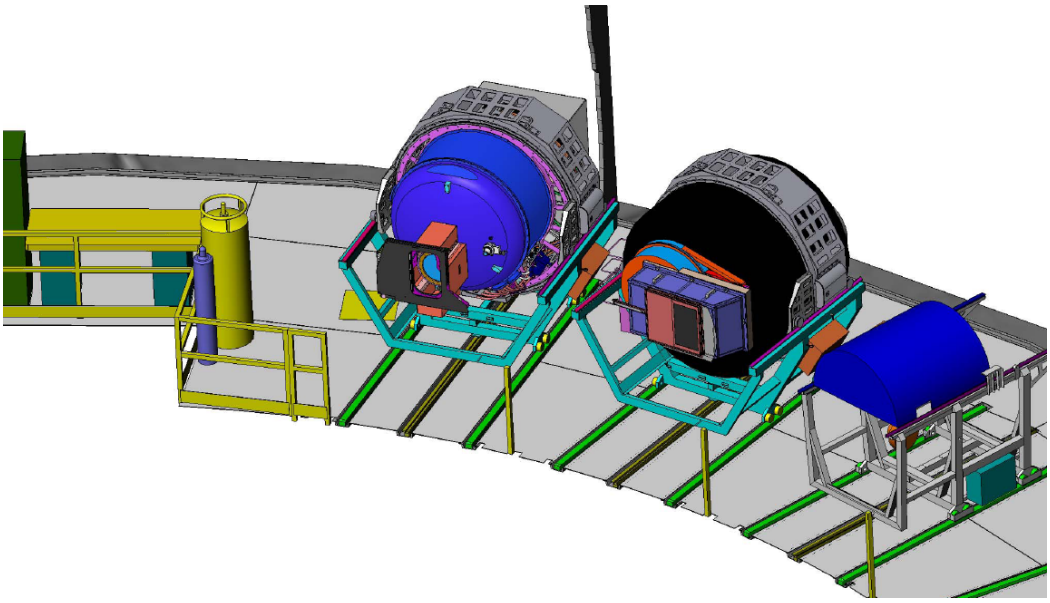

**Figure 122: Perspective View of MOSFIRE on the Keck I Nasmyth Deck**

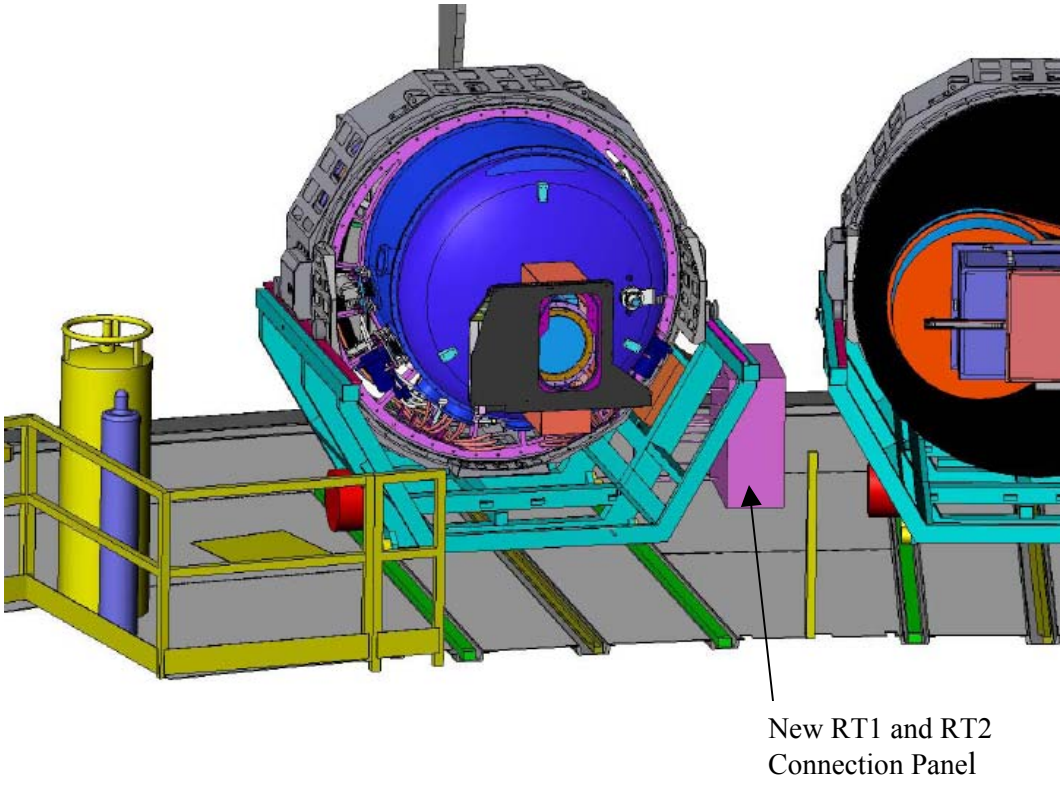


**Figure 123: MOSFIRE at RT1 with New Connection Panel**

## 5.6 Operational Concepts and Observing Scenarios

Four main observing modes are envisioned for MOSFIRE:

- direct imaging mode
- MOS acquisition imaging mode (fine acquisition mode)
- multi-object spectroscopic mode
- long-slit spectroscopic mode.

These four modes and their requirements are described in more detail below, and in MSDN03.

### 5.6.1 Direct Imaging Mode

This mode is used to perform wide-field infrared imaging. All bars of the CSU are moved to the fully open position and the imaging mirror selected. In addition to the typical exposure settings (integration time, coadds, etc.), the user must specify the field position, position angle, and filter. A user will often take a series of exposures in a dither pattern to increase the field of view or improve noise performance, or to take set of exposures with different filters.

### 5.6.2 Fine Acquisition Mode

This mode is used when acquiring a field for spectroscopy, in order to precisely place the MOSFIRE FOV in the correct position on the sky so that the slits are accurately aligned with the desired objects to be sampled.

In this mode, the telescope and rotator are set to their nominal positions, after which a pre-selected guide star is placed at the recommended guider pixel position provided by the mask design. This initial "coarse" alignment requires a constant and well-known relationship between the guider and the MOSFIRE (telescope) focal plane. The slit bars are deployed to their spectroscopic positions, except for a few (typically 3-5) which are used for alignment stars. These bars will be opened more than typical slits to create "alignment boxes" (a typical alignment box size will be 4" by 7.3") to ensure that the designated alignment stars will fall inside the slit mask opening. An image is then taken through the mask and it is analyzed to compare the predicted and observed alignment star positions within the alignment boxes. The comparison is used to calculate any necessary adjustments of telescope pointing and instrument rotation to place the alignment stars in their precise positions. This procedure can be repeated to verify that the adjustments have been successful. Once the star positions are correct, the slits used for alignment stars can be redeployed as spectroscopic slits. Users may switch back to this mode during a series of spectroscopic observations to check alignment.

### 5.6.3 Multi-Object Spectroscopic Mode

In this mode, the grating is exchanged with the flat imaging mirror and is rotated to one of two fixed positions, depending on the spectral order to be observed. An order sorting filter is used to select the desired spectral order from the grating dispersion. Typical integration times expected for

this mode are in the range of 600 to 1800 s, depending on the waveband and the detector noise characteristics.

The observer will often want to nod along the slit by a small amount to facilitate background subtraction. This requires the slit planning software to count for the nod distances to ensure that the selected objects will remain in their slits for a specified nod distance. If a high priority target is predicted to move off the slit during the nod, an adjacent bar can be used to extend the slit length.

### 5.6.4 Long-Slit Spectroscopic Mode

MOSFIRE users will sometimes want to acquire spectra from a single object using a long slit. For example, obtaining spectra for telluric or flux standards, extended objects, or any a single object of interest. The CSU bars can be positioned to produce a contiguous long slit up to 6.1' in length, but more commonly a slit length of <1' will be sufficient. Field acquisition can be accomplished using the same method employed for multi-slit masks if the user can plan observations well in advance; however, more commonly a user would either place a relatively bright target (such as a standard star) on the slit or would place a relatively bright offset star onto the slit and then perform a blind offset to a faint target. The default method for long slit acquisition would be to deploy the central ~15 bars (~2′ in length) to the center of the MOSFIRE field, except for the central bar, which would be opened wider to form a single alignment box. The target or offset star would first be placed on the guider at a position that is calibrated relative to the center of the MOSFIRE FOV, and then the telescope is offset to place the star into the alignment box. A short exposure in imaging mode will allow for an analysis program to calculate the necessary telescope offset to place the target at the center of the alignment box and then send the move command to the telescope. When the user is satisfied with the centering, the central bar can be closed down to the same width as the rest of the long slit, and the grating can then be inserted to replace the imaging mirror.

### 5.6.5 Selected Use Cases

#### 5.6.5.1 Acquiring a pre-planned multi-object spectroscopy field

- Telescope operator slews telescope to user-specified coordinates and the rotator to the desired position angle. User sets up CSU with fine alignment slit mask (i.e., science configuration with a few bars assigned to “alignment boxes” (See “Creating a science slit mask and its associated alignment slit mask”), puts the instrument in imaging mode, and selects a filter while telescope is slewing.
- Telescope operator offsets telescope to put guide star on specific predetermined pixels in guider. (See “Determining locations of guide stars on guider pixels”)
- User offsets telescope to get a sky image through the alignment slit mask. This frame is used both to measure alignment box location and for background subtraction for the alignment image.
- User takes exposure of specified integration time in specified readout mode.
- User offsets telescope back to get object image through the alignment slit mask.
- User takes exposure of specified integration time in specified readout mode.

- Software automatically calculates how to offset telescope and rotate the instrument to put alignment stars in the proper locations.
- User offsets the telescope using these values.
- User optionally takes another object image through the alignment slit mask, and if necessary, offsets the telescope.

#### 5.6.5.2 Acquiring a real-time long-slit spectroscopy field

- Telescope operator slews telescope to user-specified coordinates and position angle. During the telescope slew, the user puts instrument in imaging mode, inserts filter, and sets up CSU with long-slit mask, with center row opened to create alignment box.
- Telescope operator offsets telescope to put target or offset star on a specific guider pixel.
- Telescope operator offsets telescope to put target or offset star in center of MOSFIRE FOV.
- User offsets telescope to get sky frame through the alignment slit mask. This frame is used both to measure alignment box location and for background subtraction of alignment image (this step is necessary only when the target or offset star is fainter than K ~16).
- User takes exposure of specified integration time in specified readout mode.
- User offsets telescope back to get object image through the alignment slit mask.
- User takes exposure of specified integration time in specified readout mode.
- Software automatically calculates how to offset telescope and rotate the instrument to put the target or offset object in the proper location, or user places the object at the desired location interactively.
- User offsets the telescope using these values.
- User optionally takes another object image through the alignment slit mask, and if necessary, offsets the telescope.
- If aligning on offset star, the user performs blind offset to target.

#### 5.6.5.3 Taking a science exposure

- User sets up CSU with final science slit mask configuration. (For preplanned spectroscopic observations, see “Creating a science slit mask and its associated slit mask”; for imaging mode, CSU is opened fully).
- For spectroscopic observations, user puts instrument in spectroscopy mode.
- User specifies dither pattern parameters.
- User takes exposure of specified integration time in specified readout mode.
- Telescope is offset to perform dither.
- The above two steps are repeated for all dither positions.
- Telescope is offset to original position.

#### 5.6.5.4 Determining locations of guide stars on guider pixels

- User specifies RA, Dec, and position angle of field.
- Extents and positions of the pixels of the guider camera on the sky are determined based on optical model of instrument.

- Archives, such as the USNO catalog, are used to determine which stars are in the guider field.
- Locations of those stars in guider pixel coordinates are noted.

#### 5.6.5.5 Creating a science slit mask and its associated alignment slit mask

- User creates a prioritized list of targets in a field, including accurate RA and Dec of all potential science targets as well as potential alignment stars. Alignment stars should be bright enough to be well detected in short (~30 s) imaging exposures. User submits to optimization software.
- User specifies a position on the sky and position angle for initial mask orientation.
- User specifies the width (in arc minutes) of the MOSFIRE field in the X-direction to be used for slit placements. This choice affects both the number of targets that can be accommodated, and the common wavelength coverage of the slits.
- User specifies band for which the mask will be used (Y, J, H, K, or Ks)
- User specifies minimum distance from object to edge of slit. This choice should include any planned nodding along slitlets during observations.
- User specifies global slit width to be used for all slits (this can be modified interactively for individual slits or ranges of slits).
- Software optimizes slit mask to create a slit configuration that maximizes the cumulative priority score over the entire slit mask.
- User may interactively change the PA and pointing center, resulting in a new optimized configuration.
- User optionally manually adjusts slit positions and widths.
- Once happy with the science configuration, user specifies which alignment stars within the MOSFIRE field of view are to be used for fine alignment (they need not be within the same range of "X" as the science targets).
- Slit configuration and associated alignment configuration is written to disk. The software also produces an archival image of the guider field of view, a list of guide stars that will appear in the guider field, and the predicted pixel locations of each guide star on the guider detector. The finding chart and the guide star positions will then be used at the telescope for coarse alignment of the mask.

#### 5.6.5.6 Obtaining calibrations for MOSFIRE slitmasks

##### 5.6.5.6.1 Flat Fields and Arc Line Lamps

- During the afternoon prior to a night's observing (or, alternatively, at the end of an observing night), with the dome closed, the telescope is positioned to point at the area of the dome interior illuminated by the dome flat fielding lamps.
- User positions CSU to science slitmask configuration, including the order-sorting filter.
- User obtains flat field exposures of specified integration time in specified readout mode.
- User closes MOSFIRE front hatch and turns on arc line lamps
- User obtains arc lamp exposures of specified integration time in specified readout mode.

#### 5.6.5.6.2 Standard Star Observations

- Standard stars will generally be observed following the procedure outlined in section 5.6.5.2, "Acquiring a Real-time long-slit spectroscopy field".

### 5.6.5.7 Using the Data Reduction Pipeline

- User assembles science data and associated calibrations (arcs, flat fields, bad pixel mask)
- User enters file names into a DRP "plan file"
- User runs DRP up to desired step (e.g., either 2-D background subtracted spectrograms, or all the way to 1-D extraction of spectra).
-

## 5.6.6 Development Strategy

The development strategy for MOSFIRE is largely consistent with that of previous WMKO instruments, and the standards and conventions established by the observatory. The Concurrent Versions System (CVS) will be used for code version control (described in MSDN32). Source code will be stored in the `$KROOT/kss/mosfire` subdirectories (described in MSDN25), consistent with the conventions used for other instruments. Coding style conventions (described in MSDN31) conform to KSD-50. Editing will performed using the tool of choice, typically *`emacs`* or *`vi`*. For GUIs, development will be done in the open-source *Eclipse* IDE. Builds for all programs, including servers, GUIs, and scripts, will be performed with the GNU *`gmake`* utility, with makefiles conforming to KSD-31a and KSD-198 (described in MSDN27). Builds release executables, libraries, classes, and data files to a subdirectory of `$KROOT/rel/default/Versions/`. The subdirectory is identified with a version number, specified in the makefile used for the build. Links to the released files are created in the respective `bin/`, `lib/`, `classes/`, and `data/` subdirectories of the `$KROOT/rel/default` directory.

MOSFIRE will follow the newer convention of using multiple accounts and kroot trees to manage configuration changes (described in MSDN27). Source is developed using the `mosdev` account in a `mosdev`-owned kroot tree. When a change is finished and tested, it is checked into the CVS repository. It is then checked out as `mosbld`, the owner of the engineering tree. It is built and tested as `mosbld` and/or the engineering account, `moseng`. When the change is verified, it is released to the operational kroot tree, living in `/kroot`. This tree is also owned by `mosbld`. The change is released using *`rsync`*. The change is then tested using the MOSFIRE numbered accounts.

### 5.6.6.1 Work Distribution

The MOSFIRE Software team is comprised of Jason Weiss (JW, MOSFIRE Software Manager, UCLA), John Cromer (JC, Caltech), Chris Johnson (CJ, UCLA), and Allan Honey (AH, WMKO). Jason Weiss has experience on the WMKO instruments NIRSPEC and NIRC2, and was the software manager and primary developer for OSIRIS. John Cromer has been involved in the WMKO instruments LRIS, the LRIS blue camera and the LRIS blue camera upgrade as well as a number of instruments for Caltech's Palomar Observatory. Chris Johnson is a system administrator

in the UCLA IR Lab. Allen Honey is WMKO software engineer who has been involved from the beginning of the development of Observatory software including telescope controls and various aspects of instrumentation.

Jason Weiss (JW) will be responsible for the management of software development, including overall design, budget and scheduling, and progress reporting. He will also be responsible for the following software packages:

- All GUIs, including the MOSFIRE desktop
- MOSFIRE detector server and communication layers between the server and the ASIC control system.

John Cromer (JC) will be responsible for:

- All housekeeping servers
- All mechanism servers
- CSU server
- Scripts
- MOSFIRE automatic slit configuration generator

Allan Honey (AH) will be responsible for:

- MOSFIRE global server

Chris Johnson (CJ) will be responsible for:

- Setting up (configuring, patching) the computers
- Setting up the private network
- Installing and configuring development software and tools

#### 5.6.6.2 Incremental Builds

MOSFIRE software development will be done with an incremental build process. Each successive build results in a functional program providing incrementally more functionality than the previous version. This allows for more rapid integration, since interfaces between programs, such as the global server and the lower level servers, and the GUIs and the lower level servers, are established early and are testable throughout the development process. Unit testing occurs after each incremental build.

The philosophy for server development is as follows:

1. Implement core rpcKey_server stubs
2. Implement keyword configuration files
3. Implement status gathering keywords

4. Implement hardware control keywords

As soon as the global server is ready, integration with each lower level server can begin as soon as the keyword configuration files for that lower level server is complete. The first two steps of server development are very simple, and these steps should be completed for all servers in a couple of man-days. All servers will reach this level before development proceeds further.

The philosophy for GUI development is as follows:

1. Create entry point class, application class, and stub for parameters (constants)
2. Create stubs for model, view, and controller (MVC) classes
3. Implement model
4. Implement handling of asynchronous non-user events, such keyword change events
5. Implement view and controller simultaneously
6. Implement handling of user initiated events (e.g. button press)

The overall implementation schedule and work assignments are planned as follows:

1. Set up computers (CJ)
2. Set up working environment (CJ)
3. Set up version control (AH)
4. Set up directory structure (JW)
5. Run Scripts (JC)
6. MOSFIRE Global Server without coordinated keywords (AH)
7. MOSFIRE Desktop (JW)
8. MOSFIRE Pressure Server (JC)
9. MOSFIRE Pressure Status GUI (JW)
10. MOSFIRE Temperature Control Server (JC)
11. MOSFIRE Temperature Status GUI (JW)
12. MOSFIRE Temperature Control GUI (JW)
13. MOSFIRE Power Server (JC)
14. MOSFIRE Power Status GUI (JW)
15. MOSFIRE Rotary Motor Server (JC)
16. MOSFIRE Mechanism Status GUI (JW)
17. MOSFIRE Flexure Compensation Server (JC)
18. MOSFIRE Detector Server (JW)
19. MOSFIRE Exposure Status GUI (JW)
20. MOSFIRE CSU Server (JC)
21. MOSFIRE CSU Status GUI (JW)
22. MOSFIRE CSU Control GUI (JW)
23. MOSFIRE Global Server coordinated keywords (AH)
24. Scripts (JC)
25. MOSFIRE Automatic Slit Configuration Generator (JC)
26. MOSFIRE Mechanism Control GUI (JW)
27. MOSFIRE Exposure Control GUI (JW)

28. MOSFIRE Power Control GUI (JW)
29. MOSFIRE Calibration GUI (JW)
30. MOSFIRE Telescope GUI (JW)
31. DRP (TBD)

#### 5.6.6.3 Prototypes

To reduce risk, prototypes for many systems have been developed during the design process. The servers identical to the ones used for OSIRIS have been coded for MOSFIRE. These servers include the housekeeping servers and the rotary mechanism servers. In addition, the NIRES flexure compensation server can be considered a prototype for the MOSFIRE implementation, and the LRIS/DEIMOS slit software can be considered prototypes for MASCGEN and MSAlign.

A prototype of the GUI Builder has also been developed. It is quite functional, in that it can read in an XML GUI description and create a GUI linked to properties. The properties are not linked to server keywords, but a simple property setting utility was written to test the GUIs response to property change events. The figures for the MESGUI, MMCGUI, MMSGUI, MTCGUI, MTSGUI, MPRSGUI, MPCGUI, MPSGUI and MCGUI show the GUIs created from our prototype. MSDN36 includes the XML that created these GUIs.

A prototype of the MOSFIRE desktop has also been completed. This GUI has the ability to load in an XML GUI configuration file and place GUIs on the desktop in their saved locations. It also has the ability to save a configuration to file. The button toolbar that displays and hides GUIs is functional. The prototype does not connect to a server yet, but it does have a working property manager, and the same property setting utility described above can be used within the desktop to access the property values. The various figures showing the desktop in this document are screen captures of this prototype.

A prototype of the MAS is also in development. The prototype tests the ability to access a COM object from Java. The prototype can create a connection to the SIDECAR COM object and access and execute nearly all methods of the COM object. However, we have experienced problems with methods that pass an array by reference to be filled with return data. Currently, with *J-Interop*, attempting to call a function that returns data in an array passed in by reference crashes the prototype. With *ComfyJ*, the method would return, but the array would not have the obtained data. An example of this kind of method is the ReadScienceData method, used to obtain science data from the ASIC. Obviously, this is a critical function. Effort will continue in finding a solution. The primary programmer of *J-Interop* has been very supportive, and we are optimistic that a solution will be found. Fallback strategies exist and are discussed in the interface section.

#### 5.6.6.4 Test and Integration Plan

This section outlines the test plan for MOSFIRE software. In general we will follow a bottom to top testing plan from individual functions as they are written through successive levels of integration. Functions, libraries, tasks, and systems of tasks will be tested more or less in that

order. Extended and lifetime testing will have output automatically logged to files using standard script redirection. The files can be parsed during or after the test for performance validation.

This plan is high level and in this document only limited detail can be given. For further information, see the MOSFIRE software design notes for the test plan for each individual component.

#### 5.6.6.4.1 Servers

All of the servers use the same base code, found in the KTL section of the Keck KROOT code tree. This code has been tested effectively for the past 10 years as more revisions have been added. The application code for each server must be tested.

##### 5.6.6.4.1.1 General

- Are client-server communications working properly? What happens when communication is attempted but server is not running or is wedged? Proper health notice from the global server?
- Server to server communications.
    - Global server to individual servers.
    - Detector server to ASIC server.
- Each server keyword must be individually tested.
    - Does `show` and `modify` produce the correct result and an informative error message if unsuccessful?
    - Do out-of-range values fail and produce informative error messages?
    - Does writing to read-only keywords fail and produce informative error messages?
    - Do coordinated keywords function properly?
- Hardware problems.
    - Are power-out conditions properly reported?
    - Is power outage recovery acceptable?
    - Are hardware interface disconnects properly reported?
    - Are terminal server power-outs or errors properly reported?
    - Are fault and error messages from specific hardware controllers properly handled and reported?

##### 5.6.6.4.1.2 Detector server (MSDN44)

- Minimum exposure times handled properly.
- Sampling modes all work properly.
- Number of samples works properly.
- Coadd limits handled properly
- FITS header consistently correct and complete.
- FITS file produced with correct path.
- Abort exposure works correctly.
- Detector windowing (region of interest) works properly.

- Binning works properly.

#### 5.6.6.4.1.3 ASIC server (MSDN44)

- Forwards commands from detector server properly.
- Write image data to disk accurately. A constant flux source with a test pattern mask will be imaged. The resulting image data will be compared against what is expected.

#### 5.6.6.4.1.4 Mechanism servers

(MRMS: MSDN41, MFCS: MSDN42, MCSUS: MSDN43)

- Properly configure and initialize hardware.
- Allowed positions reached in optimum time.
- Move aborts work properly.
- Recover properly if power fails during move.
- Accuracy and precision meets requirements.
- Reliability tests. Mechanisms (where appropriate) run continuously for extended period of time.

#### 5.6.6.4.1.5 Temperature Controller (MSDN38)

- Properly configures and initializes Lake Shore hardware.
- Properly configures PID loops.
- Properly sets temperature set-points and responds properly for out of range values.
- Reliability: properly controls temperature for 7 days.
- Reliability. Poll temperatures continuously for 7 days.
- Temperature logging toggle on and off works properly.
- Polling time interval is adjustable properly.
- Out of range values are properly reported.
- Test with lab test dewar before instrument dewar is ready.

#### 5.6.6.4.1.6 Pressure Monitor (MSDN37)

- Properly configures and initializes Varian hardware.
- Reliability. Poll pressure continuously for 7 days.
- Pressure logging toggle on and off works properly.
- Polling time interval is adjustable properly.
- Out of range values are properly reported.
- Test with lab test dewar before instrument dewar is ready

#### 5.6.6.4.1.7 Power Controller (MSDN40)

- Toggle power on and off properly to individual outlets.
- Properly reports subsystem power outages.

- Reliability: Cycle power on and off for 24 hours continuously at a defined interval. Log power cycles with external test hardware.

#### 5.6.6.4.1.8 Global server (MSDN45)

- Properly handles all keywords that interface to lower level servers.
- Properly registers all lower level servers for health monitoring.
- Properly reports loss of lower level server response.
- Properly handles coordinated keywords.
- Reliability: Runs continuously for 14 days fielding keyword requests and monitoring lower level server health.

### 5.6.6.4.2 Graphical User Interfaces

#### 5.6.6.4.2.1 General

- All GUIs properly reconnect after fault or crash. Tested by stopping and restarting servers
- Control GUIs properly set keyword values.
- Control GUIs properly report failures from server.
- Control GUIs properly disallows values that are out of range.
- Status GUIs accurately displays current state of keywords.
- Status GUIs properly display errors when keyword values are in error.

#### 5.6.6.4.2.2 MECGUI - Exposure Control GUI ((MSDN54)

- Properly controls:
    - Integration time
    - Number of coadds
    - Sampling mode
    - Number of reads
    - Object/field name
    - Frame comment
    - FITS file path
    - Dither patterns

These will be tested by setting individual values, checking to see the keyword values are properly set and cause the proper actions in the server and hardware.

#### 5.6.6.4.2.3 MESGUI - Exposure Status GUI (MSDN53)

- Properly displays:
    - Integration time
    - Number of coadds
    - Sampling mode
    - Number of reads

- Object/field name
- Frame comment
- FITS file path
- Dither patterns

Check against keyword values and hardware settings read back into keywords.

#### 5.6.6.4.2.4 MMCGUI - Mechanism Control GUI (MSDN52)

The following will be checked against hardware settings and keyword values:

- Exposure mode set correctly verified by checking grating/mirror setting and keyword.
- Filter set correctly verified by checking the filter, pupil mask position, grating tilt, and detector focus mechanisms and keywords.

#### 5.6.6.4.2.5 MMSGUI - Mechanism Status GUI (MSDN51)

Each of the following will be tested against keyword values and actual hardware positions:

- Dust cover - open, closed, moving, error.
- Flexure compensation - on, off, error.
- Filter wheel 1 - position name, moving, error.
- Filter wheel 2 - position name, moving, error.
- Pupil - position angle, open, tracking, not tracking, error.
- Grating-mirror exchange - grating, mirror, moving, error.
- Grating tilt - grating, mirror, moving, error.
- Detector focus - position in microns, error.

#### 5.6.6.4.2.6 MSCGUI - CSU Control GUI (MSDN55)

- Properly reads MSC file, reports appropriate errors – file not found, bad format.
- Properly writes MSC file, reports errors - disk full, etc.
- Properly commands CSU for multi-slit setup.
- Correctly moves bar positions.
- Correctly changes slit widths.
- Correctly reads and displays archived images

#### 5.6.6.4.2.7 MSSGUI - CSU Status GUI (MSDN68)

- Correctly reflects the state of the CSU.
- Slit positions and widths will be checked against keyword values.
- Zooming works correctly.

#### 5.6.6.4.2.8 MTCGUI - Temperature Control GUI (MSDN48)

- Correctly sets the dewar temperature set-point, verified by keyword and visual check of Lake Shore 340 controller display.
- Correctly sets the detector temperature set-point, verified by keyword and visual check of Lake Shore 340 controller display.

#### 5.6.6.4.2.9 MTSGUI - Temperature Status GUI (MSDN47)

- Correct display of temperatures verified by keywords and visual check of the Lake Shore 340 display.

#### 5.6.6.4.2.10 MPRGUI - Pressure Status GUI (MSDN46)

- Correct display of pressure verified by keyword and visual check of the Varian controller display.

#### 5.6.6.4.2.11 MPCGUI - Power Control GUI (MSDN50)

- Correctly turns power on and off to all controlled subsystems, verified by keyword and physically observing the subsystem to determine its power state.

#### 5.6.6.4.2.12 MPSGUI - Power Status GUI (MSDN49)

- Correct display of power states as verified by keyword and by observing the subsystem power states.

#### 5.6.6.4.2.13 MCGUI - Calibration GUI (MSDN69 [to be written])

- Correctly turns power on and off to lamps, verified by keyword and physically observing each lamp to determine its power state.
- Dust cover position set correctly verified by checking the mechanism and keywords.

#### 5.6.6.4.2.14 MTGUI - Telescope GUI (MSDN56)

- Telescope movements performed correctly verified by checking the DCS keywords.

### 5.6.6.4.3 Additional processes

#### 5.6.6.4.3.1 watch_keywords

- Properly connect with given servers and monitors selected keywords.
- Properly commands server moves.
- Properly coordinates telescope positions with server moves.
- Properly reports loss of communications to server.

- Properly reports loss of communications to DCS.

#### 5.6.6.4.3.2 MASCGEN (MSDN59)

- Correctly creates optimized mask based on priority list. Verify against hand-calculated mask.

#### 5.6.6.4.3.3 MSAlign (MSDN65)

- Determines correct offsets from images taken with alignment mask. Verify versus measurements done by hand using image analysis tools like DS9.

### 5.6.6.4.4 Scripts (MSDN60)

The facility scripts will be tested as they are created and during commissioning. Scripts in the following categories will be tested:

- Detector control
- Exposure Setup
- Imaging
- Image Display
- Information Display
- Mechanism Control
- Power Control and Monitoring
- Start and stop
- Telescope Control and Monitoring
- Test scripts
- Utility
-

### 5.6.6.4.5 DRP - Data Reduction Pipeline (MSDN23)

The DRP will be tested by submitting data taken with the instrument with a full slit configuration.

## 5.6.7 Risk Identification and Mitigation

Most MOSFIRE software is based on heritage, and therefore, considered low risk. However, there are two technologies that are not only new to MOSFIRE and the development team, but also new to the community as a whole. The CSU is a custom piece of hardware, with new control software being developed for our use. The SIDECAR ASIC is a newly developed detector control electronics system that is just coming to the market. Both of these systems present risks, as it is difficult to predict any complications associated with unique and unfamiliar hardware.

#### 5.6.7.1 CSU

Risk associated with the use of the CSU is mitigated by the support of CSEM. Relationships between MOSFIRE programmers and CSEM engineers have been established, and despite the hemispheric distance between the two groups, lines of communication have been maintained. They have been very forthcoming with documentation and support via email and phone. This intimate relationship will continue throughout the project, and will help mitigate risk associated with the mechanism.

#### 5.6.7.2 ASIC

The control of the SIDECAR ASIC and its interface software is considered to be a black box; it is a closed-source commercial set of software with a defined interface that we must trust works as expected and documented. If it does not, communication and collaboration with Teledyne staff will be required to obtain the desired functionality. Teledyne has thus far been responsive to issues raised by the MOSFIRE team, and Teledyne has made their staff available for face-to-face meetings. Any requests for information or code changes are expected to be resolved satisfactorily.

The highest risk associated with the ASIC is the interface. This is mitigated by the various options available, both in the Java-to-COM bridge and the middleware options that could potentially replace RMI. Additionally, WMKO staff has experience with RMI, JNI, and COM, and should therefore provide a welcome source of support. Understanding of these technologies has been furthered with the MAS prototype, giving us a head start on development in this high-risk area.

### 5.6.8 Responses to Issues Raised in the PDR Report

The report of the MOSFIRE preliminary design review (PDR) committee raised several issues related to the MOSFIRE software. The MOSFIRE software team's responses to these issues are summarized here.

*"Re-configuration of the CSU bars seemed a significant cost to observing efficiency and urges any attempt at reducing that time, assuming this can be accomplished without compromising the positioning accuracy."*

Keith Matthews has been discussing the matter with the CSEM engineers. It appears a significant reconfiguration speed-up could be achieved if bars that are opposite one another could be moved simultaneously if they are not moving in opposite directions. So far CSEM has declined to agree to this for safety reasons, but are aware that it is something we would like. They have said that if they do research the issue and decide to implement the change, this would be beyond the current scope of the project and would involve an extension to our contract and an increase in cost. Discussions of this issue are ongoing.

*"The committee urges close and frequent evaluation of the progress of the ASIC development."*

The MOSFIRE Software team has developed a relationship with Teledyne personnel, in particular, software engineer Jing Chen. She has been responsive to emails and has even welcomed a visit from Jason Weiss to discuss the software implementation. Communications with her and with electrical engineer Markus Loose and program manager Murali Rao have been very fruitful.

*"Specific use-cases are recommended to refine the MOSFIRE Desktop."*

Use cases have been fully developed since MOSFIRE PDR. However, it is evident that the MOSFIRE Desktop is not required to perform all science tasks of the instrument. It is offered, rather, as a convenience. The desktop has three main advantages. First, it helps manage the myriad of GUIs that are available for instrument control and status reporting by collecting them in a common area. Second, it provides the ability to save a GUI configuration to disk and restore it at a later time. In this way, frequent users can preserve their layout from one night to the next. Additionally, support staff can maintain their preferred layout, likely to differ from a typical observing layout. Lastly, it can serve as a single point interface to the server level, minimizing the number of `KJava` concurrent connections.

*"To support integration testing of the CSU interface and to facilitate subsequent troubleshooting by the MOSFIRE team, the committee strongly recommends a handover and re-use of any test software that CSEM uses to externally exercise and validate this interface across the serial link."*

CSEM has agreed to give us their test software as a baseline for the development of our own.

*"The MOSFIRE software team should explore the possibilities for collaboration with the MAGIQ software team (developing the guider camera software for MOSFIRE and other Keck instruments) on common camera abstractions of other design concepts that could be shared across both efforts."*

The Keck Common Camera Abstraction, developed for the MAGIQ project, was presented to the team at the WMKO Software Coordination Committee meeting held on February 1 and 2, 2007. It consists wholly of Java classes, and contains no KTL. It is unclear how this abstraction would apply to MOSFIRE. Because it does not contain KTL, it would have to be a layer above the server level, presumably in or under the GUI layer. Subsequent discussions with software engineer Richard Cohen confirmed the belief that it is unlikely that any code would be directly applicable to MOSFIRE. While there are opportunities for some common classes, the MAGIQ project has just completed its PDR and so is at an earlier stage that MOSFIRE. Any possible commonality developed in the future could potentially be retrofitted to MOSFIRE.

*"The bridge software to the detector target computer combines a few different technologies, seemed challenging and not without risk, so the committee suggests some follow-up discussions and information exchange with WMKO software engineers on the proposed technical approach and possible alternatives."*

A meeting was held with WMKO software engineers to discuss the bridge from the detector server to the SIDECAR COM object. It was agreed that the approach presented by the MOSFIRE team

would be adequate. The cross-platform communication technology, RMI, is now prevalent at WMKO, who have made a commitment to the technology in its MAGIQ project. WMKO staff has had successful experiences with Java-COM bridges in the past; a possible fallback strategy would be a custom JNI object that is specific to the SIDECAR COM object. WMKO staff suggested an alternate approach to the RMI and Java-COM bridge method: the uses of cross-platform RPC, with a C interface to the COM object on the Windows side. The use of cross-platform RPC is a technology unfamiliar to the MOSFIRE team, and not in widespread use at the Observatory. Additionally, a new interface between the KTL detector server and the RPC client would have to be developed, with significant risk as well. We believe our proposed method is sufficient, and because of consistency, will be considered adequately manageable by the WMKO staff.

# 6 MANAGEMENT PLAN

## 6.1 Project Structure and Organization

The MOSFIRE project structure is a team effort involving UCLA, CIT, UCSC and WMKO. Professors Ian McLean (UCLA) and Charles Steidel (CIT) are the co-principal investigators. In addition, the co-PIs also hold specific roles within the team. McLean acts as overall Project Manager and Steidel is the Project Scientist. Professor McLean was PI and Project Manager for the NIRSPEC instrument for WMKO from 1994-1999 (McLean et al. 1998). He has 17 years of experience as Director of the Infrared Lab at UCLA and 10 years prior to that at the Royal Observatory Edinburgh Astronomy Technology Center. McLean has provided many instruments for observatories over this period of time, including the very first infrared cameras for astronomy (IRCAM: UKIRT 1986), a twin-channel camera for Lick Observatory, and a wide-field infrared camera for NASA's SOFIA. All of these instruments also had spectroscopic capability. Steidel was PI for LRIS-B, the UV/blue-optimized channel for the LRIS (WMKO) and is very experienced in multi-object and near-IR faint object spectroscopy.

To provide experienced leadership in the three critical areas of instrumentation, optics and software, Keith Matthews (CIT), Prof. Harland Epps (UCSC) and Prof. James Larkin (UCLA) oversee these areas as co-Investigators. Matthews is the overall Instrument Scientist for the entire project and will oversee the final system integration. Matthews was the PI for NIRC and NIRC2 at Keck and he has been involved in the development of infrared instruments since the inception of the field. Professor Harland Epps is one of the country's leading authorities on the optical design of astronomical spectrographs. He has provided the design of most of the Keck's existing complement of instruments, including HIRES, LRIS, ESI and DEIMOS. Professor James Larkin was PI of OSIRIS, a state-of-the-art diffraction-limited integral field spectrometer for the WMKO adaptive optics system (J.E. Larkin et al. 2002). As the Observatory's most recent instrument, this complex and sophisticated infrared instrument, with its fully automated data reduction pipeline, provides the most significant source of heritage.

The organization chart (Figure 124) shows the structure of the project team. A senior engineer or faculty member at each of the partner institutions is responsible for budget and schedule in each of the major work areas, mechanics, optics, electronics, software and observatory interfaces. Overall program management resides with the WMKO Instrument Program Manager Sean Adkins and the WMKO instrument development process is being followed. This team structure involving these four major establishments has been remarkably successful. As demonstrated by two years of productive work, this paradigm of sharing work within the WMKO community is promising.

## 6.2 Project Management

For the team, McLean at UCLA acts as executive project manager, but works very closely with the WMKO Instrument Program Manager, Sean Adkins. Technical and administrative personnel at UCLA, CIT and UCSC assist McLean to prepare the monthly reports required by WMKO and TSIP. Representatives of the TSIP program have acknowledged these reports as satisfactory. As

the Organization chart shows, senior and experienced people lead each major sub-discipline and provide regular and detailed reports in each area.

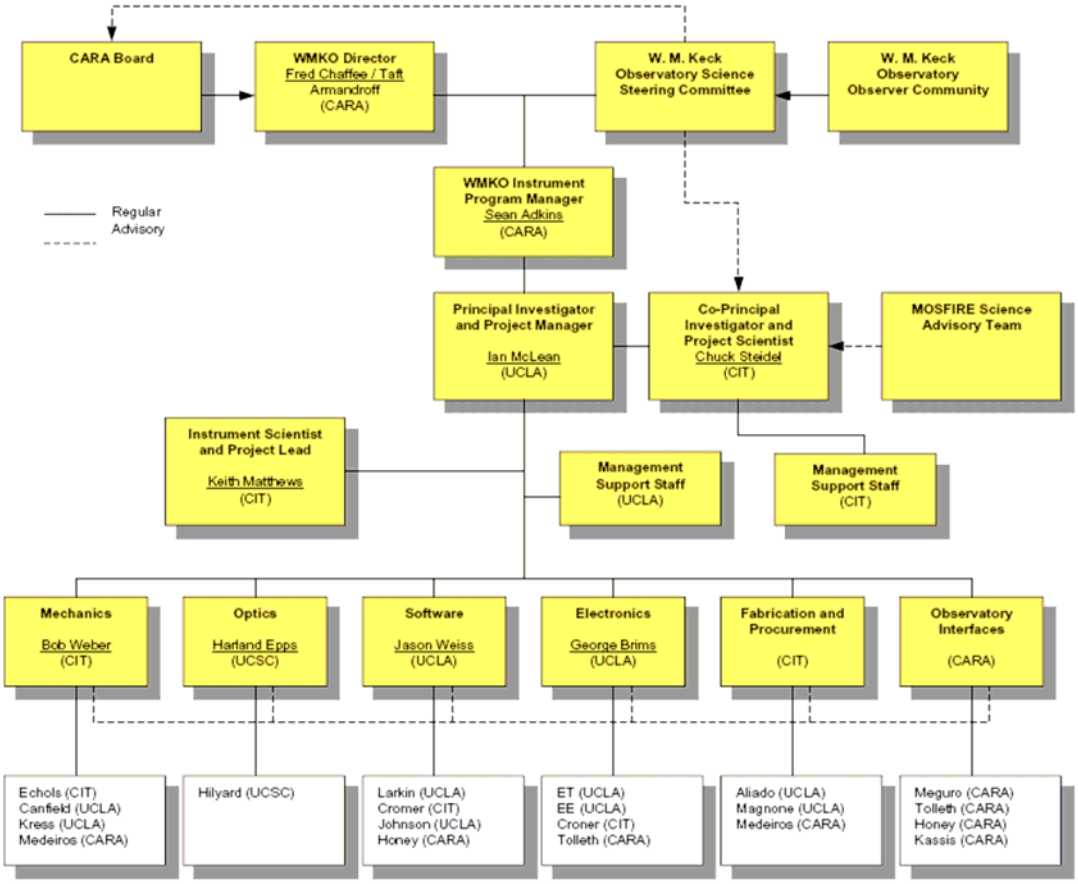


**Figure 124: MOSFIRE Organizational Chart**

## 6.3 Risk Assessment and Management

From the beginning of the MOSFIRE project several important choices were made to reduce the risks associated with an instrument of this size and complexity, as well as the potential for cost growth. Among these decisions are the following:

1. Smaller field of view – more affordable optics
2. Single infrared detector – one quarter the cost of a 4-detector mosaic; eliminates issues associated with the gaps between detectors that would be present in a mosaic.
3. Grating dispersion using multiple orders – a single two position grating is much more stable and considerably less expensive than multiple dispersion elements, a cost-effective and highly practical solution.
4. Configurable Slit mask Unit (CSU) – completely eliminates slit mask manufacture and cryogenic handling to exchange slit masks, but requires a new technology not previously

used in astronomy. We discuss below how we have handled the remaining risks in producing the CSU.

5. Re-use of software from OSIRIS and other recent WMKO projects – yields significant reduction in manpower effort for software and provides a product familiar to WMKO staff and users alike.
6. Installation at the Keck I Cassegrain focal station – eliminates handling/scheduling problems on the over-crowded Keck II telescope; heritage with LRIS is enabled and an extra reflection (the tertiary mirror) is eliminated.

As was apparent at PDR, the single greatest risk area is the CSU. From the outset, we have managed this risk through an aggressive development program with the Swiss company CSEM. First, we placed CSEM under contract to study our requirements in detail and to produce a prototype of the MOSFIRE CSU that could be tested cryogenically before the MOSFIRE detailed design was complete. CSEM has successfully met our requirements and the CSU passed an internal critical design review last month. CSEM is ready to manufacture and test the complete MOSFIRE CSU and its associated control electronics and software.

The second area of perceived risk from the outset was the large optical components required to provide the desired field of view. Again, to reduce risk in this area, we worked to get the optical design to the pre-construction level before PDR. Having achieved that goal, long-lead glass and crystalline blanks were ordered and almost all the required materials are now in hand ready for the fabrication phase. In addition, lens-mounting options were analyzed for displacements and stresses, a scheme based on flexures was developed and several prototypes constructed. In particular, cryogenic tests of the bonding strength have been carried out, two sample lens cells have been fabricated, and a prototype lens-handling jig has been built and tested. Finally, considerable effort has been expended to obtain the most reliable cryogenic indices of refraction.

Schedule slip is a risk in any engineering project involving significant development effort. For MOSFIRE we have carefully managed costs to remain within our funding profile thus far. We view this as a design-to-cost project, but so far it has not been necessary to reduce the scope of the project in any way. As we move into fabrication and procurement, we will protect against schedule slip by ensuring tight management of in-house fabrication, and close supervision of all vendors with major sub-contracts. We have already been working closely with potential suppliers for the vacuum enclosure and internal structure, and we are re-using two large handling fixtures originally built for ESI and LRIS.

Major de-scopes at this stage are unlikely, but some options remain to preserve schedule. For example, we could accept a CSU with fewer slit bars, slower operation and poorer performance. While not desirable, this option would allow a future upgrade. Optical issues may be solved by restricting the field of view. We could accept more flexure. Elimination of the pupil tracking mechanism and simplification of the flexure compensation mechanism could save component and fabrication costs and software effort. However, none of these options are desirable and we intended to make every effort to avoid any compromises in the performance or features of MOSFIRE.

## 6.4 Work Breakdown Structure

A top level WBS diagram for MOSFIRE is shown in Figure 125. Key WBS elements are also included in the MOSFIRE schedule shown in Figure 126 and Figure 127. WBS element 1.3 "Instrument Design and Fabrication" contains all of the deliverables required to produce the finished instrument. These deliverables are organized in a manner consistent with the product structure defined for the instrument (see Figure 12). For each deliverable, the work is broken down into the actual tasks required to produce the finished and qualified components of the system.

Using our combined experience building OSIRIS, NIRSPEC, NIRC2, LRIS and ESI we identify all the major components of the system, group them and execute the design, development and fabrication in the best order for sub-assembly testing and readiness for system integration. Although each partner has well-defined work packages, it is through the seamless merging of the engineering efforts at all four places that we get the greatest benefit. For example, while CIT takes the lead on all aspects of the cryo-mechanical engineering, UCLA staff will still provide drawing and fabrication support.

The division of the major work packages is as follows:

- Mechanical – CIT
- Optics – UCSC
- Electronics – UCLA
- Software – UCLA
- Interfaces – CARA
- Integration and Testing – CIT

As indicated by the final bullet above, system integration and testing for MOSFIRE will occur at CIT, but the entire team will participate in delivery and installation.

## 6.5 Schedule

A schedule to completion for the MOSFIRE project is summarized in Figure 126 and Figure 127. The overall duration of this project is estimated at 57 months, the effective start date was July 15, 2005 and the end date is projected to be March 31, 2010.

MOSFIRE passed PDR in April 2006. We strived for a detailed design phase lasting only 8-9 months, but knew that this was not probable given the pace at CSEM and the desire to produce and test prototypes. Thus, the detailed design phase has lasted 12 months, but we have accomplished all the desired tasks and more, a fully detailed solid model now represents the instrument, and we are within budget. MOSFIRE is ready for a full scale development phase lasting about 14 months followed by an integration and testing phase requiring 1 year. Our overall schedule with respect to our projections at PDR has slipped by approximately 1 month.

Fabrication of the dewar vacuum shell, internal optical benches, mechanisms and handler will begin soon after DDR in May 2007. Our goal is to receive the dewar shell in November 2007 and perform the first pump down in January 2008.

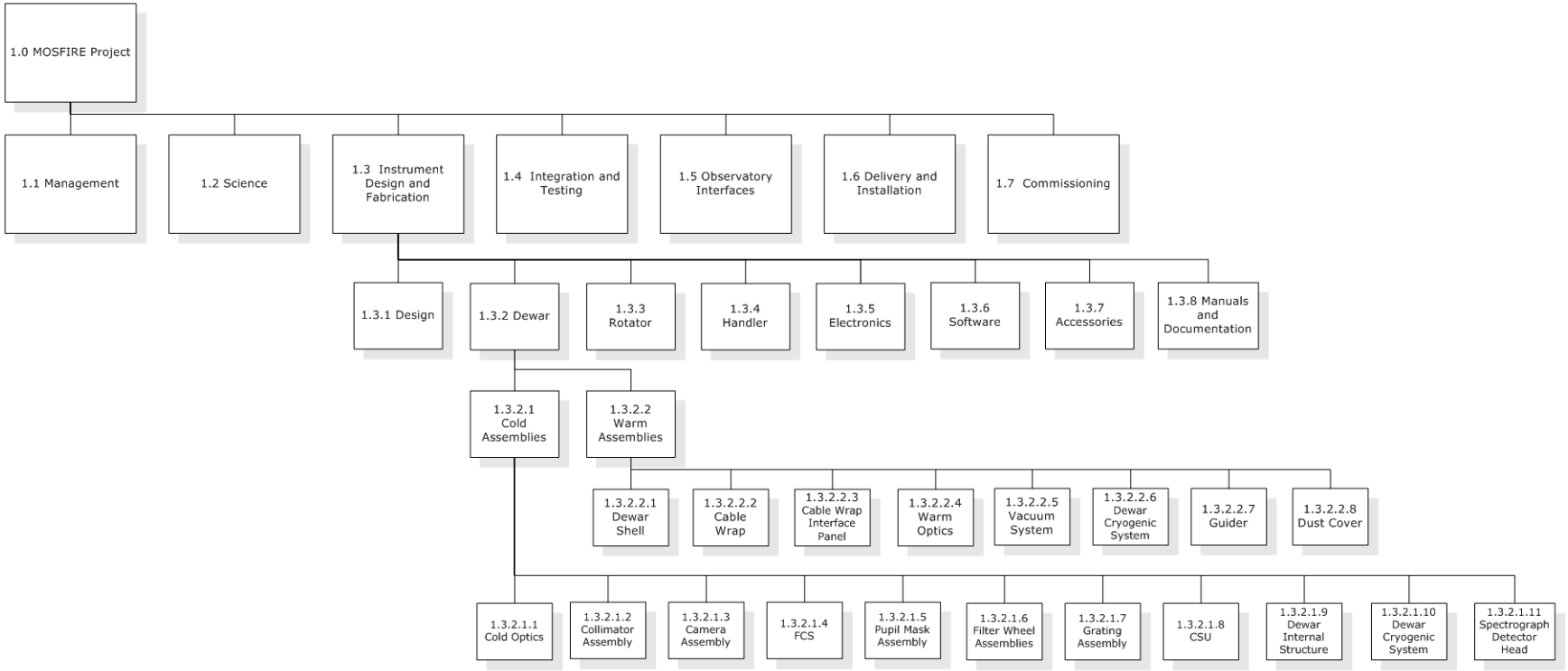


**Figure 125: MOSFIRE Top Level WBS**

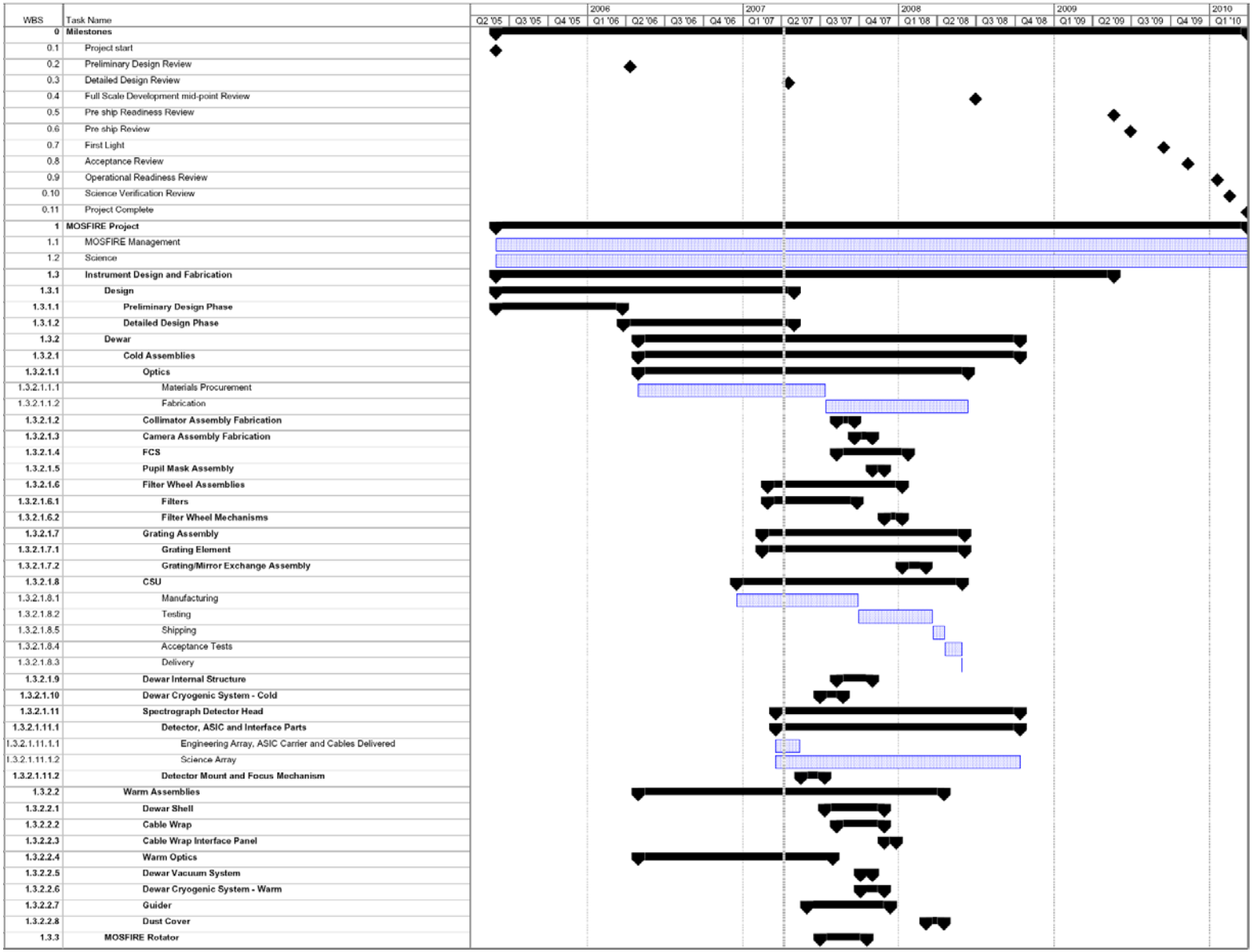


**Figure 126: MOSFIRE Schedule to Completion, Part I**

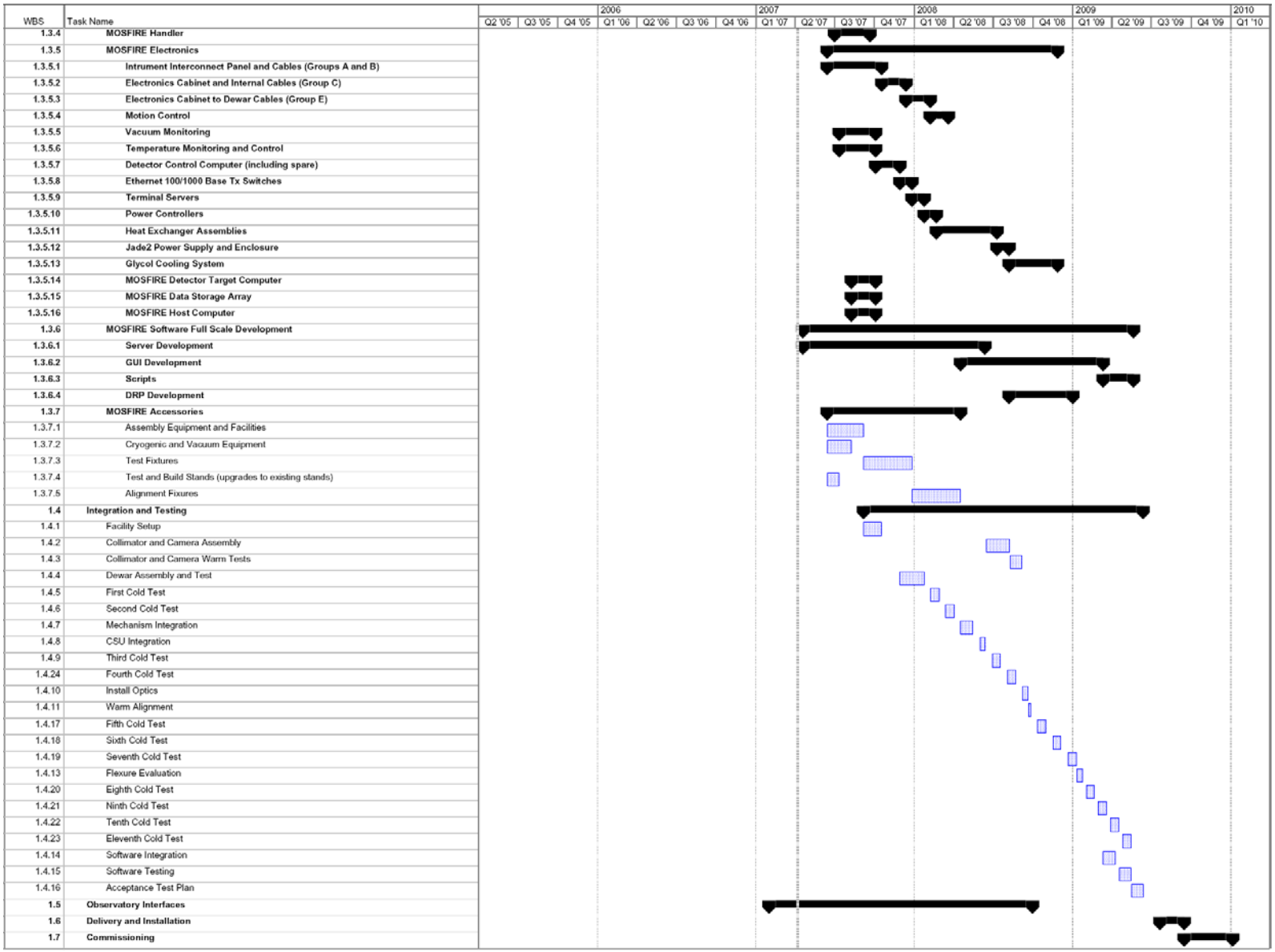


**Figure 127: MOSFIRE Schedule to Completion, Part II**

Two cold tests are planned prior to beginning integration of the mechanisms including the CSU prior to the third cold test. Delivery of the CSU is expected in at the end of May 2008.

Starting with the third cold test, each cold test is planned as a 3 week cycle, separated by periods of 2 weeks for warm adjustments and additional integration activities.

Electronics fabrication and test parallels the fabrication of the mechanisms, with the sequence of electronics activities planned to support testing of the server software, and to prepare for the initial cold tests and the warm testing of the MOSFIRE mechanisms. Since the MOSFIRE servers are all keyword based, once the servers are tested the instrument can be operated using the command line or scripts, allowing integration and test of the instrument to proceed in parallel with the development of the MOSFIRE GUIs, operating scripts and DRP. The servers will also be completed in an order that matches the integration plan, with the final servers being completed in June 2008.

Delivery of the finished science optics is expected in June 2008, and the fabrication of the collimator and camera assemblies is planned to match this delivery date. The optics will be assembled into the mounts and bench tested prior to integration into the dewar for warm alignment using a multiplexer. The fifth cold test will include the optics and optical and mechanism testing using the engineering grade detector will continue through cold test 6. Delivery of the science grade detector is expected no later than October 2008. The science grade detector will be installed for cold test 7, planned for late December 2008, and flexure evaluation will be performed during this cold test.

Four more cold tests are planned prior to performing the acceptance test plan in May 2009. Software integration and testing with the instrument will begin during cold test 9. At the completion of cold test 11 and the completion of software testing a pre-ship readiness review will be held to establish readiness for the pre-ship review. The acceptance test plan will be completed in mid-June 2009 and the pre-ship review is planned for June 30, 2009.

First light on Keck I is planned for September 2009. Handover of the instrument will occur in January 2010 with shared risk operations beginning in Semester 2010A.

## 6.6 Deliverables

WMKO and the MOSFIRE team have agreed to a list of deliverables, including the following items:

- Reports and budget information as requested
- The completed MOSFIRE instrument, with all electronics, computers, cables and accessories needed to operate and service the instrument
- Operating software and source code including a DRP
- Handling Equipment
- Documentation, including all engineering drawings, schematics, etc.
- Acceptance Test Report

- User's Manual
- Shipping containers
- A reasonable set of spare parts as agreed with WMKO

## 6.7 Milestones and Reviews

The major project milestones are shown in Table 28. Included in these milestones are 8 reviews, 4 of which involve invited external review panels.

| Milestone | Date |
|---|---|
| Project start | 7/15/2005 |
| **Preliminary Design Review** | 4/12/2006 |
| **Detailed Design Review** | 4/19/2007 |
| **Full Scale Development mid-point Review** | 7/1/2008 |
| **Pre ship Readiness Review** | 5/14/2009 |
| **Pre ship Review** | 6/30/2009 |
| First Light | 9/16/2009 |
| **Acceptance Review** | 11/12/2009 |
| **Operational Readiness Review** | 1/20/2010 |
| **Science Verification Review** | 2/18/2010 |
| Project Complete | 3/31/2010 |

**Table 28: Milestones and Reviews**

Reviews are organized and conducted by the WMKO instrument program manager and the report of the review panel is formally made to the WMKO director and the WMKO Science Steering Committee.

## 6.8 Budget

The overall budget for the MOSFIRE project is shown in Table 29. The total cost for the project is estimated at $12,266,084 including an allowance for inflation and a contingency on labor and materials. The budget shown in Table 29 includes actual expenditures for the first year of the project, and projections for the second year of the project, currently in progress.

The project began in July 2005 and is expected complete in March 2010. This represents total duration of 57 months, 3 months longer than projected at the PDR. This increase reflects an allowance for time to complete documentation at the end of the project. A postdoctoral research associate has been added to the project to assist with pre-shipment testing, commissioning activities and to support the completion of the documentation. A graduate student is also participating in the project.

The project has been awarded a total of $7,366,293 from the Telescope System Instrumentation Program (TSIP) in exchange for 24 nights of observing time in year 1, and 12 nights per year for

years 2 through 5. The balance of the project is being funded through a gift of $4.9M from Gordon and Betty Moore. This gift has been offered in annual amounts to complement the funding from the TSIP for years 2 through 5 of the project and years 2 and 3 have been received.

In year 2 the project has completed the detailed phase, and based on a successful DDR the project will continue through the remaining phases consisting of full scale development, installation and commissioning of the instrument. Design and construction of the instrument is subcontracted by WMKO to UCLA, CIT and UCSC. WMKO is implementing the observatory interfaces and support facilities required by the instrument as well as provide program management, reporting and reviews. It should be noted that none of the collaborating organizations are applying their normal indirect cost rates to the project.

To develop the budget estimate for MOSFIRE the instrument was broken down into discrete components using a product structure approach and this breakdown was used to establish labor and materials estimates. This budget has been reviewed as part of the detailed design phase and represents the current best estimate of the cost to design and build MOSFIRE. All of the major subcontracted fabrications are based on current quotations from suppliers, and the majority of the COTS items are based on quotations or current (2007) list prices. Based on the fidelity of these estimates we have reduced the materials contingency to 8%. 5% contingency is also included for the CSEM contact.

The project budget includes an allowance of 4% inflation for labor costs in project years 2 through 5 and a contingency of 15% for labor. Current liens on this contingency are for the additional cost of the graduate student and postdoctoral research associate. There were no expenditures of contingency in year 1 of the project.

The development of the CSU by CSEM represents a major cost component at $2.5M. 5% contingency is included for the CSEM contact. $76,014 of this contingency has been allocated to cover the cost of adding the 46$^{th}$ masking bar, improved impregnation of the clutch coils to prevent outgassing, and the procurement of spares for long lead custom items. These consist of sufficient spares for the equivalent of 4 slit assemblies: spare clutch actuator assemblies (common to ratchet clutches and brakes), spare masking bars, parts for the spare ratchet clutches (spare sapphire teeth, springs, supports, etc.), and parts for the corresponding brake actuators (brake pads, flex supports, springs, etc.).

Foreign travel is included in the project budget to allow for at least 2 people to travel to CSEM in year three of the project to participate in the acceptance testing of the CSU.

| | | Actuals | Projections | | | | |
|---|---|---|---|---|---|---|---|
| **Expenses** | **Notes** | **Year 1 (6/1/05 to 7/31/06)** | **Year 2 (8/1/06 to 7/31/07)** | **Year 3 (8/1/07 to 7/31/08)** | **Year 4 (8/1/08 to 7/31/09)** | **Year 5 (8/1/09 to 03/31/10)** | **Total for Project** |
| Senior Personnel | | | | | | | |
| Ian S. McLean, PI | | $ 15,481 | $ 30,963 | $ 30,963 | $ 30,963 | $ 30,963 | $ 139,333 |
| James E. Larkin, Co-I | | $ 10,267 | $ 10,267 | $ 10,267 | $ 10,267 | $ 10,267 | $ 51,335 |
| Charles C. Steidel, Project Scientist | | $ - | $ - | $ - | $ - | $ - | $ - |
| Keith Matthews, Instrument Scientist | 1 | $ 101,263 | $ 105,314 | $ 109,526 | $ 113,907 | $ 118,464 | $ 548,474 |
| Harland Epps, Co-I | | $ 15,582 | $ 15,891 | $ 16,209 | $ 16,533 | $ 16,864 | $ 81,079 |
| **Total Senior Personnel** | | $ 142,593 | $ 162,435 | $ 166,965 | $ 171,670 | $ 176,558 | $ 820,221 |
| Other Personnel | | | | | | | |
| Post Doctoral Associates | | $ - | $ - | $ - | $ 64,896 | $ 43,264 | $ 108,160 |
| Other Professionals (Technician, Programmer, Etc.) | 1 | $ 376,827 | $ 484,389 | $ 655,582 | $ 741,470 | $ 337,767 | $ 2,596,035 |
| Graduate Students | | $ - | $ 20,000 | $ 20,800 | $ 21,632 | $ 14,999 | $ 77,431 |
| Undergraduate Students | | $ - | $ - | $ - | $ - | $ - | $ - |
| Secretarial - Clerical (If Charged Directly) | 1 | $ - | $ 7,296 | $ 2,596 | $ 2,700 | $ 2,808 | $ 15,400 |
| Other | | $ - | $ - | $ - | $ - | $ - | $ - |
| **Total Salaries and Wages** | | $ 519,420 | $ 674,120 | $ 845,943 | $ 1,002,368 | $ 575,396 | $ 3,617,247 |
| Fringe Benefits | 2 | $ 102,007 | $ 177,058 | $ 223,357 | $ 265,950 | $ 152,239 | $ 920,611 |
| **Total Salaries, Wages and Fringe Benefits** | | $ 621,427 | $ 851,178 | $ 1,069,300 | $ 1,268,318 | $ 727,635 | $ 4,537,858 |
| Equipment | | $ 4,837 | $ 511,109 | $ 1,706,876 | $ 700,496 | $ - | $ 2,923,318 |
| Travel | | | | | | | |
| Domestic | | $ - | $ 10,500 | $ 10,500 | $ 9,750 | $ 32,000 | $ 62,750 |
| Foreign | | $ - | $ - | $ 8,000 | $ - | $ - | $ 8,000 |
| Other Direct Costs | | | | | | | |
| Materials and Supplies | | $ 21,208 | $ 7,541 | $ 23,833 | $ 10,812 | $ - | $ 63,394 |
| Publication Costs/Documentation/Dissemination | | $ - | $ - | $ 4,000 | $ 6,750 | $ 4,000 | $ 14,750 |
| Consultant Services | 3 | $ - | $ 30,000 | $ - | $ - | $ - | $ 30,000 |
| Computer Services | | $ - | $ 5,150 | $ 5,000 | $ 5,000 | $ - | $ 15,150 |
| Subawards (Subcontracts) | | $ - | $ - | $ - | $ - | $ - | $ - |
| Other | | $ - | $ 4,000 | $ 4,000 | $ 4,000 | $ 4,000 | $ 16,000 |
| **Total Other Direct Costs** | | $ 21,208 | $ 46,691 | $ 36,833 | $ 26,562 | $ 8,000 | $ 139,294 |
| **Total Direct Costs** | | $ 647,472 | $ 1,419,478 | $ 2,831,509 | $ 2,005,126 | $ 767,635 | $ 7,671,220 |
| Indirect Costs | | $ - | $ - | $ - | $ - | $ - | $ - |
| **Total Indirect Costs** | | $ - | $ - | $ - | $ - | $ - | $ - |
| **Total Direct and Indirect Costs** | | $ 647,472 | $ 1,419,478 | $ 2,831,509 | $ 2,005,126 | $ 767,635 | $ 7,671,220 |
| | | | | | | | |
| **Contingency** | | | | | | | |
| Materials (Equipment, Materials and Supplies) | 4 | $ - | $ 51,865 | $ 173,071 | $ 71,131 | $ 73,133 | $ 369,200 |
| Labor (Total Salaries, Wages and Fringe Benefits) | 5 | $ - | $ 124,677 | $ 157,275 | $ 177,269 | $ 100,406 | $ 559,627 |
| Less Usage of Contigency | 6 | $ - | $ (20,000) | $ (20,800) | $ (86,528) | $ (58,263) | $ (185,591) |
| **Total Contingency** | | $ - | $ 156,542 | $ 309,546 | $ 161,872 | $ 115,276 | $ 743,236 |
| **Total Cost including contingency** | | $ 647,472 | $ 1,576,020 | $ 3,141,055 | $ 2,166,998 | $ 882,911 | $ 8,414,456 |
| | | | | | | | |
| **Contract to CSEM for CSU** | 7 | $ 750,000 | $ 1,144,614 | $ 562,900 | | $ - | $ 2,457,514 |
| 5% Contingency on CSEM Contract | | $ - | $ 90,930 | $ 28,145 | $ - | $ - | $ 119,075 |
| Less Usage of Contingency | 8 | | $ (76,014) | | | | |
| **Total Cost including contingency for CSEM Contract** | | $ 750,000 | $ 1,159,530 | $ 591,045 | $ - | $ - | $ 2,500,575 |
| | | | | | | | |
| **Observatory Interfaces** | | | | | | | |
| Labor (Total Salaries, Wages and Fringe Benefits) | 9 | $ 25,110 | $ 46,495 | $ 189,735 | $ 550,786 | $ 5,235 | $ 817,361 |
| Materials (Equipment, Materials and Supplies) | | $ - | $ - | $ 277,143 | $ 79,943 | $ - | $ 357,086 |
| Travel | | $ 3,000 | $ 17,000 | $ 17,000 | $ 17,000 | $ - | $ 54,000 |
| Contingency | 10 | $ - | $ 6,975 | $ 28,461 | $ 82,618 | $ 4,553 | $ 122,607 |
| **Total Interface Costs** | | $ 28,110 | $ 70,470 | $ 512,339 | $ 730,347 | $ 9,788 | $ 1,351,054 |
| **Total Project Costs** | | $ 1,425,582 | $ 2,806,020 | $ 4,244,439 | $ 2,897,345 | $ 892,699 | $ 12,266,084 |
| | | | | | | | |
| **Funding Profile** | | | | | | | |
| Actual (Year 1) + Projected TSIP funding | 11 | $ 2,452,629 | $ 1,228,416 | $ 1,228,416 | $ 1,228,416 | $ 1,228,416 | $ 7,366,293 |
| Private funding | 12 | $ - | $ 1,662,764 | $ 1,581,290 | $ 1,374,363 | $ 281,458 | $ 4,899,875 |
| **Total Funding** | | $ 2,452,629 | $ 2,891,180 | $ 2,809,706 | $ 2,602,779 | $ 1,509,874 | $ 12,266,168 |

Notes:
1. Inflation allowed for labor costs at 4% per year for years 2 through 5
2. Benefits are 28% for UCLA and UCSC, and 26% for CIT
3. Contract to SDL for thermal analysis
4. Materials contingency is 8%
5. Labor contingency is 15%
6. Usage of contingency for graduate student and post doctoral associate costs
7. Contract is for design and manufacture of CSU
8. $76,014 for addition of 46th masking bar, impregnation of clutch coils and long lead spares
9. WMKO benefits are 29%
10. Contingency is 10% for materials and 15% for labor
11. TSIP funding based on 12 nights per year for years 2 through 5, value per night $102,368.
12. Private funding commitment made for years 2 through 5, years 2 and 3 amounts have been received.

**Table 29: Detailed MOSFIRE Project Budget**

### 6.8.1 Fabrication Costs

The fabrication cost for MOSFIRE, not including the contract to CSEM is estimated at $2.86M as shown in Table 30. This cost estimate may be compared to the PDR materials cost estimate of $2.7M. The difference between these two estimates is primarily due to the inclusion of fabrication labor costs in all of the assemblies and components that will be produced at UCLA and CIT. This was done in order to place these costs on the same basis as the costs from outside fabrication shops that are being used for some fabrications such as the dewar shell. This accounts for approximately $124K of the increase with the balance attributable to refinement of costs for large fabrications such as the dewar shell and the identification of additional costs relating to assembly and alignment equipment.

| Product Structure Element | Cost |
|---|---|
| MOSFIRE Dewar | $ 2,505,005 |
| MOSFIRE Electronics | $ 121,467 |
| MOSFIRE Accessories | $ 207,053 |
| Crating and Shipping | $ 24,675 |
| **Total** | $ 2,858,200 |

**Table 30: MOSFIRE Fabrication Cost Summary**

Additional details of the estimates for the major product structure elements of MOSFIRE are given in Table 31 and Table 32.

### 6.8.2 Observatory Interface Costs

The observatory interface costs are detailed in Figure 128. These costs include a 4% inflation rate for labor costs in project years 2 through 5. In the overall project budget we have allowed a 15% contingency on labor and a 10% contingency on equipment and materials for the observatory interface costs.

| Item | Labor $ | Material $ | Total Cost |
|---|---|---|---|
| Rotator | $ 110,192 | $ 158,700 | $ 268,892 |
| Handler | $ 29,478 | $ 38,500 | $ 67,978 |
| Support Package | $ 20,431 | $ - | $ 20,431 |
| Instrument Program Management | $ 130,420 | $ - | $ 130,420 |
| Keck I Cassegrain Focal Station | $ 36,464 | $ 32,780 | $ 69,244 |
| CCR Helium Connections | $ 101,137 | $ 67,925 | $ 169,062 |
| Keck I Nasmyth Deck RT1 Position | $ 72,575 | $ 52,580 | $ 125,155 |
| Computing Facilities | $ 32,863 | $ 6,600 | $ 39,463 |
| Software Reconfiguration | $ 56,873 | $ - | $ 56,873 |
| Reviews | $ 92,449 | $ - | $ 92,449 |
| Installation and Commissioning | $ 134,479 | $ - | $ 134,479 |
| **Totals** | $ 817,361 | $ 357,085 | $ 1,174,446 |

**Figure 128: Observatory Interface Cost Details**

| Product Structure Element | Cost |
|---|---|
| MOSFIRE Dewar | |
| Cold Assemblies | |
| Cold Optics | |
| Lenses, Mirrors, Windows | $ 821,400 |
| Mountings | $ 22,450 |
| Inner Window Assembly | $ 22,132 |
| FCS | $ 103,700 |
| Pupil Mask Assembly | $ 12,056 |
| Filter Wheel Assemblies | |
| Filters | $ 100,000 |
| Mechansim | $ 11,156 |
| Grating Assembly | |
| Grating | $ 101,523 |
| Mechansim | $ 24,280 |
| Dewar Internal Structure | |
| Major Optical Assembly Mountings | |
| Optical Benches | $ 98,875 |
| Main G-10 Ring | $ 7,000 |
| Other Mounts and Standoffs | $ 9,052 |
| Cold Strapping | $ 50,000 |
| Temperature Sensors | $ 2,450 |
| Cold Shields | $ 80,013 |
| MLI | $ 60,000 |
| Dewar Cryogenic System - Cold | $ 2,935 |
| Spectrograph Detector Head | |
| Head Assmebly, Focus Mechanism, Heater and Sensor | $ 22,845 |
| Detector, ASIC, Jade 2 and Interface Parts | $ 485,000 |
| Internal Wiring Assemblies (Groups F and G) | $ 24,327 |
| Warm Assemblies | |
| Dewar Shell | $ 190,534 |
| Cable Wrap | $ 15,231 |
| Cable Wrap Interface Panel | $ 1,440 |
| Warm Optics | |
| Mounts, Baffles, Heaters | $ 17,116 |
| Dewar Vacuum System | $ 5,316 |
| Dewar Cryogenic System - Warm | $ 48,610 |
| Guider | |
| Optics | $ 86,000 |
| Mounts, Stucture, Focus Mechanism | $ 19,350 |
| Guide Camera and Controller | $ 44,880 |
| Dust Cover | |
| Door and Drive System | $ 8,614 |
| Calibration Lamp Assembly | $ 6,720 |
| **MOSFIRE Dewar Total** | $ 2,505,005 |

**Table 31: MOSFIRE Dewar Cost Details**

| | | |
|---|---|---|
| MOSFIRE Electronics | | |
| Intrument Interconnect Panel and Cables (Groups A and B) | $ | 8,500 |
| Electronics Cabinet and Internal Cables (Group C) | $ | 21,627 |
| Electronics Cabinet to Dewar Cables (Group E) | $ | 12,870 |
| Motion Control | $ | 6,935 |
| Vacuum Monitoring | $ | 3,636 |
| Temperature Monitoring and Control | $ | 6,863 |
| Detector Control Computer (including spare) | $ | 9,238 |
| Ethernet 100/1000 Base Tx Switches | $ | 4,048 |
| Terminal Servers | $ | 1,676 |
| Power Controllers | $ | 1,498 |
| Heat Exchanger Assemblies | $ | 13,064 |
| Jade2 Power Supply and Enclosure | $ | 1,500 |
| Glycol Cooling System | $ | 11,000 |
| MOSFIRE Detector Target Computer | $ | 6,743 |
| MOSFIRE Data Storage Array | $ | 5,526 |
| MOSFIRE Host Computer | $ | 6,743 |
| **MOSFIRE Electronics Total** | $ | 121,467 |

| | | |
|---|---|---|
| MOSFIRE Accessories | | |
| Assembly Equipment and Facilities | $ | 135,694 |
| Cryogenic and Vacuum Equipment | $ | 28,300 |
| Test Fixtures | $ | 25,000 |
| Test and Build Stands (upgrades to existing stands) | $ | 8,806 |
| Alignment Fixures | $ | 9,253 |
| **MOSFIRE Accessories Total** | $ | 207,053 |

**Table 32: MOSFIRE Electronics and Accessories Cost Details**

# 7 APPENDICES

Separate documents (pdf) for each of the items listed below are posted on the MOSFIRE web site.

## 7.1 Requirements Document

Requirements for MOSFIRE: Multi-Object Spectrometer for Infra-Red Exploration, Version 1.4, March 30, 2007

## 7.2 Interface Control Document

Draft Interface Control Document for MOSFIRE, Version 1.3, March 31, 2007, W. M. Keck Observatory

## 7.3 Compliance Matrix

Draft Requirements Compliance Matrix for MOSFIRE, Version 1.1, March 30, 2007

## 7.4 CSEM Documents

CDR Documentation status_March23.pdf
MOSFIRE_CSU_CDR_ADP Doc log March23.pdf
MOSFIRE_CSU Compliance matrix_01_Feb2305_CDR.pdf
RSM_CSE_MA01_User_Manual_Iss1Draft.pdf
RSM_CSE_RP01_CSU Design and Analysis Report_Iss2A.pdf
RSM_CSE_RP02_CSU Control Rack User Manual_Iss2.pdf
RSM_CSE_RP03_CSU Thermal Analysis_2.2.pdf
RSM_CSE_TN02_Operational_Reference_Def_Iss2.pdf
RSM_CSE_TN07_User function list_Iss3C.pdf
RSM_CSE_TN13_Iss3_State_machine_control_description.pdf
RSM_CSE_TN16_CSU_Electronics_connectors_and_cabling_Iss3.pdf
RSM_CSE_TR10_Control_rack_acceptance_test_report_Iss5.pdf

## 8 REFERENCES

1. Alcock, Charles et al. 2004, "Building the System from the Ground Up, Second Community Workshop on the Ground-based O/IR System", National Optical Astronomy Observatory.

2. Erb, D.K., Steidel, C.C., Shapley, A.E., Pettini, M., and Reddy, N.A. 2006, ApJ, submitted. "The Stellar, Gas, and Dynamical Masses of Star-Forming Galaxies at z~2".

3. Martini, P., and DePoy, D.L., SPIE, 4008, 695 "Optimal Resolutions for IR Spectroscopy Through the OH Airglow".

4. R. Kibrick et al. 2000, "Active Flexure Compensation Software for the Echellette Spectrograph
and Imager on Keck-II", Proc. SPIE 4009, p. 262-273.

5. R. Kibrick et al. 2003, "A comparison of open versus closed loop flexure compensations for two Keck optical imaging spectrographs: ESI and DEIMOS", Proc. SPIE 4841, p. 1385-1398.

6. S. B. Larson 1996, "NIRSPEC Optics Design Note 2.02: Guider Camera".

7. S. M. Faber et al. 2002, Proc. SPIE 4841.

8. S.M Faber et al. 2003, SPIE, 4841,1657

9. S. Henein et al. 2003, "Mechanical Slit Mask Mechanism for the James Webb Space Telescope Spectrometer", in Proc. 10th European Space Mechanisms and Tribology (ESMAT) Symposium, San Sebastian, Spain, ESA SP-524, pp.201-208.

10. P. Spanoudakis et al. 2004, in Opticon: Workshop on Reconfigurable Slit Masks.

11. I. S. McLean et al. 1998, Proc. SPIE Vol. 3354, 566.

12. J.E. Larkin et al. 2002, Proc. SPIE 4841.

# 9 MOSFIRE ACRONYMS

- API: Application Programming Interface
- ASIC: Application Specific Integrated Circuit
- BCS: Balanced Composite Substrate
- Cass: Cassegrain
- CDS: Correlated Double Sampling
- COM: Component Object Model
- COO: Caltech Optical Observatories
- CSEM: Centre Suisse d'Electronique et de Microtechnique (Swiss Center for Electronics and Microtechnology)
- CSU: Cryogenic Slit Unit
- DEIMOS: Deep Imaging Multi-Object Spectrograph
- DLL: Dynamically Linked Library
- DRP: Data Reduction Pipeline
- ESI: Echellette Spectrograph and Imager
- FCS: Flexure Compenstation System
- FITS: Flexible Image Transport System
- GUI: Graphical User Interface
- HAL: Hardware Abstraction Layer
- HgCdTe: Mercury-Cadmium-Teluride
- IDL: Interactive Data Language
- IR: InfraRed
- JAR: Java Archive
- JNI: Java Native Interface
- KTL: Keck Task Library
- LRIS: Low Resolution Imaging Spectrograph

- LVDT: Linear Voltage Differential Transformer
- MAS: MOSFIRE ASIC Server
- MASCGEN: MOSFIRE Automatic Slit Configuration Generator
- MCDS: Multiple Correlated Double Sampling (Fowler Sampling)
- MCSS: MOSFIRE CSU Server
- MDFS: MOSFIRE Detector Focus Server
- MDS: MOSFIRE Detector Server
- MECGUI: MOSFIRE Exposure Control GUI
- MESGUI: MOSFIRE Expsoure Status GUI
- MFCS: MOSFIRE Flexure Compensation Server
- MGS: MOSFIRE Global Server
- MMCGUI: MOSFIRE Mechanism Control GUI
- MMSGUI: MOSFIRE Mechanism Status GUI
- MOSFIRE: Multi-Object Spectrograph for InfraRed Exploration
- MPCGUI: MOSFIRE Power Control GUI
- MPRGUI: MOSFIRE Pressure Status GUI
- MPRS: MOSFIRE Pressure Server
- MPSGUI: MOSFIRE Power Status GUI
- MPWS: MOSFIRE Power Server
- MRMS: MOSFIRE Rotary Mechanism Server
- MSC: MOSFIRE Slit Configuration File
- MSCGUI: MOSFIRE CSU Control GUI
- MSSGUI: MOSFIRE CSU Status GUI
- MTCGUI: MOSFIRE Temperature Control GUI
- MTCS: MOSFIRE Temperature Control Server
- MTGUI: MOSFIRE Telescope GUI

- MTMS: MOSFIRE Temperature Monitor Server
- MTSGUI: MOSFIRE Temperature Status GUI
- MVC: Model-View-Controller Architecture
- NIRC2: Near InfraRed Camera 2
- NIRES: Near InfraRed Echelle Spectrometer
- NIRSPEC: Near InfraRed Spectrograph
- OIR: Optical/Infrared
- OSIRIS: OH-Suppressing InfraRed Imaging Spectrograph
- PI: Physik Instrumente
- RMI: Remote Method Invocation
- RPC: Remote Procedure Call
- SCA: Sensor Chip Assembly
- TCP/IP: Transmission Control Protocol/Internet Protocol
- UCLA: University of California, Los Angeles
- UCO: University of California Observatories
- UCSC: University of California, Santa Cruz
- UI: User Interface
- USB: Universal Serial Bus
- WMKO: W. M. Keck Observatory